CONTRATO

IICA / INDRHI / CSU

INSTITUTO INTERAMERICANO
DE COOPERACION PARA LA
AGRICULTURA (IICA)

INSTITUTO NACIONAL DE RECURSOS
HIDRAULICOS (INDRHI)

UNIVERSIDAD DEL
ESTADO DE COLORADO
(CSU)

ESTUDIOS SOBRE LA OPERACION Y SEGURIDAD DEL SISTEMA DE EMBALSES DE VALDESIA

FINAL REPORT

VOLUME I

HYDROLOGIC STUDIES 1/

DOCUMENTO No. 36
/08/86

Serie Publicaciones Misceláneas
A1/DO-86-002
ISSN-0534-5391

FINAL REPORT

VOLUME I

HYDROLOGIC STUDIES [1/]

1/ This document was prepared by J.T.B. Obeysekera, G.Q. Tabios III, F.A. Pons, J.D. Salas and H.W. Shen, Colorado State University, Fort Collins, Colorado.

PRESENTACION

Los estudios de Operación y Seguridad del Sistema de Embalses de Valdesia fueron ejecutados conjuntamente por el Instituto Nacional de Recursos Hidráulicos (INDRHI) de la República Dominicana, la Universidad del Estado de Colorado (CSU) y el Instituto Interamericano de Cooperación para la Agricultura (IICA) a través del Contrato IICA/INDRHI/CSU firmado el 6 de abril de 1984. Los estudios se iniciaron el 6 de agosto de 1984 y finalizaron el 31 de agosto de 1986.

Los estudios fueron financiados por el INDRHI a través del préstamo 1655-DO del Banco Mundial.

La ejecución de los estudios se desarrolló en seis áreas:

a) Estudios Hidrológicos
b) Operación Normal
c) Operación de Emergencia
d) Inspección, Mantenimiento y Seguridad de Presas
e) Organización para la Operación del Sistema de Embalses
f) Entrenamiento y Transferencia de Tecnología

En este documento se incluye parte del material técnico del Informe Final, el cual consta de los siguientes volúmenes:

-Resumen
-Estudios Hidrológicos
-Operación Normal
-Estudios de Operación de Crecidas
-Estudios de Inspección, Mantenimiento y Seguridad de Presas
-Organización y Funciones para la Operación del Sistema de Embalses de Valdesia.

-Transferencia de Tecnología y Capacitación.

-Plan de Operación de Emergencia para el Sistema de Embalses de Valdesia.

-Plan de Operación Normal para el Sistema de Embalses de Valdesia: (1) Riego y Energía, (2) Control de Crecidas.

-Manuales de Operación de Modelos Computarizados para la Operación Normal del Sistema de Embalses.

-Manual de Usuario de Modelos de Sistemas Hidrológicos.

Santo Domingo, República Dominicana
31 de agosto de 1986

DR. JOSE D. SALAS
Coordinador por CSU

DR. AGUSTIN A. MILLAR
Coordinador General
Estudios Embalse Valdesia
(IICA)

ING. JULIO M. LLINAS
Coordinador por INDRHI

VOLUME I
HYDROLOGIC STUDIES

TABLE OF CONTENTS

VOLUME I. HYDROLOGIC STUDIES

1.1 INTRODUCTION

The Valdesia reservoir system, located on the Nizao River in the Dominican Republic, was designed to provide irrigation water to the Nizao project areas and hydroelectric energy to the national electrical network system. The reservoir system consists of a main reservoir, dam and spillway, a power plant and outflow regulating works, together with an afterbay, diversion and spillway system a short distance downstream.

The study on the operational management of the Valdesia system reported in a series of volumes including this one, involved several interrelated areas. This volume reports in detail the basic hydrologic studies including rainfall-runoff modeling, flood forecasting and stochastic data generation which are essential components of the entire study. The products reported in this volume are used for developing emergency and normal operation plans for the Valdesia system.

1.2 METHODS OF INVESTIGATION

Hydrologic studies are a prerequisite to any water resources management project. The required studies necessary for this project can be categorized under four topics:

1. Design storms
2. Rainfall-runoff modeling
3. Streamflow forecasting
4. Stochastic data generation

Hypothetical design storms are required to compute hypothetical floods which are necessary for developing emergency operating procedures. Two types of hypothetical storms are considered: (a) Standard Project Storms (SPS); and (b) Probable Maximum Precipitation

(PMP). The rationale behind the use SPS is discussed in many documents of the U.S. Army Corps of Engineers (U.S. Army, 1971). Both types of hypothetical storms require depth-area-duration curves. These are developed from about 25 observed historic storms. Since two regimes of storms, namely hurricane and non-hurricane, are present in the Dominican Republic, two types of SPS are developed. The time distribution of SPS is also derived from the observed storms. The PMP is based on the Hurricane model of the U.S. National Weather Service (U.S. Weather Bureau, 1961) modified by the counterparts in the Dominican Republic.

An event type rainfall-runoff model suitable for conditions in the Nizao basin is necessary to compute hypothetical floods from hypothetical storms. The HEC-1 model of the U.S. Army Corps of Engineers is used for this purpose. It is calibrated by using data of historic storms and floods and a few flood data derived from Valdesia reservoir levels during storm events. The calibrated model is used to compute hypothetical floods for three different antecedent basin conditions. The model is also used to reconstruct the possible hydrographs from the precipitation that occurred during the Hurricane DAVID which struck the island on August 30, 1979.

For real-time forecasting, a modified version of the U.S. National Weather Service River Forecast Model is employed. The modification is necessary to (a) develop a version which will fit in the computing facilities at INDRHI/CDE; and (b) incoporate kinematic wave flood routing procedure in the model. The model is calibrated using several years of daily streamflow data and hourly precipitation data.

Synthetically generated data are necessary to develop and test the normal operating rules. Multivariate stochastic models of streamflow of

three gauging stations (Ermitano, Palo de Caja, Rancho Arriba) are developed from extended existing historic data. The generated data at Ermitano is employed to generate another synthetic series of number of hours of energy production at Valdesia dam. Both series are used for developing and testing of normal operating rules.

1.3 SUMMARY OF CONCLUSIONS

Following is a summary of conclusions based on the hydrologic studies reported in this section:

1. Significant amount of errors and inconsistencies are found in various precipitation and streamflow data collected. A careful review of data collection processing and reporting of all hydrologic data is warranted.

2. The standard project storm (for 48-hour duration) based on non-hurricane storms is 260 mm whereas the same based on hurrican precipitation is 493 mm.

3. The watershed average PMP of 1338 mm was obtained by the counterpart based on the hurricane model of U.S. Weather Brueau.

4. The nonhurricane SPS simulated a peak inflow to Valdesia reservoir of 3469 m^3/s for dry antecedent conditions whereas it gave 7544 m^3/s for wet antecedent conditions.

5. The hurricane SPS simulated a peak inflow to Valdesia reservoir of 10185 m^3/s for dry antecedent conditions whereas it gave 16548 m^3/s for wet antecedent conditions.

6. The flood peak simulated by using the calibrated HEC-1 model and observed precipitation during hurricane DAVID was 5332 m^3/s for dry antecedent conditions and 10358 m^3/s for wet antecedent conditions. The

calibrated SAC-KW model resulted in peak of 7074 m^3/s for the same event.

7. The PMP supplied by counterparts produces a PMF of 20,000 m^3/s for dry antecedent conditions. For wet antecedent conditions it increases to 23,000 m^3/s.

8. The calibration of the developed flood forecasting model for Nizao basin was performed on a year-to-year basis using the data from 1972 to 1975. It is concluded from this exercise that the best model calibration is in year 1972. Subsequent use of the 1972-model parameters to forecast the streamflow regime during Hurricane DAVID (August, 1979) gave a hourly peak flow at Paso del Ermitano of 7074 m^3/s.

9. For stochastic modeling and data generation, a trivariate, contemporaneous firt-order autoregressive process with seasonal parameters has been found to adequately describe the streamflows of Rancho Arriba, Palo de Caja and Paso del Ermitano. On both monthly and weekly levles, the streamflows are concluded to be log-Pearson Type III distributed as indicated by the normalizing transformation used which is the combination of logarithmic and Wilson-Hilferty transformations. A similar model structure has also been found for modeling and generation of turbine operating hours time series at the Valdesia reservoir with bivariate dependence on Paso del Ermitano streamflows.

1.4 ORGANIZATION OF THE VOLUME

The work involved in hydrologic studies are reported in five subsections. The general characteristics of the watershed physiography, vegetation, etc. and the details of availability and quality of data are included in Section 1.5. The development of hypothetical storms

Standard Project Storm and the Probable Maximum Precipitation is discussed in Section 1.6. The details of rainfall-runoff modeling including the calibration of the selected HEC-1 model and its application to compute hypothetical floods are included in Section 1.7. In Section 1.8, the development, calibration, testing and application of the SAC-KW model for real-time flood forecasting is discussed. Finally, Section 1.9 deals with the development and application of the stochastic models of streamflow and number of hours of energy generation.

1.5 NIZAO WATERSHED

1.5.1 Physiography

The Nizao Watershed is located in the south central part of the Dominican Republic (Figure 1.5.1). The Valdesia Dam is located approximately 50 km upstream from the confluence of Nizao river and the Atlantic Ocean. The drainage area at Valdesia Dam is about 850 sq. km. The watershed has a distinct elongated shape with a predominant orientation in the NW-SE direction (see Figure 1.5.2). Most of the headwater areas have high relief with main channel slopes reaching as much as 8 to 10 percent. The drop in elevation from the highest point to the Valdesia dam site is about 2500 meters. No significant flood plains exist in the entire Nizao watershed.

1.5.2 Vegetation

The watershed is covered primarily with forest and pasture. Less than 8 percent of the watershed is covered with agricultural lands.

1.5.3 Hydrometeorological Data

Precipitation data: A list of the precipitation data received from INDRHI and the Meteorology Agency is included in Table 1.5.1. Table 1.5.2 shows the available hourly precipitation data that was obtained in computer tape. For purposes of data analysis the nine computer files corresponding to these stations were used to create yearly files containing the hourly data. The precipitation data availability for station in and around Nizao watershed is shown in the form of a bar chart in Figure 1.5.3.

Climatological Data: Table 1.5.3 shows the stations in and around Nizao, for which climatological data is available. The evaporation data was used in the calibration of the real-time streamflow forecast model.

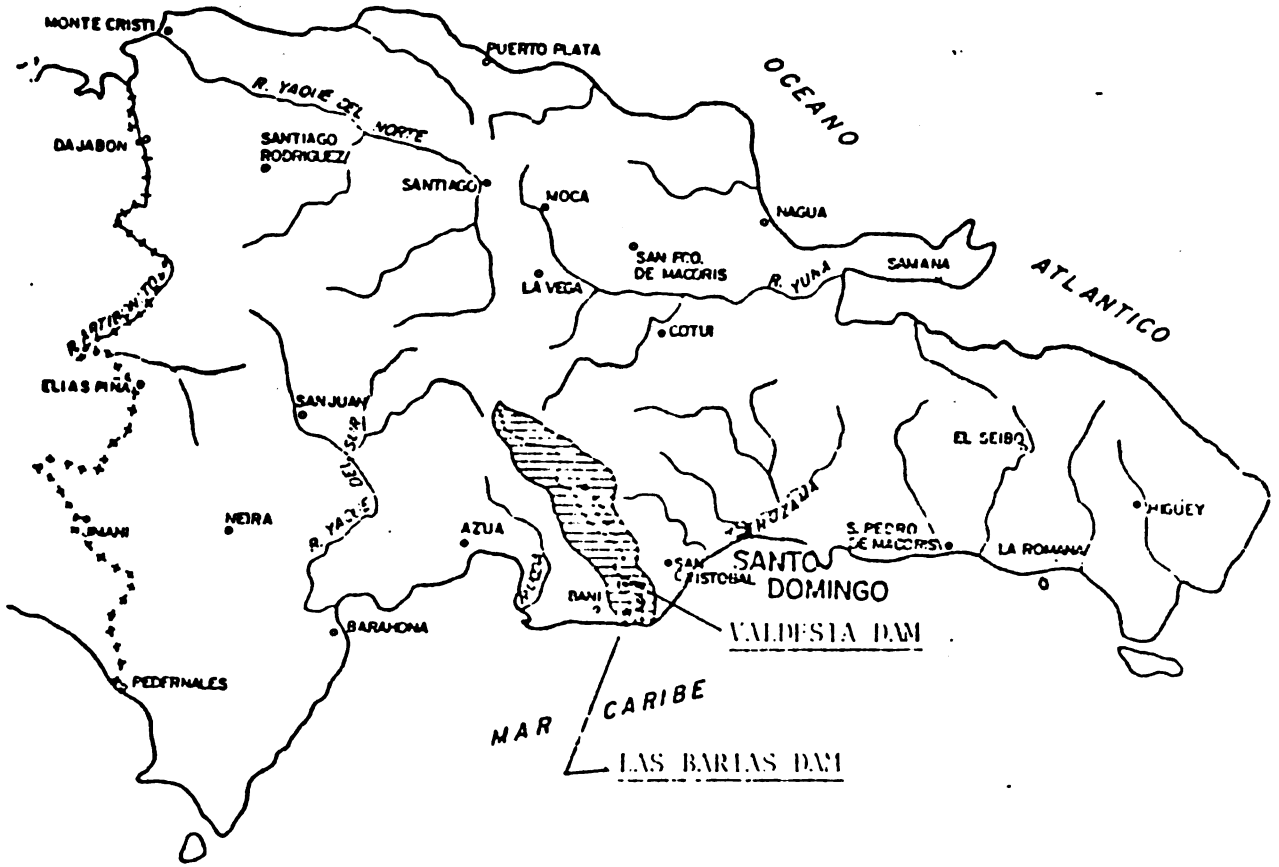

Figure 1.5.1. Location of the Nizao watershed in the Dominican Republic.

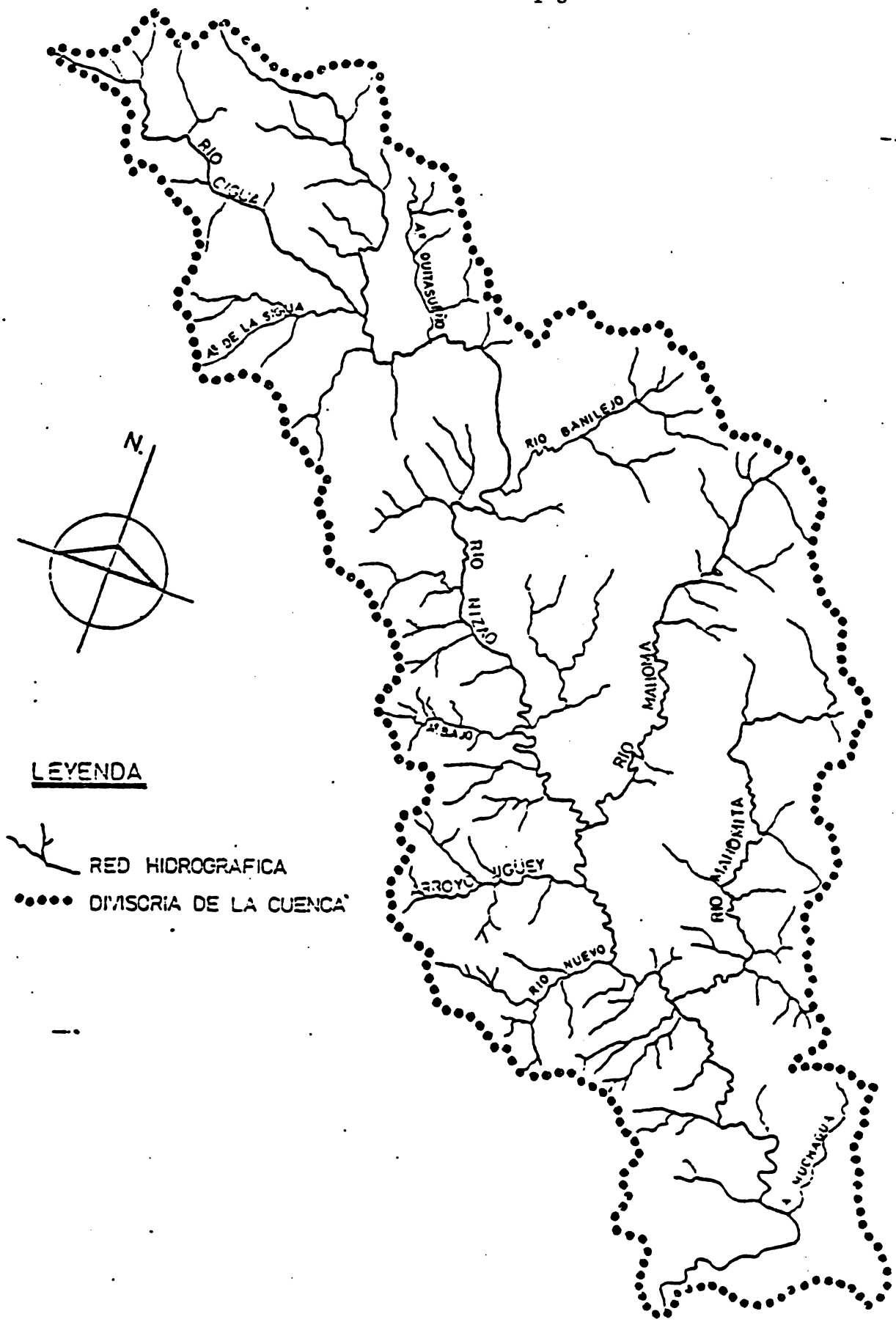

Figure 1.5.2. Nizao river basin.

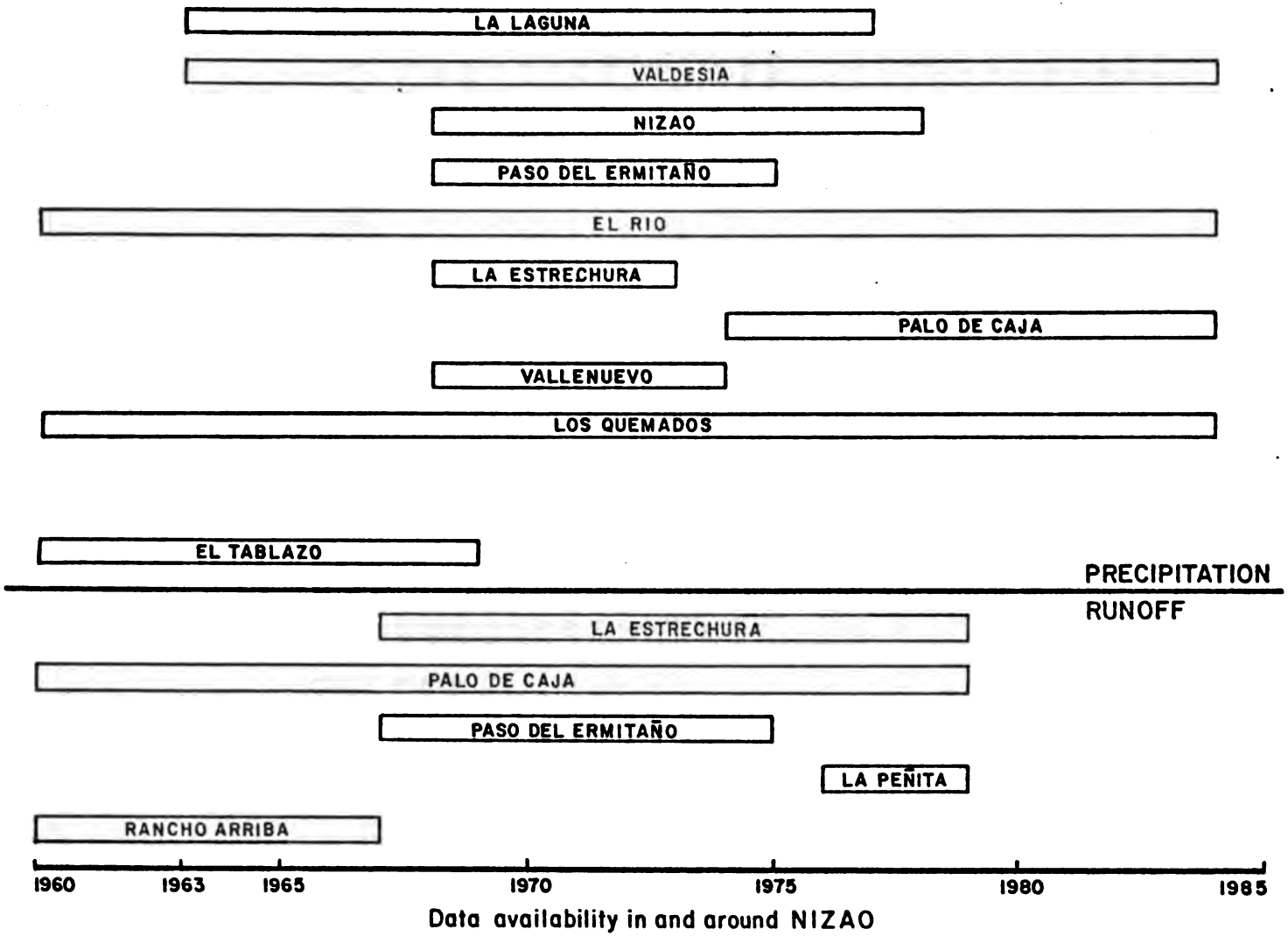

Data availability in and around NIZAO

Figure 1.5.3. Precipitation and runoff data availability for stations in and around Nizao watershed.

TABLE 1.5.1 PRECIPITATION DATA

Station Name	Basin	Type	Start	End	Lat.	Lon.	Tap
La Laguna	Nizao	Day	12/62	12/77	18°32'30"	70°24'45"	Yes
Nizao	Nizao	Day	1/68	3/78	18°36'53"	70°27'07"	Yes
Paso Del Ermitano	Nizao	Day	4/68	11/75	18°26'00"	70°16'00"	Yes
Los Cacaos	Nizao	Day	8/67	7/70	18°31'40"	70°18'00"	Yes
Azua Hatillo	Ocoa	Day	8/69	3/84	18°23'40"	70°32'20"	Yes
Valdesia	Nizao	Day	2/63	7/84	18°24'30"	70°16'50"	Yes
La Estrechura	Nizao	Day	1/68	12/73	18°43'40"	70°29'00"	Yes
Presa Mana	Haina	Day	11/82	7/84	18°36'28"	70°12'55"	Yes
Presa Isa	Haina	Day	11/82	7/84	18°36'28"	70°12'32"	Yes
Quija Quieta	Nizao	Day	10/76	4/79	18°13'49"	70°27'31"	Yes
Engombre	Haina	12 hr	1/77	7/83	18°27'00"	70°00'07"	No
Palo De Caja	Nizao	Day	5/74	10/84	18°31'50"	70°24'00"	Yes
Valle Nuevo	Y. Del Sur	Day	1/68	6/74	18°49'27"	70°40'58"	Yes
Constanza	Y. Del Sur	Day	1/68	12/79	18°54'40"	70°43'00"	Yes
Guayabal	Y. Del Sur	Day	3/79	9/84			Yes
Los Quemados	Yuna	Day	1/60	10/84	18°53'30"	70°27'30"	Yes
Juma-Bonao	Yuna	Day	12/70	9/84	18°54'00"	70°23'10"	Yes
El Rio (Constanza)	Y. Del Sur	Day	6/60	9/84	18°58'30"	70°37'40"	Yes
Esta Bania	Grande Del Med.	Day	9/69	10/84	18°27'20"	70°38'45"	Yes
El Tablazo	Nigua	Day	8/60	1/69	18°29'10"	70°10'50"	Yes
Rancho Arriba	Nizao	Mon	1/39	12/80	18°42'	70°27'	No
Padre Las Casas	Y. Del Sur	Mon	1/38	12/83			No
Bani	Bani	Mon	1/36	12/83	18°16'	70°20'	No
Villa Autagracia	Haina	Mon	1/38	12/83			No
Azua	Via	Mon	1/31	12/83			No
Valdesia	Nizao	Hour	2/63	5/83	18°24'30"	70°16'50"	No
La Laguna	Nizao	Hour	12/62	11/77	18°32'30"	70°24'45"	No
Nizao	Nizao	Hour	1/63	4/78	18°36'53"	70°27'07"	No
Medina	Haina	12 hr	10/79	7/84	18°32'06"	70°08'40"	No
Quija Quieta	Nizao	12 hr	4/79	4/79	18°13'49"	70°27'31"	No
Medina	Haina	Day	3/76	12/84	18°32'06"	70°08'40"	Yes
Rancho Arriba	Nizao	Day	3/39	12/84	18°42'	70°27'	No
Padre Las Casas	Y. Del Sur	Day	10/38	12/84			No
Bani	Bani	Day	1/36	12/84	18°16'	70°20'	No
Villa Altagracia	Haina	Day	8/38	12/84			No
Azua	Via	Day	1/31	12/84			No

TABLE 1.5.2 HOURLY PRECIPITATION

STATION NAME	BASIN	START	END
Valdesia	Nizao	2/63	5/83
La Laguna	Nizao	12/62	5/78
Nizao	Nizao	1/63	4/78
Engombe	Haina	5/72	6/84
Palo De Caja	Nizao	2/79	9/83
Valle Nuevo	Y. Del Sur	9/77	3/83
El Eio (Const.)	Y. Del Sur	1/77	12/84
Los Quemados	Yuna	1/65	7/84
Juma-Bonao	Yuna	7/71	5/82

TABLE 1.5.3 CLIMATOLOGICAL DATA

CLIMATOLOGICAL REPORTS: Precipitation, evaporation, temperature, humidity, wind speed, cloudiness , radiation, pressure (printouts)

CODE	STATION	BASIN	START	END	LAT.	LON.
34001	Engombe	Haina	10/68	7/84	18°27'00"	70°00'07"
34002	Medina	Haina	10/79	7/84	18°32'06"	70°08'40"
38002	Valdesia	Nizao	10/67	7/84	18°24'30"	70°16'50"
38001	Nizao	Nizao	10/67	4/78	18°36'53"	70°27'07"
38009	Quija Quieta	Nizao	10/76	4/79	18°13'49"	70°27'31"

EVAPORATION (Tape)

CODE	STATION	BASIN	START	END	LAT.	LONG.	TYPE
34001	Engombe	Haina	/77	/84	18°27'00"	70°00'07"	Daily

1.5.4 Streamflow Data

Daily Runoff Data: Table 1.5.4 shows the daily runoff data available for gauging stations in Nizao and other surrounding watersheds. The daily streamflow data at stations La Estrechura, Palo De Caja, Paso Del Ermitano, and Rancho Arriba were used for stochastic streamflow generation and in the calibration of the real-time streamflow forecast model. The data availability at these stations is summarized in the form of a bar chart in Figure 1.5.3.

Storm Hydrograph (Stage) Data: Table 1.5.5 presents the data availibility on selected storm hydrographs for stream gauging stations La Estrechura, Palo de Caja, Paso del Ermitano and La Penita. It is noted that the original raw data corresponds to stages observed during storm events and calibrated rating curves needed to be employed to convert them to actual discharges.

Rating Curves: The counterparts provided stage-discharge relations for stations La Estrechura, Palo De Caja, La Penita, and Paso del Ermitano to be used in transforming the hourly stage data to discharges. The plots of these curves are shown in Figures 1.5.4 to 1.5.13. In view of some inconsistencies present in these curves, the raw stage-discharge data were used to develop a new set of rating curves for this study. The development of these new rating curves is explained in detail in Appendix 1.5.A.

Reservoir Levels: In order to supplement the gauged storm hydrograph data, reservoir levels at Valdesia dam for certain major events were obtained from CDE. Hourly reservoir levels were obtained for following periods:

TABLE 1.5.4 RUNOFF DATA

Station Name	Basin	Type	Start	End	Lat.	Long.	Tape
La Estrechura	Nizao	Day	10/67	8/79	18°43'47"	70°29'00"	Yes
Palo De Caja	Nizao	Day	10/56	8/79	18°33'17"	70°22'52"	Yes
Paso Del Ermitano	Nizao	Day	11/67	10/75	18°26'02"	70°15'43"	Yes
Rio Abajo	Nizao	Day	5/58	10/67	18°35'08"	70°25'05"	Yes
La Penita	Nizao	Day	10/76	7/79	18°27'19"	70°16'32"	Yes
Caobal	Haina	Day	9/57	7/84	18°35'08"	70°08'57"	Yes
Los Corozos	Haina	Day	6/82	7/84	18°31'23"	70°07'10"	Yes
Arroyo Limon	Ocoa	Day	3/70	11/83	18°29'37"	70°30'43"	Yes
El Recodo	Bani	Day	2/79	9/83	18°22'27"	70°20'24"	Yes
Los Quemados	Yuna	Day	4/62	8/79	18°53'31"	70°27'25"	Yes
Blanco	Yuna/Bl.	Day	11/77	6/84	18°52'56"	70°31'17"	Yes
Maimon	Yuna/Mai.	Day	1/68	6/84	18°53'47"	70°17'71"	Yes
El Tablazo	Nigua	Day	1/59	3/84	18°28'39"	70°10'15"	Yes
Rancho Arriba	Nizao	Day	5/59	10/67	18°42'58"	70°27'59"	Yes
El Cacao	Nizao	Day	1/62	11/83	18°31'41"	70°17'59"	Yes
Los Ranchitos	Ocoa	Day	1/61	12/67	18°26'58"	70°29'55"	Yes
Carrizal	Jura	Day	10/64	10/81	18°32'27"	70°49'14"	Yes
Palomino	Y. Del. S.	Day	1/78	12/83	18°48'06"	70°58'26"	Yes
Mendez	Ocoa	Day	1/56	4/61	18°28'29"	70°30'48"	Yes
La Higuana	Nizao	Day	1/56	12/61	18°22'46"	70°16'22"	Yes

TABLE 1.5.5 HYDROGRAPH DATA OF SELECTED STORMS

arting			Ending			Estrec	Palo de	La Peni	Trattan	STORM ID
MON	DAY	HR	YR	MON	DAY	HR					
Jul	13	[illegible]	60	Jul	22	24	Incom	N/A	N/A	Incomp	[illegible]
Jul	7	1	70	Jul	12	21	Incom	N/A	N/A	Comp	3
Nov	6	1	70	Nov	12	21	N/A	N/A	N/A	Comp	[illegible]
Dec	7	1	70	Dec	10	21	N/A	N/A	N/A	Comp	9
Mar	'0	1	72	Mar	13	24	Comp	Comp	N/A	Comp	[illegible]
May	20	1	72	May	25	24	Incom	Comp	N/A	Comp	[illegible]
Aug	1	1	71	Aug	13	13	Incom	Comp	N/A	Comp	G
Sep	11	1	71	Sep	19	21	Incom	Comp	N/A	Comp	H
Oct	21	1	74	Oct	26	24	Incom	Comp	N/A	Incom	I
Sep	16	1	75	Sep	21	11	Incom	N/A	N/A	Comp	J
Oct	22	1	75	Oct	27	14	Incom	N/A	N/A	Comp	K
Nov	1	1	75	Nov	12	12	Incom	N/A	N/A	Comp	L
May	20	1	77	May	25	24	Incom	Comp	Comp	N/A	M
Nov	21	1	77	Nov	27	21	Incom	Comp	Comp	N/A	N
Dec	27	1	78	Jan	6	21	N/A	Comp	Comp	N/A	O
May	28	1	78	May	31	21	Incom	Comp	Comp	N/A	P
Aug	2	1	78	Aug	8	21	Incom	Comp	Comp	N/A	Q
Jan	29	1	79	Jul	5	21	N/A	N/A	Comp	N/A	R

Notes: Incom = Some hourly data is missing
Comp = Complete - we have this data at CSU
N/A = Not available - No record available

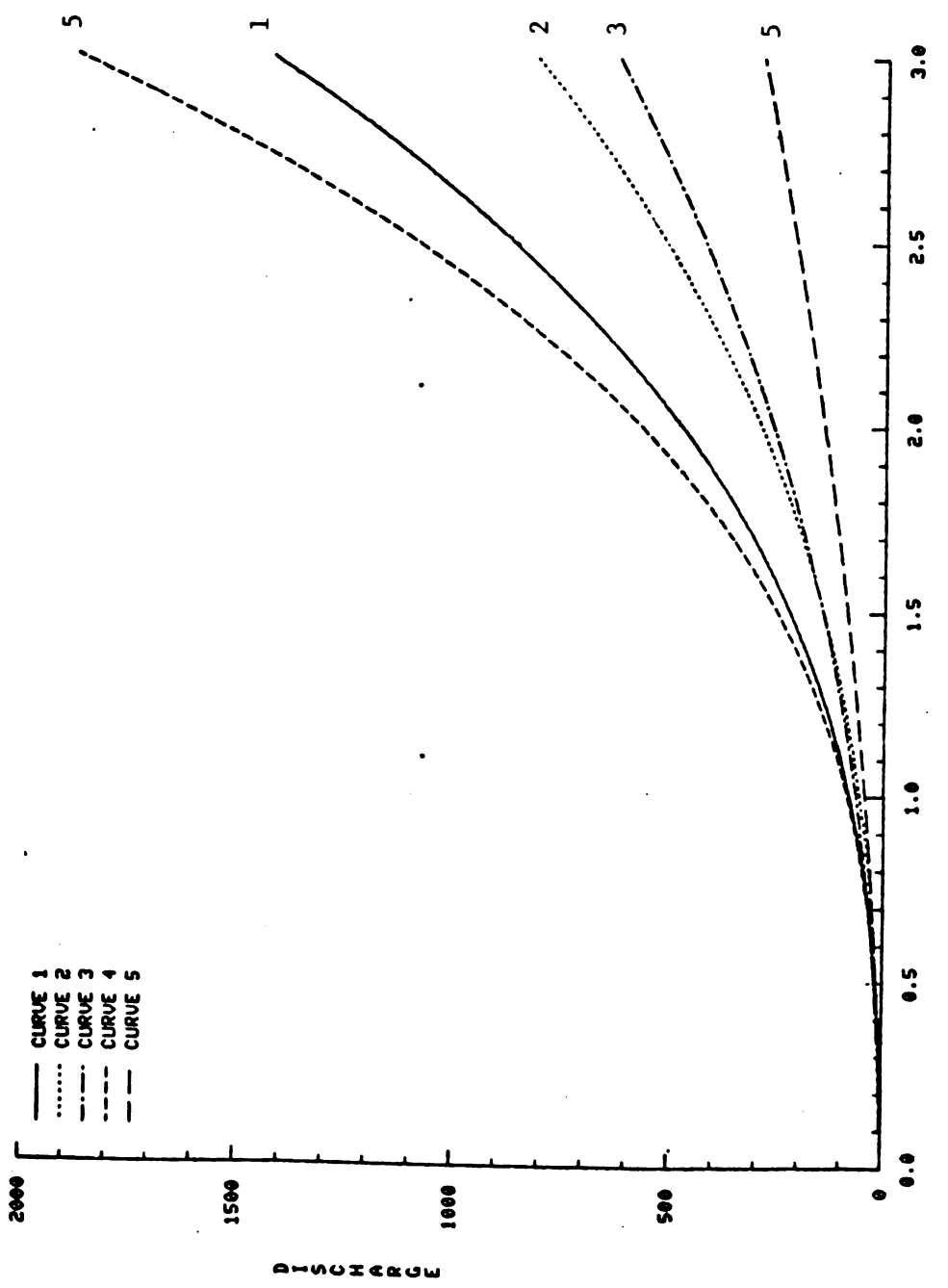

Figure 1.5.4 RATING CURVES FOR LA ESTRECHURA

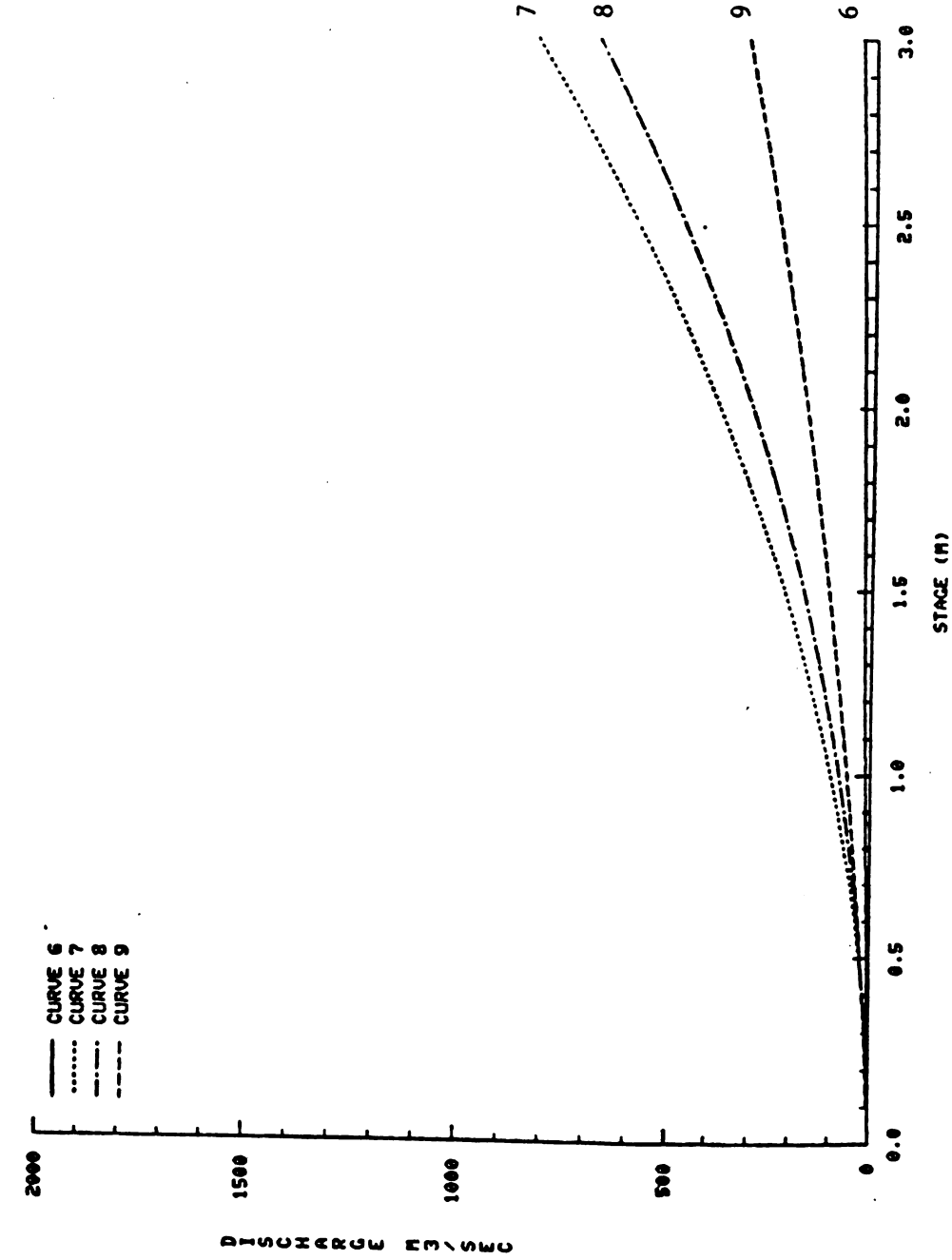

Figure 1.5.5 RATING CURVES FOR LA ESTRECHURA

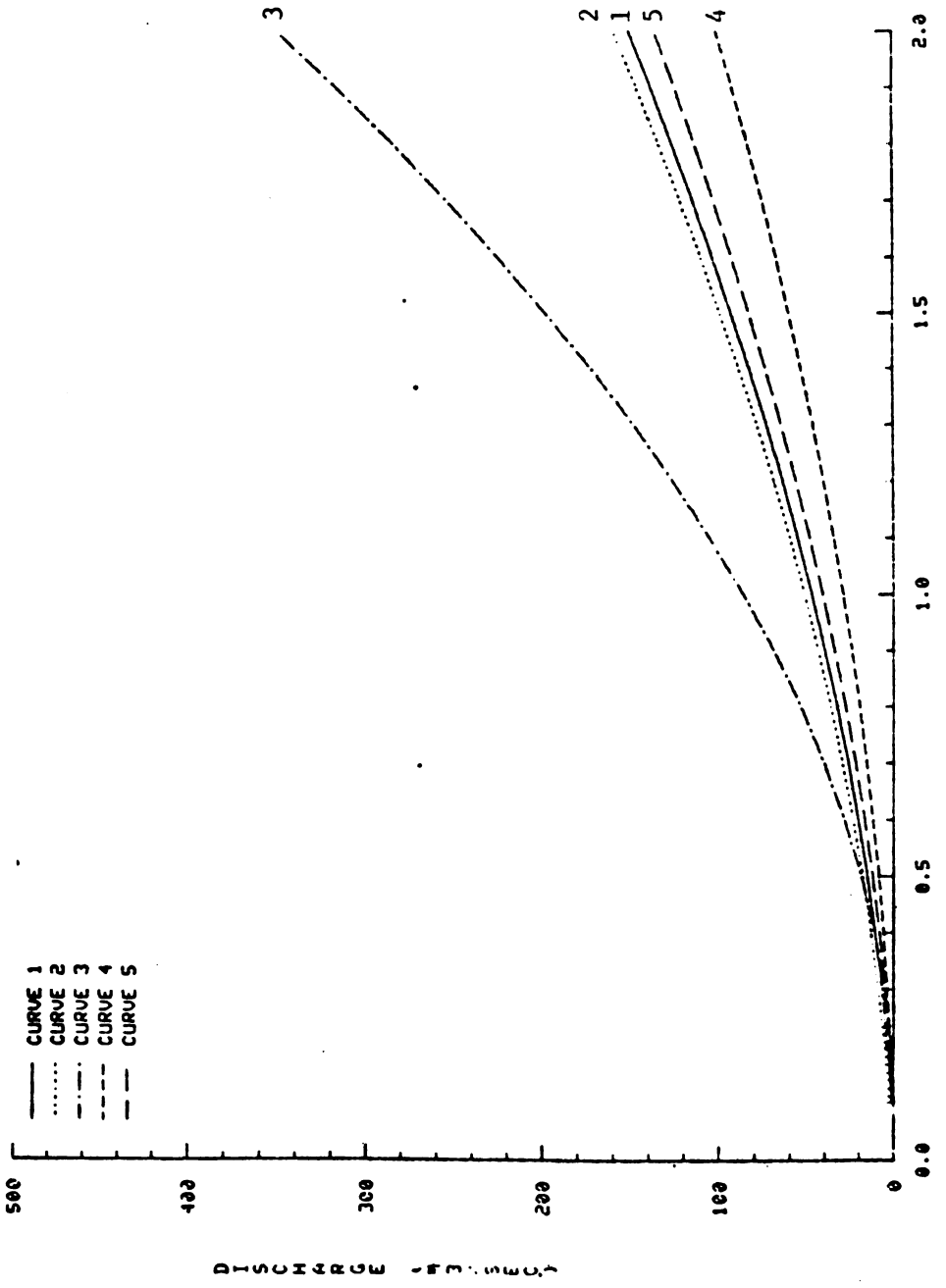

Figure 1.5.6 RATING CURVES FOR PALO DE CAJA

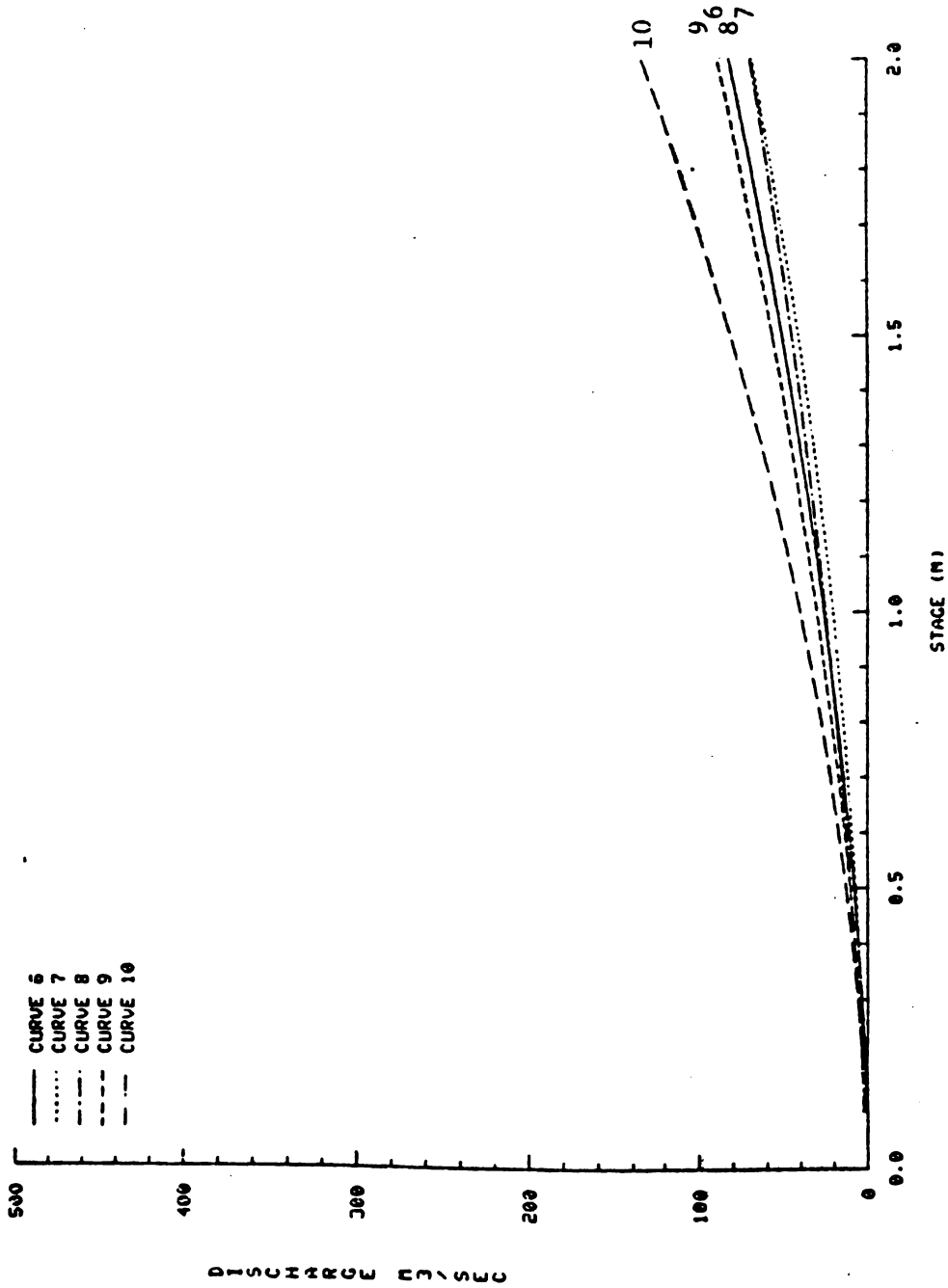

Figure 1.5.7 RATING CURVES FOR PALO DE CAJA

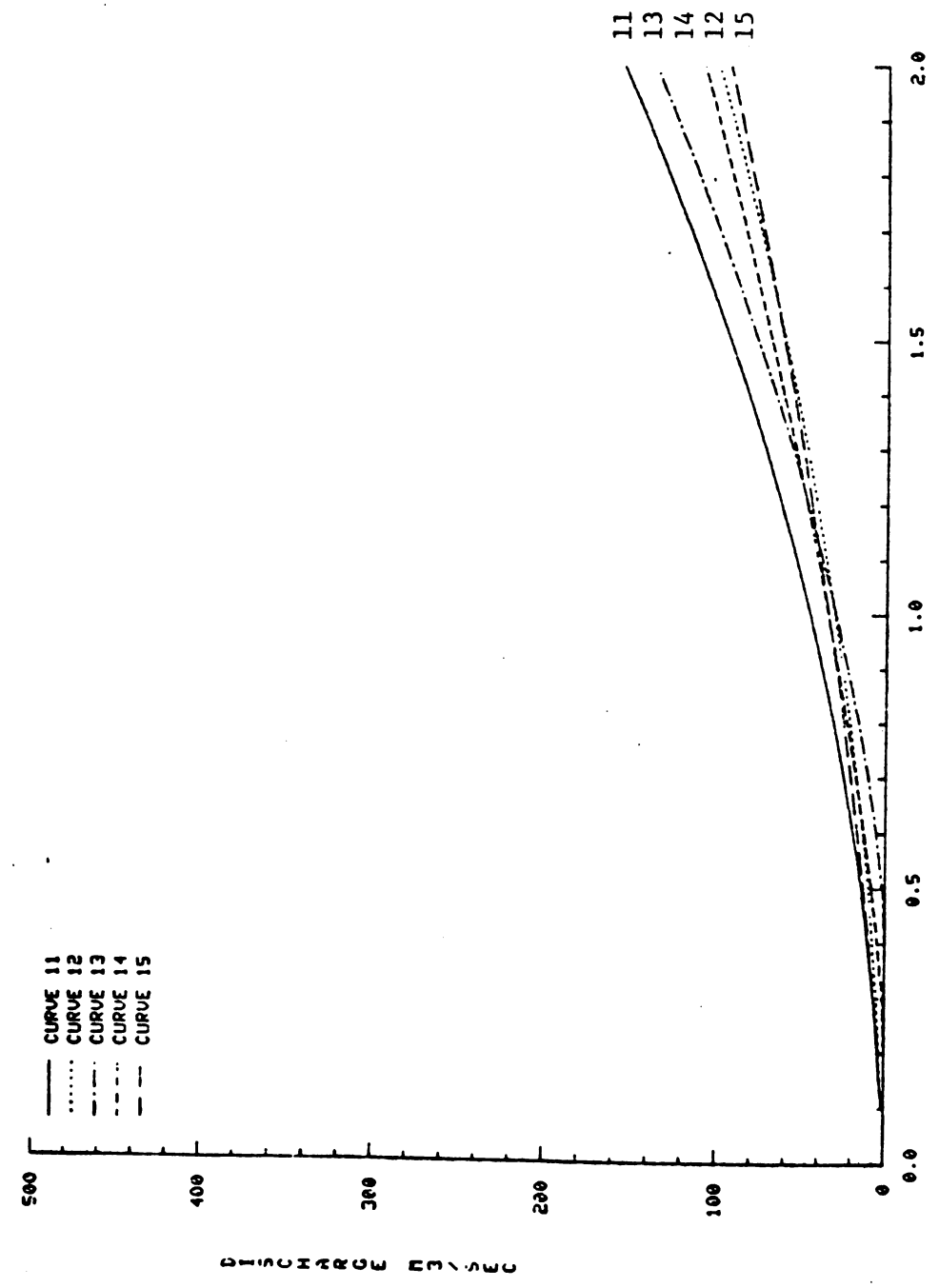

Figure 1.5.8 RATING CURVES FOR PALO DE CAJA

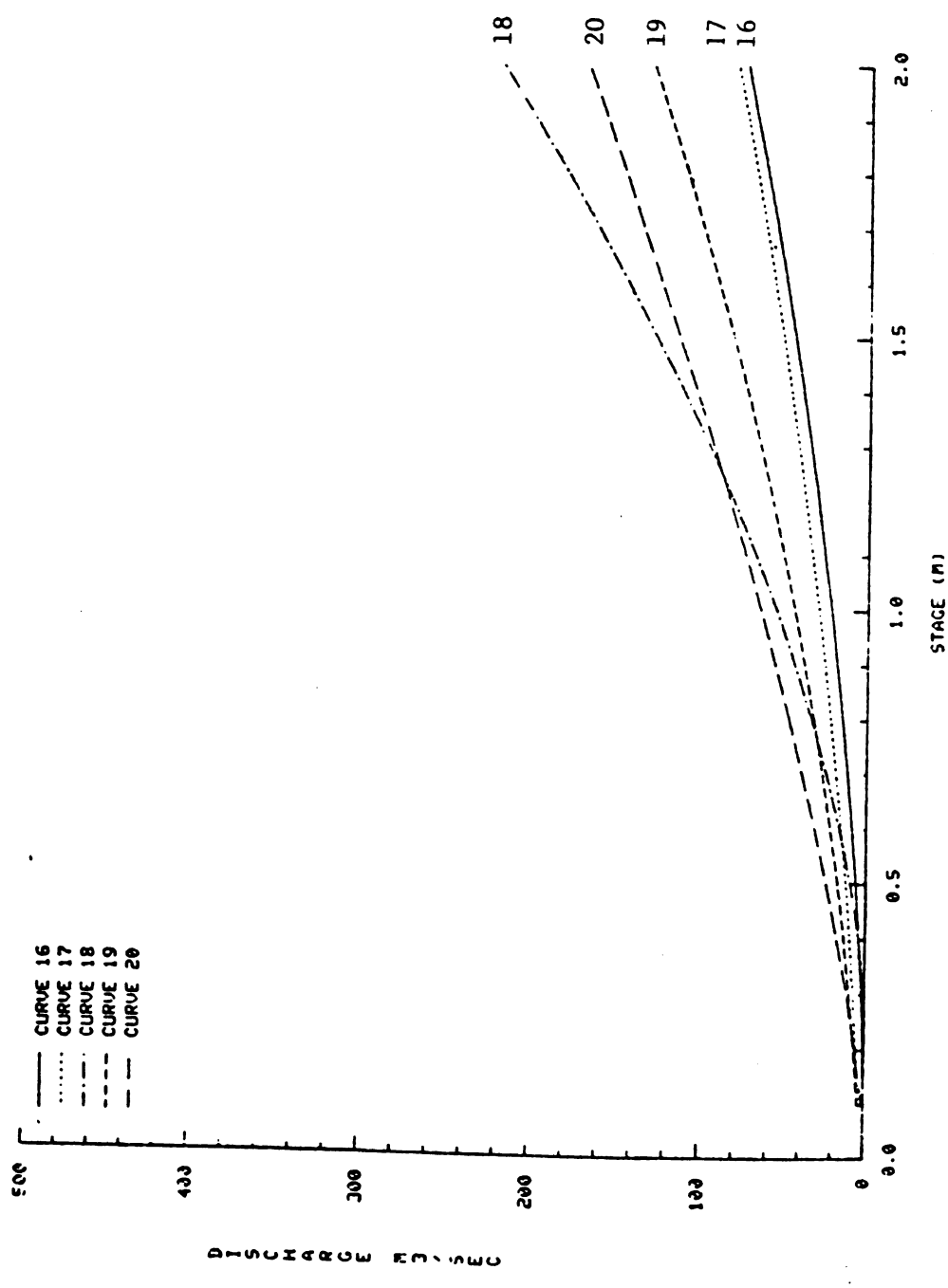

Figure 1.5.9 RATING CURVES FOR PALO DE CAJA

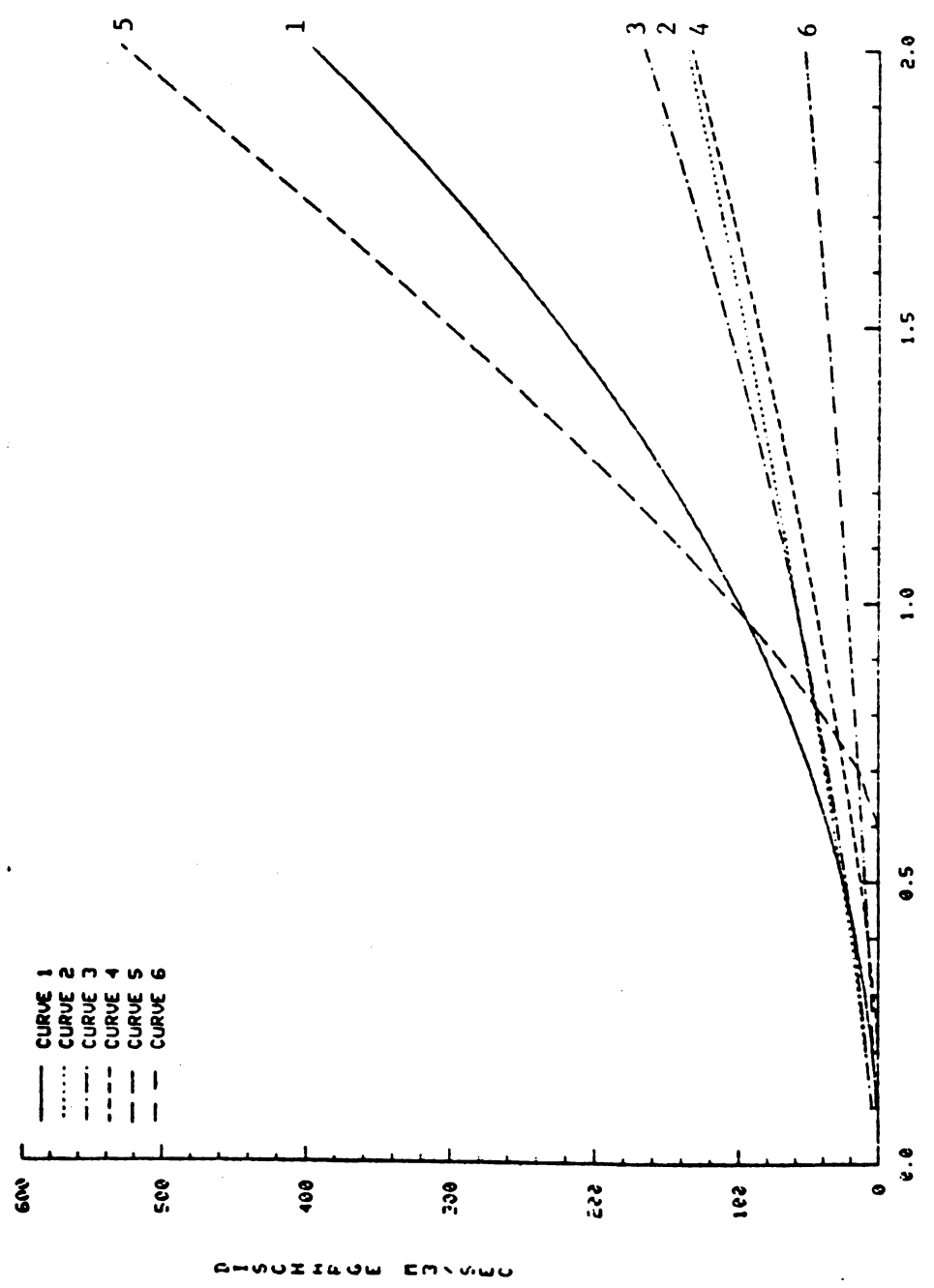

Figure 1.5.10 RATING CURVES FOR PASO DEL ERMITANO

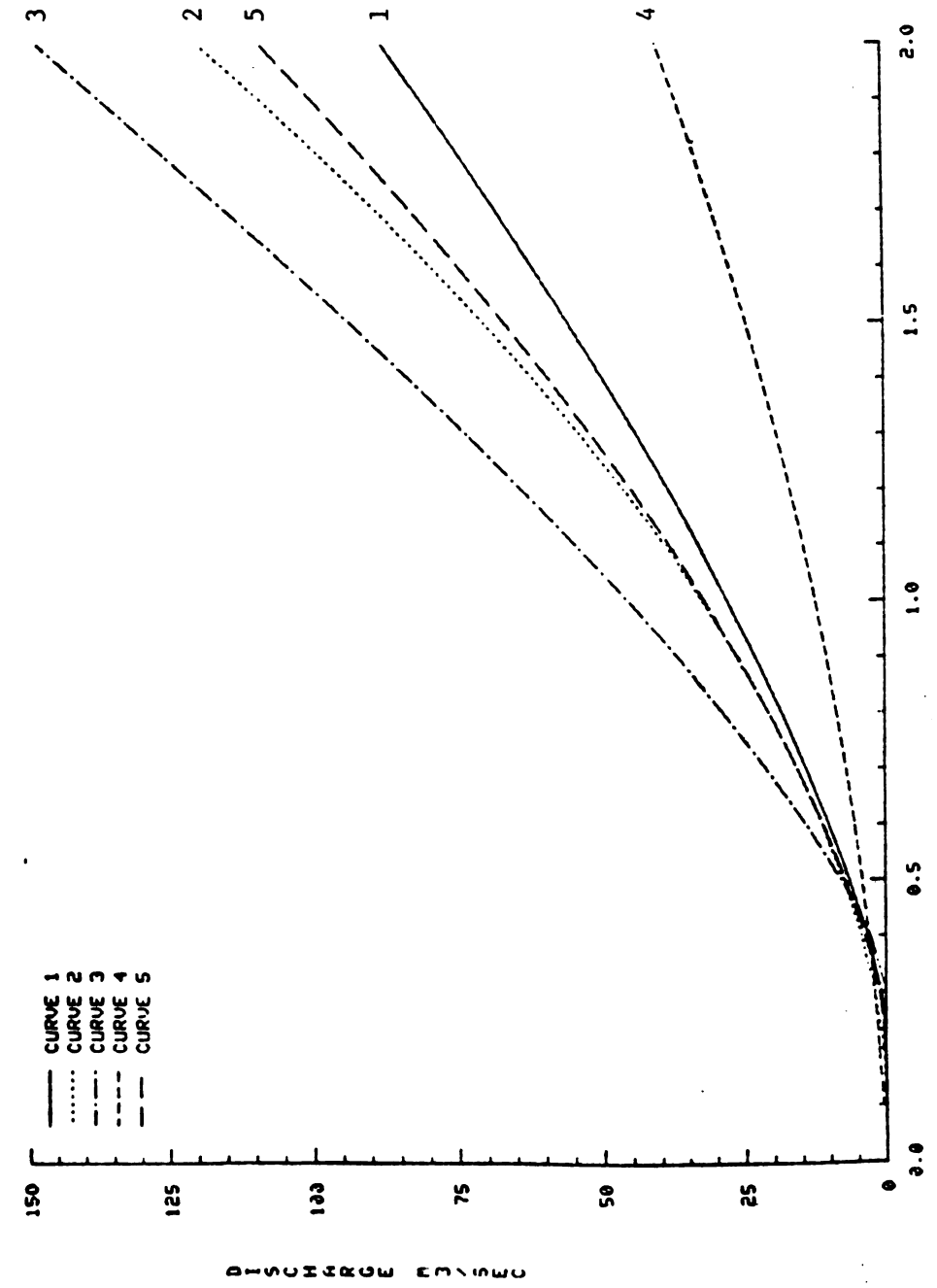

Figure 1.5.11 RATING CURVES FOR LA PENITA

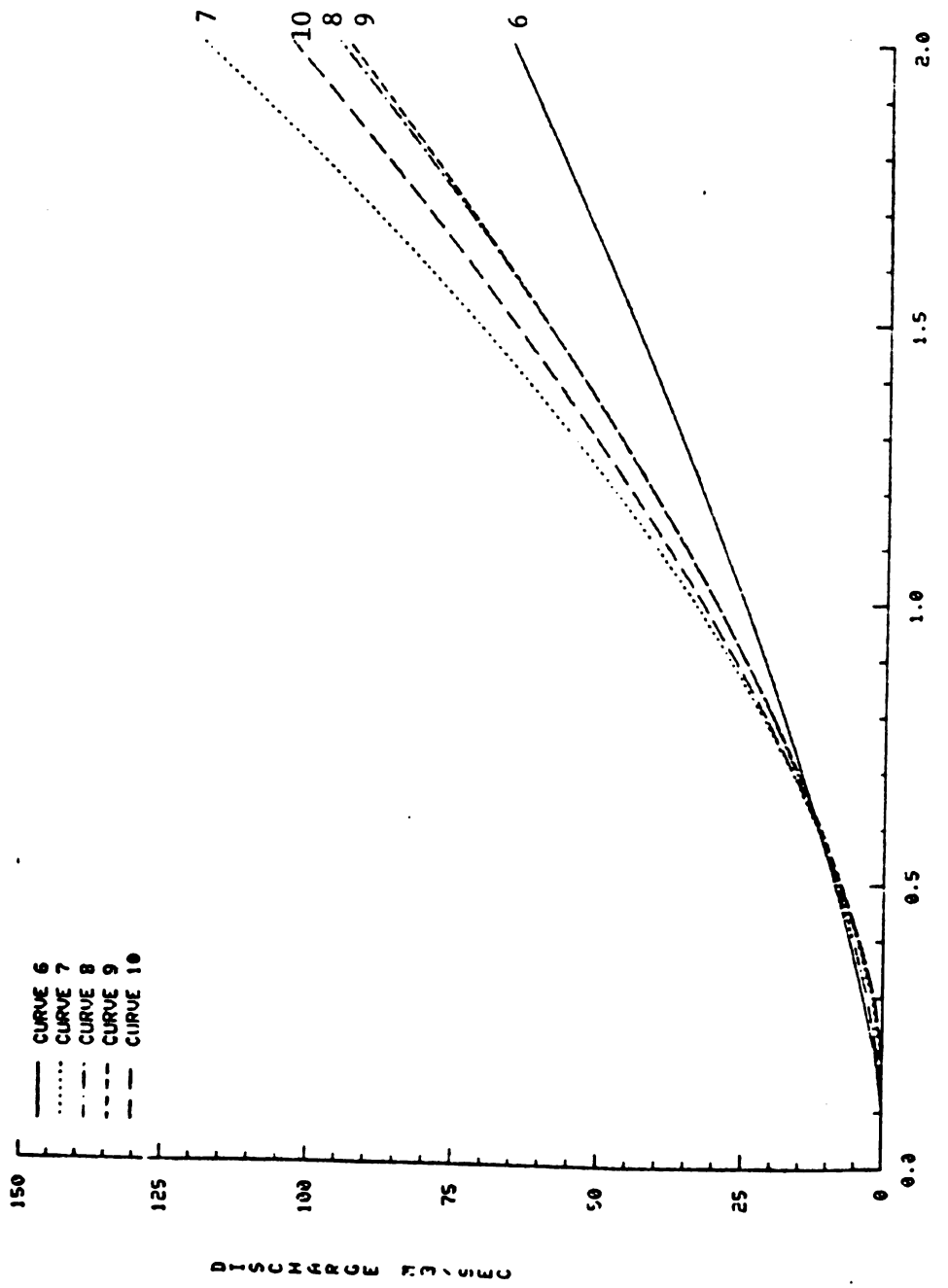

Figure 1.5.12 RATING CURVES FOR LA PENITA

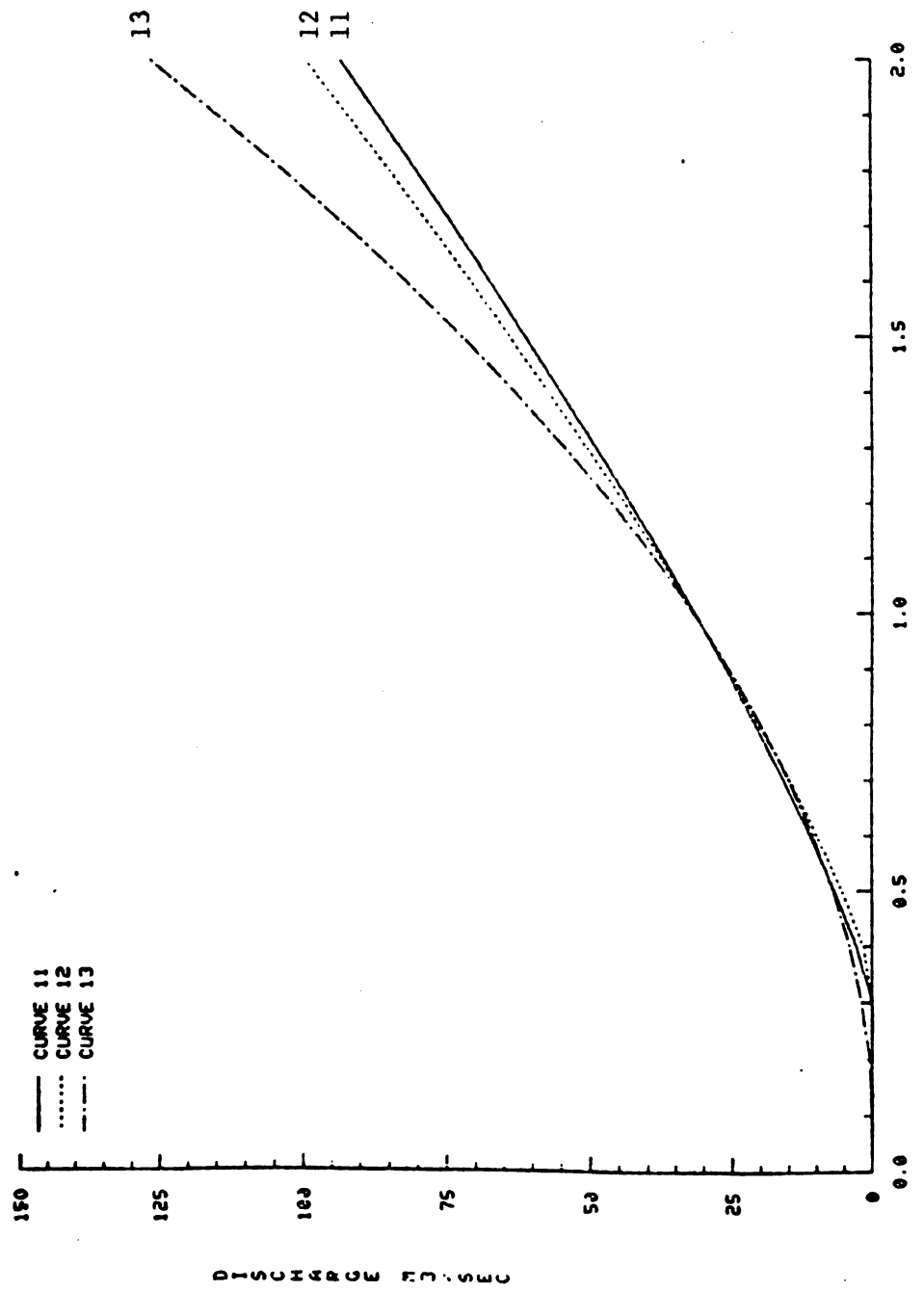

Figure 1.5.13 RATING CURVES FOR LA PENITA

1. August 1-13, 1980

2. May 6-20, 1981

3. April 10-20, 1983

4. September 13-14, 1985

5. October 23-26, 1985

For the two events in 1985, the data on operation of the spillway gates and turbines of Valdesia dam were also obtained. The two inflow hydrographs reconstructed using these data were found to be very valuable in rainfall-runoff model calibration.

1.5.5 Quality of Data

During the course of the study several obvious inconsistencies in rainfall and streamflow data were detected. The quality of data was of utmost concern since majority of modeling work to be carried out depended heavily on the accuracy of data. In general, it was felt that the entire data recording and processing procedures of INDRHI needs a careful review. Some specific problems are described below.

The first problem was encountered when the stage hourly data were transformed into discharges using the stage discharge relations provided by INDRHI. The curve numbers shown in Figures 1.5.4 to 1.5.13 refer to different equations corresponding to different time interval in which each is applicable. The equation parameters and dates are shown in Tables 1.5.6 to 1.5.11.

Very large differences are observed in some cases between consecutive curves; such is the case of curves 3 and 4 at La Penita, 5 and 6 at Paso del Ermitano, 4 and 5 at Estrechura and 3 and 4 at Palo De Caja. Curves 3 and 4 at La Penita are applicable at two consecutive periods with break point at May 22, 1977. This date coincides with

Table 1.5.6. Coefficients of rating curve equation $Q=C1(H+C2)^{C3}$ for La Estrechura gaging station provided by the counterparts.

```
**********************************************************************************
**                                                                              **
**      CLAVE IMPRESION DE-W9     POR USUARIO-MORILLO     15/03/85     12.28.11  **
**                                                                              **
**********************************************************************************
```

*** DATOS EXISTENTES EN EL ARCHIVO DE CURVAS DE CALIBRACION ***

ESTACION 204 TIPO Q1 CUENCA 38 NST 1

CUENCA NIZAO — ESTACION LA ESTRECHURA

CURVA NO.	DIA	MES	AÑO	C1	C2	C3	HP
1	30	1	69	46.60770	0.20490	2.93600	9.98
2	10	11	70	32.93860	0.21500	2.74770	9.98
3	17	12	72	42.82300	0.20500	2.30390	9.98
4	3	12	73	35.60100	0.30500	3.31600	9.98
5	4	8	74	41.45441	0.03500	1.76290	9.98
6	13	10	76	12.72110	0.02500	0.86770	-9.98
7	13	10	76	107.27660	-0.04500	1.87530	9.98
8	6	8	78	61.82739	0.11500	2.10210	9.98
9	1	9	79	48.12910	0.11500	1.65020	9.98
10	**	**	**	0.25098	0.25098	0.25098	0.25

OPCION PARA PROCEGUIR 00= SIGUIENTE PAGINA
-1= PAGINA ANTERIOR

Table 1.5.7. Coefficients of rating curve equation $Q=C1(H+C2)^{C3}$ for Palo de Caja (1956-1974) gaging station provided by the counterparts.

```
**********************************************************************************
**                                                                              **
**      CLAVE IMPRESION DE-W9     POR USUARIO-MORILLO     15/03/85     12.28.34  **
**                                                                              **
**********************************************************************************
```

*** DATOS EXISTENTES EN EL ARCHIVO DE CURVAS DE CALIBRACION ***

ESTACION 205 TIPO Q1 CUENCA 38 NST 2

CUENCA NIZAO — ESTACION PALO DE CAJA

CURVA NO.	DIA	MES	AÑO	C1	C2	C3	HP
1	11	9	56	44.91780	0.03000	1.70740	9.98
2	2	9	58	43.53909	0.10000	1.74770	9.98
3	18	8	67	105.76849	-0.10500	1.87140	9.98
4	11	9	67	28.67450	0.01000	1.80610	9.98
5	22	1	68	43.48500	-0.03500	1.68810	9.98
6	17	2	69	26.94740	-0.01500	1.63240	9.98
7	10	5	70	14.43730	0.20000	1.98760	9.98
8	10	12	72	18.54150	0.20000	1.68690	9.98
9	16	10	73	29.94270	0.01000	1.56390	9.98
10	29	6	74	33.79080	0.10000	1.87360	9.98

OPCION PARA PROCEGUIR 00= SIGUIENTE PAGINA
-1= PAGINA ANTERIOR

Table 1.5.7. Coefficients of rating curve equation $Q=C1(H+C2)^{C3}$ for Palo de Caja (1956-1974) gaging station provided by the counterparts.

```
**********************************************************************************
**                                                                              **
**      CLAVE IMPRESION DE-W9     POR USUARIO-MORILLO     15/03/85     12.28.34  **
**                                                                              **
**********************************************************************************
```

*** DATOS EXISTENTES EN EL ARCHIVO DE CURVAS DE CALIBRACION ***

ESTACION 205 TIPO Q1 CUENCA 38 NST 2

CUENCA NIZAO — ESTACION PALO DE CAJA

CURVA NO.	DIA	MES	AÑO	C1	C2	C3	HP
1	11	9	56	44.91780	0.03000	1.70740	9.98
2	2	9	58	43.53909	0.10000	1.74770	9.98
3	18	8	67	105.76849	-0.10500	1.87140	9.98
4	11	9	67	28.67450	0.01000	1.80610	9.98
5	22	1	68	43.48500	-0.03500	1.68810	9.98
6	17	2	69	26.94740	-0.01500	1.63240	9.98
7	10	5	70	14.43730	0.20000	1.98760	9.98
8	10	12	72	18.54150	0.20000	1.68690	9.98
9	16	10	73	29.94270	0.01000	1.56390	9.98
10	29	6	74	33.79080	0.10000	1.87360	9.98

OPCION PARA PROCEGUIR 00= SIGUIENTE PAGINA
-1= PAGINA ANTERIOR

Table 1.5.8. Coefficients of rating curve equation $Q=C1(H+C2)^{C3}$ for Palo de Caja (1974-1983) gaging station provided by the counterparts.

```
**********************************************************************************
**                                                                              **
**      CLAVE IMPRESION DE-W9     POR USUARIO-MORILLO     15/03/85     12.28.43  **
**                                                                              **
**********************************************************************************
```

*** DATOS EXISTENTES EN EL ARCHIVO DE CURVAS DE CALIBRACION ***

ESTACION 205 TIPO Q1 CUENCA 38 NST 2

CUENCA NIZAO — ESTACION PALO DE CAJA

CURVA NO.	DIA	MES	AÑO	C1	C2	C3	HP
11	5	8	74	38.39900	0.10000	1.88770	9.98
12	3	9	74	25.92999	0.10000	1.82850	9.98
13	23	10	74	67.16380	-0.40500	1.53280	9.98
14	7	11	75	50.38040	-0.23500	1.35860	9.98
15	11	10	76	33.19110	0.03000	1.46740	9.98
16	28	5	77	23.96001	-0.04500	1.71730	9.98
17	31	8	79	21.93730	0.20000	1.66120	9.98
18	26	3	81	89.56500	-0.25500	1.61390	9.98
19	10	2	82	32.25369	0.20000	1.77360	9.98
20	1	8	83	70.21440	-0.05500	1.32240	9.98

OPCION PARA PROCEGUIR 00= SIGUIENTE PAGINA
-1= PAGINA ANTERIOR

Table 1.5.9. Coefficients of rating curve equation $Q=C1(H+C2)^{C3}$ for Paso del Ermitano gaging station provided by the counterparts.

```
**********************************************************************************
**                                                                              **
**      CLAVE IMPRESION DE-W9     POR USUARIO-MORILLO     15/03/85     12.33.09  **
**                                                                              **
**********************************************************************************
```

*** DATOS EXISTENTES EN EL ARCHIVO DE CURVAS DE CALIBRACION ***
ESTACION 206 TIPO Q4 CUENCA 38 NST 3
CUENCA NIZAO ESTACION PASO DEL ERMITAÑO

CURVA NO.	DIA	MES	AÑO	C1	C2	C3	HP
1	7	8	68	99.45490	0.00500	1.99660	9.98
2	18	5	69	58.28030	0.01490	1.22850	9.98
3	14	1	71	49.65660	0.12490	1.61130	9.98
4	20	5	72	62.38860	-0.20490	1.30910	9.98
5	15	9	72	357.57153	-0.62490	1.25100	9.98
6	1	1	76	21.84320	0.02490	1.28920	9.98
7	**	**	**	0.25098	0.25098	0.25098	0.25
8	**	**	**	0.25098	0.25098	0.25098	0.25
9	**	**	**	0.25098	0.25098	0.25098	0.25
10	**	**	**	0.25098	0.25098	0.25098	0.25

OPCION PARA PROCEGUIR 00= SIGUIENTE PAGINA
-1= PAGINA ANTERIOR

Table 1.5.10. Coefficients of rating curve equation $Q=C1(H+C2)^{C3}$ for La Penita (1976-1978) gaging station provided by the counterparts.

```
**********************************************************************************
**                                                                              **
**      CLAVE IMPRESION DE-W9     POR USUARIO-MORILLO     15/03/85     12.33.40  **
**                                                                              **
**********************************************************************************
```

*** DATOS EXISTENTES EN EL ARCHIVO DE CURVAS DE CALIBRACION ***

ESTACION 211 TIPO Q1 CUENCA 38 NST 9

CUENCA NIZAO ESTACION LA PEÑITA

CURVA NO.	DIA	MES	AÑO	C1	C2	C3	HP
1	11	12	76	40.91248	-0.24500	1.35256	9.98
2	24	1	77	41.40970	-0.13500	1.69410	9.98
3	19	2	77	75.62613	-0.32500	1.29730	9.98
4	22	5	77	10.35230	0.10500	1.82360	9.98
5	4	8	77	45.90889	-0.21500	1.48397	9.98
6	15	8	77	29.06615	-0.10500	1.29024	9.98
7	2	5	78	44.39969	-0.15500	1.62325	9.98
8	20	5	78	36.22534	-0.11500	1.54355	9.98
9	23	6	78	41.52792	-0.20500	1.40991	9.98
10	6	8	78	45.83560	-0.21500	1.42376	9.98

OPCION PARA PROCEGUIR 00= SIGUIENTE PAGINA
-1= PAGINA ANTERIOR

Table 1.5.11. Coefficients of rating curve equation $Q=C1(H+C2)^{C3}$ for La Penita (1978-1980) gaging station provided by the counterparts.

```
**********************************************************************************
**                                                                              **
**       CLAVE IMPRESION DE-W9     POR USUARIO-MORILLO     15/03/85     12.33.51  **
**                                                                              **
**********************************************************************************
```

*** DATOS EXISTENTES EN EL ARCHIVO DE CURVAS DE CALIBRACION ***

ESTACION 211 TIPO Q1 CUENCA 38 NST 9

CUENCA NIZAO — ESTACION LA PEÑITA

CURVA NO.	DIA	MES	AÑO	C1	C2	C3	HP
11	10	9	78	49.14186	-0.30500	1.21599	9.98
12	2	10	78	53.32401	-0.34500	1.23592	9.98
13	1	1	80	39.71759	-0.11500	1.82813	9.98
14	0	0	0	0.00000	0.00000	0.00000	0.00
15	0	0	0	0.00000	0.00000	0.00000	0.00
16	0	0	0	0.00000	0.00000	0.00000	0.00
17	0	0	0	0.00000	0.00000	0.00000	0.00
18	0	0	0	0.00000	0.00000	0.00000	0.00
19	0	0	0	0.00000	0.00000	0.00000	0.00
20	0	0	0	0.00000	0.00000	0.00000	0.00

OPCION PARA PROCEGUIR — 00= SIGUIENTE PAGINA
-1= PAGINA ANTERIOR

the occurrence of a flood event and could mean that the flood wave modified the cross section at the station. But curve 4 gives discharges more than three times smaller than those obtained with curve 3, and that is very unlikely to be true. Usually a big flood causes scour which should increase discharges for a given level. The same case is present in curves 4 and 5 at La Estrechura, with break point at August 8, 1974, which coincides with another flood event in the record.

Once these problems were detected, the basic information on the stage-discharge data from which these curves were obtained were requested from INDRHI. When available, they were analyzed in conjunction with cross section data to come out with the new stage-discharge relations. While developing the new stage-discharge curves, some inconsistencies were found with the data. All of them are explained in Appendix 1.5.A dealing with the development of the new stage-discharge relations, but a special case will be pointed out here. In the data received for station El Ermitano, there are two stages measured on December 11, 1970. The values in the stage-discharge data give readings of 1.75 m and 1.93 m. However, the hydrograph data available for the same day shows that the maximum observed stage is only 1.55 m. The same case is observed on the data from December 14, 1970. Two stages 1.81 and 1.89 m are observed on that date, but the hydrograph data show a maximum of 1.43 m. On March 13, 1972 a stage of 0.47 m is observed while the recorded stage hydrograph shows a minimum of 0.64 m for that day.

Even after the new stage-discharge hydrographs were developed, some unrealistic situations still exist. For example, consider the three hydrographs corresponding to storm F (see Figure 1.7.4 in Section 1.7).

The basin area upstream El Ermitano is 800 km^2 and the basin area upstream Palo De Caja is 535 km^2. The volume under the hydrograph at El Ermitano is 123.2 MCM while at Palo De Caja is 28.5 MCM. This means that the subbasins downstream Palo De Caja, that is an area of 265 km^2, must contribute to the total flow with 94.7 MCM, or 357 mm of equivalent excess rainfall depth, but the observed total storm depths have a maximum of only 231 mm at station Valdesia.

From the 18 storms for which hourly streamflow data are available, only four storms were selected for model calibration. In many other cases the runoff appears before the rainfall stations start recording any data. In some others, the volume under the hydrograph at station Palo De Caja is larger than the one at La Penita, even though very significant precipitation was observed in the lower subbasins.

When the precipitation data used in the development of the DAD curves was compiled, several discrepancies between the hourly data and the daily data at the same station were detected. In many cases the hourly values added to values completely different from the daily ones.

The results of the HEC-1 calibration presented in Section 1.7 also point out some severe problems in the timing of the hydrographs. This was confirmed after checking the calibrated model with two hydrographs reconstructed from reservoir levels. In these two cases the timing seems to be correct, but in the cases of storms A, B, F, and M (Figures 1.7.2 through 1.7.5 in Section 1.7) sharp differences were observed in the timing of the hydrographs.

APPENDIX 1.5.A

Calibration of Stage-Discharge Curves

Reliable stage-discharge curves are essential tools to convert stage readings into flow discharges, since normally measured are only the variations of flow stages. Unfortunately the data used to correlate stage with flow discharge have been collected at low flows. Thus a great deal of effort was made to construct and extend stage-discharge curves for gaging stations at La Estrechura, Palo de Caja, La Penita and Ermitano. The procedures of developing these stage-discharge curves are described below:

Step 1: Number of curves to be used for each station:
After plotting all stage-discharge data on logarithm papers for each station, (see Figures 1.5.A.1 through 1.5.A.4) the number of curves to describe the stage-discharge relationship for each station were decided by visual inspection.

Step 2: Separation of the low and high stage data:

For each curve chosen in step 1, data were divided in two parts. The first part corresponds to stages lower than or equal to the stage of an expected break point which corresponds to the upper end of the low flow cross section. The second part includes stages higher than that of the above break point. For sake of illustration of the curve separation criterion a sketch is shown in Figure 1.5.A.5.

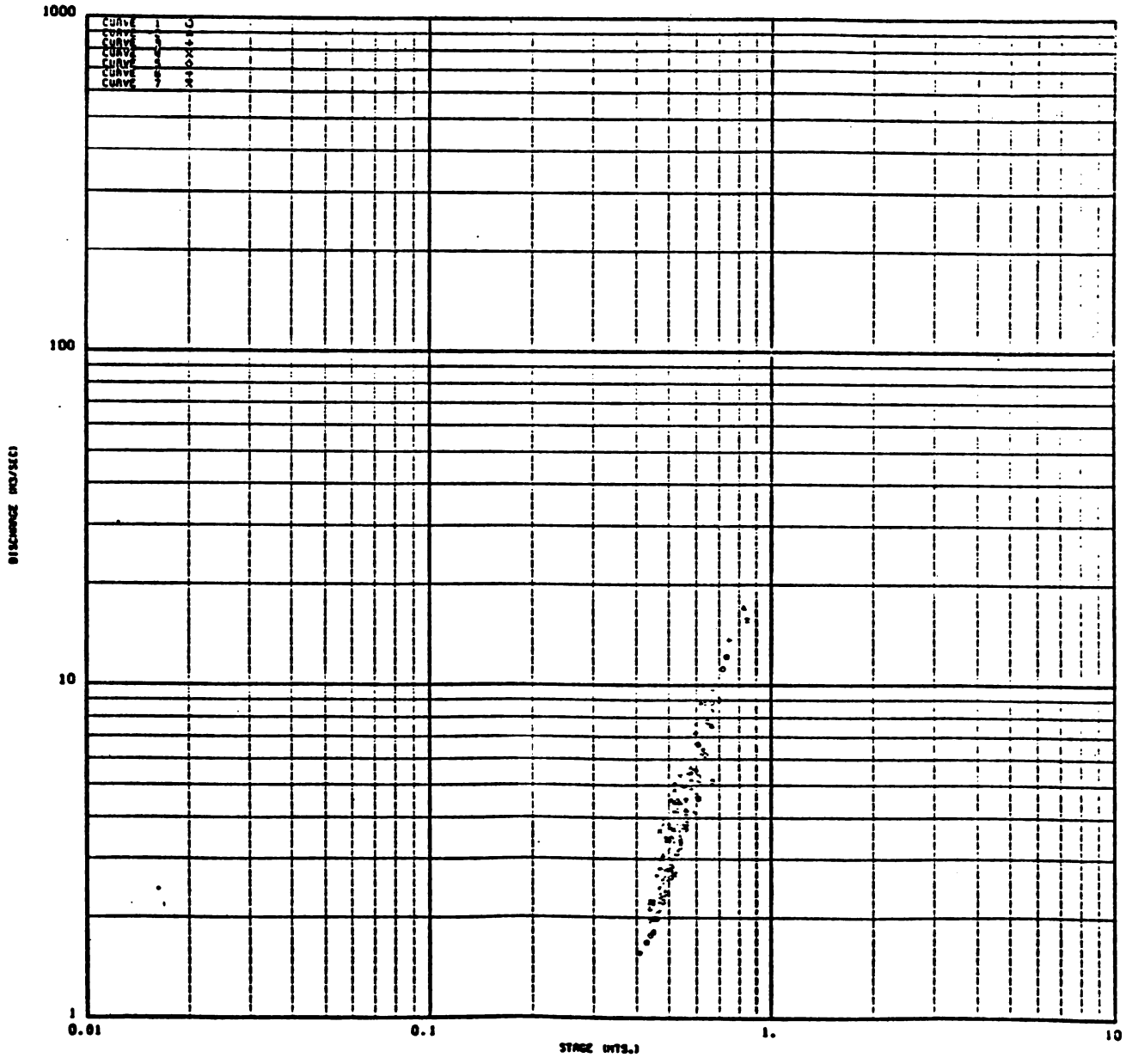

Figure 1.5.A.1. La Estrechura stage-discharge calibration points.

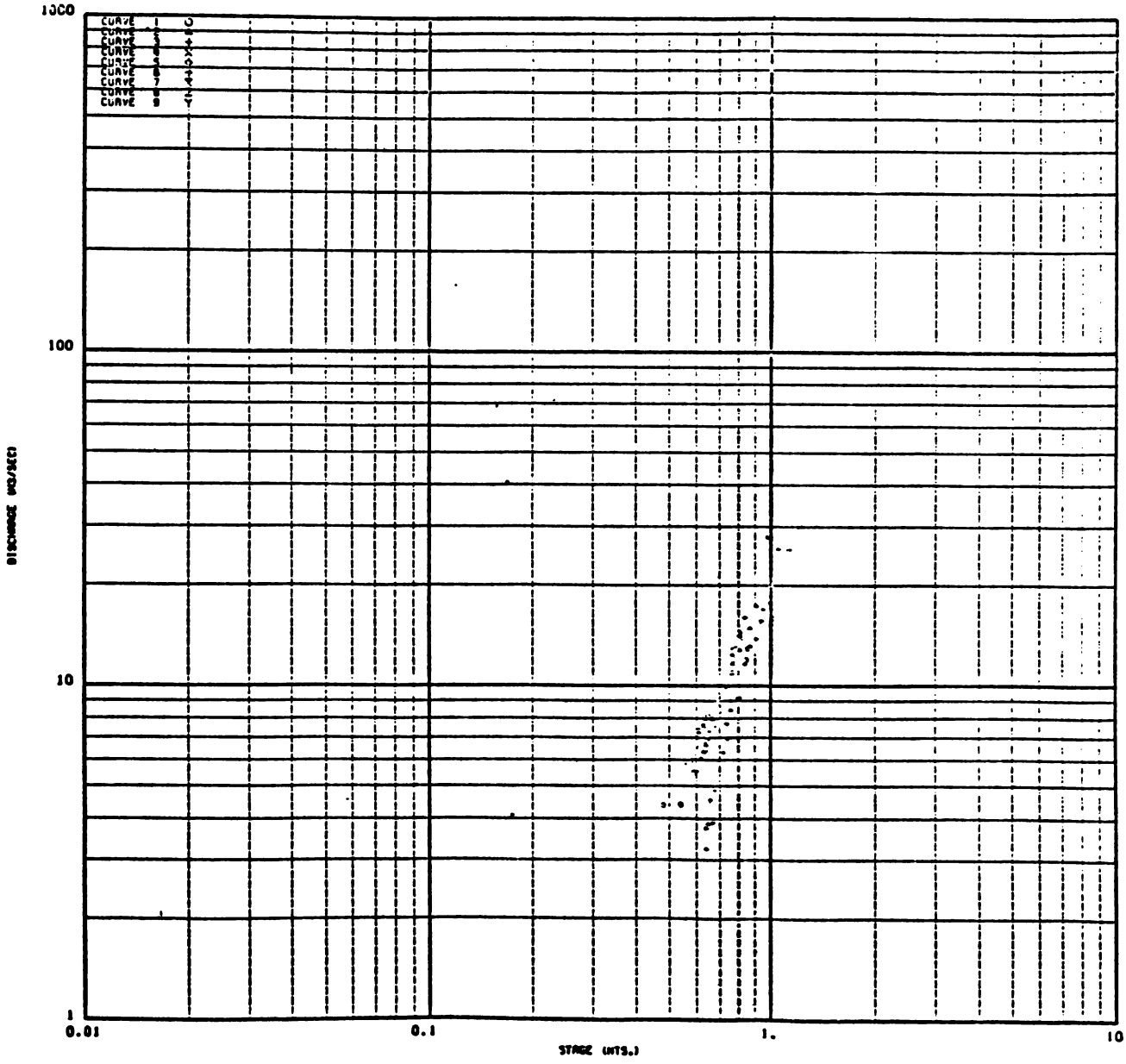

Figure 1.5.A.2. Palo de Caja stage-dishcarge calibration points.

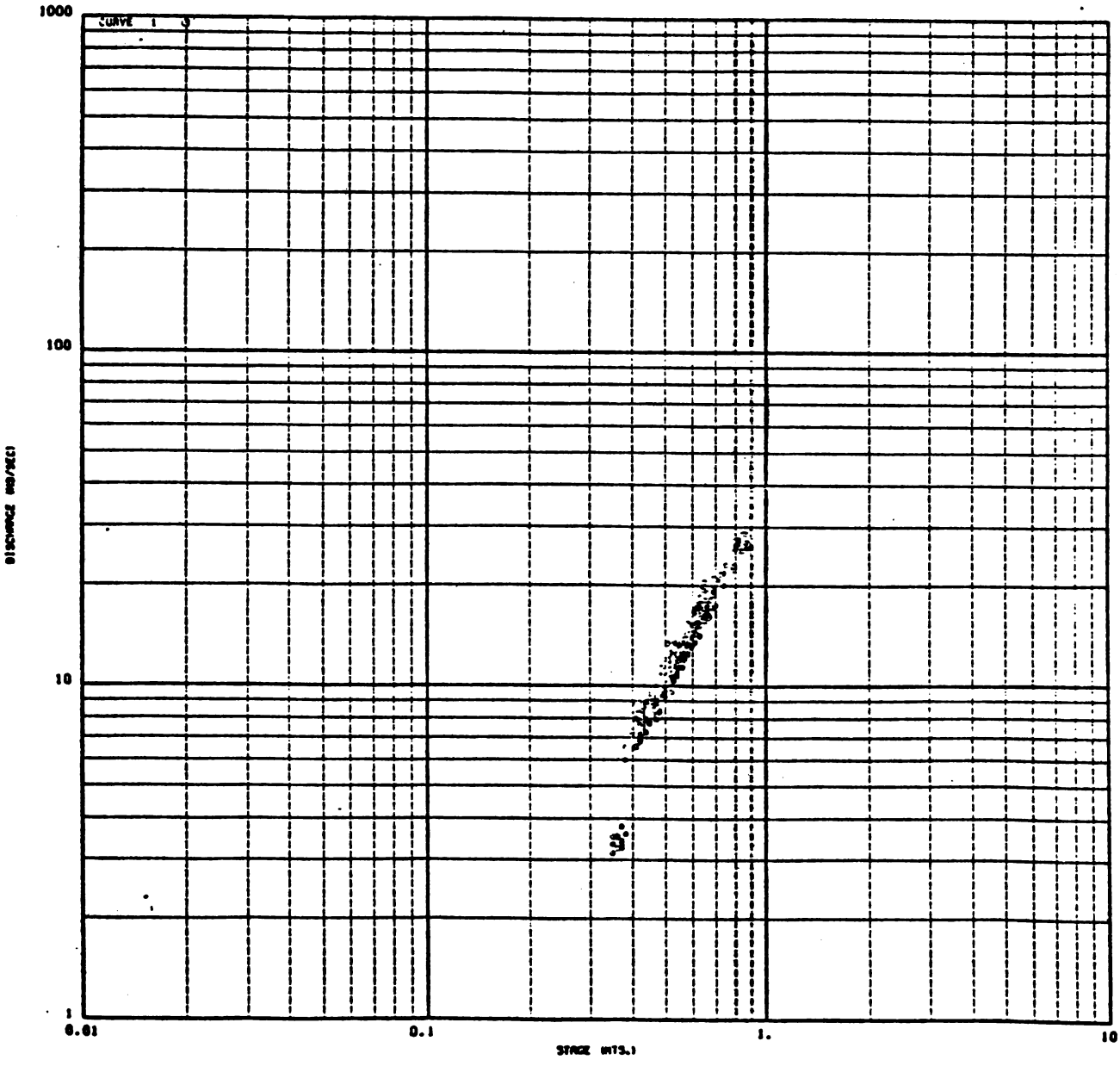

Figure 1.5.A.3. La Penita stage-discharge calibration points.

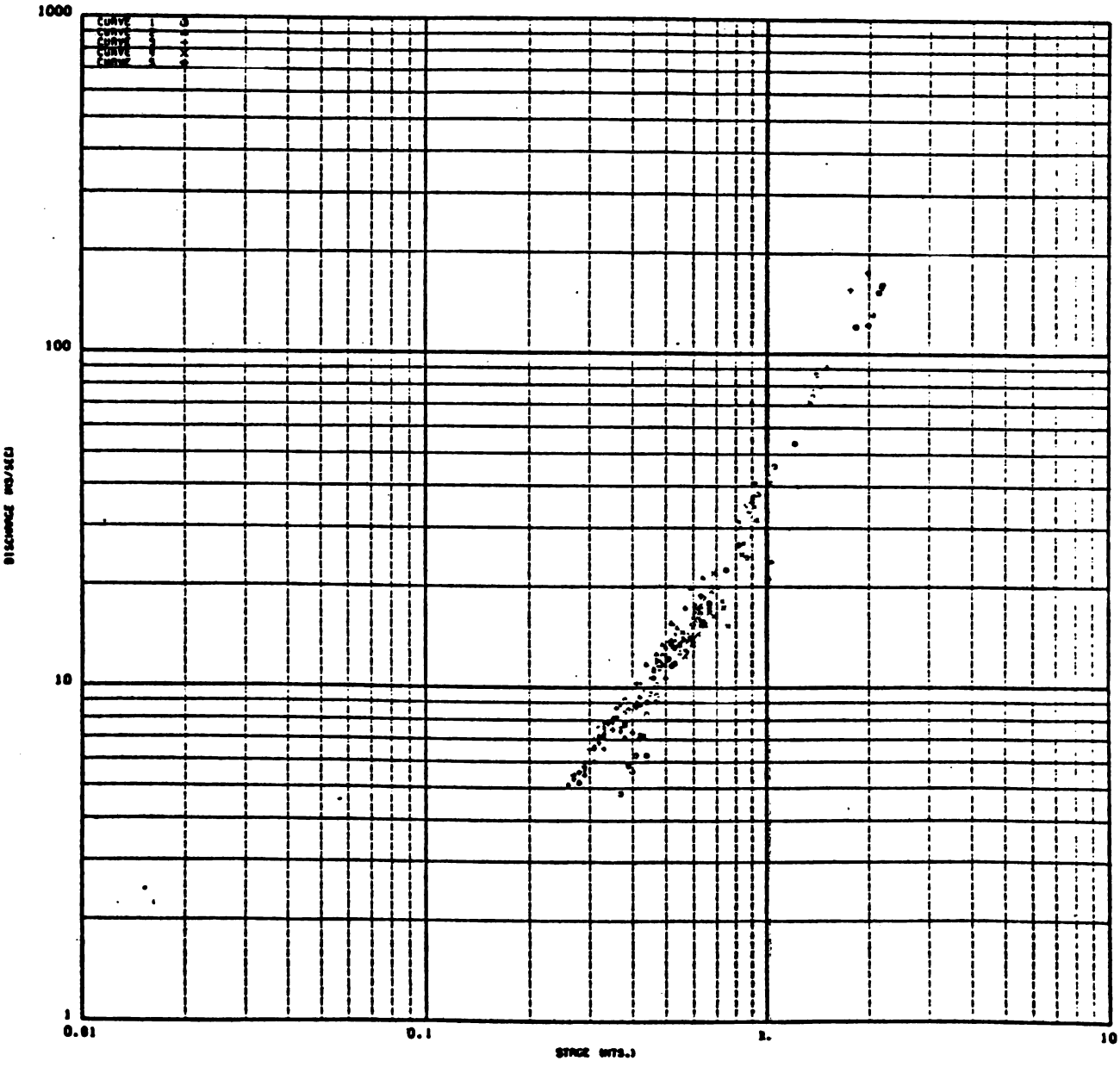

Figure 1.5.A.4. Paso del Ermitano stage-dishcarge calibration points.

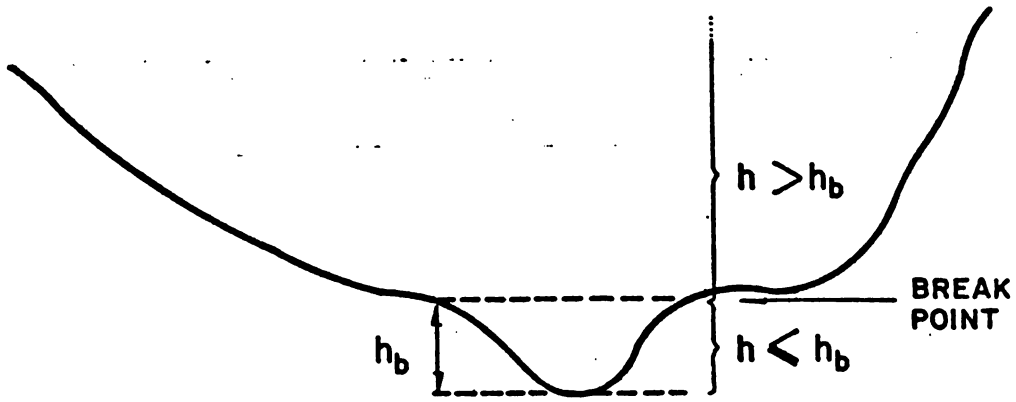

Figure 1.5.A.5 Possible gaging stations cross section shape.

Sometimes the data could not be separated into two parts because all the stages were either lower or higher than h_b. In such cases, only one curve was fitted to the data.

Since only those cross sections of May 1985 were available, a rough estimate of h_b was deduced from the shape of these cross sections.

Step 3: Development of the stage-discharge curves for low stages:

By using the stage and discharge data at low stages (as defined in step 2), and an optimization scheme of the polynomial function, the parameters of the stage-discharge relation were computed. This procedure is explained below:

Consider the stage-discharge relation:

$$Q = c(h + h_o)^m$$

The estimation of the parameters c, h_o and m is carried out by solving the following optimization problem:

$$\min \sum_{i=1}^{N} [Q_i - c_i(h_i - h_o)^m]^2$$

subject to:

$$0 < c \leq 500$$

$$h_{min} < h_o \leq 5.0$$

$$0.8 \leqslant m \leqslant 8.0 \text{ (see the footnote below)*}$$

where Q_i = observed discharge in m^3/s

h_i = observed gage height in m

N = number of observations.

The above constraints are based on the values found in the literature. The optimization problem is solved by using Rosenbrock Hillclimb procedure. Same procedure was used for all stages greater than h_b.

---

*Reference is made to Hydrometry: Principles and Practices, edited by R.W. Herschy, Page 416, John Wiley & Sons.

Step 4: Decision on the number of curves to be used for stages above h_b:

First, the discharges Q versus $(h+h_o)$ were plotted on a log-log paper, where h_o corresponds to the values obtained in step 3. If all points showed a tendency to scatter around a single straight line at high stages, only one curve was used. Otherwise several straight lines were used for each group of points.

Step 5: Development of stage-discharge curve for higher stages:

A single straight line at high stages, in the logarithmic plot of Q versus $(h+h_o)$ usually indicates that the upper part of the cross section $(h>h_b)$ can be considered as stable. In this case all the cross section rating curves will have the same parameters of the polynomial function except the value of h_o. Each of the rating curves will have its respective h_o.

More than one straight line at high stages, in the logarithmic plot of Q versus $(h+h_o)$ may be caused by a nonstable upper part of the cross section or a change of the site of the cross section.

Once the high stage-discharge curves are fitted, they may be used for purpose of extension. It should be stressed that the extension or extrapolation is valid only for the range of the observed hourly stages at a given station and storm.

Results

Some inconsistency has been detected in the stage-discharge data of La Estrechura, La Penita and Ermitano. The inconsistant or questionable data were either deleted or corrected.

All the stations, except La Penita, have shown an instability in the lower part of the cross section and a stability in the upper part of

the cross section. Therefore, more than one rating curve was used in the low stages and a single expression was used for the upper part of the Q versus $(h+h_o)$ logarithmic plot. The value of h_o differs from one rating curve to another. The actual break points between the upper curve and each of the low stage discharge curves are determined by simultaneous solution of both polynomial equations corresponding to each of the lower and the upper portion of the rating curve.

La Penita logarithmic plot of Q versus $(h+h_o)$ shows a single straight line for the whole range of data, except the inconsistant points which have been deleted. This indicates that a single control is effective for the complete range of discharge. The stability of La Penita station might be due to its location just upstream the Valdesia reservoir.

A detailed description of the above results are given below for each station.

La Estrechura

Inconsistant data: The reliability of data measured on 11-03-69 with h=0.36 m and a corresponding discharge of 5.14 m^3/s is doubtful. The error seems to be more related to an inadequate stage height reading rather than an inadequate measurement of the flow discharge.

Correction: Since there is no objective evidence regarding the origin of the error and since enough data was available to fit the observations of curve 1 (which includes the above questionable data), the above doubtful observation was deleted.

Fitting and extrapolation of the stage-discharge curves: After a close study of the data, seven rating curves were selected. Three of the latter have different polynomial expressions in each of their low

and high portion. The other four rating curves have a single polynomial expression.

Palo De Caja

Inconsistant data: None.

Fitting and extrapolation of the stage-discharge curves: Nine rating curves have been selected. Four of these curves have different polynomial expressions for low and high flows. The remaining five curves have one unique polynomial expression for all flows.

La Penita

Inconsistancy: Both the plot of Q versus h on arithmetic scale and the logarithmic plot of Q versus $(h+h_o)$ showed that the 14 data points observed for the time periods 03-03-77 to 03-15-77 were questionable. The latter doubtful data points would be due to inaccurate readings of the rate of revolution of the propeller-type meter. If the discharges corresponding to the above data are multiplied by 2, these 14 adjusted data points would join the same straight line as determined by all the other data. Next a logarithmic plot of Q versus $(h+h_o)$ was performed. Again the 392 data points (except the same 14 data points) defined a single curve. Fourteen questionable stage-discharge observations were discarded.

Fitting and extrapolation of the stage-discharge curve: Only one curve is used for the whole range of data since a plot of Q versus $(h+h_o)$ of the above 392 data points follow a single straight line.

Ermitano

Inconsistancy: After a comparison of the stages of the stage-discharge measurements with those of the hourly storms observations we

found that the stage-discharge data measured on the 12-11-70, the 12-14-70 and the 03-13-72 might be subject to inaccurate stage height reading. For the two rating curve measurements of the 12-11-70 the stages were set respectively to 1.75 and 1.89 m but, the maximum hourly stage observed during the same day was only 1.55 m. The same remark can be done for the 12-14-70 measurements where the maximum hourly observed stages is 1.43 m and the two stage-discharge data were set respectively to 1.81 m and 1.89 m. The 03-13-72 stage of the rating curve was 0.47 m, whereas the minimum hourly observed stage on the same day was 0.64 m. All the above five questionable stage discharge observations were deleted. A plot of Q versus $(h+h_o)$ has shown that the stage-discharge data measured from 05-22-72 to 05-24-72 were doubtful. The error might be due to incorrect rate of revolution of the propeller-type meter. It was decided to correct the above observation on account of the need for higher stage-discharge data in the period between 05-22-72 to 09-14-72.

Correction: The questionable stage-discharge data measured from 05-22-72 to 05-24-72 were corrected by dividing their corresponding discharges by 2.

Fitting and extrapolation of the stage-discharge curves: Five rating curves have been selected. One rating curve as a single polynomial expression for both low and high stages. Each of the other four curves has two polynomial expressions, one for the low portion and the other for the higher portion.

The polynomial parameters of all the rating curves, the date of validity, and some observations are shown in a tabular form for each station in Tables 1.5.A.1 through 1.5.A.4.

Table 1.5.A.1 Rating Curve Equations $Q = c(h + h_o)^m$ for La Estrechura

Station	Date	h_o in m	C	m	Stage in m	Observations
La Estrechura	10/20/67 to 7/15/70	0.31	38.75	3.51	h≥0.10	
	12/9/70 to 12/16/72	0.36	46.05	3.75	h≤0.13	
		0.36	38.75	3.51	h>0.13	
	1/12/73 to 11/15/73	0.30	38.75	3.51	h≥0.10	
	12/11/73 to 7/9/74	0.25	38.75	3.51	h≥0.15	
	8/10/74 to 10/8/76	0.34	56.66	4.30	h≤0.27	
		0.34	38.75	3.51	h>0.27	
	11/9/76 to 7/12/78	0.35	38.75	3.51	h≥0.05	
	8/23/78 to 3/7/79	0.45	40.20	4.11	h≤0.49	
		0.45	38.75	3.51	h>0.49	

Table 1.5.A.2 Rating Curves for Palo De Caja

Station	Date	h_o in m	C	m	Stage in m	Observations
Palo De Caja	6/22/71 to 9/12/73	0.26	20.26	2.20	h≥0.20	
	4/4/74 to 6/11/74	0.31	22.06	2.62	h≤0.50	
		0.31	20.26	2.20	h>0.50	
	7/5/74 to 7/29/74	0.44	19.29	3.49	h≤0.60	
		0.44	20.26	2.20	h≥0.60	
	8/6/74 to 8/30/74	0.22	20.26	2.20	h≥0.48	
	9/6/74 to 10/16/74	0.04	20.26	2.20	h≥0.60	
	10/28/74 to 10/22/75	0.27	38.39	5.35	h≤0.55	
		0.27	20.26	2.20	h≥0.55	
	2/26/76 to 9/17/76	0.30	19.80	2.11	h≤0.47	
		0.30	20.26	2.20	h>0.47	
	11/9/76 to 5/12/77	0.09	20.26	2.20	h≥0.50	
	6/23/77 to 3/22/79	0.33	20.26	2.20	h≥0.20	

Table 1.5.A.3 Rating Curves for La Penita

Station	Date	h_o in m	C	m	Stage in m	Observations
La Penita	11/30/76 to 8/9/79	-0.14	40.00	1.63	$h \geq 0.40$	The 14 points observed between 3/3/77 3/15/77 are deleted. This curve will be to get the observed hydrograph.
		-0.08	36.81	1.79	$h \geq 0.40$	The above 14 points are corrected by multiplying their discharges by 2.

Table 1.5.A.4 Rating Curves for Ermitano

Station	Date	h_o in m	C	m	Stage in m	Observations
Ermitano	8/27/68 to 12/14/70	0.25	42.42	1.999	$h \leq 0.80$	Curve 1.
		0.25	43.11	1.70	$h > 0.80$	The data corresponding to h=1.75, 1.93, 1.81, and 1.89 are deleted.
	1/14/71 to 5/16/72	-0.01	43.11	1.70	$h \geq 0.40$	The data corresponding to h = is deleted.
	5/22/72 to 9/14/72	0.30	20.73	2.98	$h \leq 1.47$	The discharge
		0.30	43.11	1.70	$h > 1.47$	corresponding to $h \geq 0.95$ are multiplied by 2.
	10/3/72 to 8/12/74	-0.22	20.86	1.48	$h \leq 0.25$	
		-0.22	43.11	1.70	$h > 0.25$	
	1/22/75 to 10/17/75	-0.07	43.11	1.70	$h > 0.50$	

1.6 DESIGN STORMS

1.6.1 Historic Storms

Analysis of critical historic storms is a prerequisite to the development of Depth-Area-Duration (DAD) curves which are required to develop hypothetical floods such as the standard project flood (SPF). The past records of hourly rainfall and daily runoff were examined to single out a critical storm for every year. A preliminary analysis of maximum 1-day, 2-day, and 3-day rainfall data at each station and the inspection of daily runoff plots allowed a rough determination of the dates of occurrence of the critical storms. The daily streamflow hydrographs were inspected to identify storms which caused major floods. The hourly precipitation records were also inspected to investigate the magnitude and spatial extent of storms. More than one critical storm were included for certain years. The initial selection included the rainfall due to hurricane David (August 30, 1979), and the tropical storm Frederic (September 5, 1979). Then a careful inspection of the hourly rainfall records at many gages enabled the selection of exact dates and times of occurrence of the storms which are to be analyzed further. Table 1.6.1 below presents the historic storms selected for further analysis. The mass curves of rainfall for these storms, are shown in Appendix 1.6.A.

1.6.2 Isohyetal Mapping

To derive the depth-area-duration curves, the first step is to analyze each storm for its isohyetal pattern. The isohyets are computed by a spatial interpolation technique known as multiquadric interpolation. In multiquadric interpolation, the influence of each sampling point is represented by quadric cones as a function of the

TABLE 1.6.1 HISTORIC STORMS SELECTED FOR ANALYSIS

	Beginning Date and Time				Ending Date and Time			
	Year	Month	Date	Hour	Year	Month	Date	Hour
1	1963	Oct.	1	20	1963	Oct.	5	5
2	1964	Aug.	6	8	1964	Aug.	7	3
3	1965	May	2	8	1965	May	5	8
4	1966	May	25	8	1966	May	27	8
5	1966	Sept.	28	20	1966	Sept.	30	8
6	1967	Sept.	10	8	1967	Sept.	13	8
7	1968	Aug.	8	8	1968	Aug.	10	8
8	1969	July	19	8	1969	July	20	8
9	1970	Aug.	22	8	1970	Aug.	23	8
10	1971	Feb.	19	8	1971	Feb.	21	8
11	1972	May	20	8	1972	May	23	8
12	1973	Oct.	14	8	1973	Oct.	21	8
13	1974	Aug.	30	8	1974	Aug.	31	8
14	1975	Sept.	16	8	1975	Sept.	18	8
15	1976	Oct.	10	8	1976	Oct.	12	8
16	1977	May	21	8	1977	May	24	8
17	1977	Dec.	28	8	1978	Jan.	1	8
18	1978	Aug.	3	8	1978	Aug.	6	8
19	1979	Aug.	30	8	1979	Sept.	2	8*
20	1979	Sept.	5	8	1979	Sept.	8	3**
21	1980	Aug.	4	8	1980	Aug.	7	8
22	1981	May	8	8	1981	May	11	8
23	1982	May	9	8	1982	May	13	8
24	1983	April	12	8	1983	April	13	8
25	1984	Aug.	1	8	1984	Aug.	3	8

*Hurricane David
**Tropical Storm Frederick

coordinates of these points. The estimate for a given point with coordinates (x_o, y_o) is thus obtained by the sum of the contributions from all those quadric cones. This is mathematically expressed as

$$h_o = \sum_{i=1}^{n} c_i d_{oi} \tag{1.6.1}$$

where h_o is an estimate of rainfall process at any point (x_o,y_o), c_i is the multiquadric coefficient of sampling point with coordinates (x_i,y_i), d_{oi} is the distance between point (x_o,y_o), and (x_i,y_i), and n is the number of sampling points. The distance d_{oi} is computed from the formula:

$$d_{oi} = \sqrt{(x_o - x_i)^2 + (y_o - y_i)^2} \tag{1.6.2}$$

The estimate h_o at any point (x_o,y_o) can be represented by a weighted linear combination of the observed values h_j at each sampling point (x_j,y_j) as

$$h_o = \sum_{j=1}^{n} w_j h_j \tag{1.6.3}$$

where w_j is the weight at sampling point j. To estimate the coefficients c_i and express Eq. (1.6.1) in terms of the weights as in Eq. (1.6.3), we do the following.

Let h_j of each sampling point (x_j,y_j) assume Eq. (2.1) as

$$h_j = \sum_{i=1}^{n} c_i d_{ji} \qquad \text{for } j = 1,2,\ldots,n$$

Then the coefficients c_i are determined by

$$c_i = \sum_{j=1}^{n} \delta_{ij} j_j \qquad \text{for } i = 1,2,\ldots,n \quad (1.6.4)$$

where δ_{ij} is an element of the inverse of the nxn interstation distance matrix with element d_{ji}, $j = 1,\ldots,n$ and $i=1,\ldots,n$. Substitution of Eq. (1.6.4) in Eq. (1.6.1) yields

$$h_o = \sum_{i=1}^{n} d_{oi} \sum_{j=1}^{n} \delta_{ij} h_j$$

or upon rearranging the numeration terms,

$$h_o = \sum_{j=1}^{n} [\sum_{i=1}^{n} \delta_{ij} d_{oi}] h_j$$

Thus, the interpolation equation (1.6.3) has weights

$$w_j = \sum_{i=1}^{n} \delta_{ij} d_{oi} \qquad \text{for } j = 1,\ldots,n \quad (1.6.5)$$

For this study, Eqs. (1.6.3) and (1.6.5) are used to compute the isohyetal pattern of each storm at any point (x_o,y_o) in the study area using the data h_j at each sampling point (x_j,y_j) available from j=1,...,n stations.

A microcomputer version of a precipitation data analysis program which contains the above procedure as an optionis included in the accompanying users manual on the software package Colorado State

University Hydrologic Modeling Systems (CSU-HMS) prepared for the project.

From the previous explanation it is noted that rainfall interpolates at any point in the basin area of interest are solely function of the distances between such point and the observation points (rainfall stations) available in the area. By virtue of this method, rainfall pattern anomalies due to orographic effects or bias in rainfall information due to topography are not accounted for in the interpolation. The Hydrology Group at INDRHI strongly suggested that perhaps such rainfall pattern anomalies should be considered in the derivation of the isohyetal patterns. In this connection, two approaches are tried which are briefly described below.

First is the adoption of the precipitation weighing method given by the U.S. Corps of Engineers in the HEC-1 Flood Hydrograph Package which was likewise suggested by the INDHRI Hydrology Group. This method is based on the weighting equation given by

$$h_o = h_{B_o} \frac{\sum_{j=1}^{n} h_j w_j}{\sum_{j=1}^{n} \bar{h}_j w_j} \qquad (1.6.6)$$

where h_o is the rainfall interpolate at any point in the area, h_{B_o} is the interpolated (using optimal interpolation) normal annual precipitation at any point in the area, h_j is the total storm precipitation at sampling station j and $\bar{h}_j$ is the jth station normal annual precipitation. The weight w_j of station j can likewise be obtained using the multiquadric interpolation technique such that

$$w_j = \sum_{i=1}^{n} \delta_{ij} d_{oi} \qquad \text{for } j=1,\ldots,n \qquad (1.6.7)$$

where d_{oi} is the distance between the point with coordinates (x_o, y_o) and jth station point with coordinates (x_j, y_j), and δ_{ij} is an element of the inverse of an n x n interstation distance matrix with elements d_{ij}, j=1,...,n rows and i=1,...,n columns.

As indicated by the U.S. Corps of Engineers, the above approach could correct rainfall estimation bias associated to elevation effects which is accounted for by the station normal annual precipitation term $\bar{h}_j$. However, this claim may be rather dubious since the elevation is not explicitly parameterized in the weighting scheme and that any adjustments for bias affected by incorporating either or both terms h_B and $\bar{h}_j$ can be associated to rainfall anomalies other than elevation effects.

In view of this, the second approach tried accounts for orographic effects which explicitly parameterized the basin elevation. This approach is based on representing the rainfall by a polynomial function written as

$$h_o = a_o + \sum_{k=1}^{m} a_k E_o^k + H_o \qquad (1.6.8)$$

where h_o is the rainfall estimate at any point (x_o, y_o), the a's are polynomial coefficients, E_o is the elevation at point (x_o, y_o) and H_o is the elevation-free rainfall values. Similarly, the observed rainfall values at the available station points can be represented as in the above equation as

$$h_j = a_o + \sum_{j=1}^{n} a_k E_j + H_j \qquad (1.6.9)$$

where w_j is the jth station weight obtained by the multiquadric interpolation technique. Finally, the rainfall interpolate in the actual domain can be obtained using Equation (1.6.8) given the elevation E_o.

Note that an elevation map is required in the above approach for interpolating over an area. The multiquadric interpolation technique is used also to derive the elevation map for the basin.

The two approaches above were tried in this study followed by developing a new set of depth-area-duration (DAD) curves. A comparison was made using the two approaches as well as the previously obtained DAD curves based on rainfall isohyetal patterns without considering orographic effects.

From results obtained, it is found that using the second approach in which the elevation of the basing is explicitly parameterized gave the most reasonable and constant rainfall isohyetal pattern. The elevation map required in this approach on multiquadric interpolation is based on more than 200 elevation data points. A first-order polynomial is found sufficient to represent the rainfall-elevation anomaly function such that m=1 in Equation (1.6.8).

1.6.3 Development of Depth-Area-Duration (DAD) Curves

Given the rainfall isohyetal patterns described in the previous section and the Mass Curves shown in Appendix 1.6.A, the procedure to develop the Depth-Area-Duration curves can be summarized as follows.

First, define class intervals based on the observed range of precipitation depths. Based on the 25 storms selected (see Table 1.6.1)

the range is taken as 0 to 625 mm. Twenty five classes of class widths 25 mm each (i.e., class 1 is defined as 600-625, class 2 as 575-600, etc.) were selected. From the derived isohyetal pattern map of a given storm, the total area and average depth for each class are computed using the following equations:

$$A_i = \Delta A \sum_{j-1}^{NG} I_j \tag{1.6.10}$$

and

$$D_i = \frac{\sum_{j-1}^{NG} d_j I_j}{\sum_{j-1}^{NG} I_j} \tag{1.6.11}$$

where:

A_i = area corresponding to class interval i

ΔA = unit area of one grid point

NG = total number of grids

D_i = average depth of class interval i

d_j = depth at grid point j

I_j = $\begin{cases} 1 \text{ if } L_i \leq d_j < U_i \\ 0 \text{ otherwise} \end{cases}$

L_i = lower class limit of class i

U_i = upper class limit of class i

After obtaining the area and average depth corresponding to each class interval cumulative areas and corresponding average depths were computed using the following equations:

$$AC_i = \sum_{j-1}^{i} A_j \tag{1.6.12}$$

$$DC_i = \frac{\sum_{j=1}^{i} A_j D_j}{AC_i} \qquad (1.6.12)$$

where

AC_i = cumulative area of classes greater than or equal to class i

DC_i = weighted average depth corresponding to classes greater than or equal to class i.

Note that the cumulative areas and average depths computed above correspond to what is referred to as "extended class" where each extended class always has an upper limit of 625 mm and a lower limit equal to the lower class limit of class i defined earlier.

The above defines the Depth-Area curve for the total duration of the given storm. Now, the Depth-Area curves for shorter durations are derived by using mass curves of rainfall. To do this, one has to compute the weights that will be used in obtaining an average mass curve for each class interval.

The weight given to each recording station vary according to the distribution of the area assigned to a certain class interval. Since it is known which grid points belong to each class interval, one can compute the distance between a point and the recording stations and determine the closest one. Then, the fraction of the total area assigned to each station can be counted and the weights can be computed using the equation below.

$$W_i(k) = \frac{\sum_{j=1}^{NG} S_j(k)}{\sum_{j=1}^{NG} I_j} \qquad (1.6.14)$$

where

$W_i(k)$ = Weight assigned to station k in class interval i

$S_j(k) = \begin{cases} 1 \text{ if } L_i \leq d_j < U_i \text{ and k is the nearest station to grid point i} \\ 0 \text{ otherwise} \end{cases}$

The cumulative weights corresponding to each extended class is computed by using the equation.

$$WC_i = \frac{\sum_{j=1}^{i} W_j(k)A_j}{AC_i} \qquad (1.6.15)$$

Using the cumulative weights an average mass curve for each cumulative class is computed. From this average mass curve one obtains the maximum precipitation recorded at different durations and compute the fraction of the total storm depth for each duration. These fractions are multiplied by the depth at the corresponding class interval to obtain the depths for different storm durations. The procedure is repeated for all the extended classes. The individual DAD curves for the 25 selected storms as well as the enveloping curves obtained by picking the maximum observed depth for each area and duration are included in Appendix 1.6.B.

As explained in the previous section, two methods were tried to account for topographic effects in the rainfall interpolation program. The results from both trials were used to derive two new sets of DAD curves. The performance of the two methods were judged based on the comparison of the isohyetal patterns with those obtained without considering the topographic effects as well as by observing the DAD curves obtained with each method. Based on these it was decided that

parameterizing the elevation in the interpolation function gave the most realistic results.

Before obtaining the enveloping DAD curve from the individual curves computed with the selected method, the 25 storms used were divided into two groups: (a) hurricane and (b) non-hurricane. Table 1.6.2 shows this classification. Then the "hurricane" DAD curves and the "non-hurricane" DAD curves were derived from the corresponding groups. Based on these, a third set of curves that represent the worst conditions observed in the basin was derived. The "hurricane", "non-hurricane", and "enveloping" DAD curves are shown in Figures 1.6.1 to 1.6.3.

1.6.4 Standard Project Storm (SPS)

From the three sets of DAD curves shown in Figures 1.6.1 through 1.6.3, the standard project storms corresponding to duration of 24 hours and 48 hours for an area of 820 sq. km. (Nizao basin upstream of Valdesia dam) were derived. The total precipitation magnitudes of these standard projects storms are given in Table 1.6.3.

It is seen that precipitation magnitude corresponding to hurricane conditions is almost twice as big as the corresponding depth for non-hurricane conditions from the same storm duration.

1.6.5 Temporal Distribution of SPS

During the course of the study two different criteria have been used for temporal distribution of the total precipitation magnitudes reported in Table 1.6.3. First approach is to select two critical patterns from the 25 historic storms selected for detailed analysis in the derivation of DAD curves. Specifically, the temporal distributions corresponding to hurricane David and tropical storm Frederick were

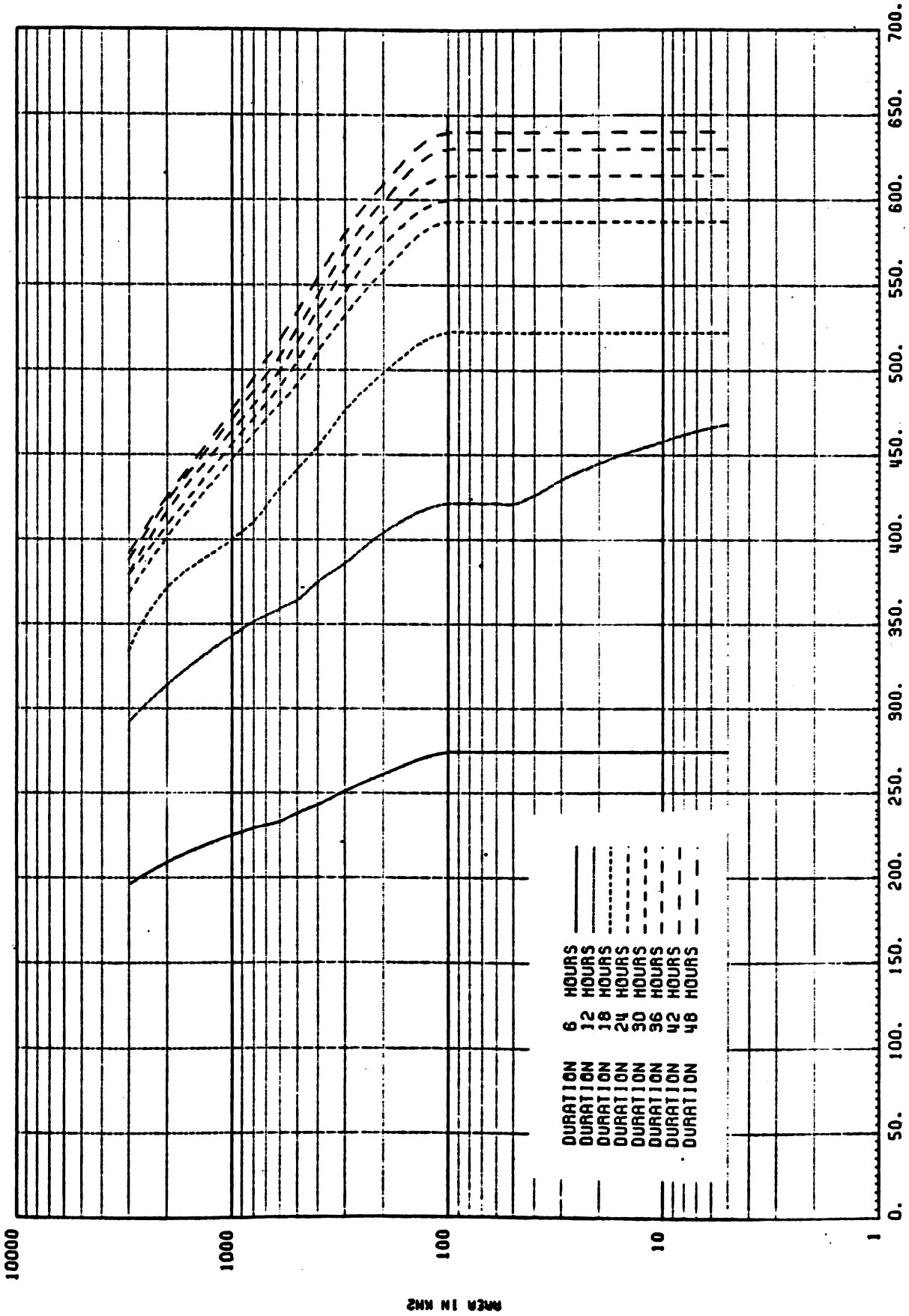

Figure 1.6.1. Hurricane depth-area-duration curves for Nizao basin.

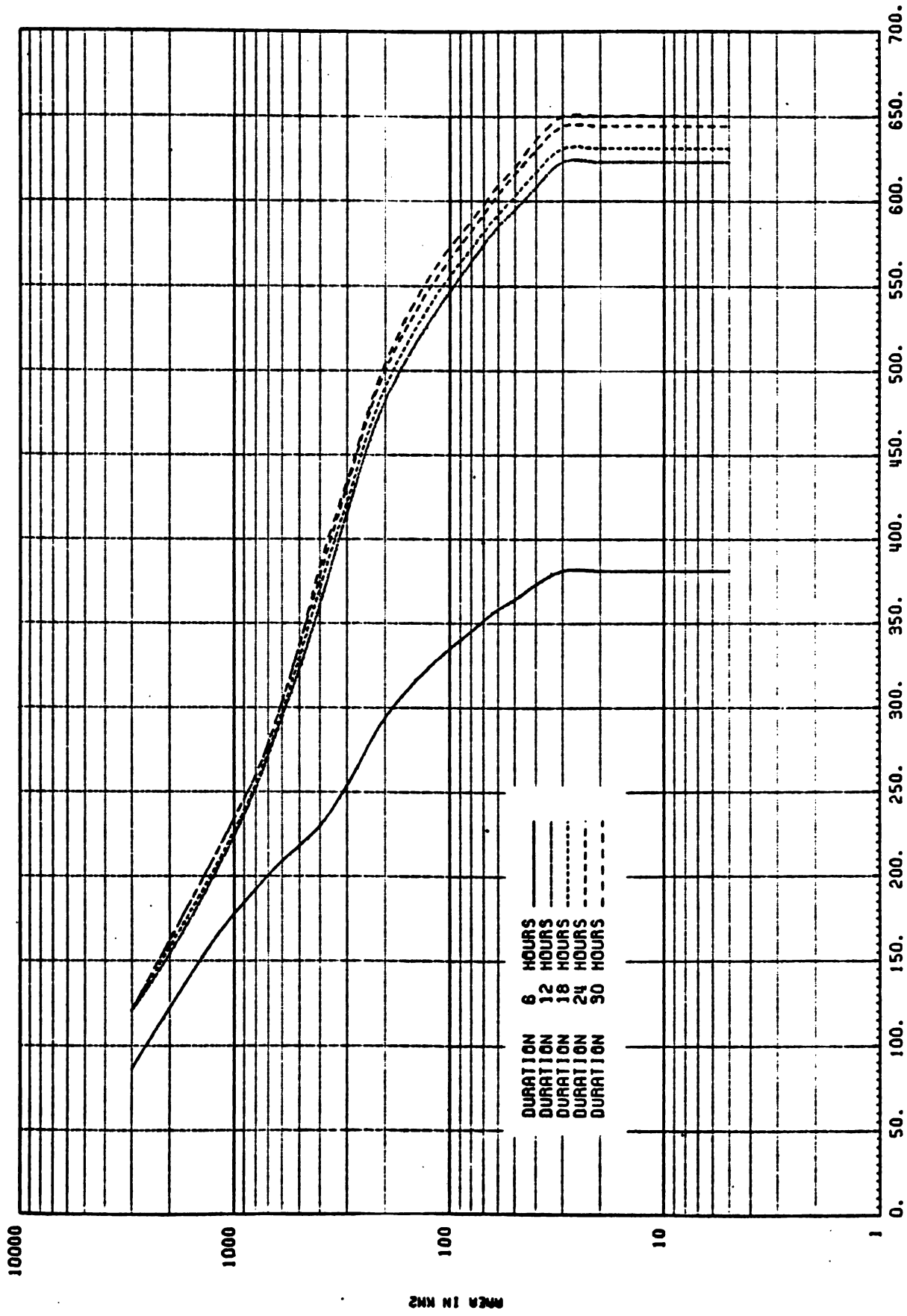

Figure 1.6.2. Non-hurricane depth-area duration curves for Nizao basin.

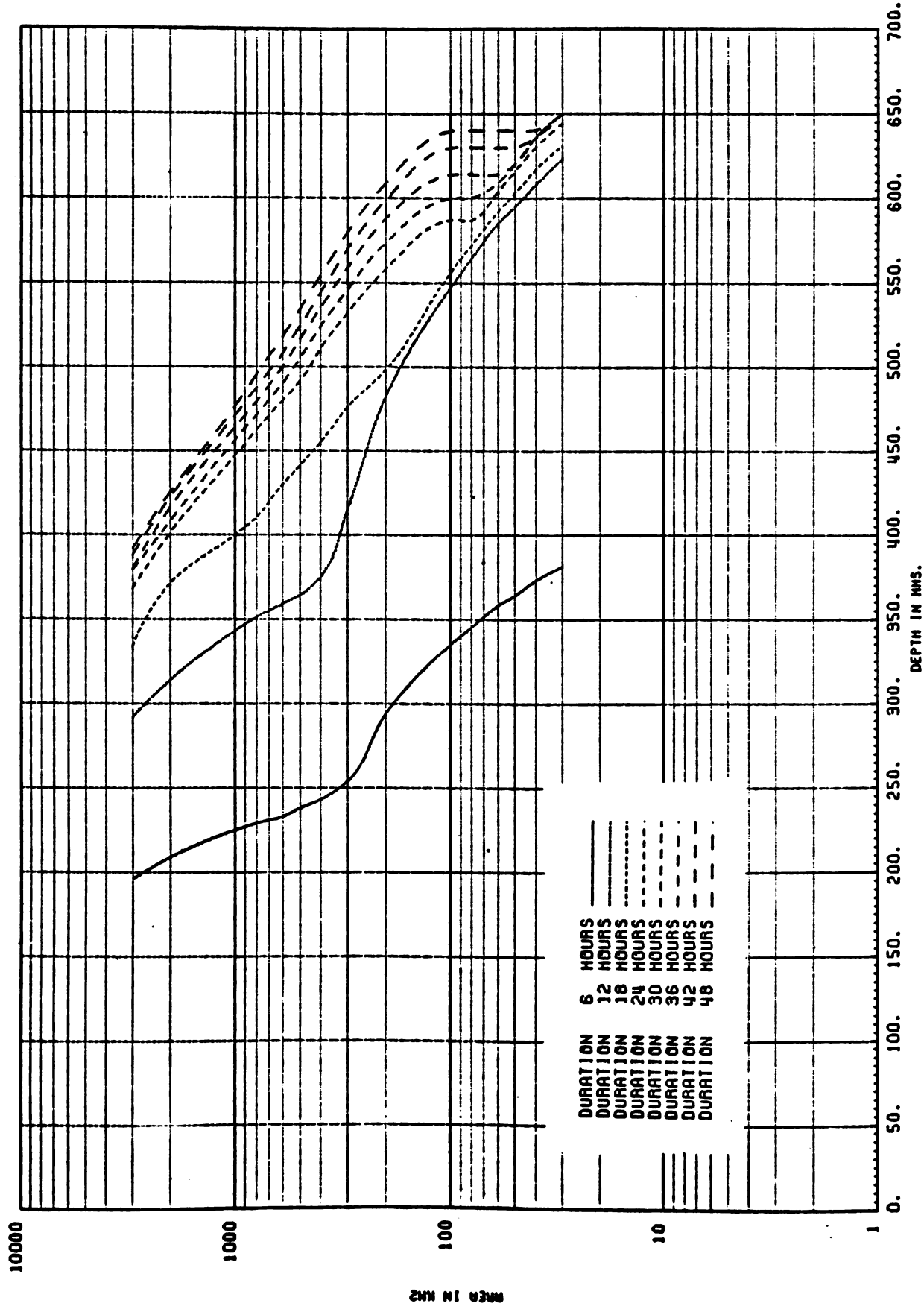

Figure 1.6.3. Enveloping depth-area-duration curves for Nizao basin.

TABLE 1.6.2 CLASSIFICATION OF STORMS USED IN DAD CURVES COMPUTATION

STARTING DATE	CLASSIFICATION	
8/1/84	non-hurricane	
4/12/83	non-hurricane	
5/9/82	non-hurricane	
5/8/81	non-hurricane	
8/4/80	hurricane	Hurricane Allen
9/5/79	hurricane	Tropical Storm Frederick
8/30/79	hurricane	Hurricane David
8/3/78	non-hurricane	
12/28/77	non-hurricane	
5/21/77	non-hurricane	
10/10/76	non-hurricane	
9/16/75	hurricane	Hurricane Eloise
8/30/74	hurricane	Hurricane Carmen
10/14/73	hurricane	Tropical Storm Gilda
5/20/72	non-hurricane	
2/19/71	non-hurricane	
8/22/70	hurricane	Tropical Storm Dorothy
7/19/69	non-hurricane	
8/8/68	non-hurricane	
9/10/67	hurricane	Hurricane Beulah
9/28/66	hurricane	Hurricane Inez
5/25/66	non-hurricane	
5/2/65	non-hurricane	
8/6/64	non-hurricane	
10/1/63	hurricane	Hurricane Flora

TABLE 1.6.3 Standard Project Storm (Hurricane, Non-Hurricane) and Enveloping) Precipitation Depth

DURATION (hrs)	PRECIPITATION DEPTH (mm)		
	HURRICANE	NON-HURRICANE	ENVELOPING
24	460	255	460
48	493	260	493

selected. . After recognizing the subjective nature of this first approach, a second approach which proved to give a more critical temporal distribution was used as follows. The percentage magnitude versus percentage duration plots were made for all 48 hour storms selected earlier. Then an enveloping curve, which lies below all the curves at small percentage duration, and above all curves for larger durations, was plotted. This exercise is illustrated in Figure 1.6.4.

Combining the enveloping temporal distribution shown in Figure 1.6.4 and the standard project storm magnitudes in Table 1.6.3, the 48 hour standard project storm isohyetal patterns were generated. These design storms are presented in Figure 1.6.5 and 1.6.6.

1.6.6 Probable Maximum Precipitation (PMP)

Given the location of the Nizao basin, a hurricane is most likely to produce the PMP. This is supported by the almost twice the precipitation depths obtained for hurricane conditions than for non-hurricane conditions for a given area and a duration (see DAD analysis). The Hurricane Model of U.S. Weather Bureau (1961) has been used by INDRHI/CDE to produce a hurricane PMP pattern for the Nizao basin. The original model has been modified for conditions existing in the Dominican Republic and has been applied to compute PMP for the Tavera-Bao Watershed (CDE, personal communication). The precipitation pattern of average PMP over Nizao watershed obtained from the Hurricane model is presented in Figure 1.6.7. It is noted that the PMP total averages to 1338 mm over Nizao which is substantially greater than the hurricane SPS reported in Table 1.6.3.

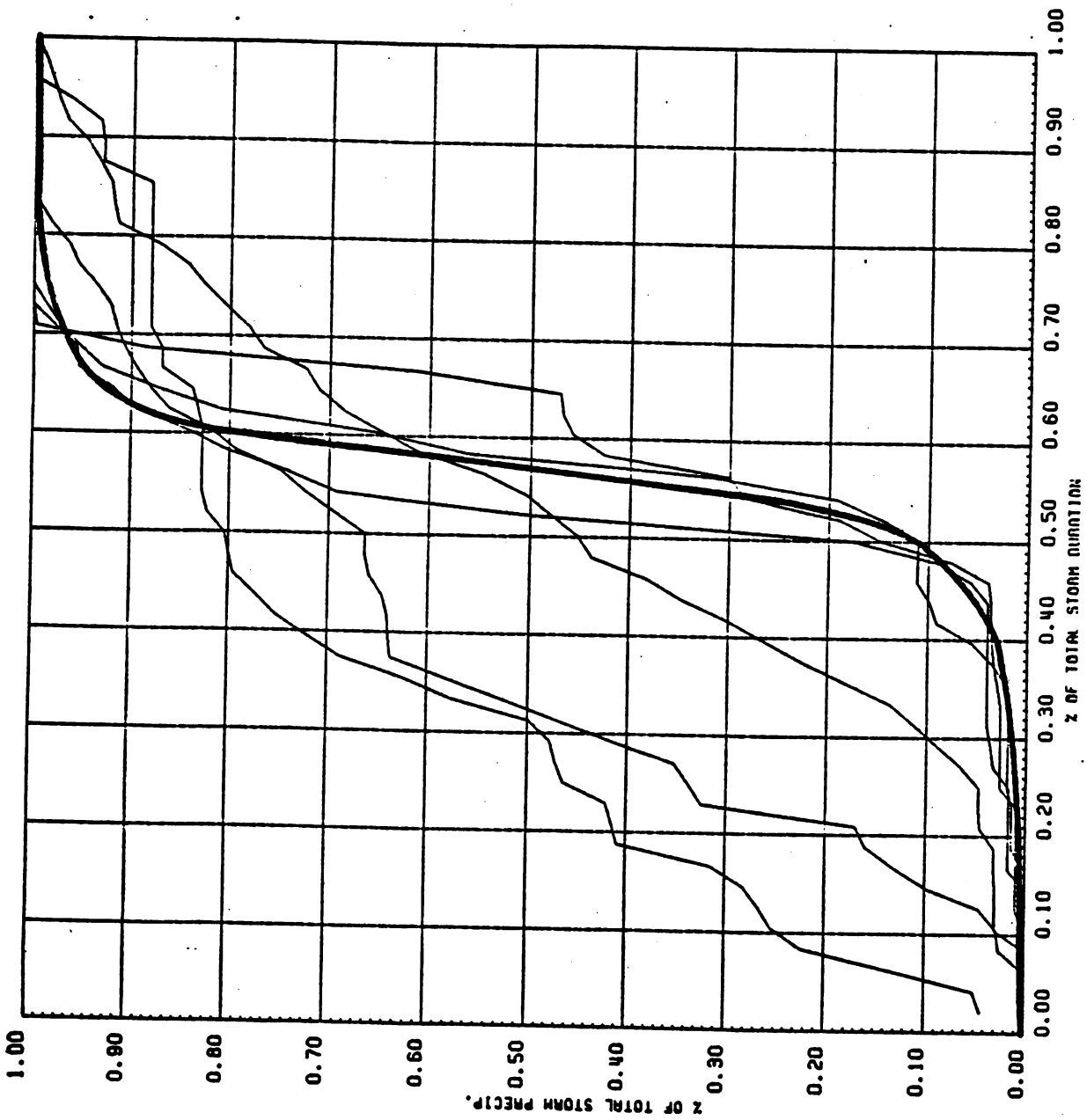

Figure 1.6.4. Historic rainfall patterns and selected design temporal distributions.

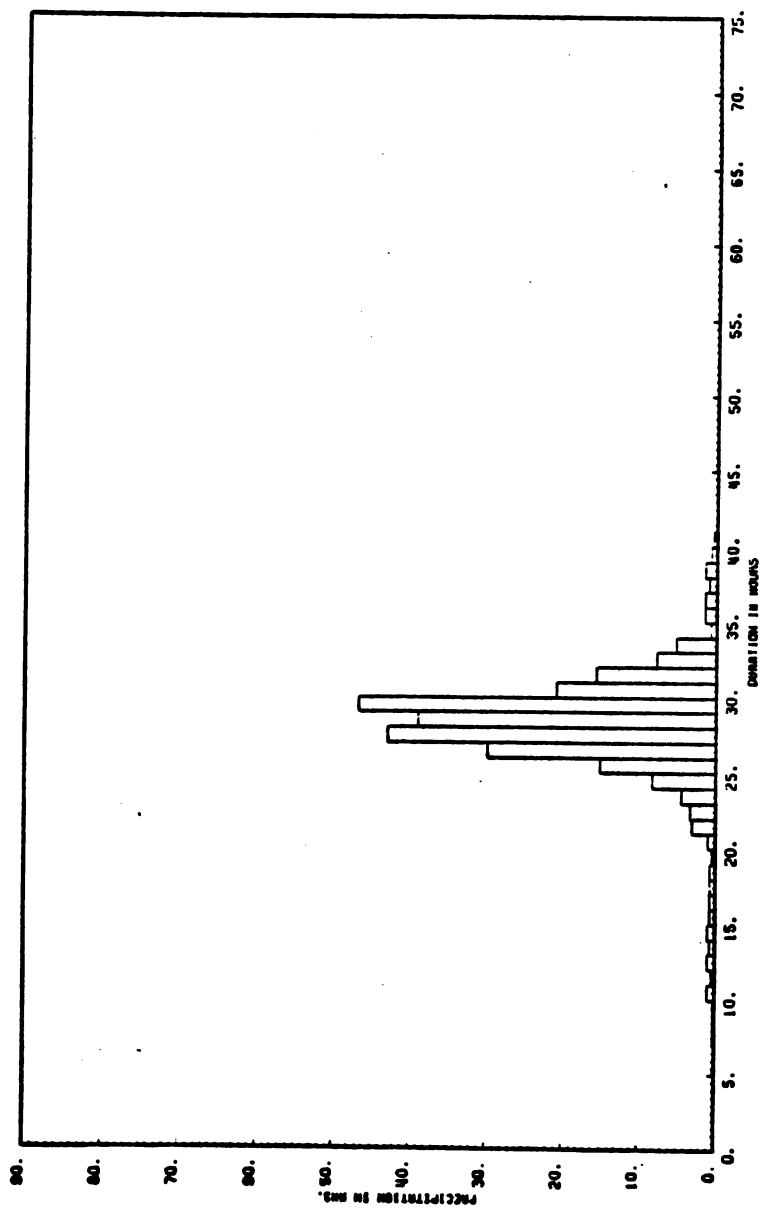

Figure 1.6.5. Non-hurricane standard project storm (48 hours).

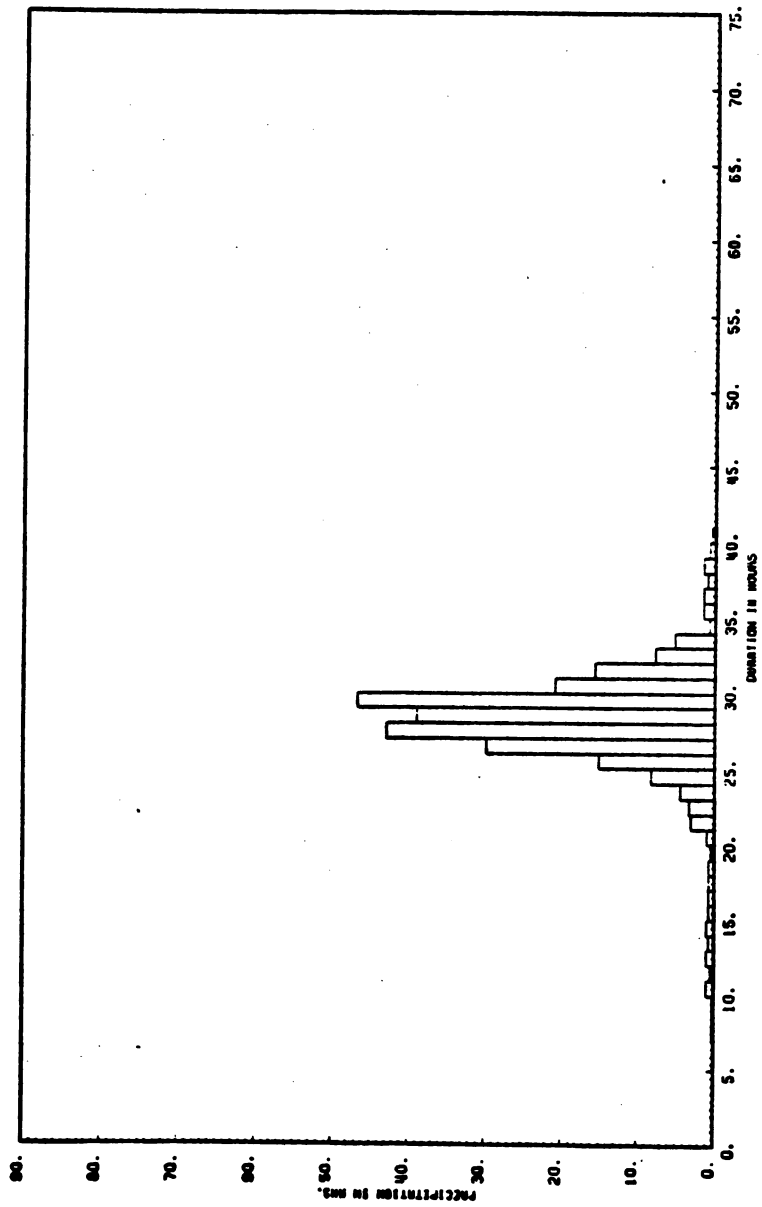

Figure 1.6.5. Non-hurricane standard project storm (48 hours).

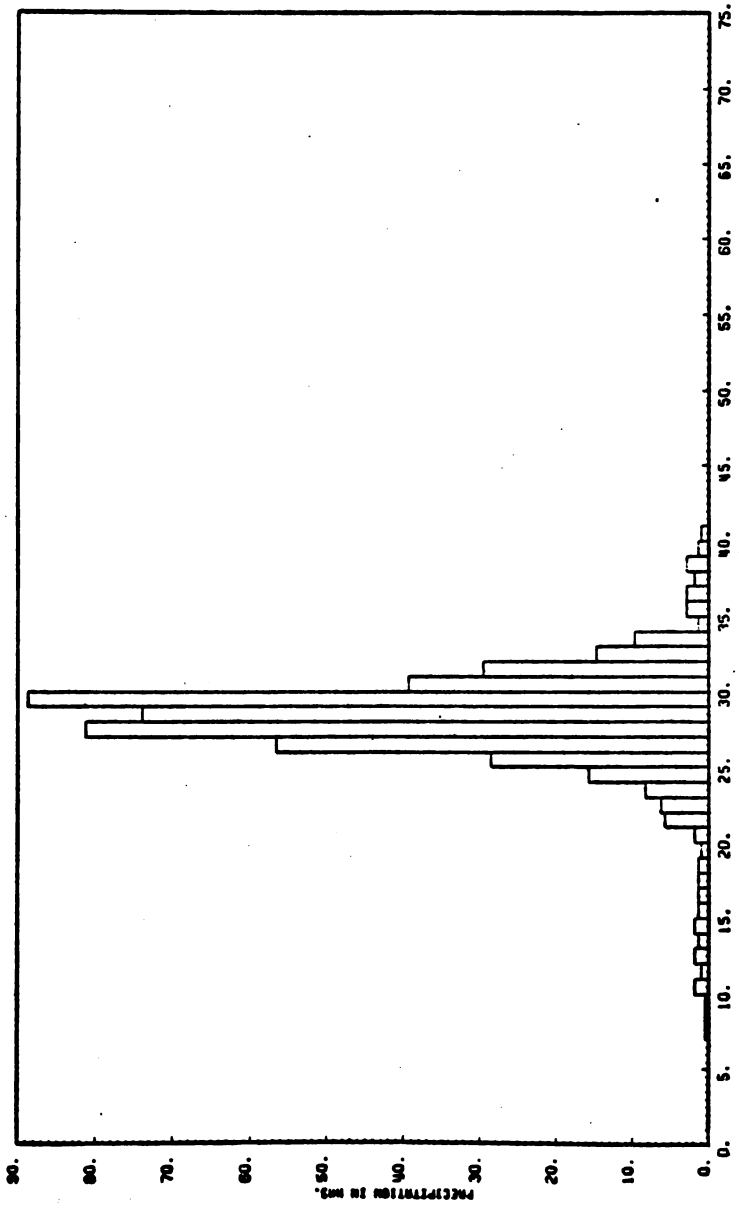

Figure 1.6.6. Hurricane standard project storm (48 hours).

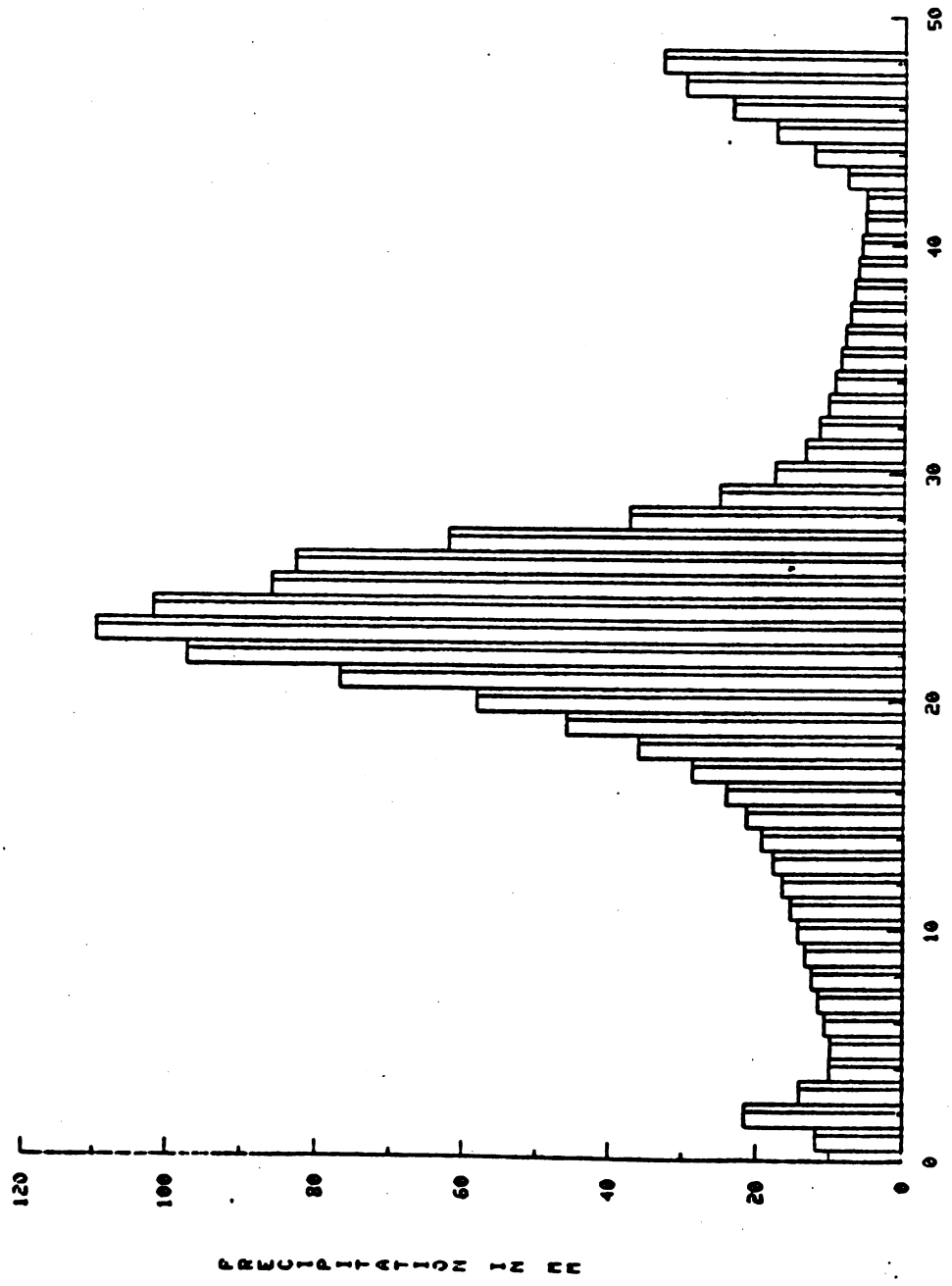

Figure 1.6.7. Precipitation pattern of average Probable Maximum Precipitation over Nizao watershed.

APPENDIX 1.6.A

MASS CURVES OF RAINFALL FOR SELECTED STORMS

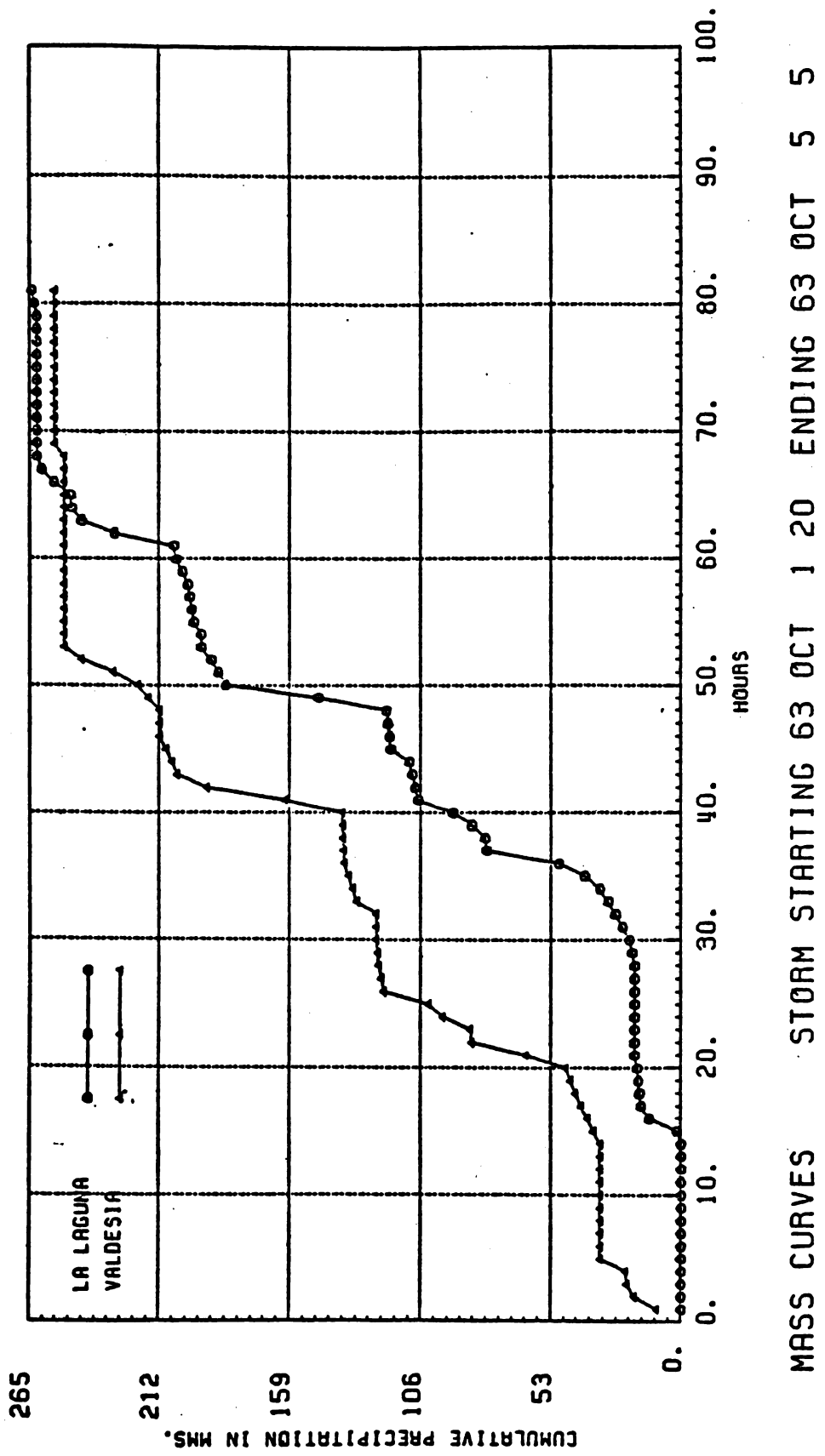
MASS CURVES STORM STARTING 63 OCT 1 20 ENDING 63 OCT 5 5
CUMULATIVE PRECIPITATION IN MMS.
265
212
159
106
53
0.
0.
10.
20.
30.
40.
50.
60.
70.
80.
90.
100.
HOURS
LA LAGUNA
VALDESIA

Figure 1.6.A.1.

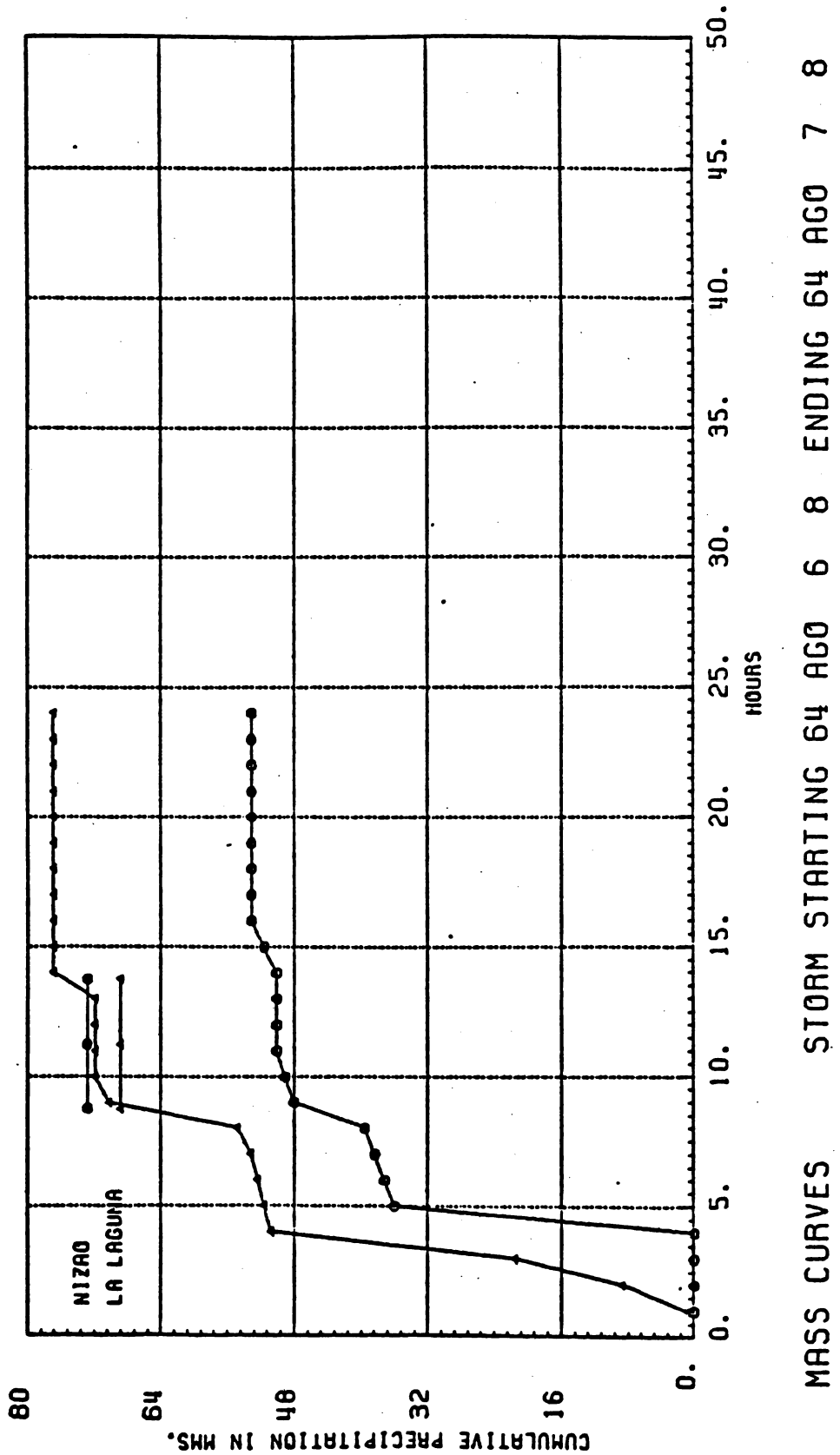
MASS CURVES STORM STARTING 64 AGO 6 8 ENDING 64 AGO 7 8
CUMULATIVE PRECIPITATION IN MMS.
80
64
48
32
16
0.
HOURS
0.
5.
10.
15.
20.
25.
30.
35.
40.
45.
50.
NIZAO
LA LAGUNA

Figure 1.6.A.2

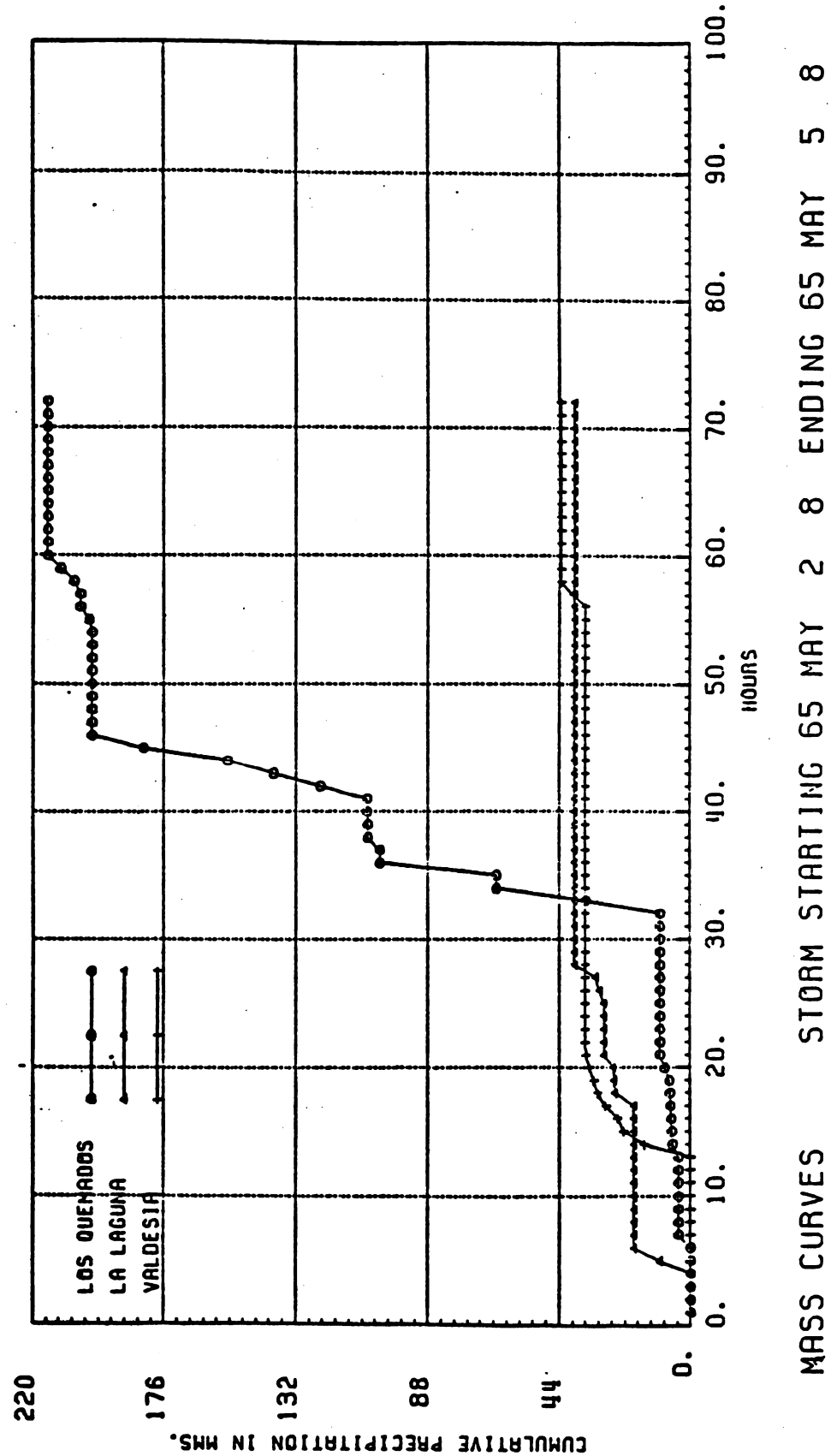
MASS CURVES STORM STARTING 65 MAY 2 8 ENDING 65 MAY 5 8
CUMULATIVE PRECIPITATION IN MMS.
220
176
132
88
44
0.
0.
10.
20.
30.
40.
50.
60.
70.
80.
90.
100.
HOURS
LOS QUEMADOS
LA LAGUNA
VALDESIA

Figure 1.6.A.3.

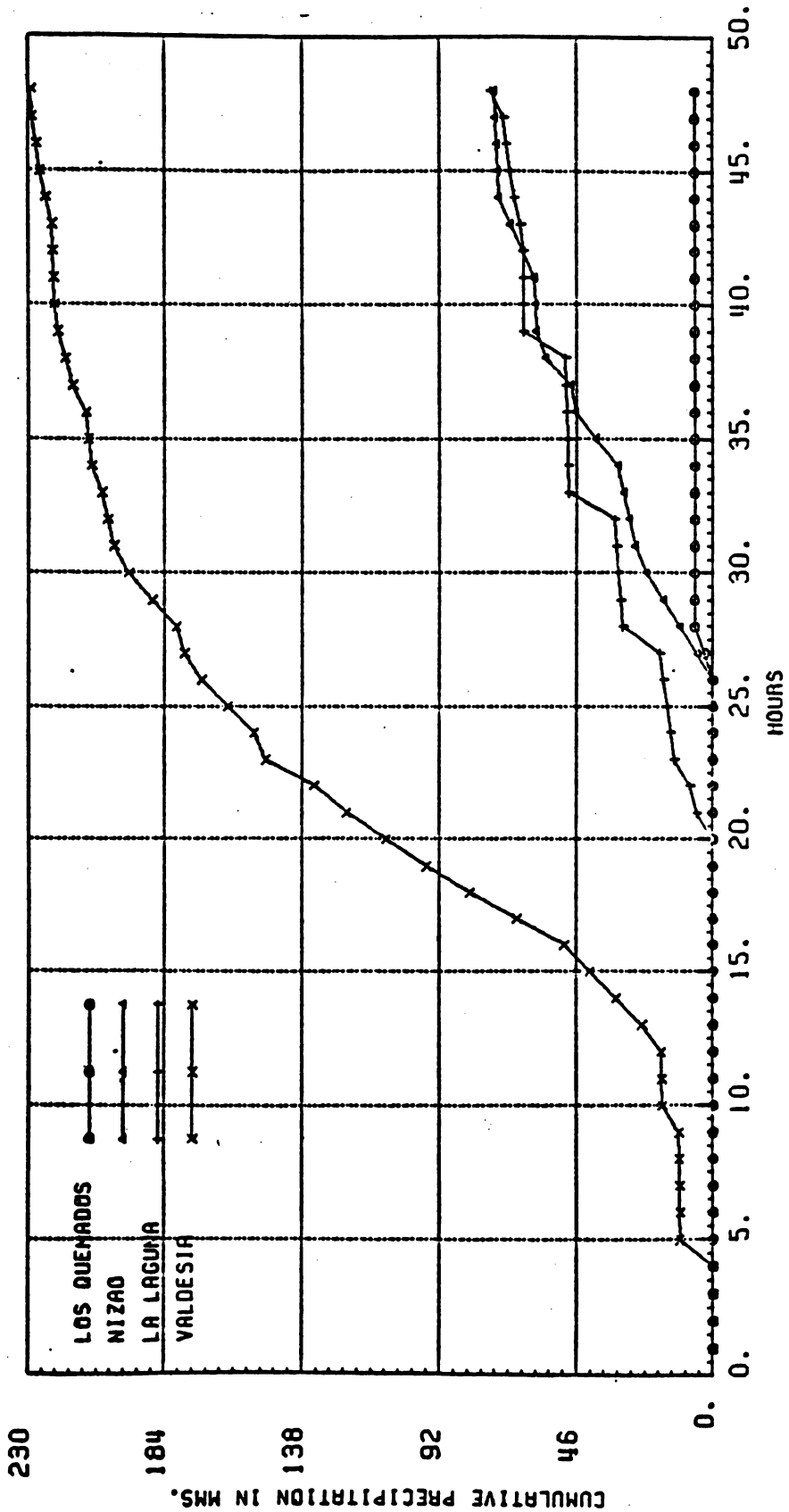
MASS CURVES STORM STARTING 66 MAY 25 8 ENDING 66 MAY 27 8
CUMULATIVE PRECIPITATION IN MMS.
230
184
138
92
46
0.
0.
5.
10.
15.
20.
25.
30.
35.
40.
45.
50.
HOURS
LOS QUEMADOS
NIZAO
LA LAGUNA
VALDESIA

Figure 1.6.A.4

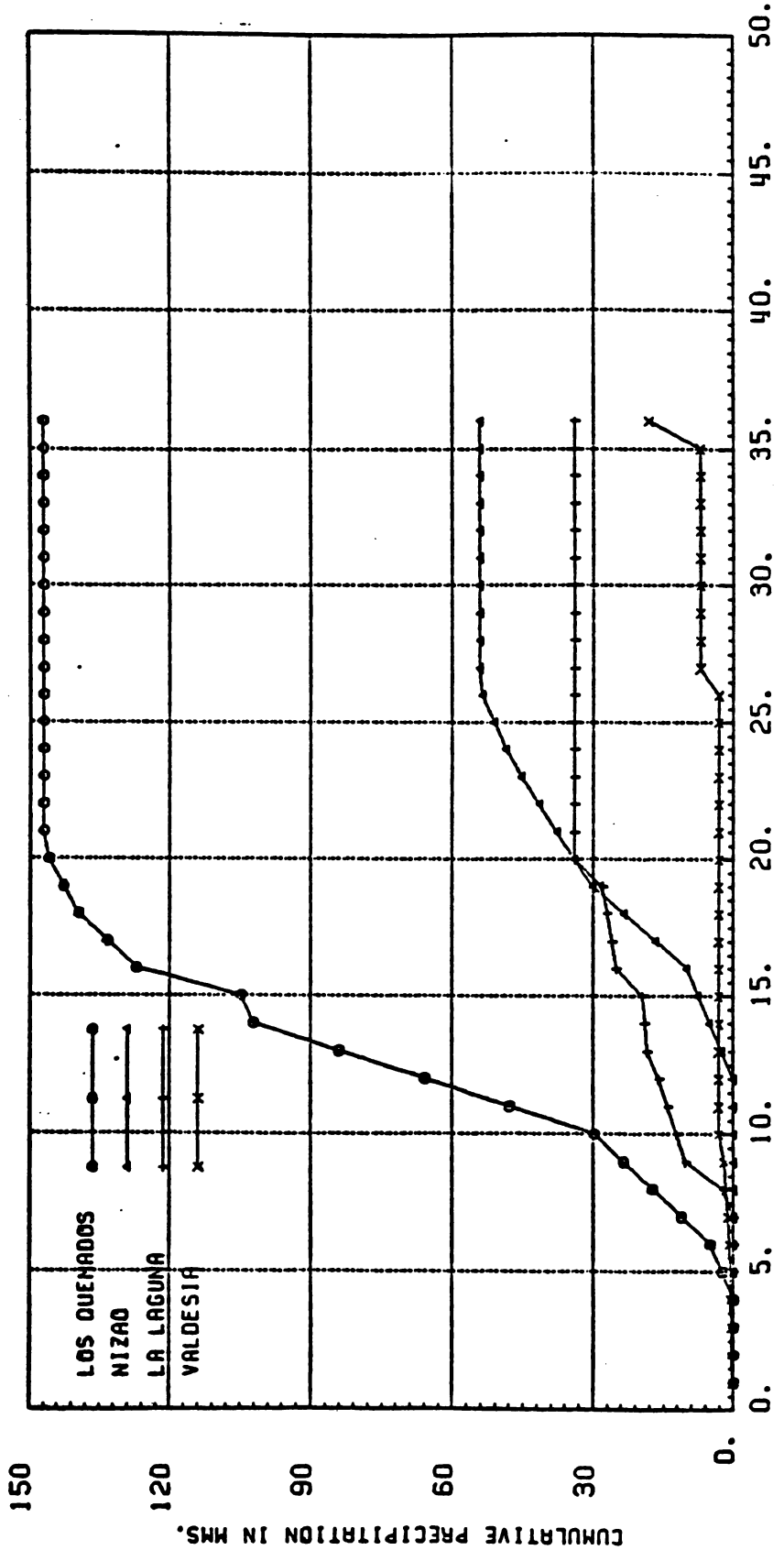
MASS CURVES STORM STARTING 66 SEP 28 20 ENDING 66 SEP 30 8
CUMULATIVE PRECIPITATION IN MMS.
HOURS
LOS QUEMADOS
NIZAO
LA LAGUNA
VALDESIA
0.
30
60
90
120
150
0.
5.
10.
15.
20.
25.
30.
35.
40.
45.
50.

Figure 1.6.A.5

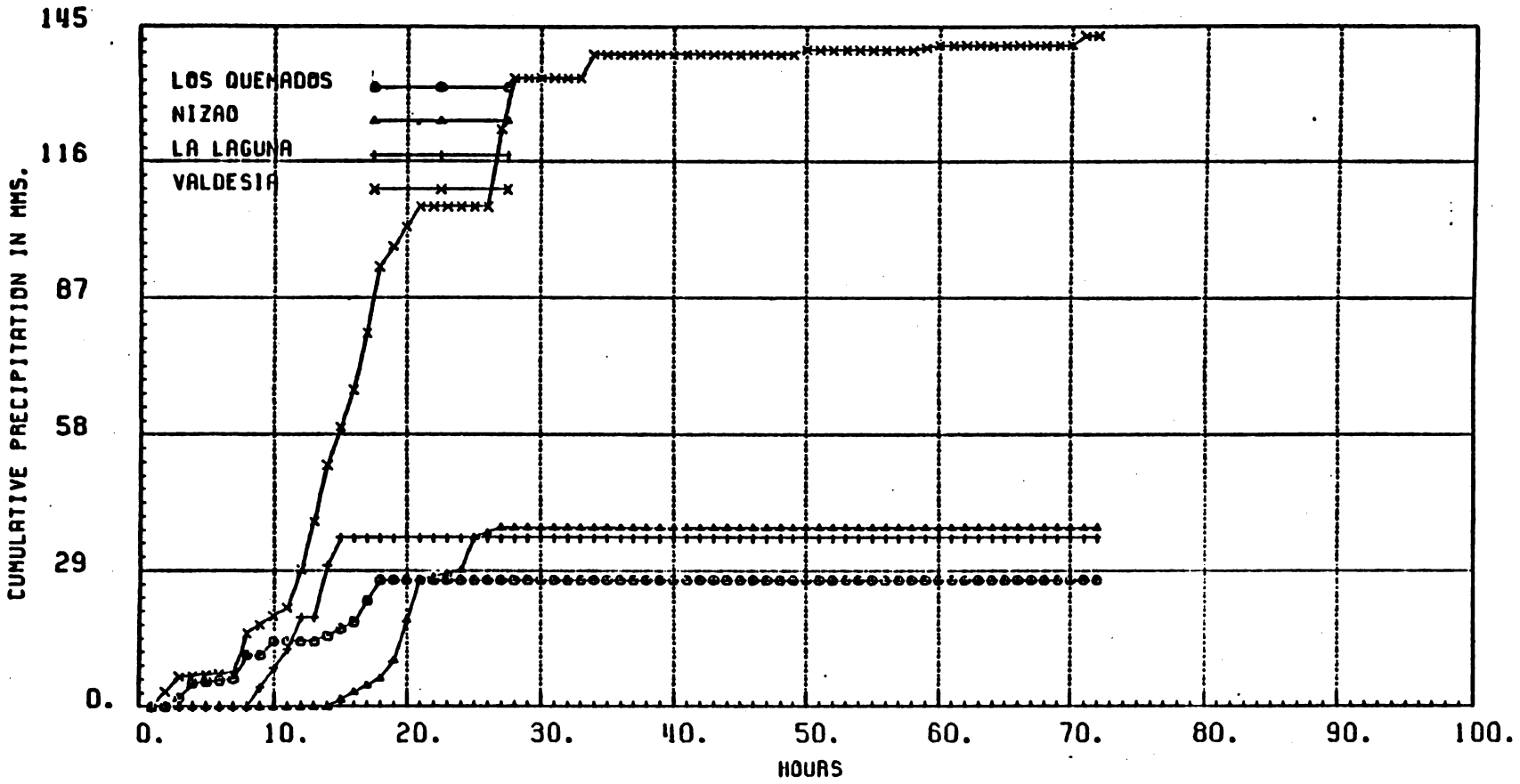

MASS CURVES STORM STARTING 67 SEP 10 8 ENDING 67 SEP 13 8

Figure 1.6.A.6

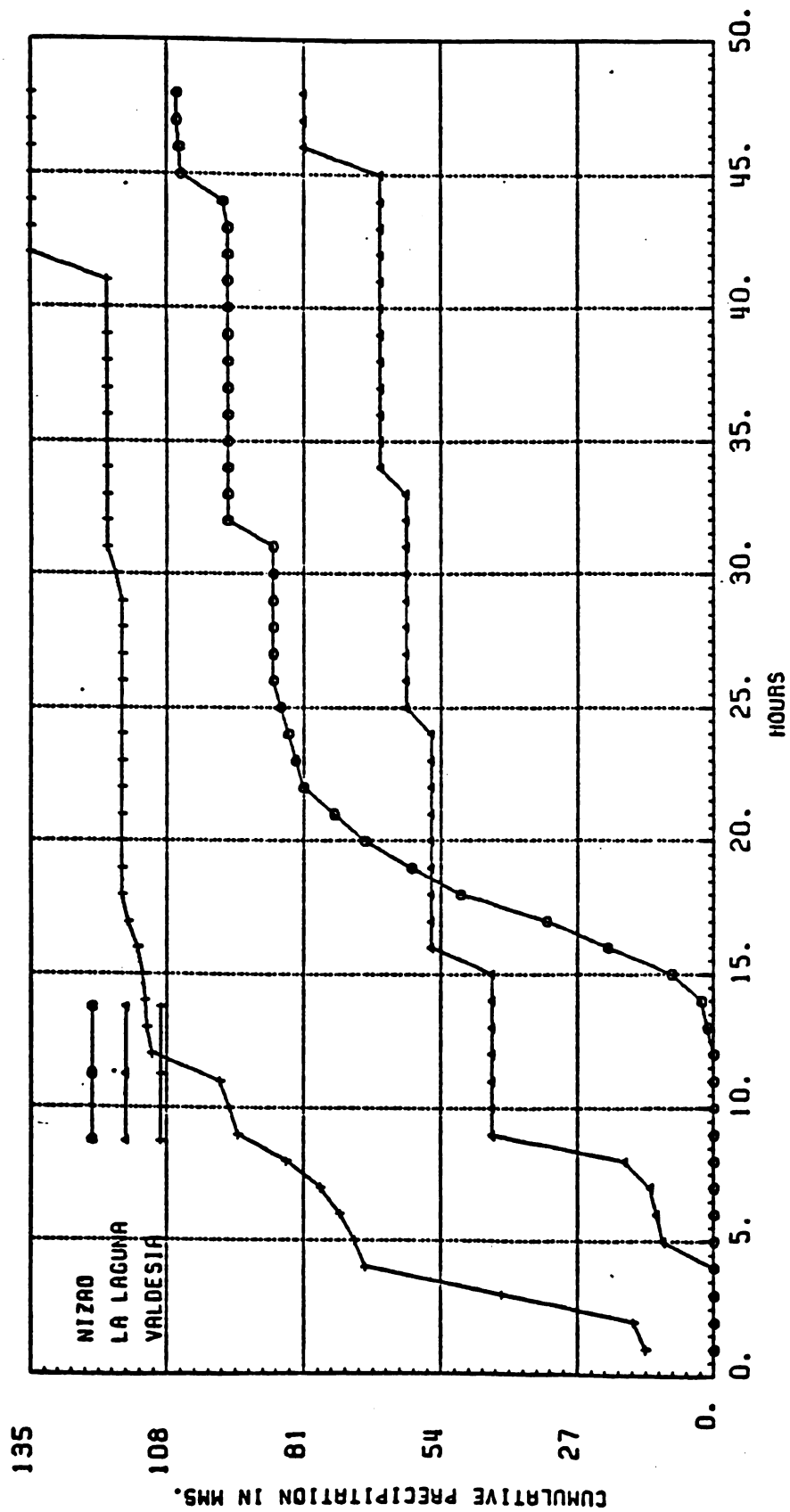
MASS CURVES STORM STARTING 68 AGO 8 8 ENDING 68 AGO 10 8
CUMULATIVE PRECIPITATION IN MMS.
HOURS
NIZAO
LA LAGUNA
VALDESIA
0.
27
54
81
108
135
0.
5.
10.
15.
20.
25.
30.
35.
40.
45.
50.

Figure 1.6.A.7

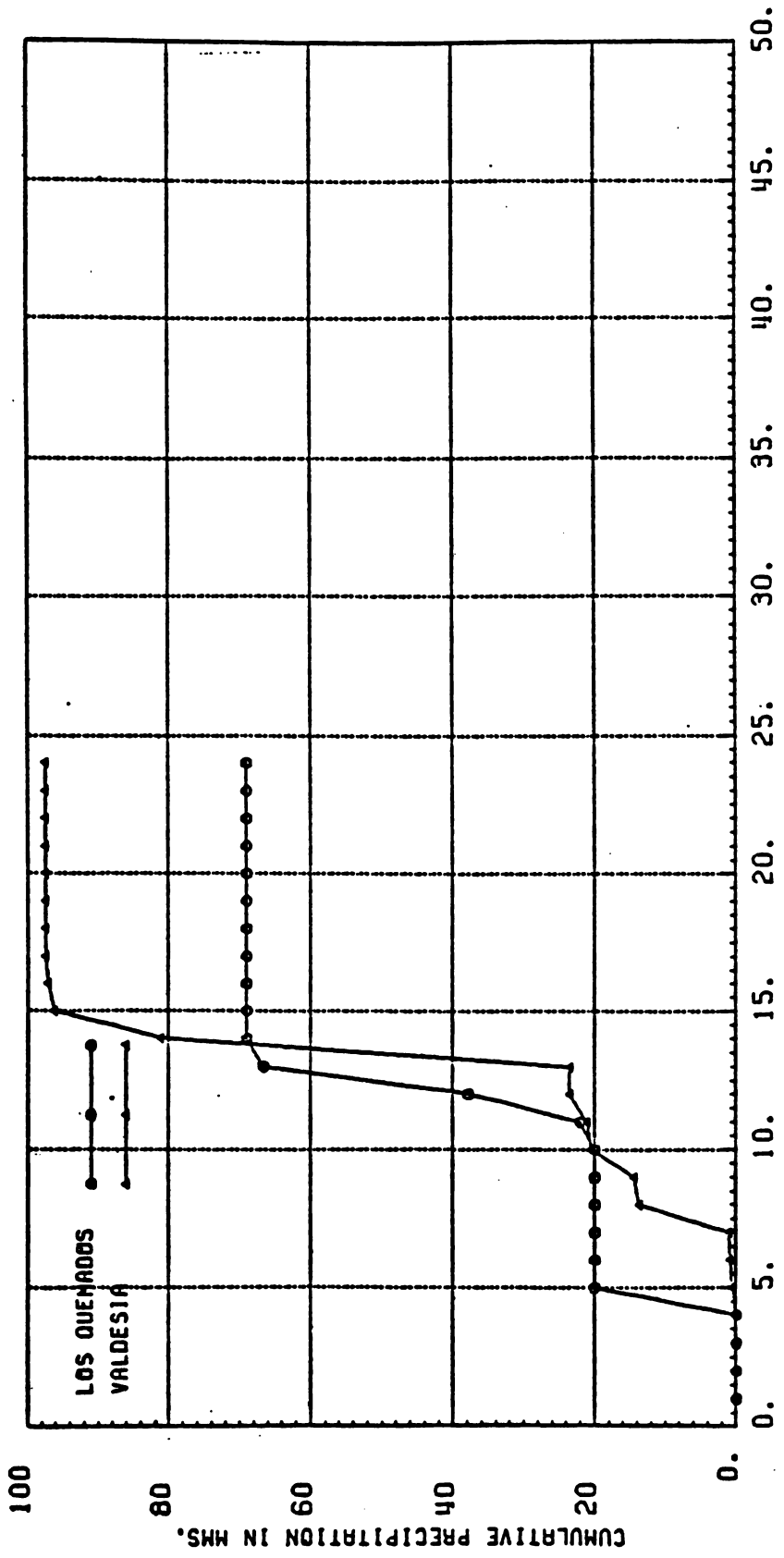
MASS CURVES STORM STARTING 69 JUL 19 8 ENDING 69 JUL 20 8
CUMULATIVE PRECIPITATION IN MMS.
HOURS
LOS QUEMADOS
VALDESIA
0.
20
40
60
80
100
0.
5.
10.
15.
20.
25.
30.
35.
40.
45.
50.

Figure 1.6.A.8

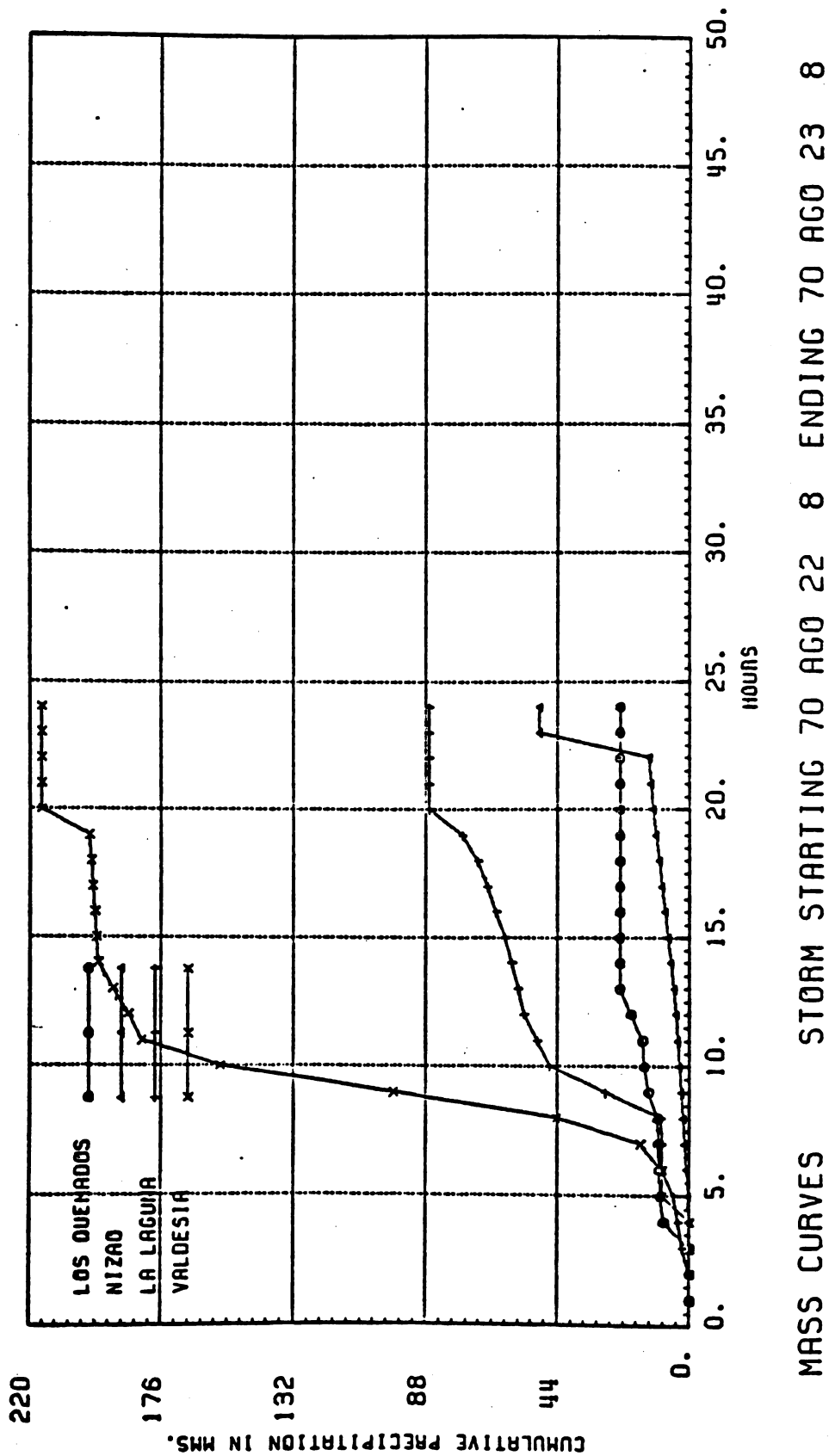
MASS CURVES STORM STARTING 70 AGO 22 8 ENDING 70 AGO 23 8
CUMULATIVE PRECIPITATION IN MMS.
220
176
132
88
44
0.
0.
5.
10.
15.
20.
25.
30.
35.
40.
45.
50.
HOURS
LOS OVENADOS
NIZAO
LA LAGUNA
VALDESIA

Figure 1.6.A.9

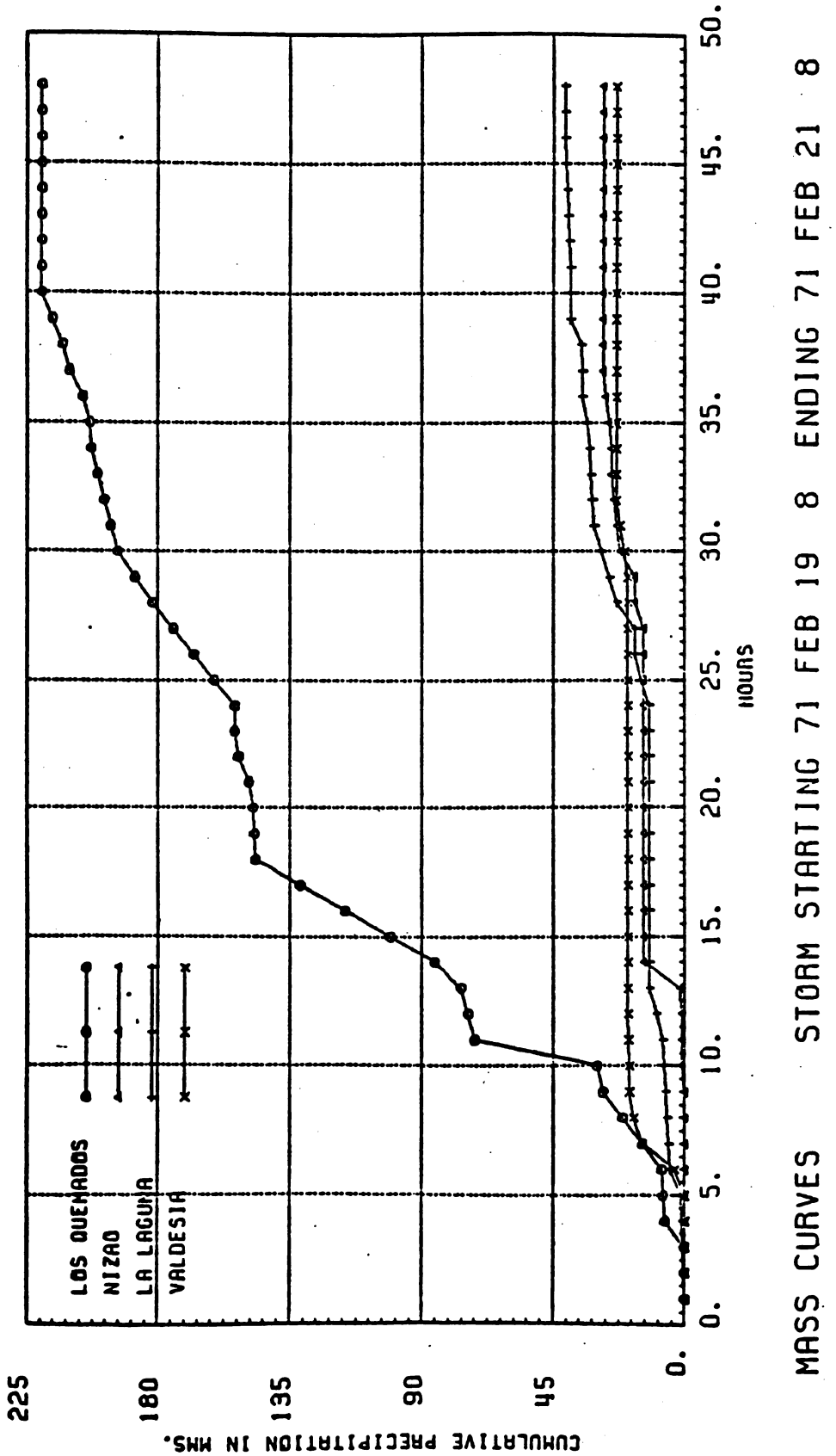

Figure 1.6.A.10

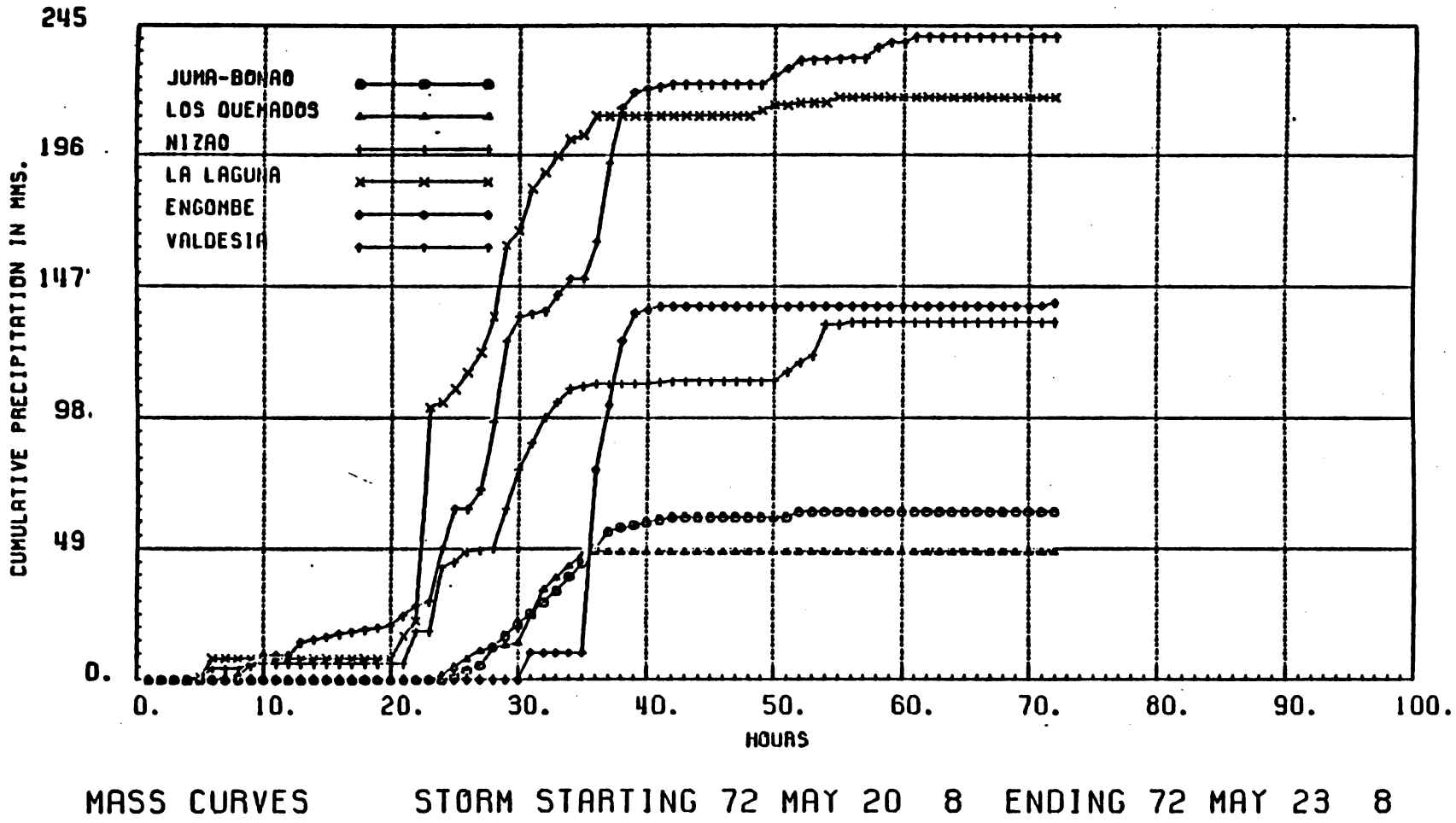

Figure 1.6.A.11

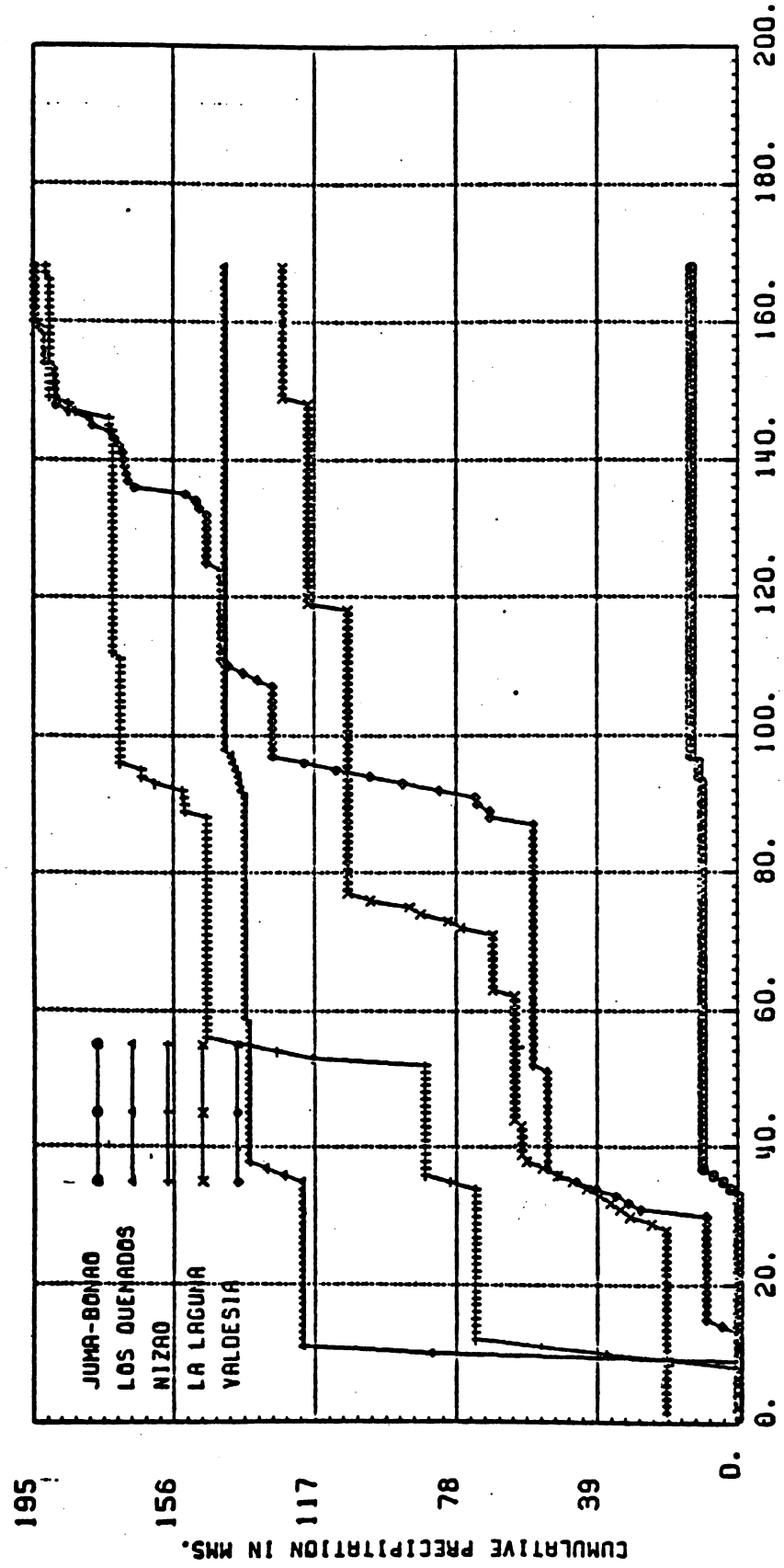

Figure 1.6.A.12

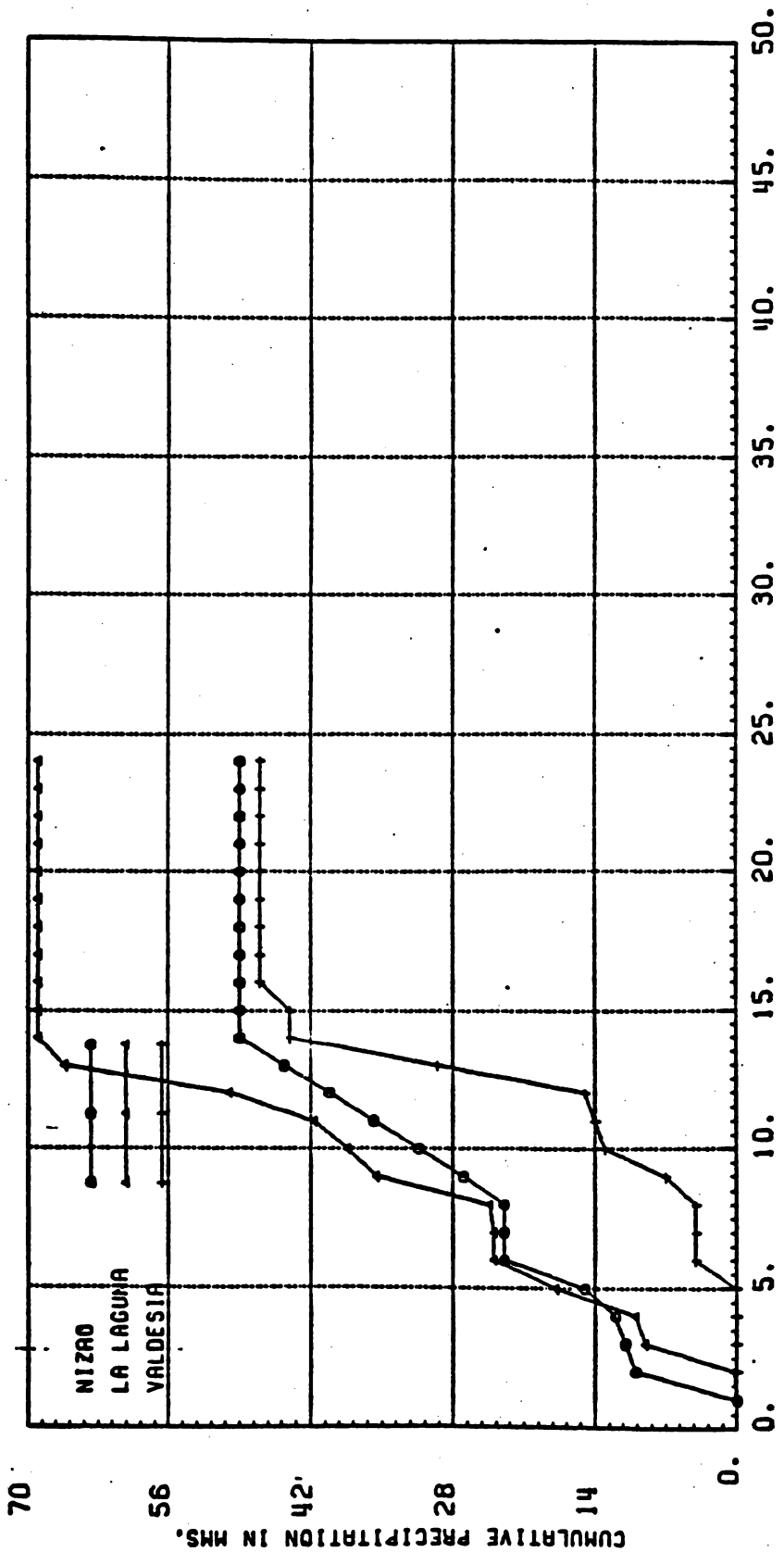

Figure 1.6.A.13

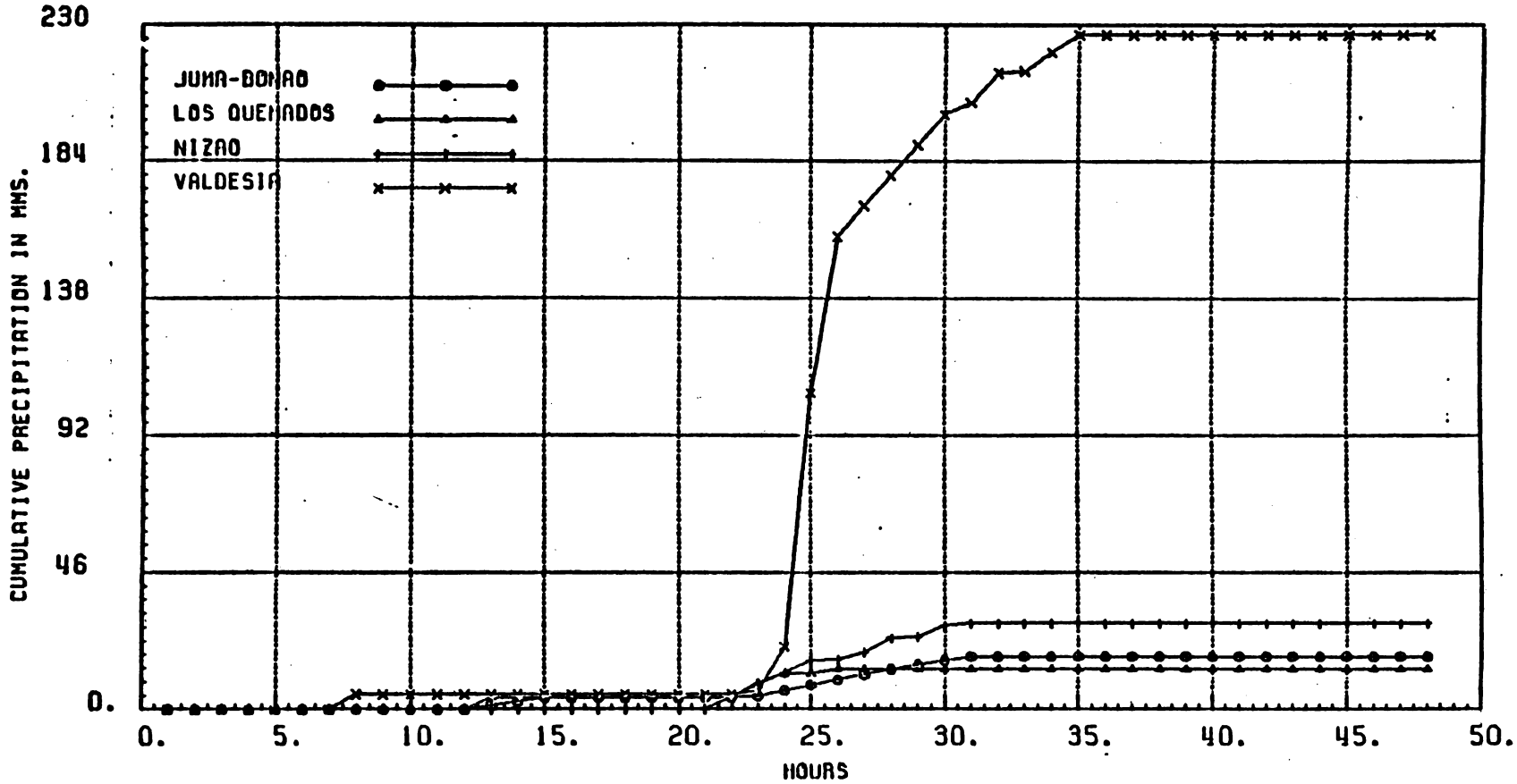

MASS CURVES STORM STARTING 75 SEP 16 8 ENDING 75 SEP 18 8

Figure 1.6.A.14

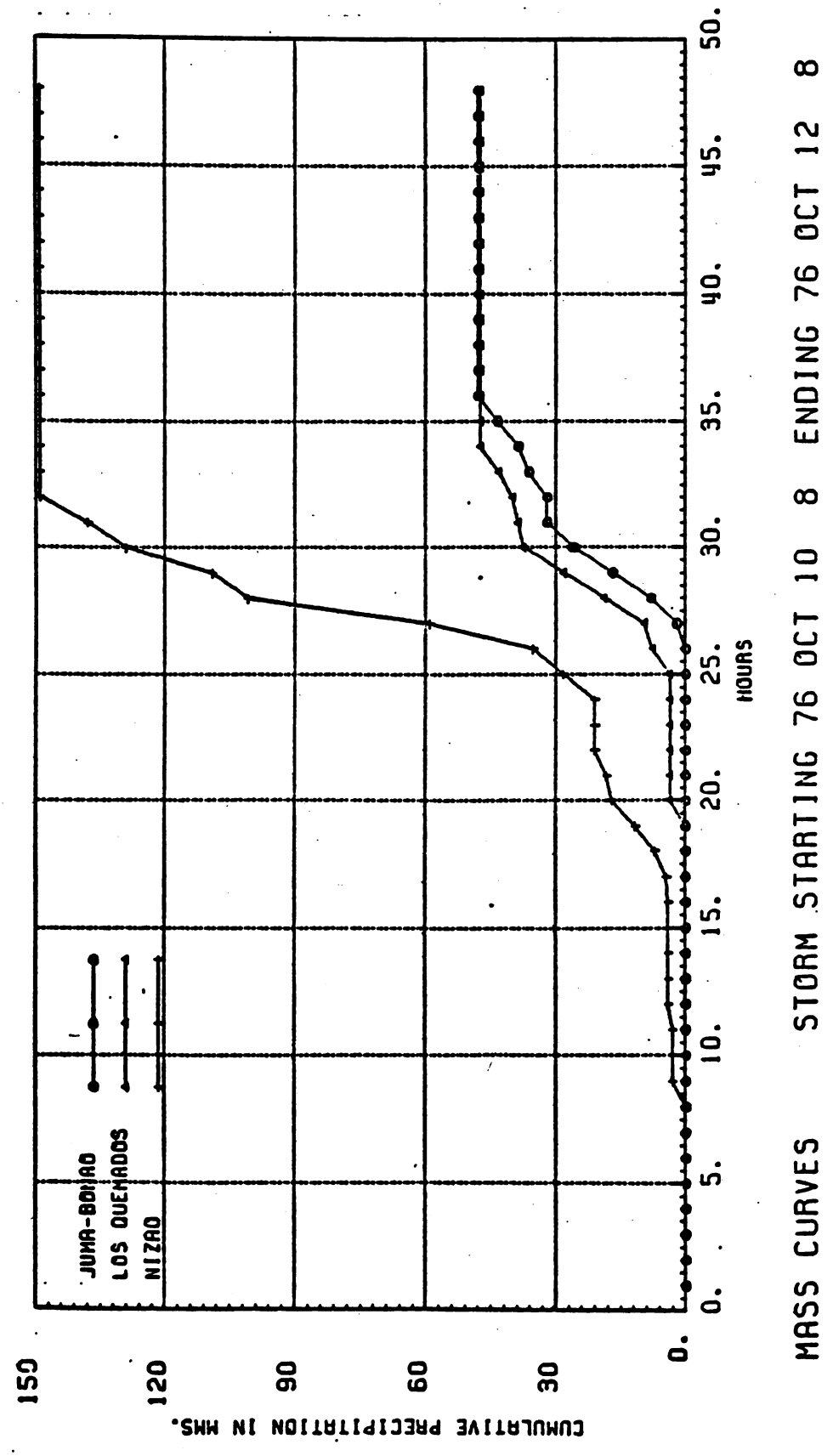

Figure 1.6.A.15

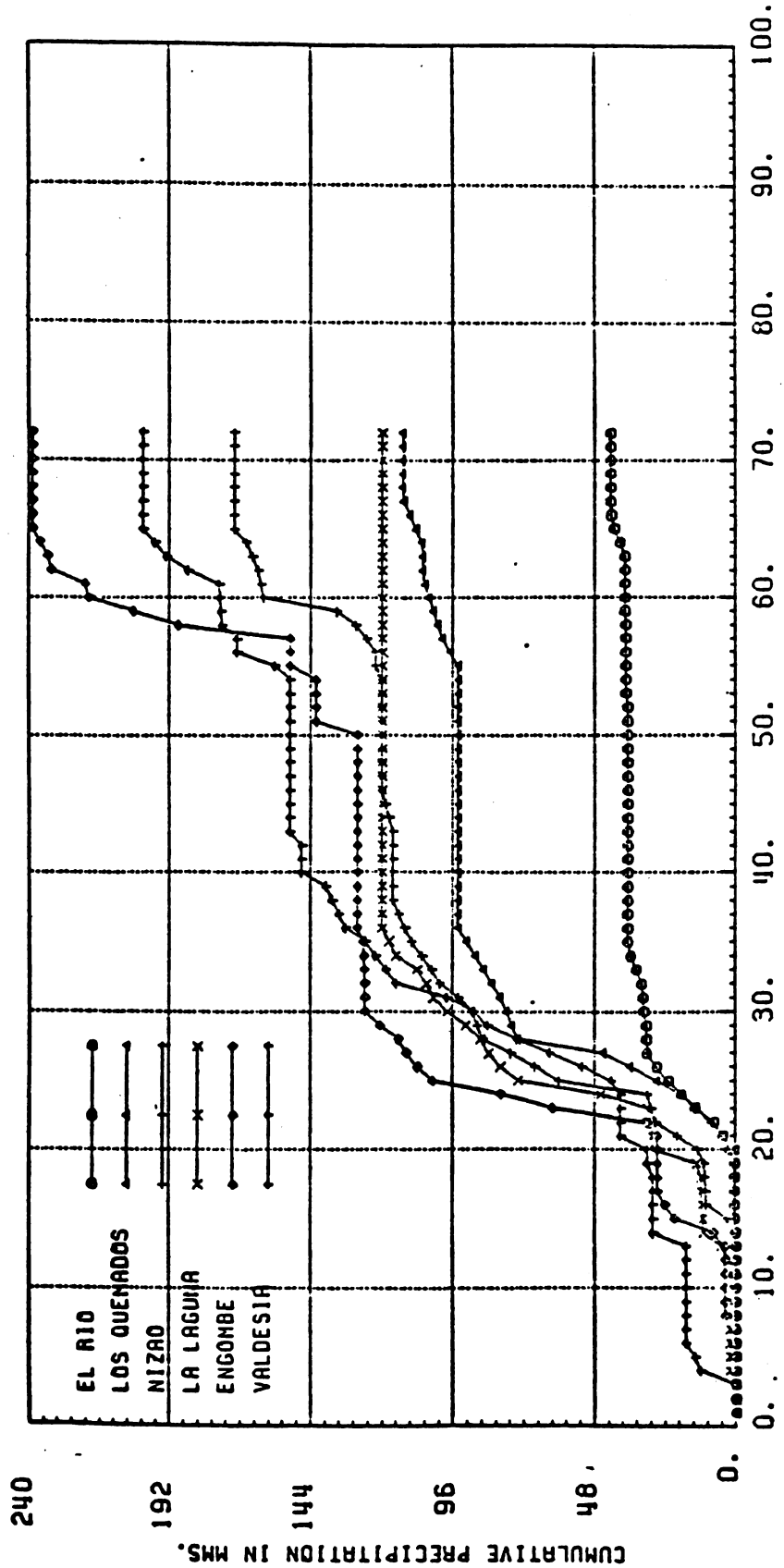

Figure 1.6.A.16

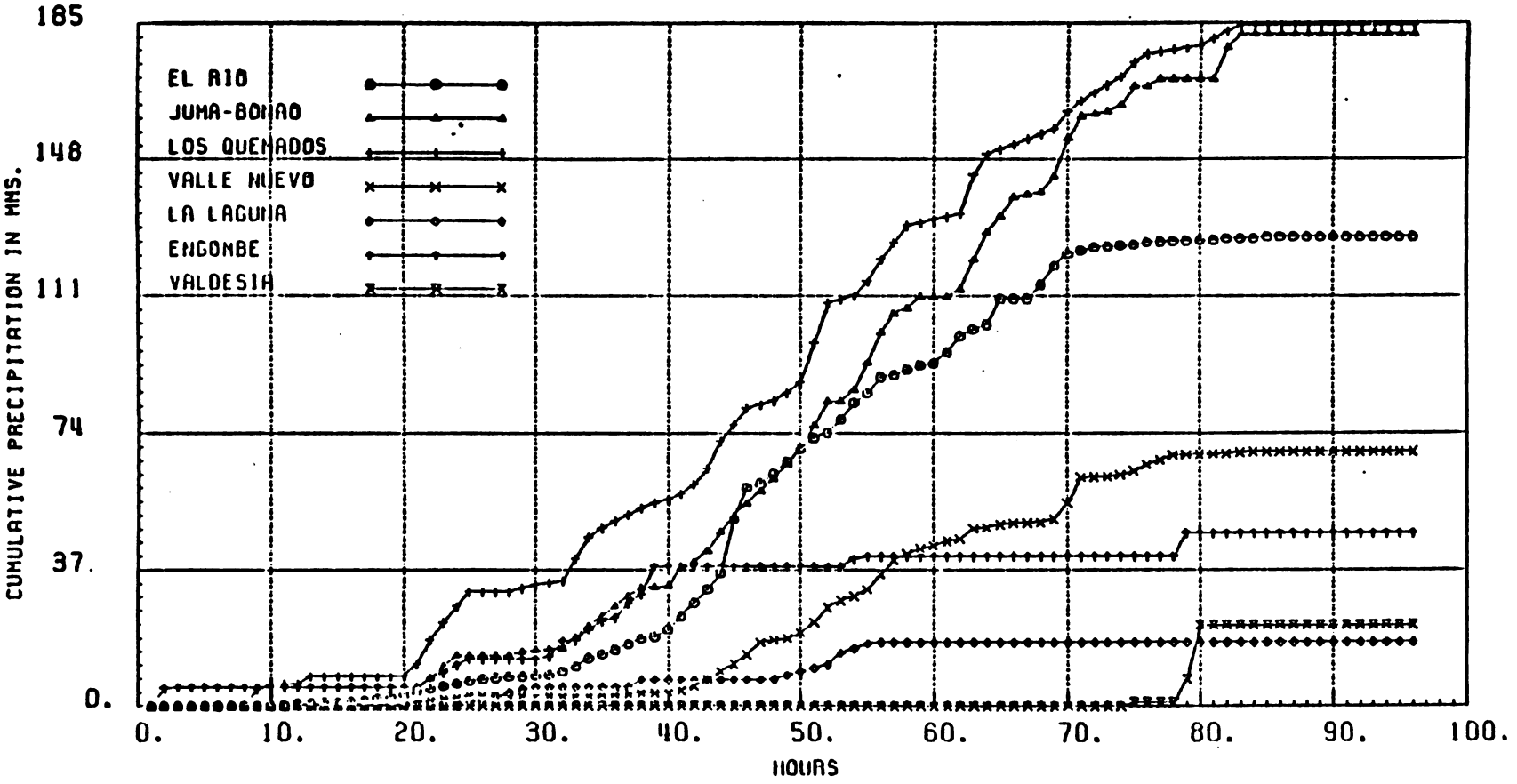

MASS CURVES STORM STARTING 77 DIC 28 8 ENDING 78 ENE 1 8

Figure 1.6.A.17

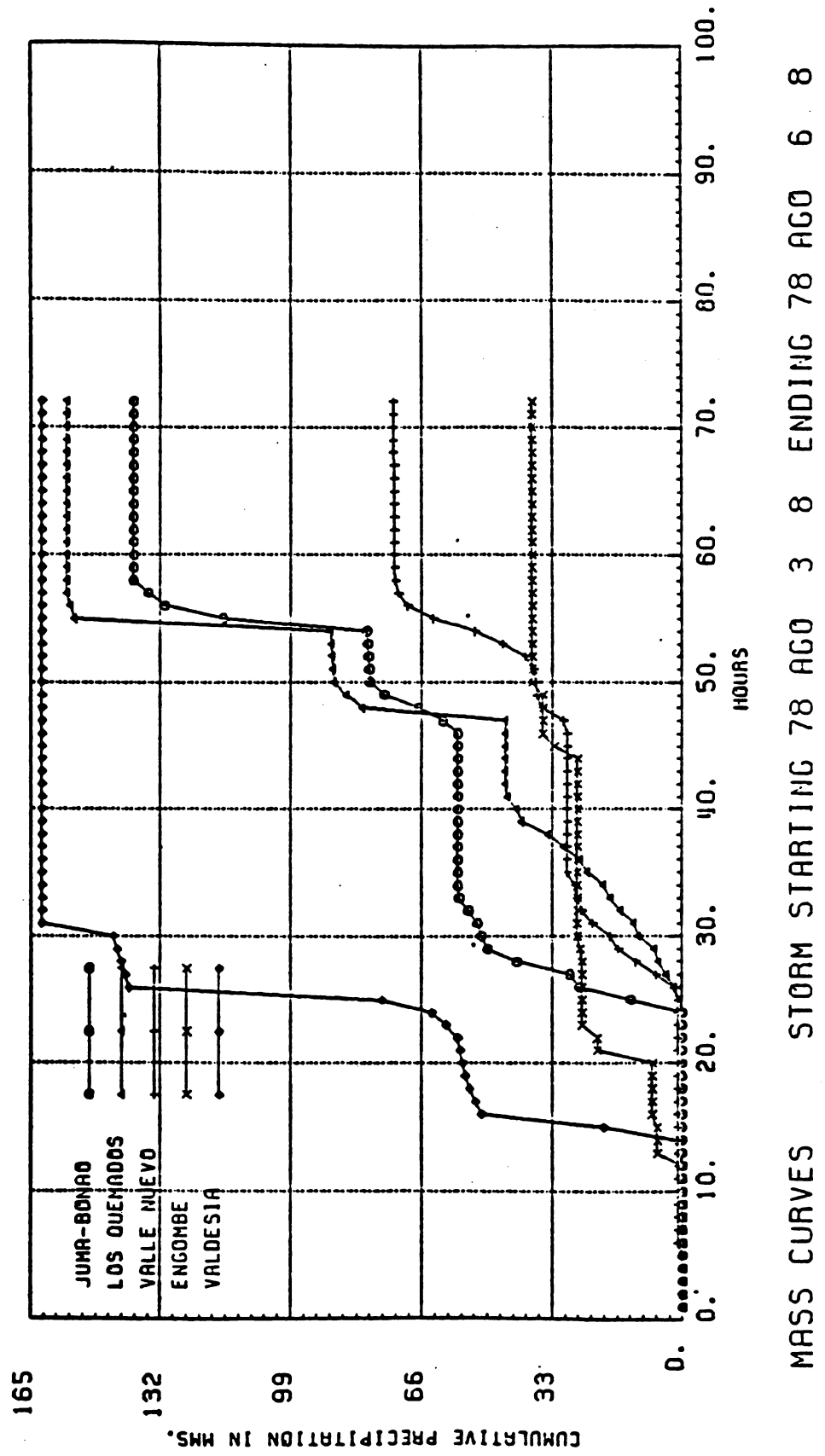

Figure 1.6.A.18

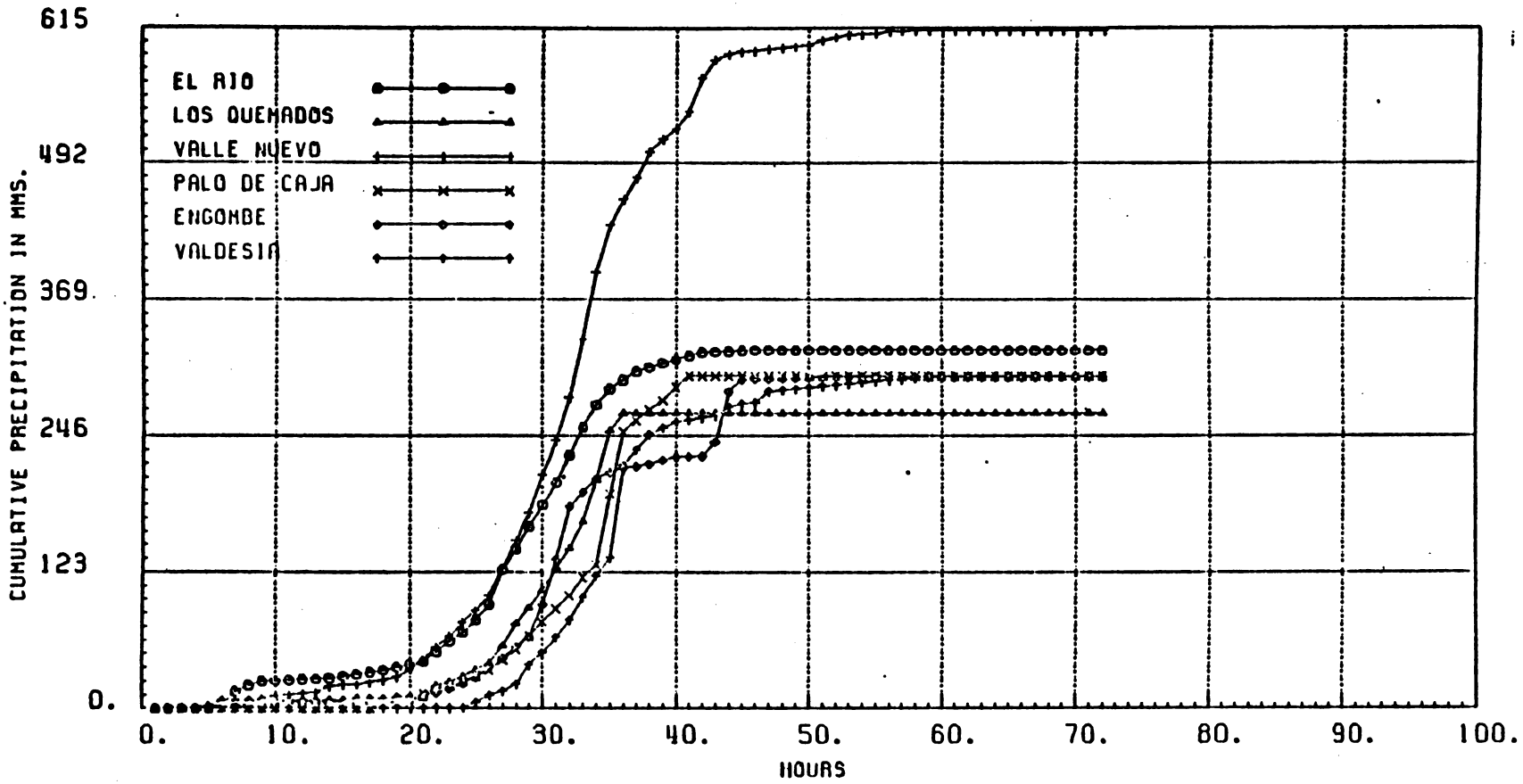

Figure 1.6.A.19

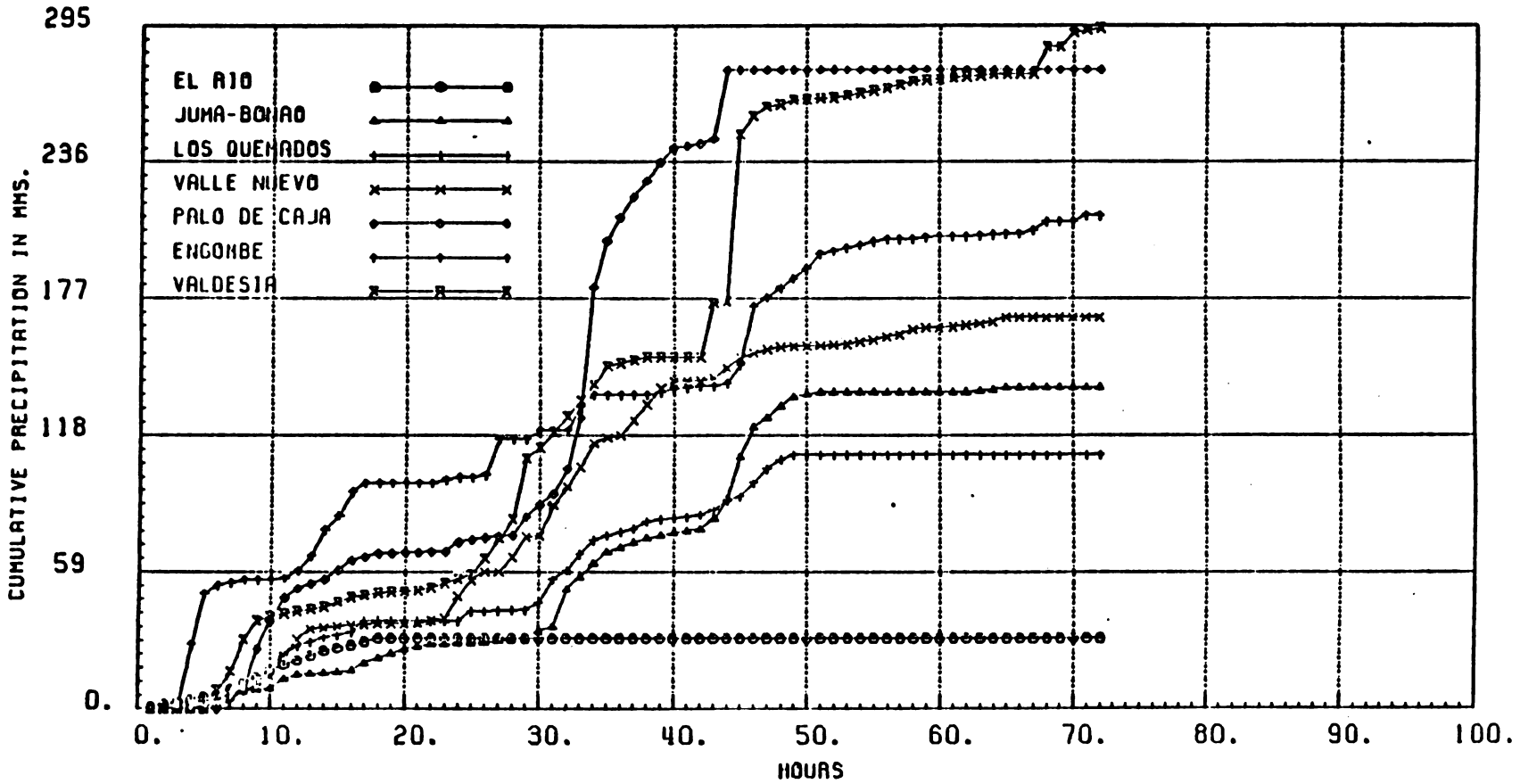

MASS CURVES STORM STARTING 79 SEP 5 8 ENDING 79 SEP 8 8

Figure 1.6.A.20

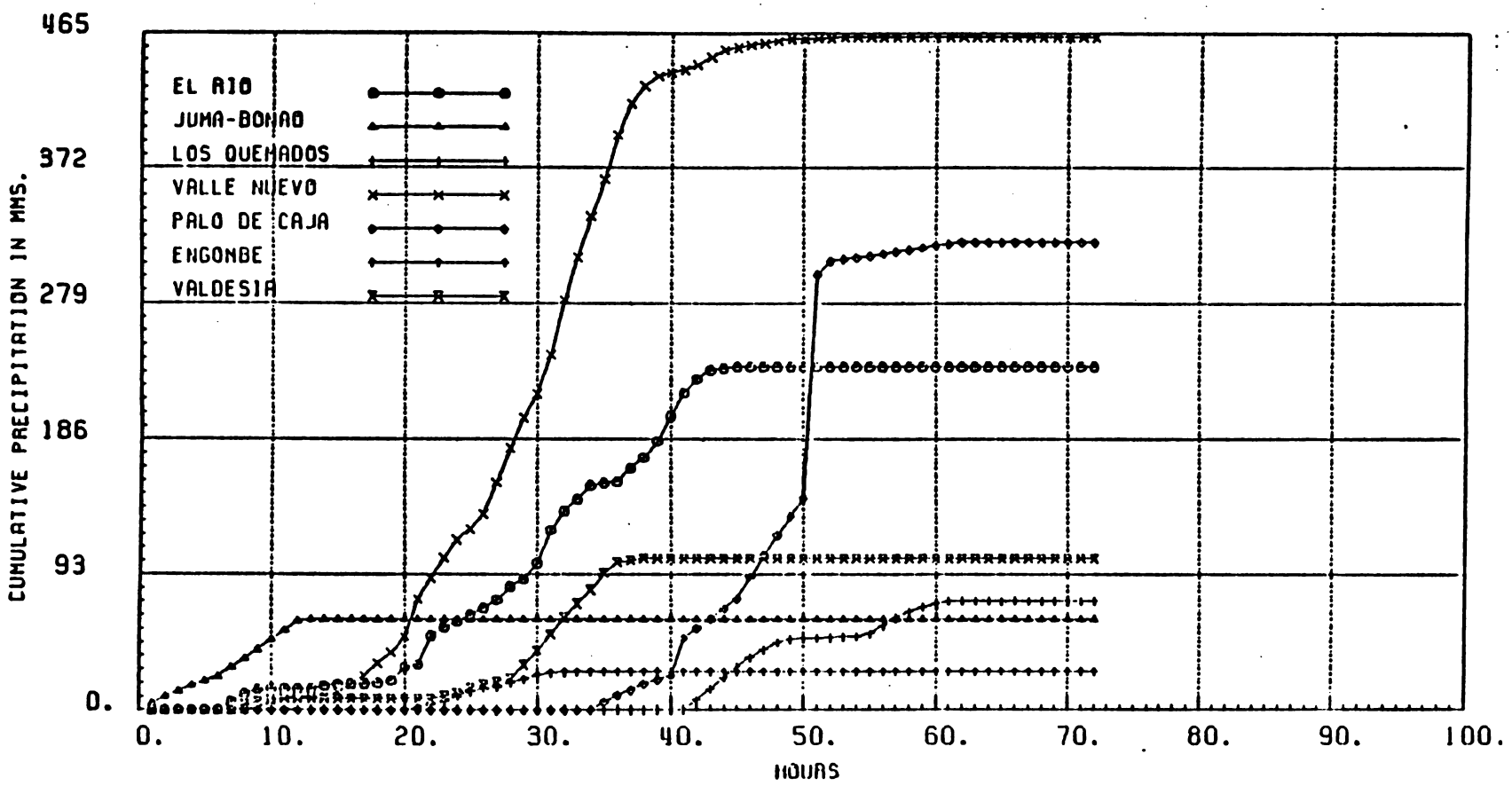

MASS CURVES STORM STARTING 80 AGO 4 8 ENDING 80 AGO 7 8

Figure 1.6.A.21

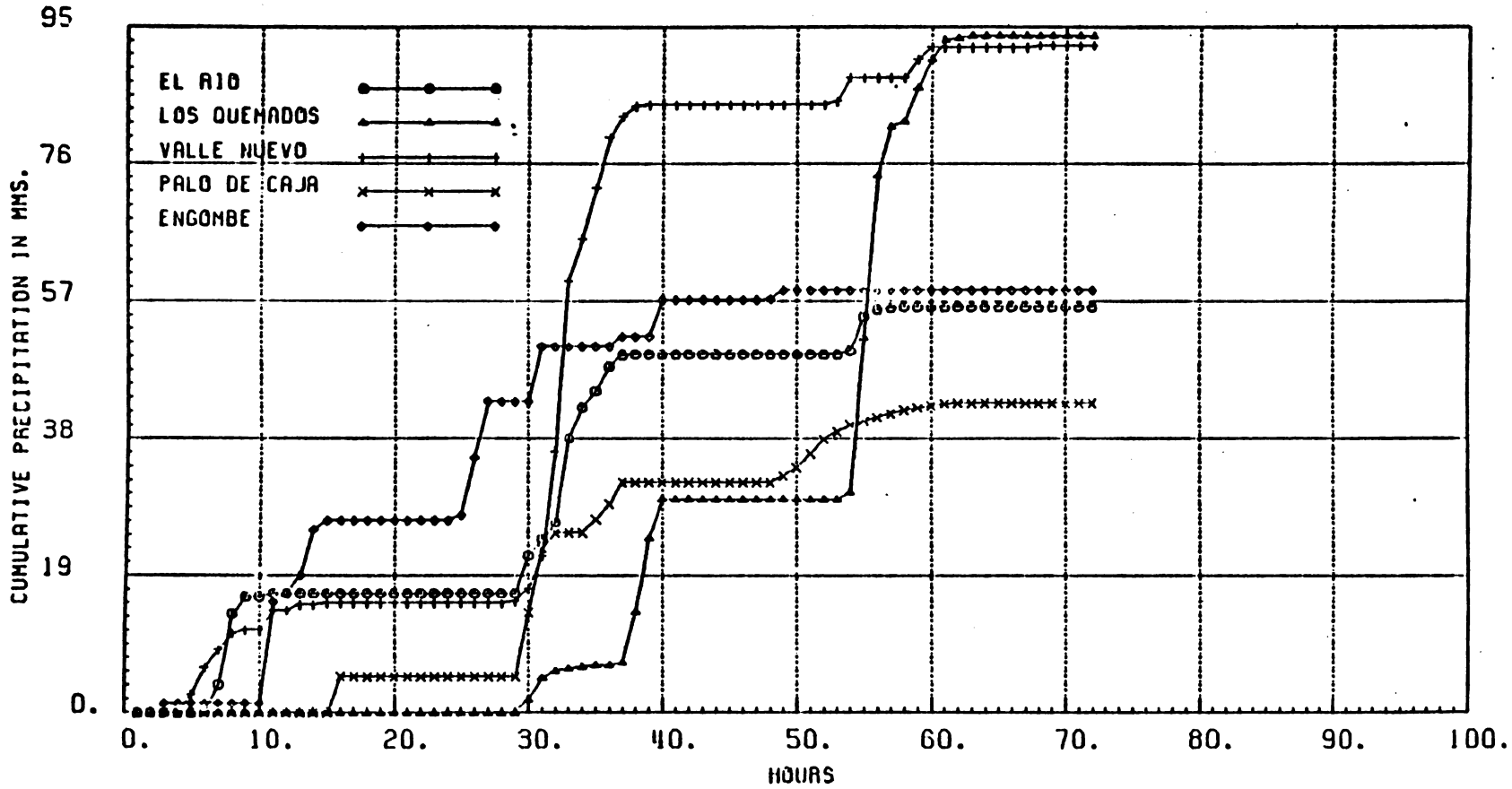

MASS CURVES STORM STARTING 81 MAY 8 8 ENDING 81 MAY 11 8

Figure 1.6.A.22

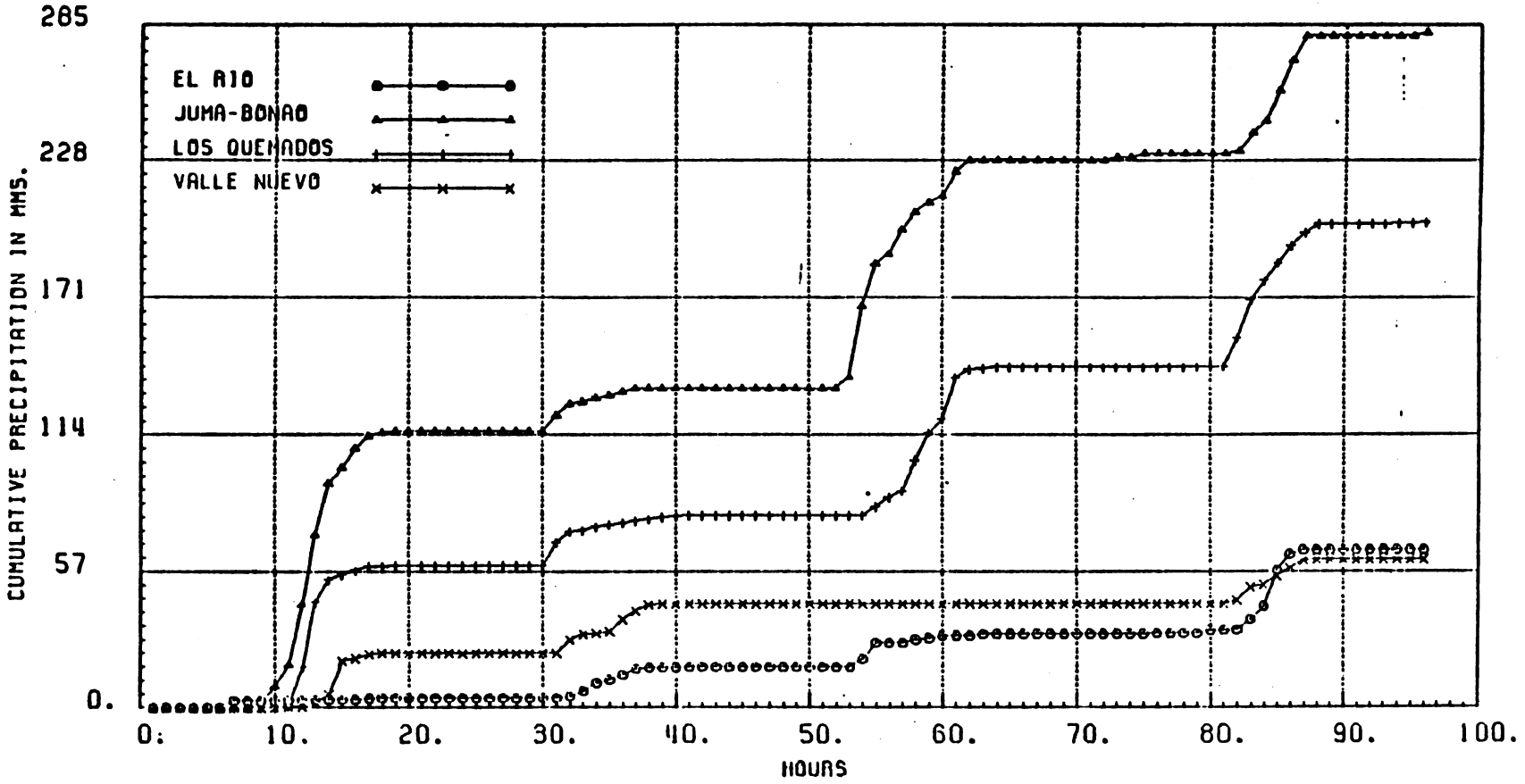

MASS CURVES STORM STARTING 82 MAY 9 8 ENDING 82 MAY 13 8

Figure 1.6.A.23

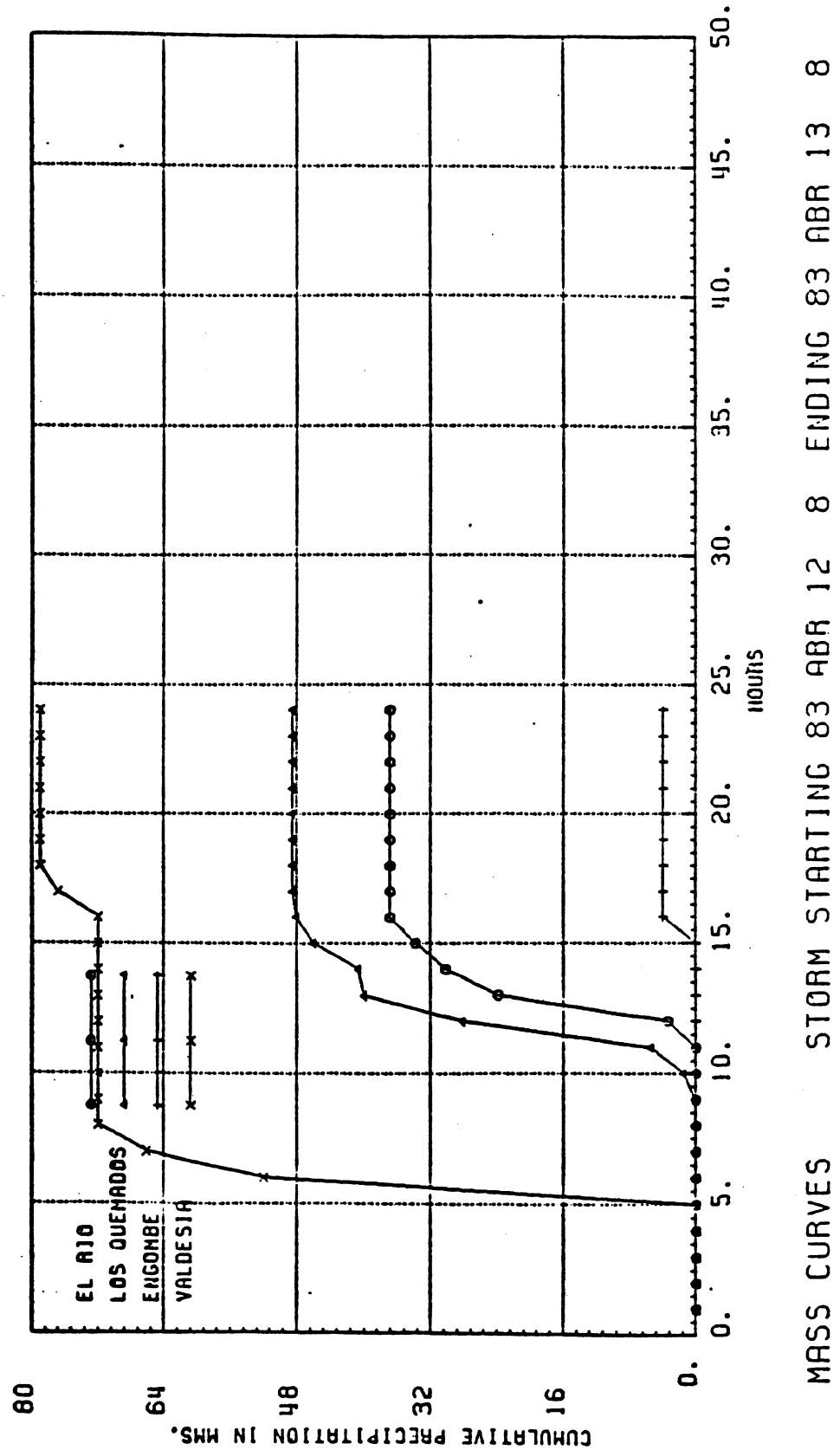

Figure 1.6.A.24

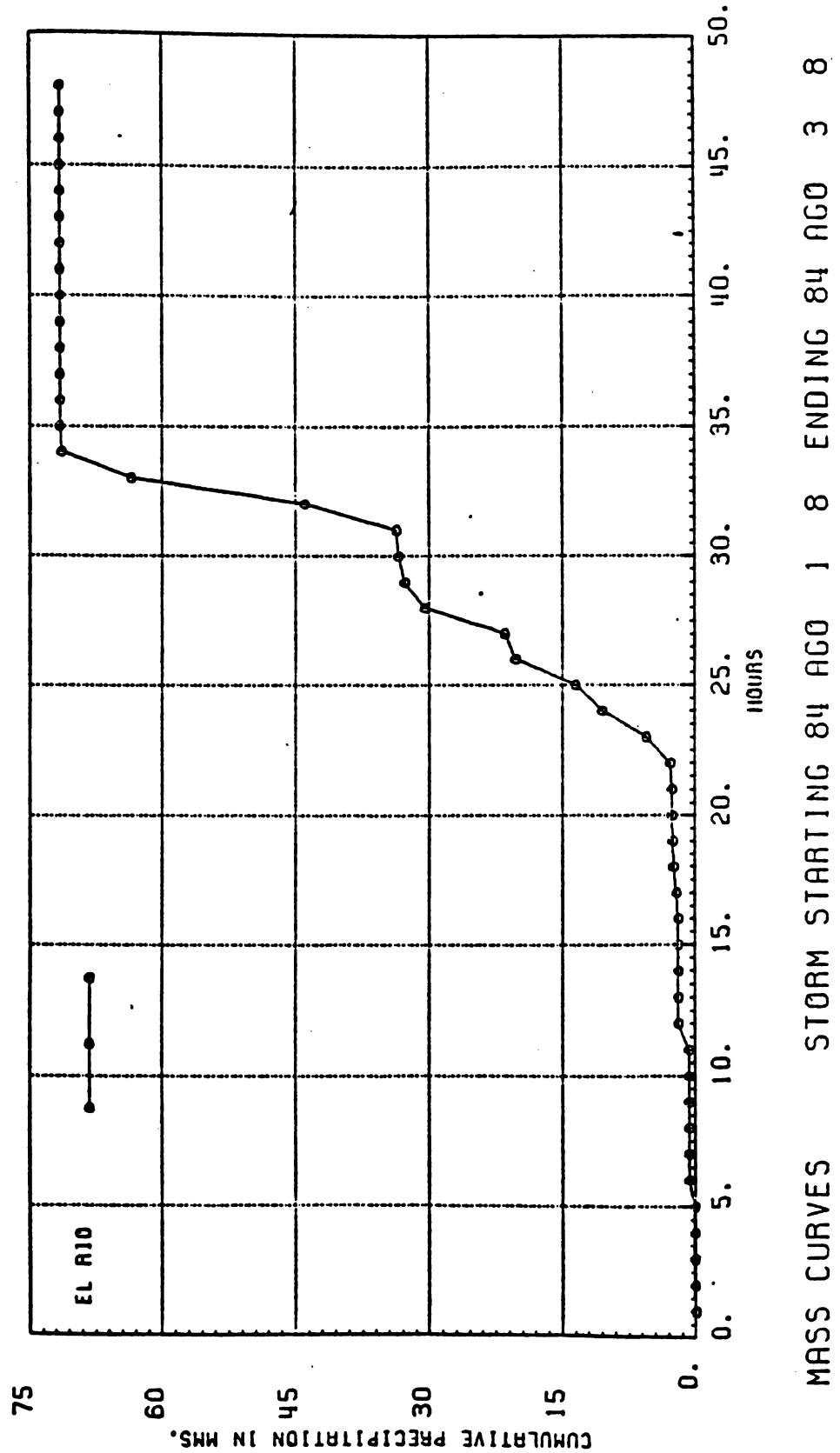

Figure 1.6.A.25

APPENDIX 1.6.B

DEPTH-AREA-DURATION CURVES FOR SELECTED STORMS

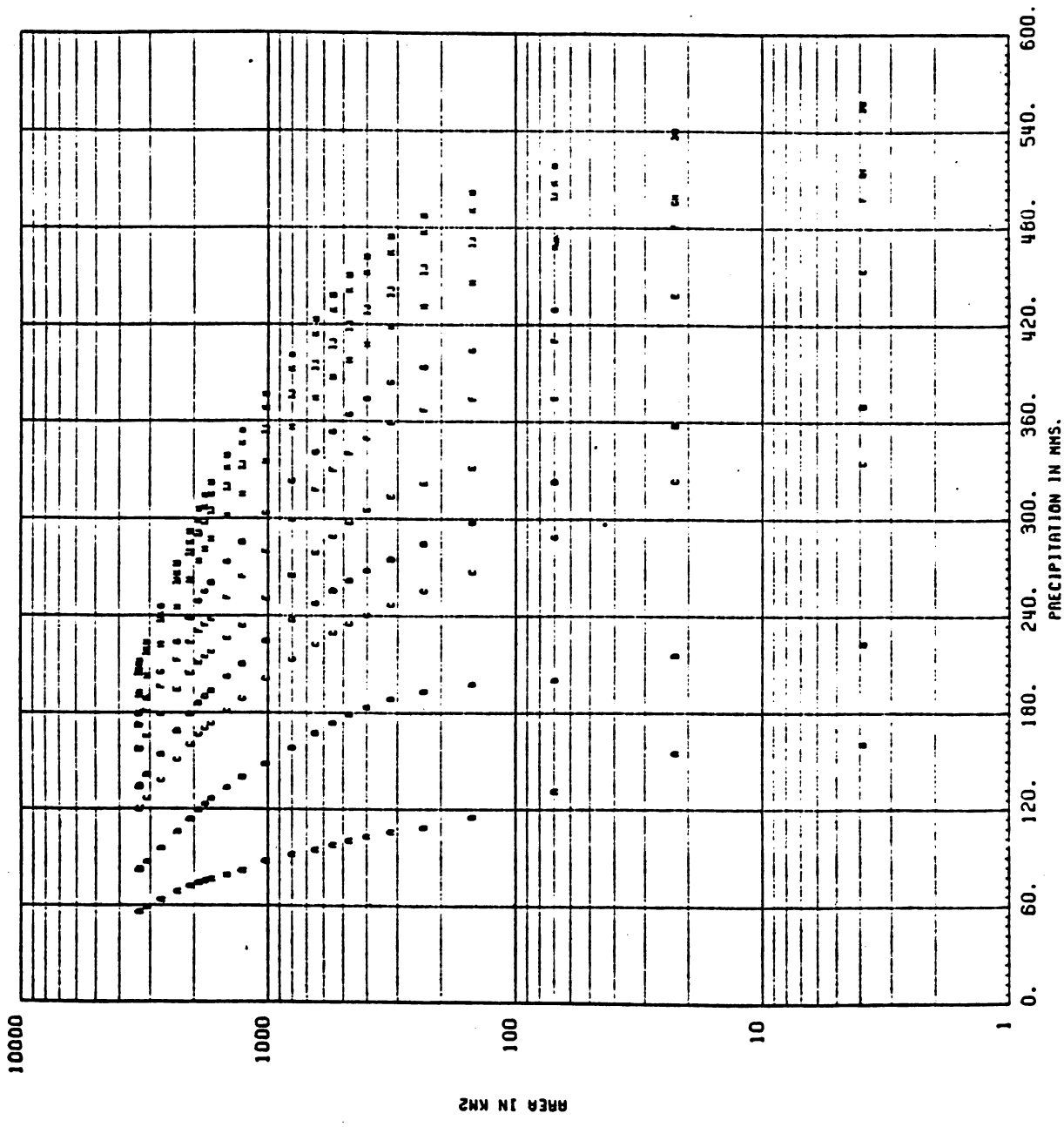
DEPTH AREA DURATION STORM STARTING 63 OCT 1 20 ENDING 63 OCT 5 5
AREA IN KM2
10000
1000
100
10
1
0.
60.
120.
180.
240.
300.
360.
420.
460.
540.
600.
PRECIPITATION IN MMS.

Figure 1.6.B.1

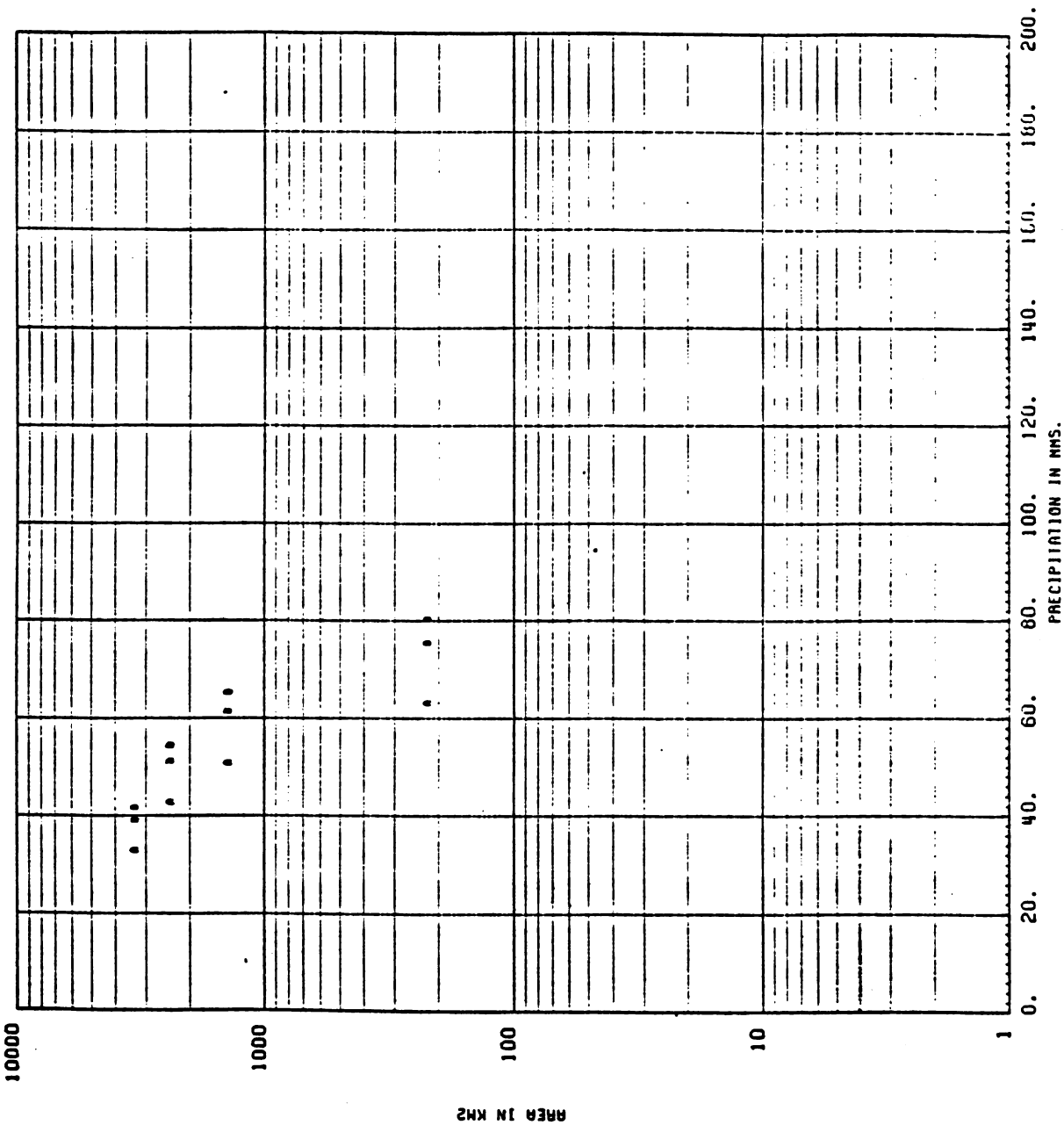
DEPTH AREA DURATION STORM STARTING 64 AGO 6 8 ENDING 64 AGO 7 8
AREA IN KM2
10000
1000
100
10
1
0.
20.
40.
60.
80.
100.
120.
140.
160.
180.
200.
PRECIPITATION IN MMS.

Figure 1.6.B.2.

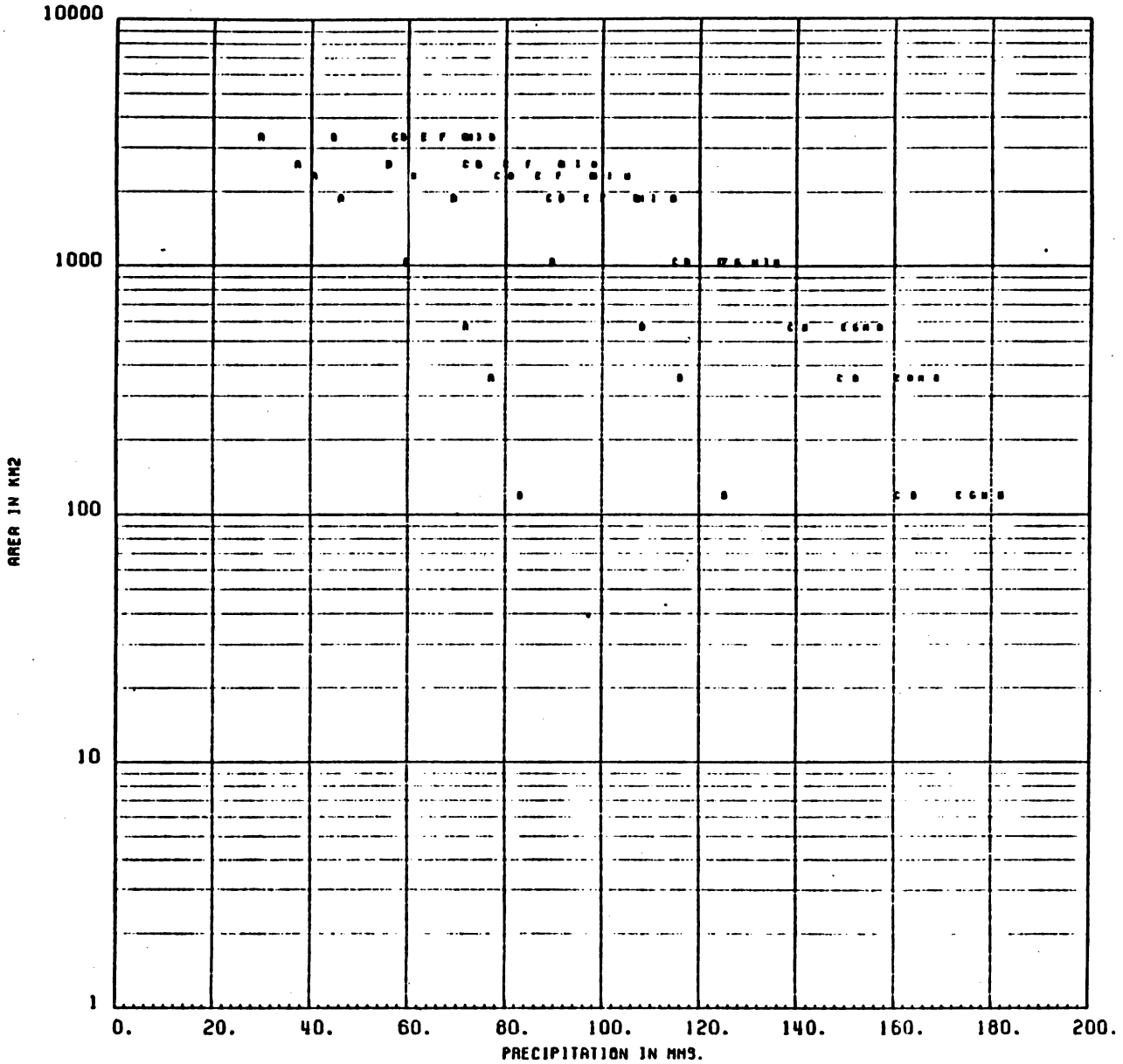
10000
1000
100
10
1
AREA IN KM2
0.
20.
40.
60.
80.
100.
120.
140.
160.
180.
200.
PRECIPITATION IN MMS.
DEPTH AREA DURATION STORM STARTING 65 MAY 2 8 ENDING 65 MAY 5 8

Figure 1.6.B.3.

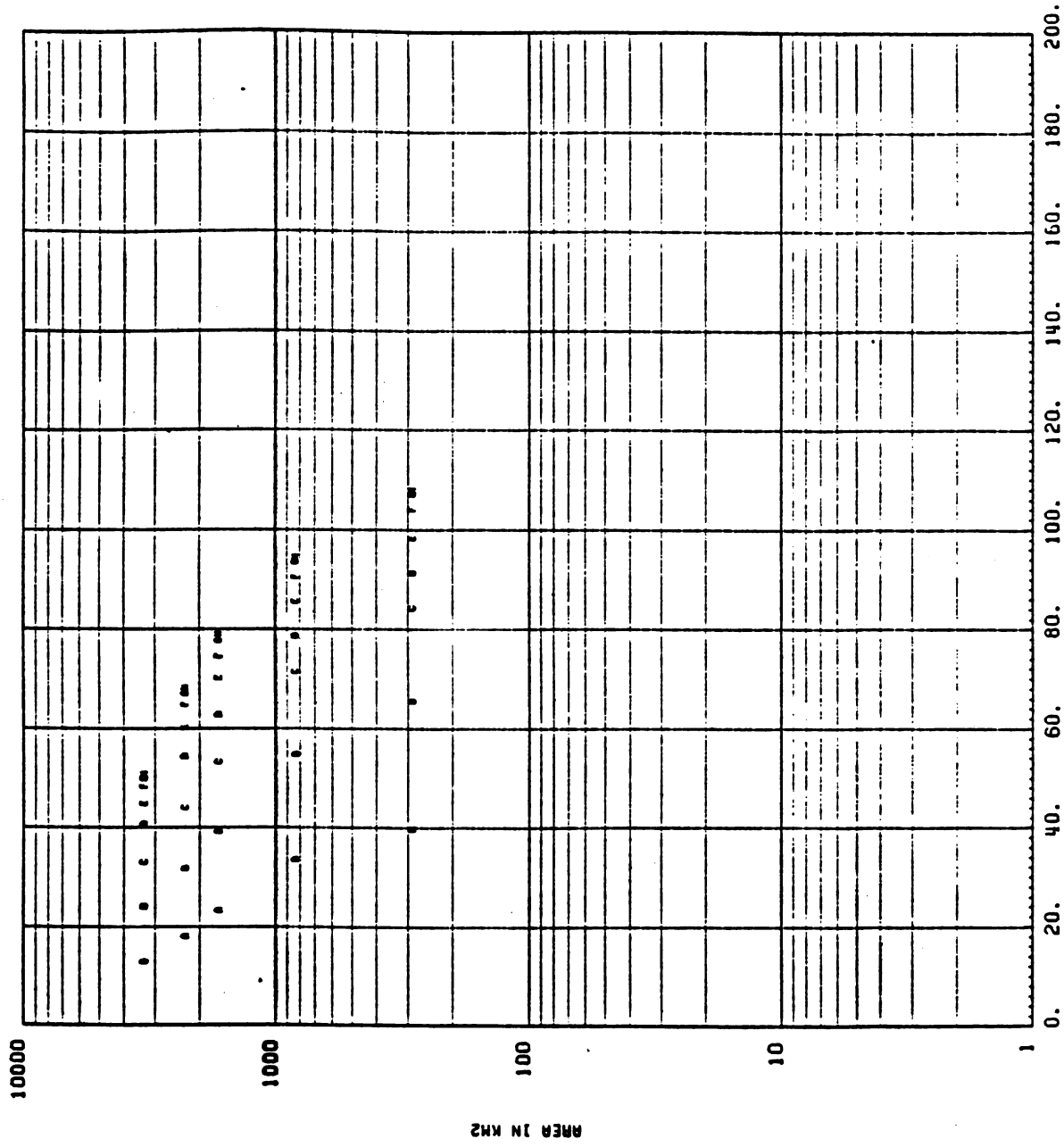
DEPTH AREA DURATION STORM STARTING 66 MAY 25 8 ENDING 66 MAY 27 8
AREA IN KM2
10000
1000
100
10
1
0.
20.
40.
60.
80.
100.
120.
140.
160.
180.
200.
PRECIPITATION IN MMS.

Figure 1.6.B.4.

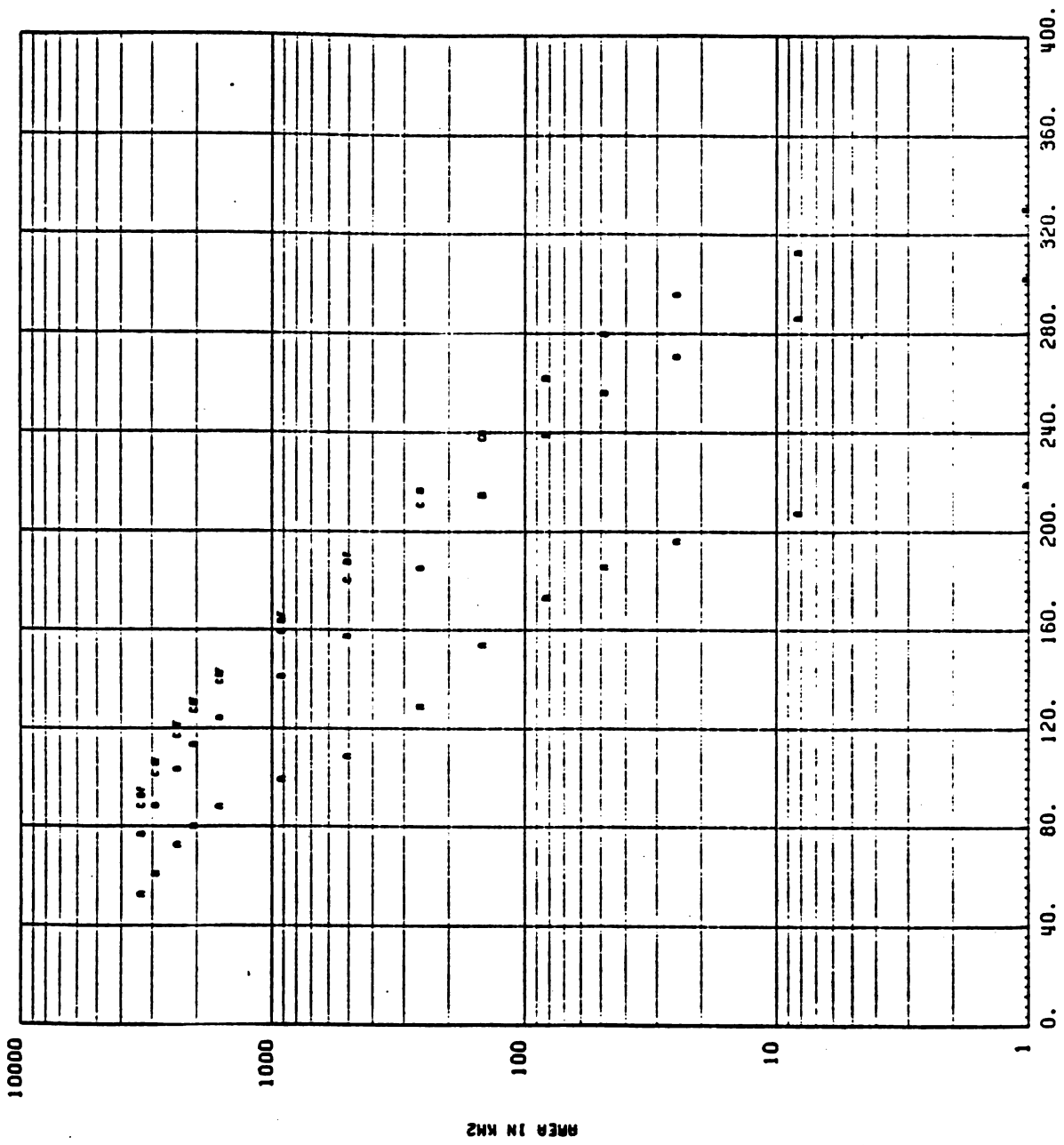
DEPTH AREA DURATION STORM STARTING 66 SEP 28 20 ENDING 66 SEP 30 8
AREA IN KM2
10000
1000
100
10
1
0.
40.
80.
120.
160.
200.
240.
280.
320.
360.
400.
PRECIPITATION IN MMS.

Figure 1.6.B.5.

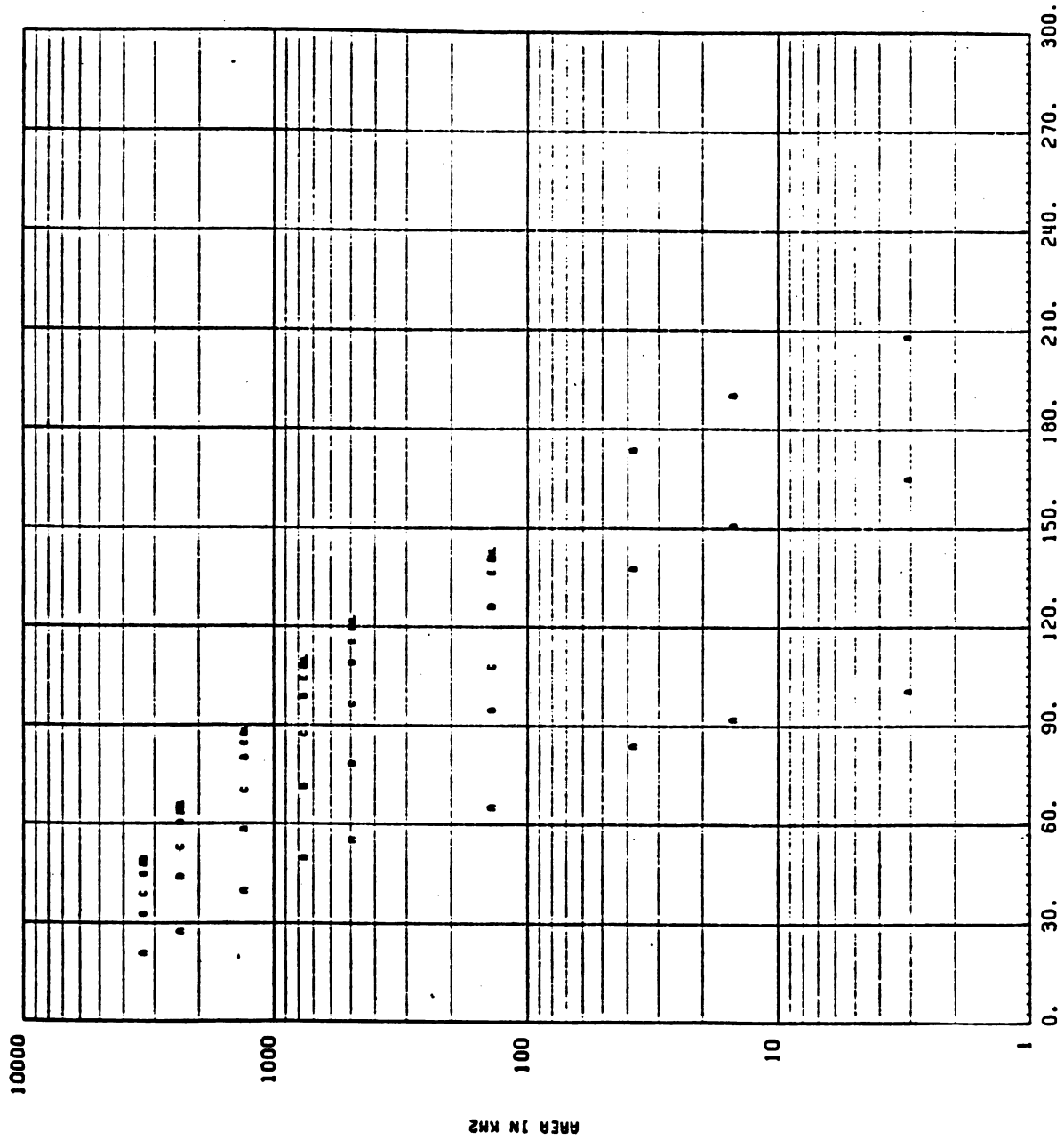
DEPTH AREA DURATION STORM STARTING 67 SEP 10 8 ENDING 67 SEP 13 8
AREA IN KM2
10000
1000
100
10
1
0.
30.
60.
90.
120.
150.
180.
210.
240.
270.
300.
PRECIPITATION IN MMS.

Figure I.6.B.6.

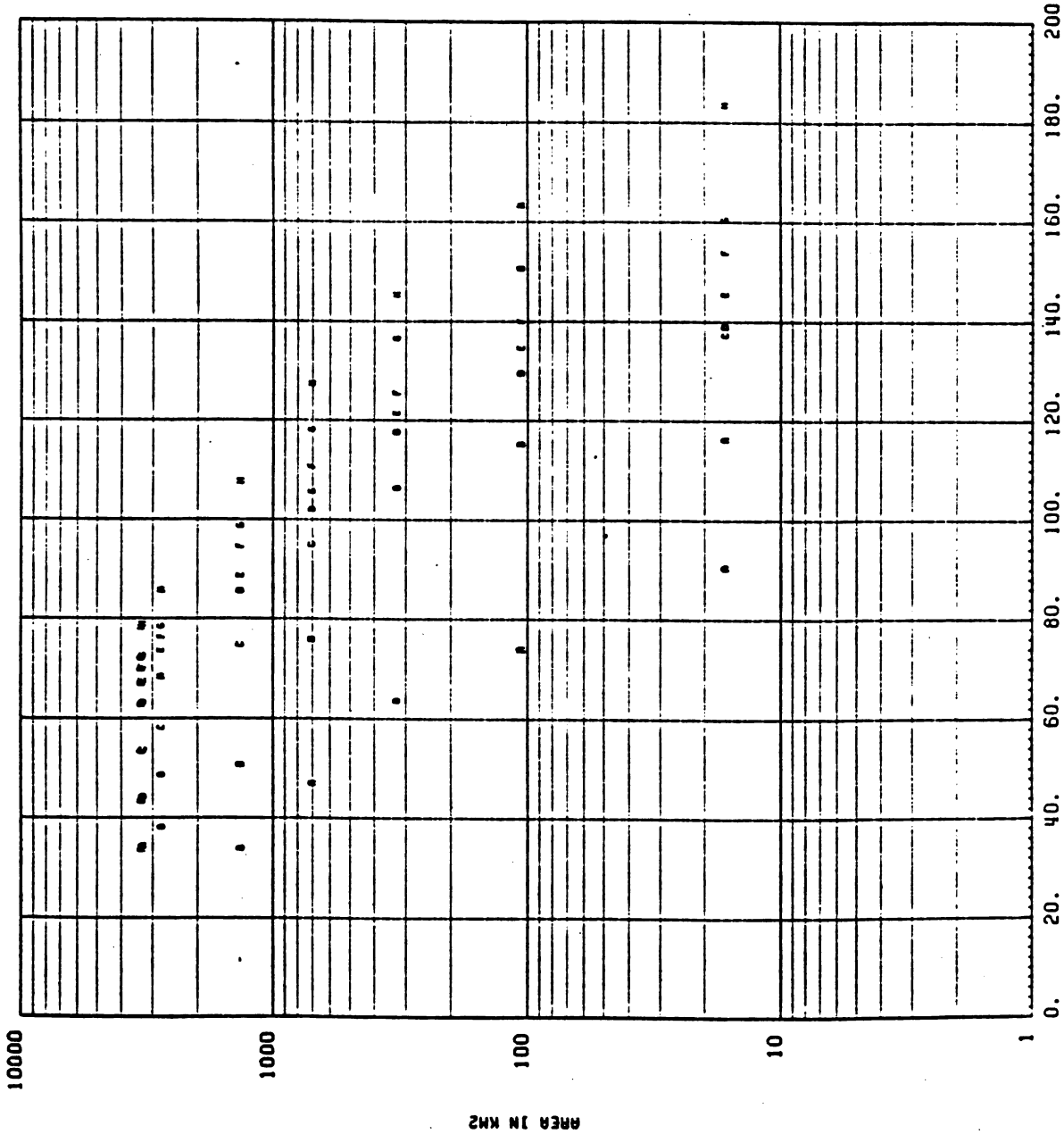
DEPTH AREA DURATION STORM STARTING 68 AGO 8 8 ENDING 68 AGO 10 8
AREA IN KM2
10000
1000
100
10
1
0.
20.
40.
60.
80.
100.
120.
140.
160.
180.
200.
PRECIPITATION IN MMS.

Figure I.6.B.7.

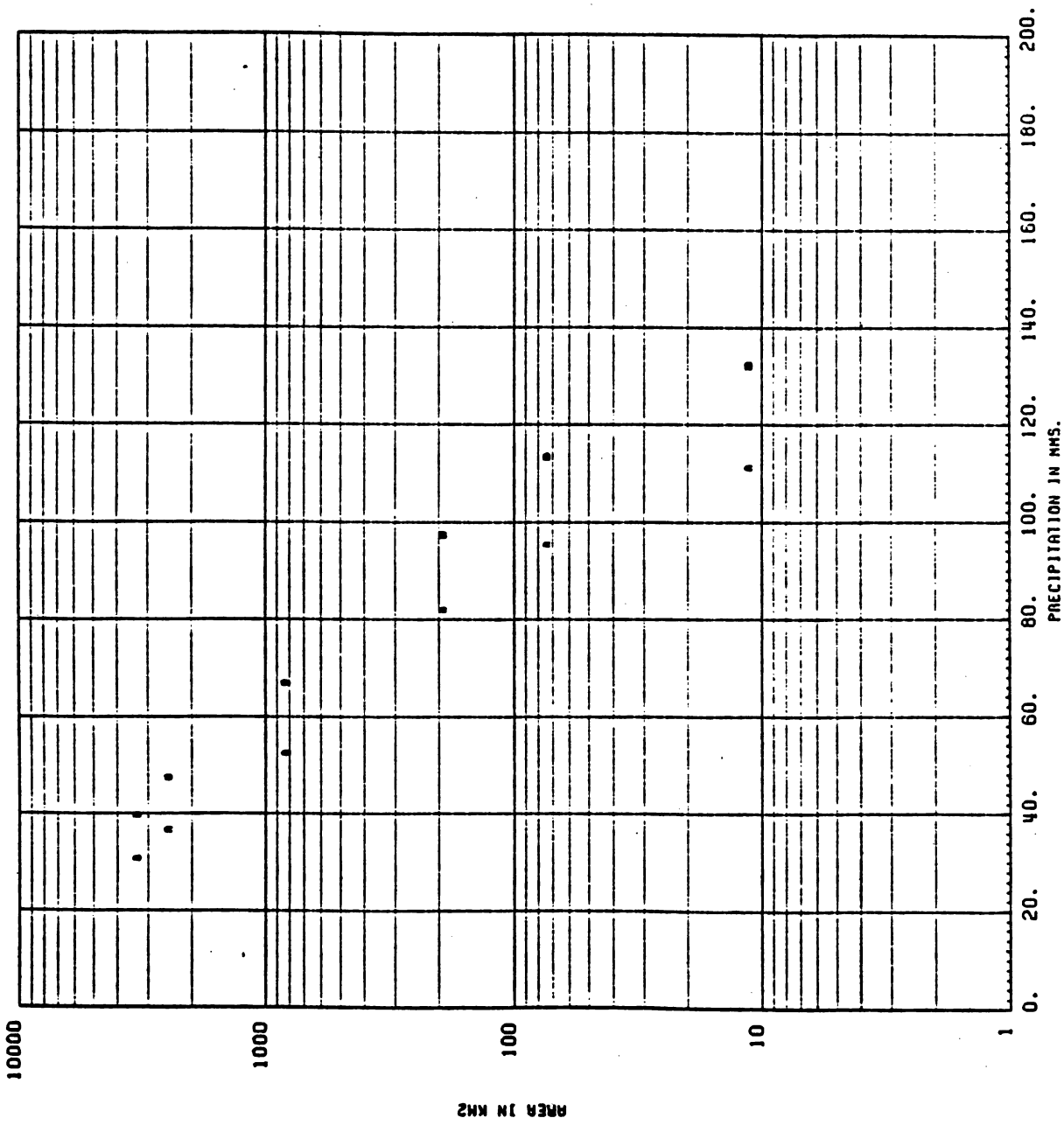
DEPTH AREA DURATION STORM STARTING 69 JUL 19 8 ENDING 69 JUL 20 8
AREA IN KM2
10000
1000
100
10
1
0.
20.
40.
60.
80.
100.
120.
140.
160.
180.
200.
PRECIPITATION IN MMS.

Figure 1.6.B.8.

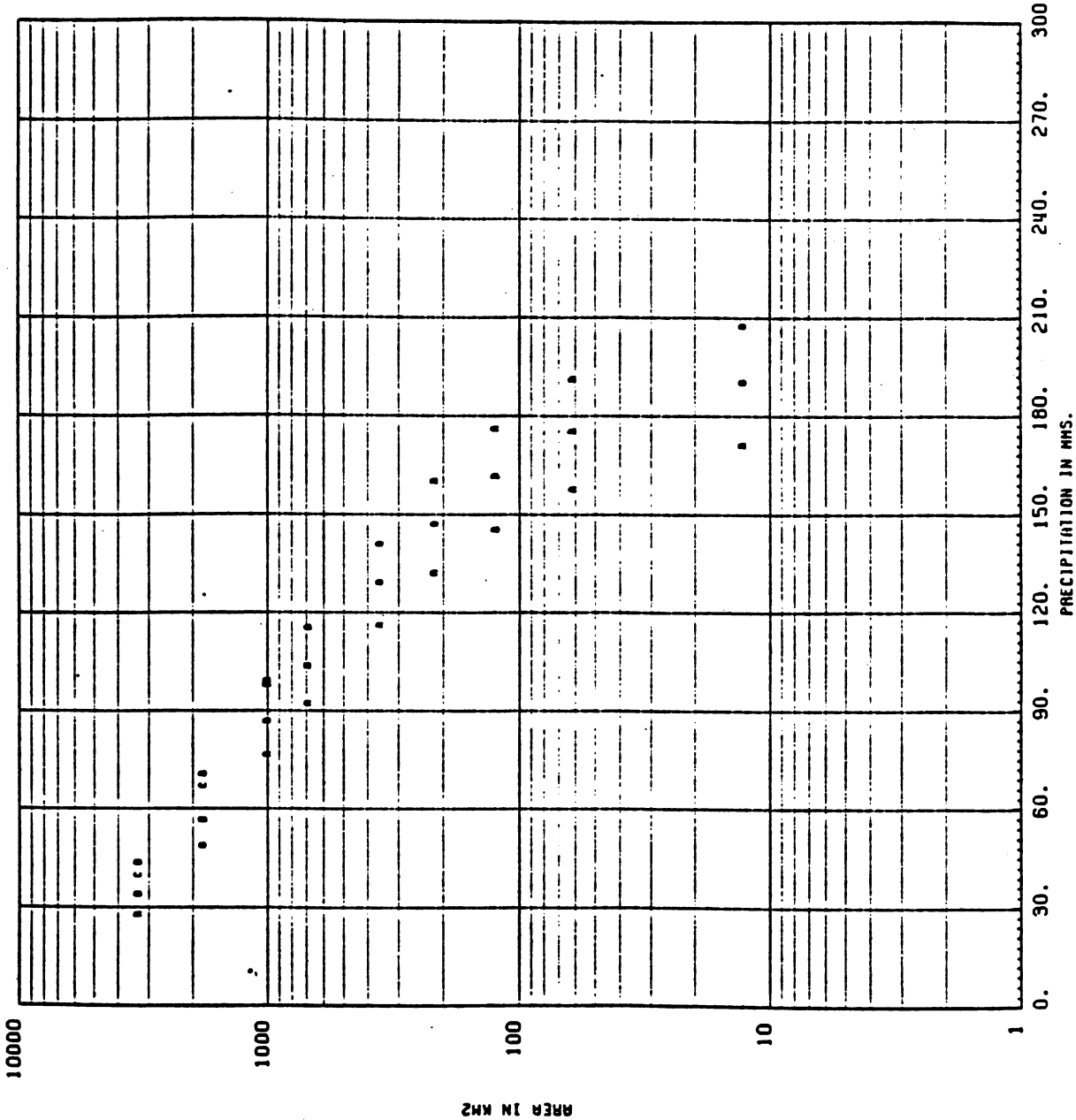
DEPTH AREA DURATION STORM STARTING 70 AGO 22 8 ENDING 70 AGO 23 8
AREA IN KM2
10000
1000
100
10
1
0.
30.
60.
90.
120.
150.
180.
210.
240.
270.
300.
PRECIPITATION IN MMS.

Figure 1.6.B.9.

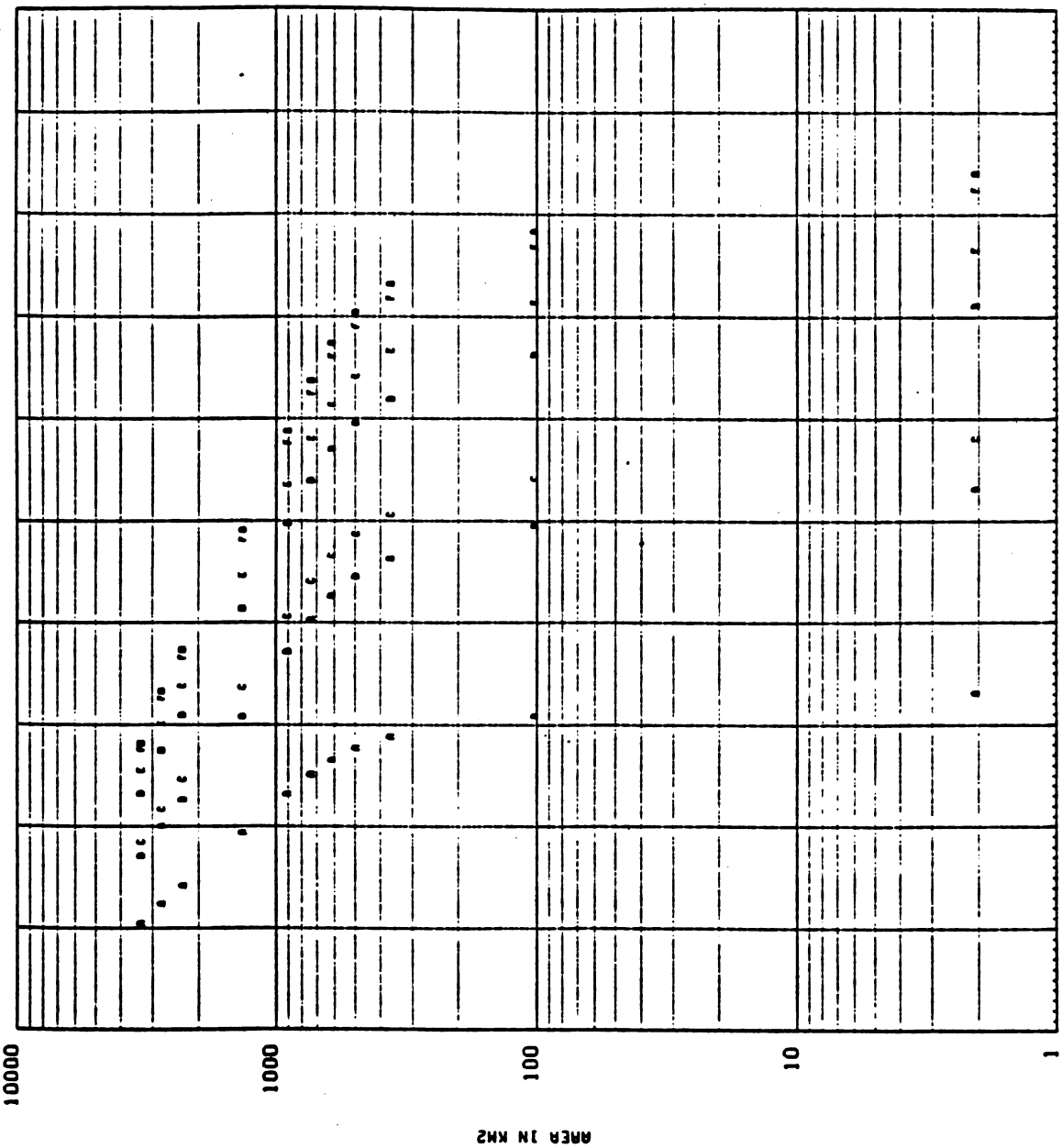

Figure 1.6.B.10

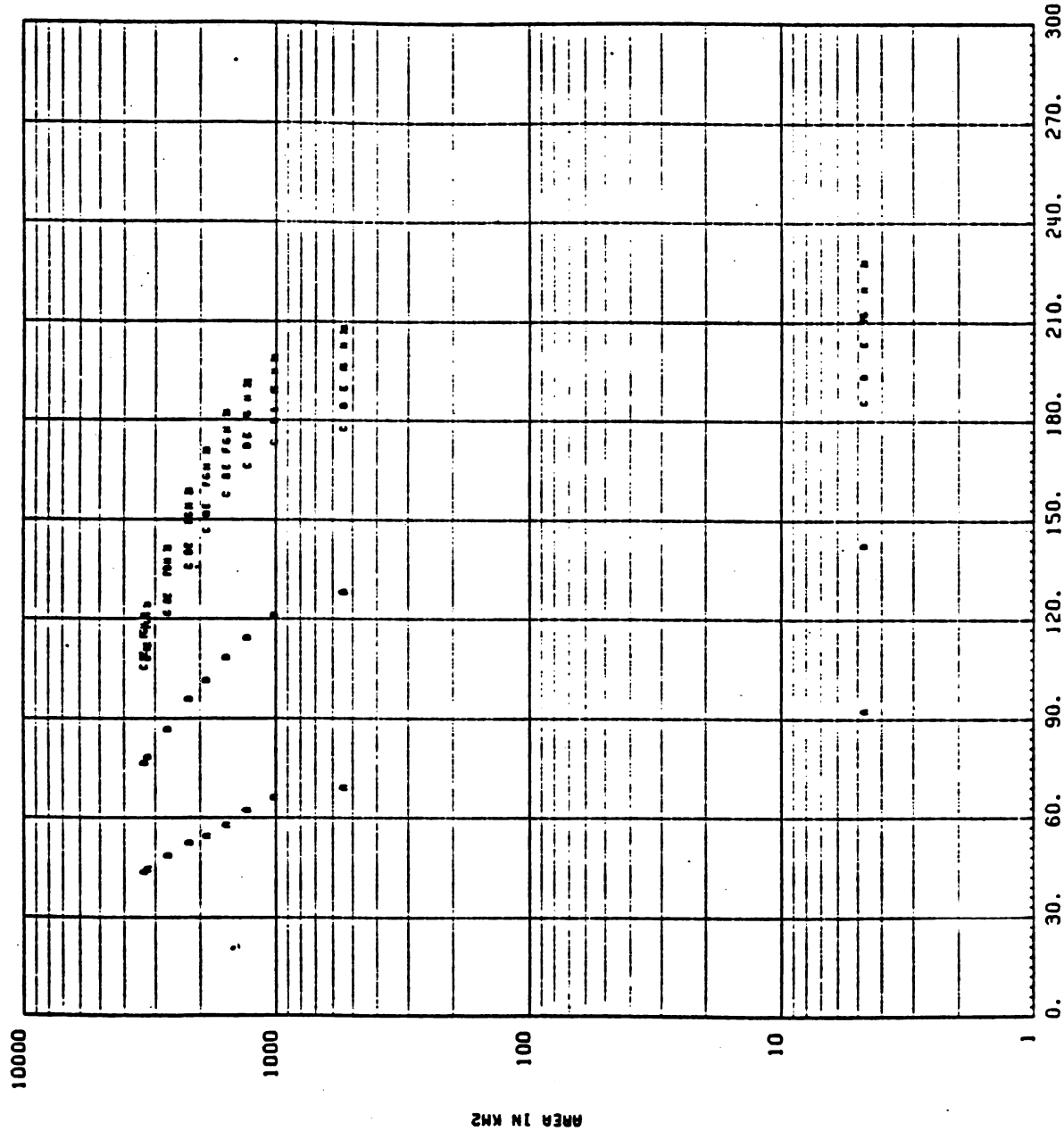

Figure 1.6.B.11.

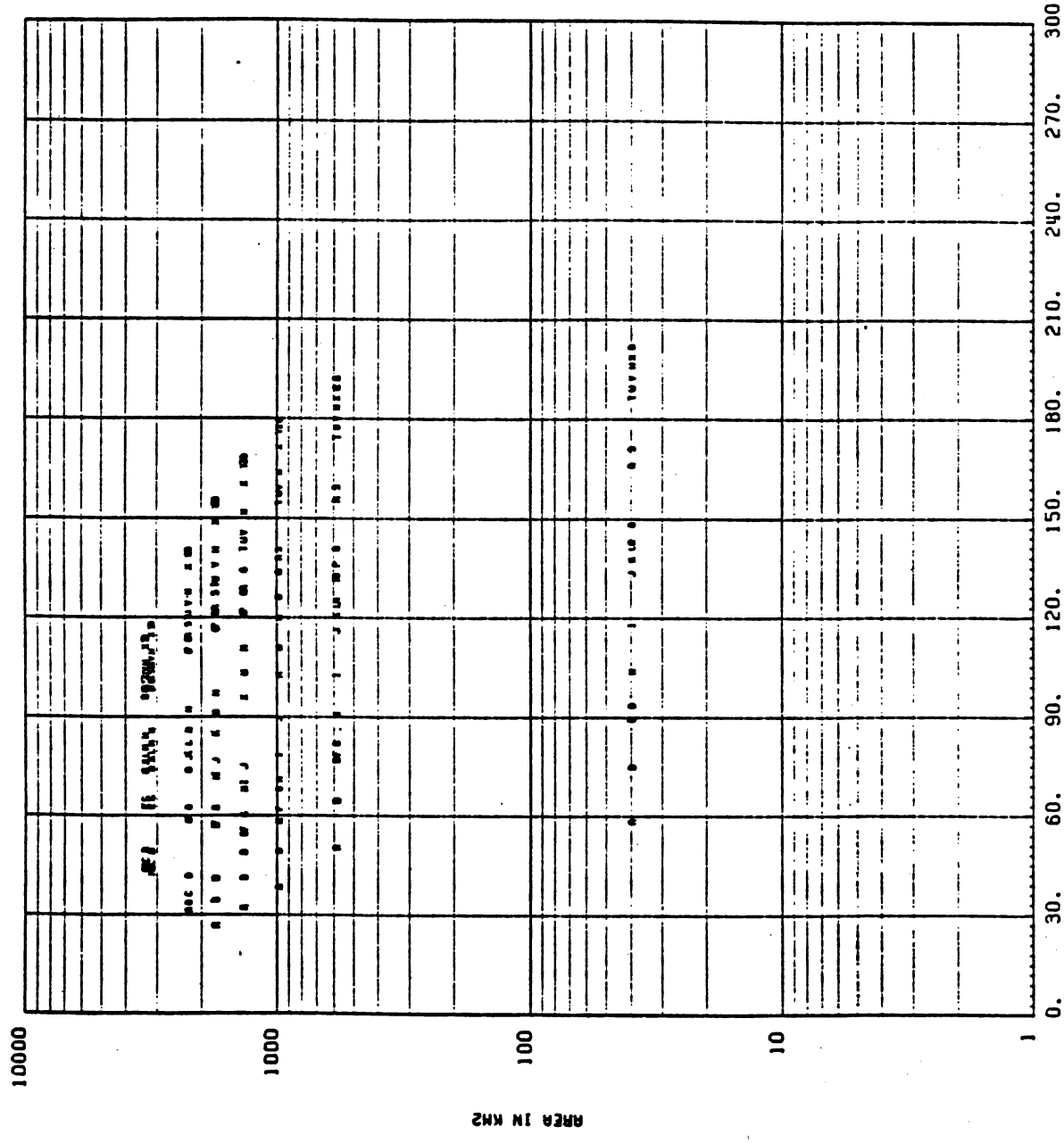

DEPTH AREA DURATION STORM STARTING 73 OCT 14 8 ENDING 73 OCT 21 8

Figure 1.6.B.12

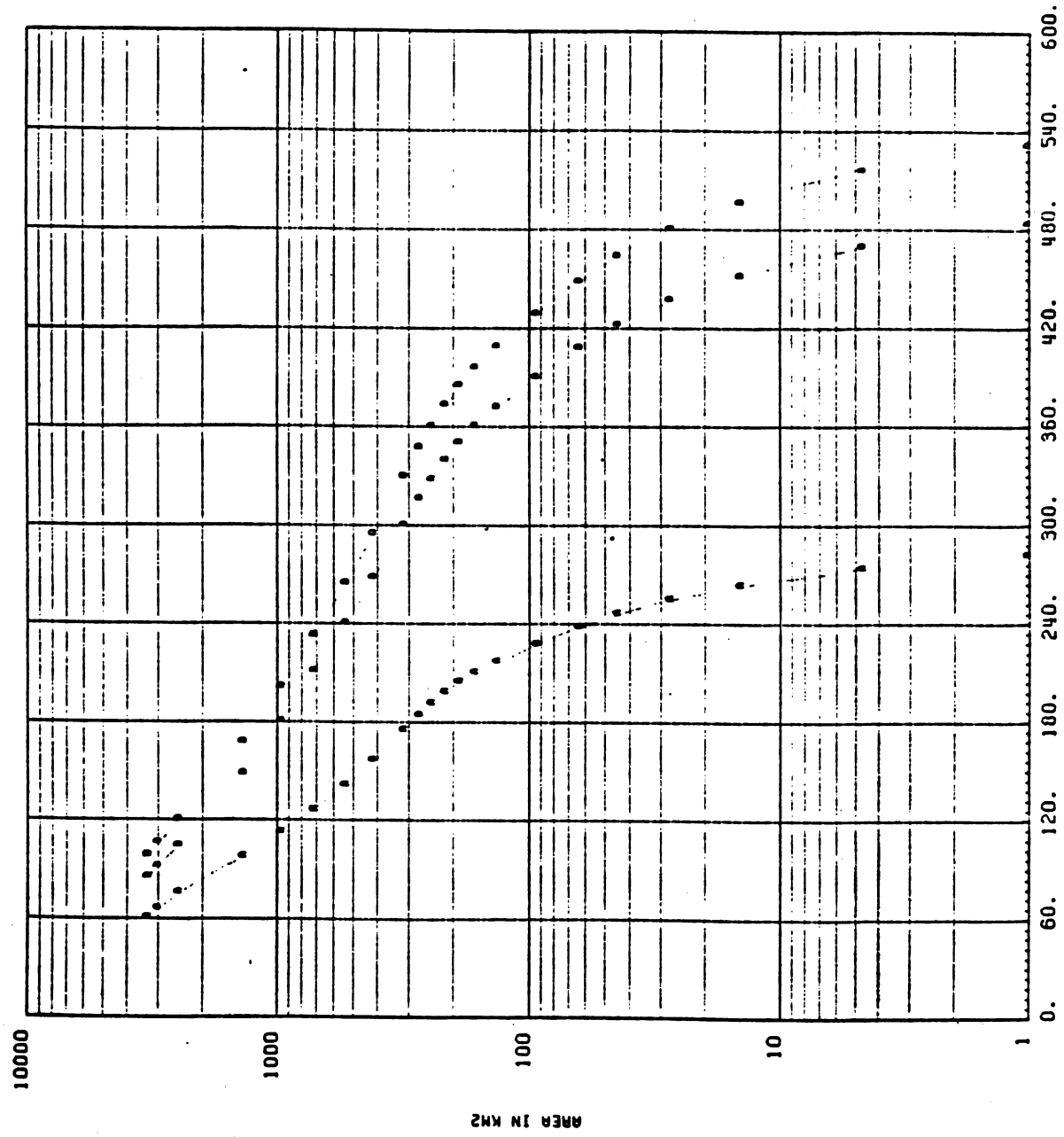

Figure 1.6.B.13.

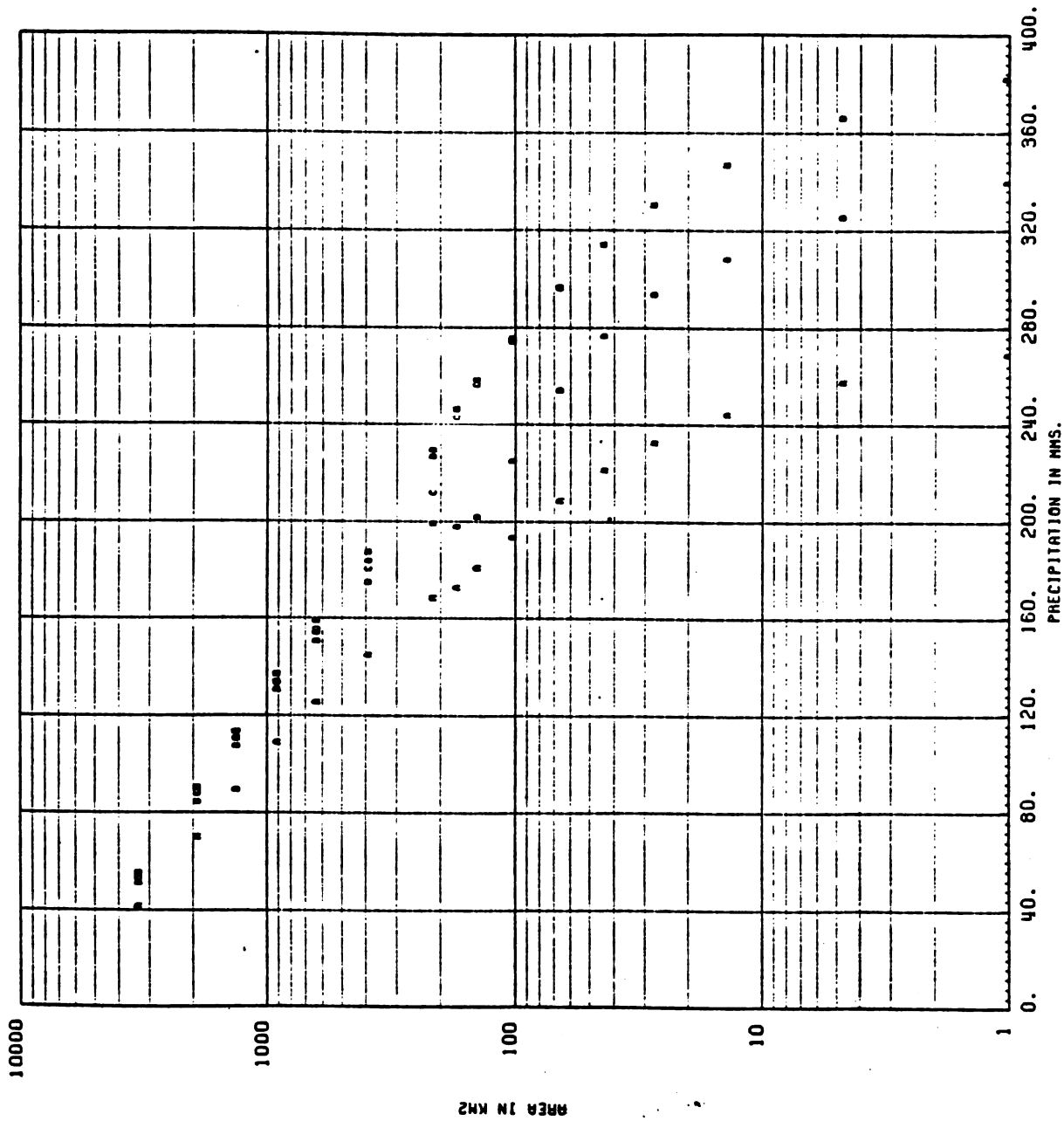

Figure 1.6.B.14

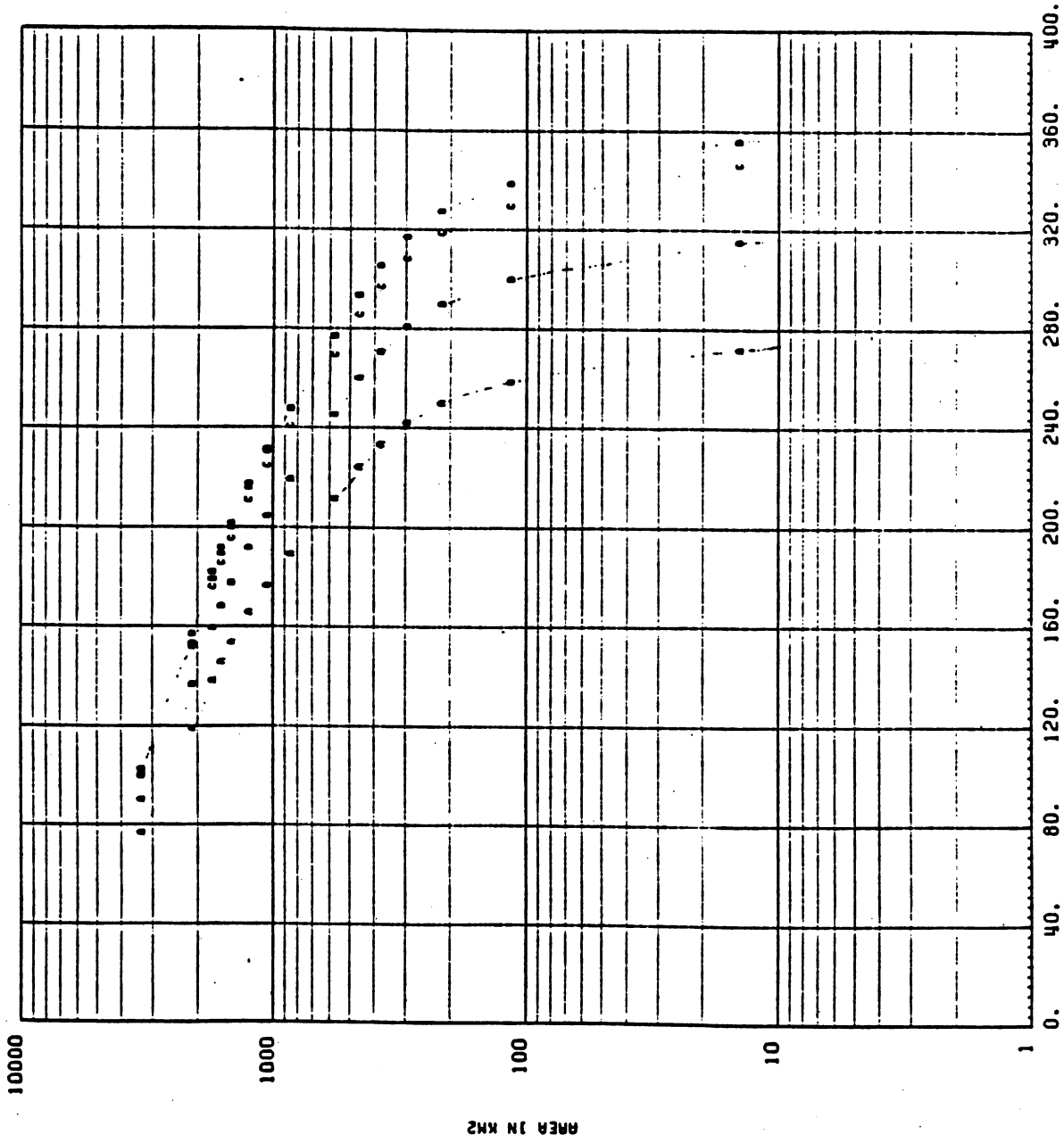

Figure 1.0.B.15

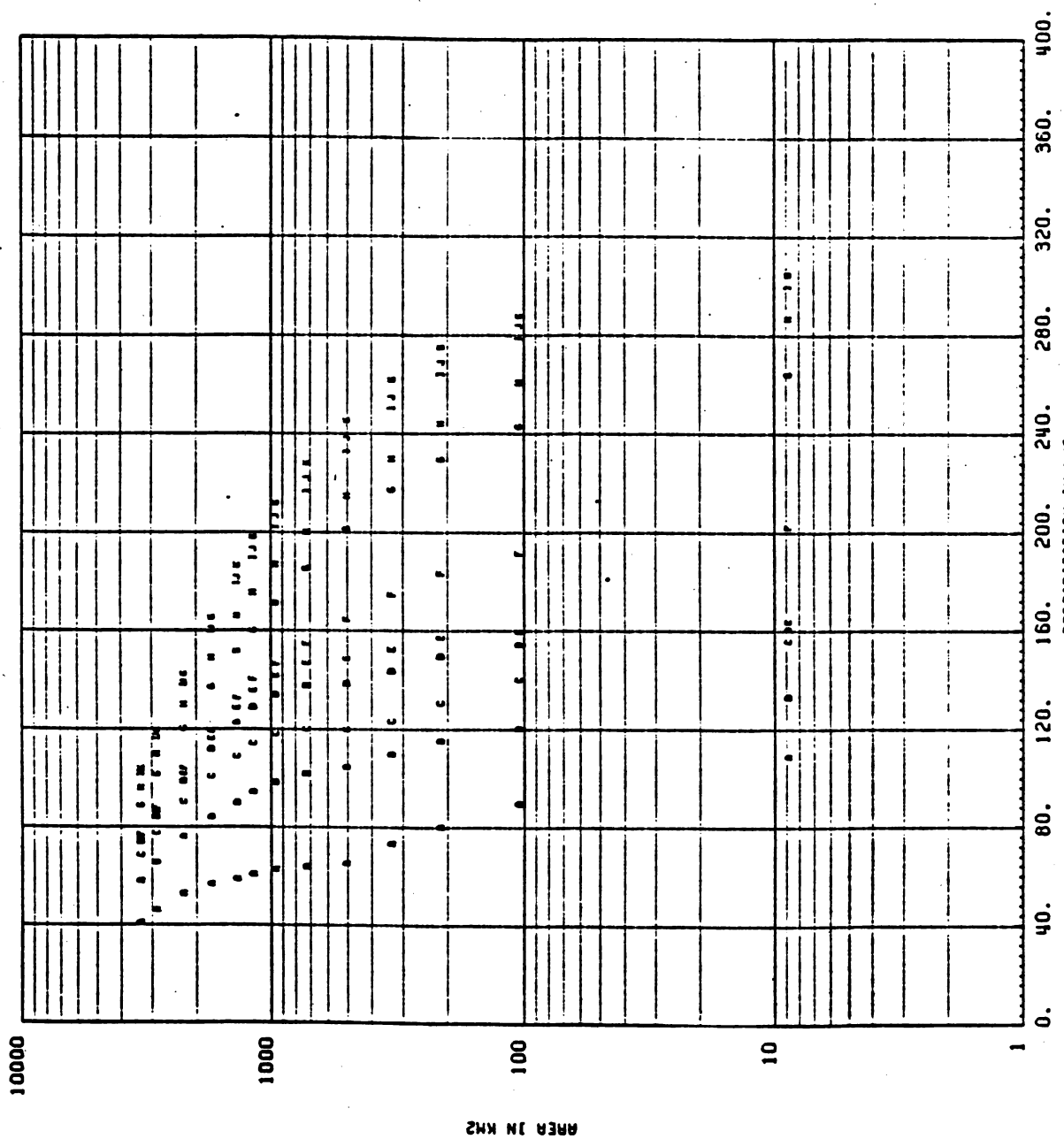

Figure 1.6.B.16

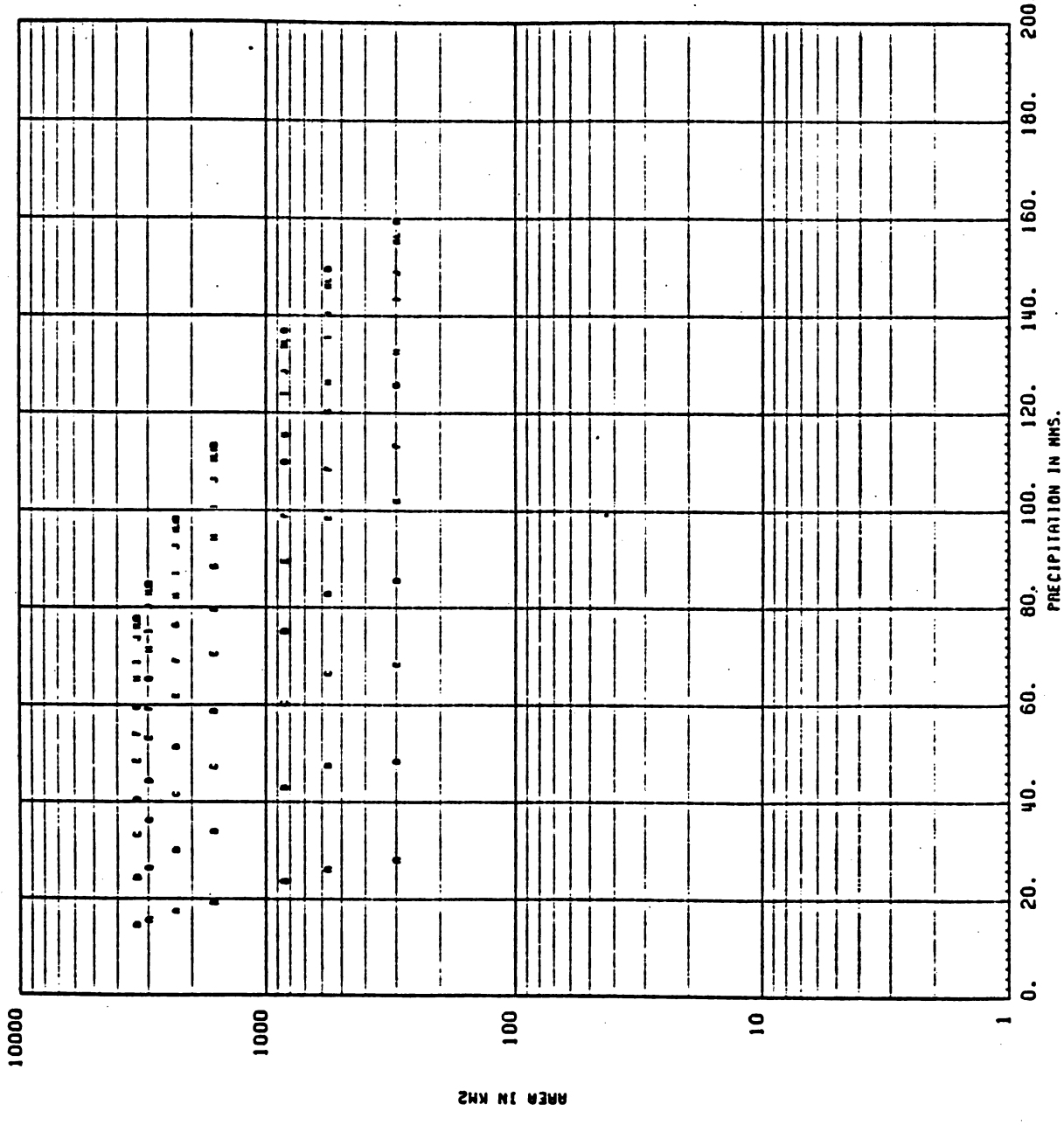

DEPTH AREA DURATION STORM STARTING 77 DIC 28 8 ENDING 78 ENE 1 8

Figure 1.6.B.17

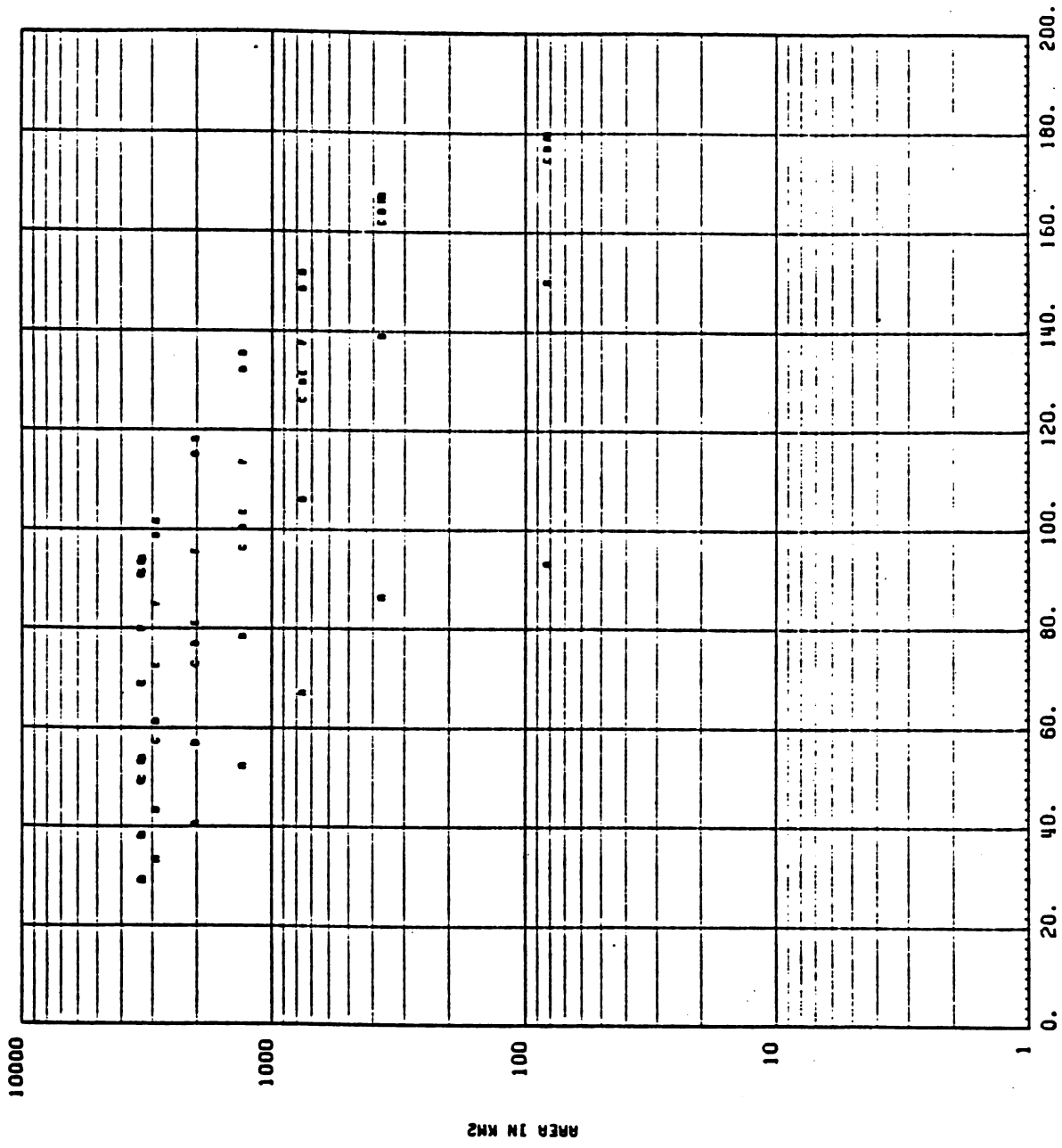

Figure 1.6.B.18

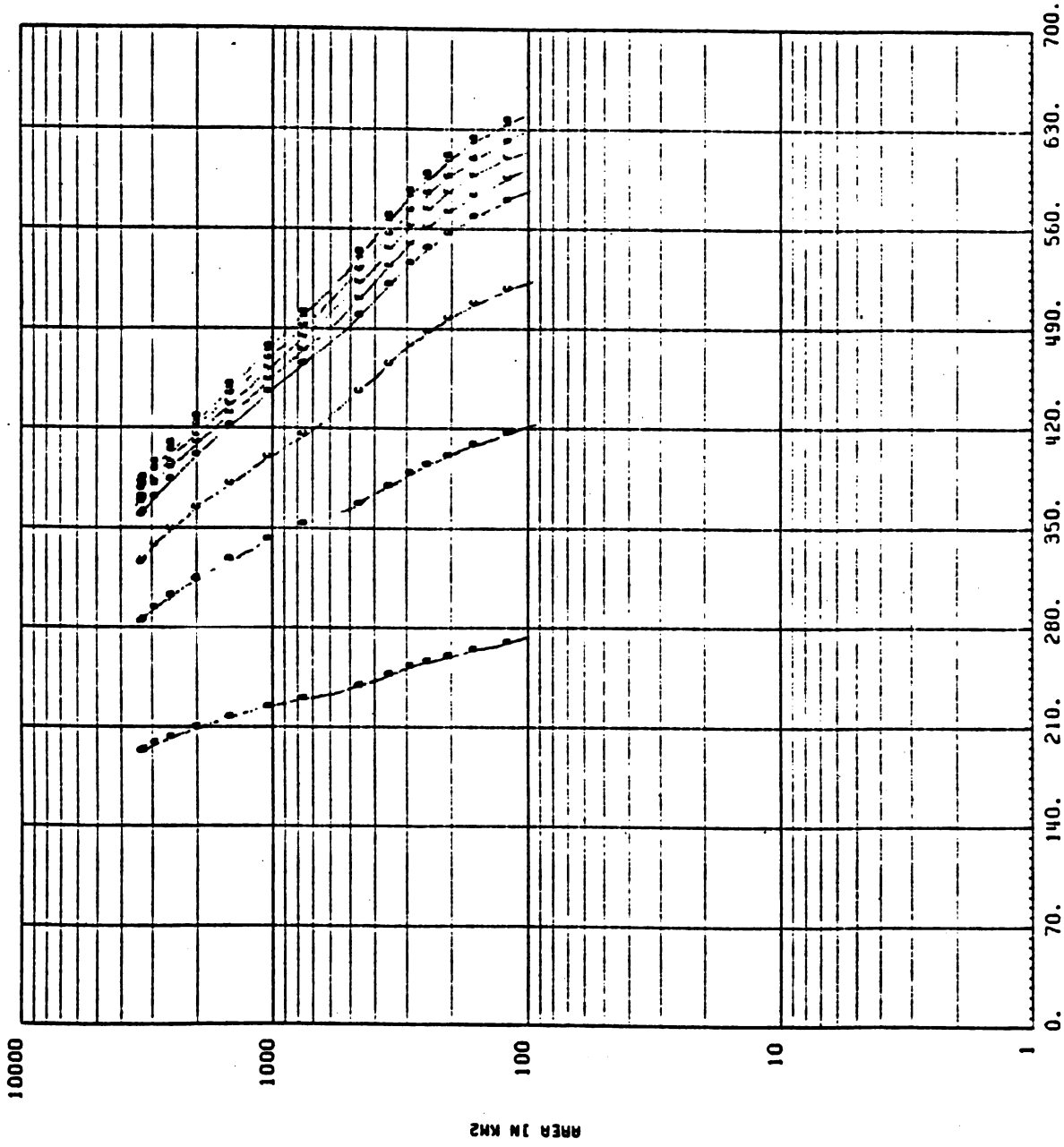

Figure 1.6.B.19

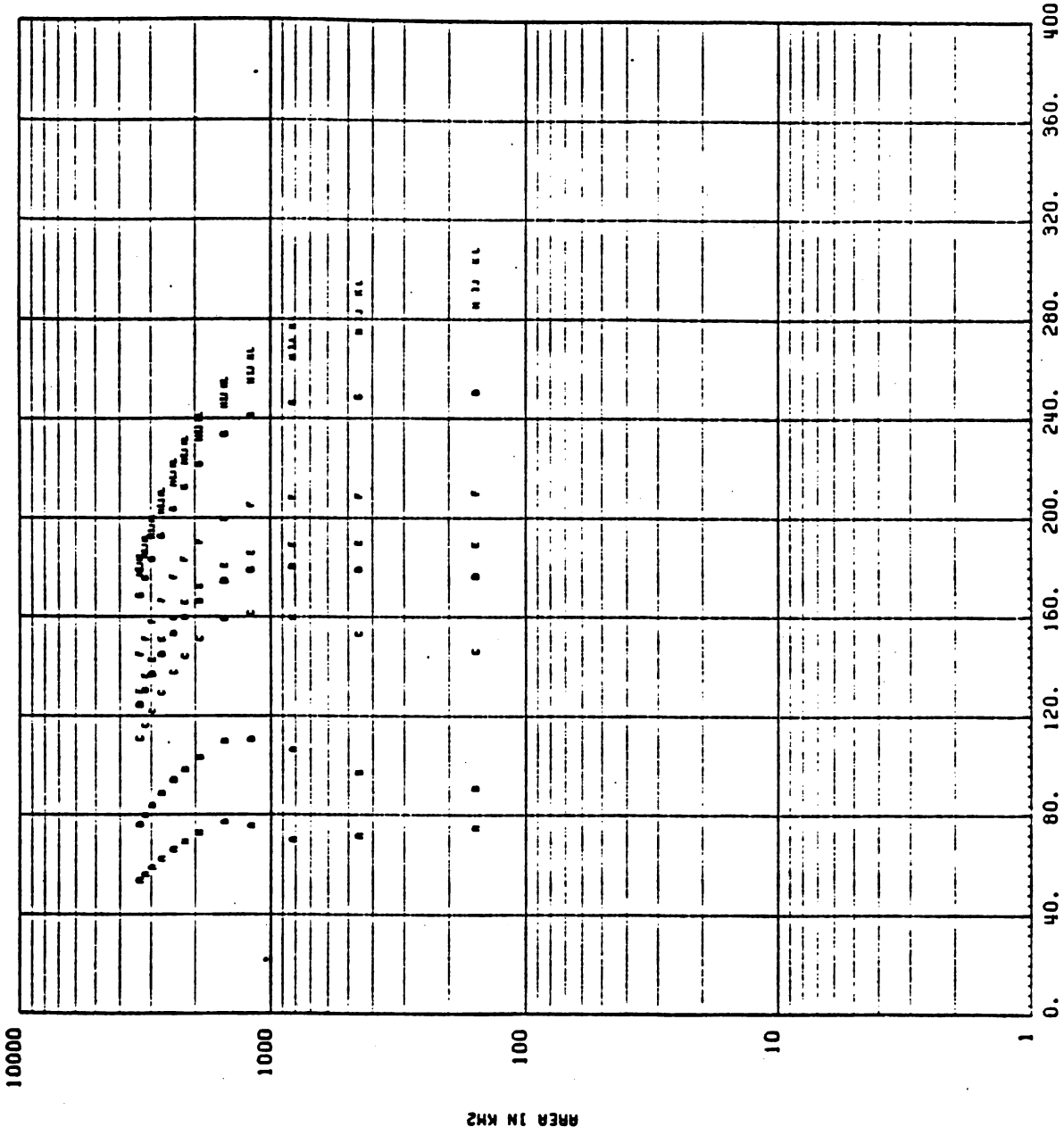

Figure 1.6.B.20

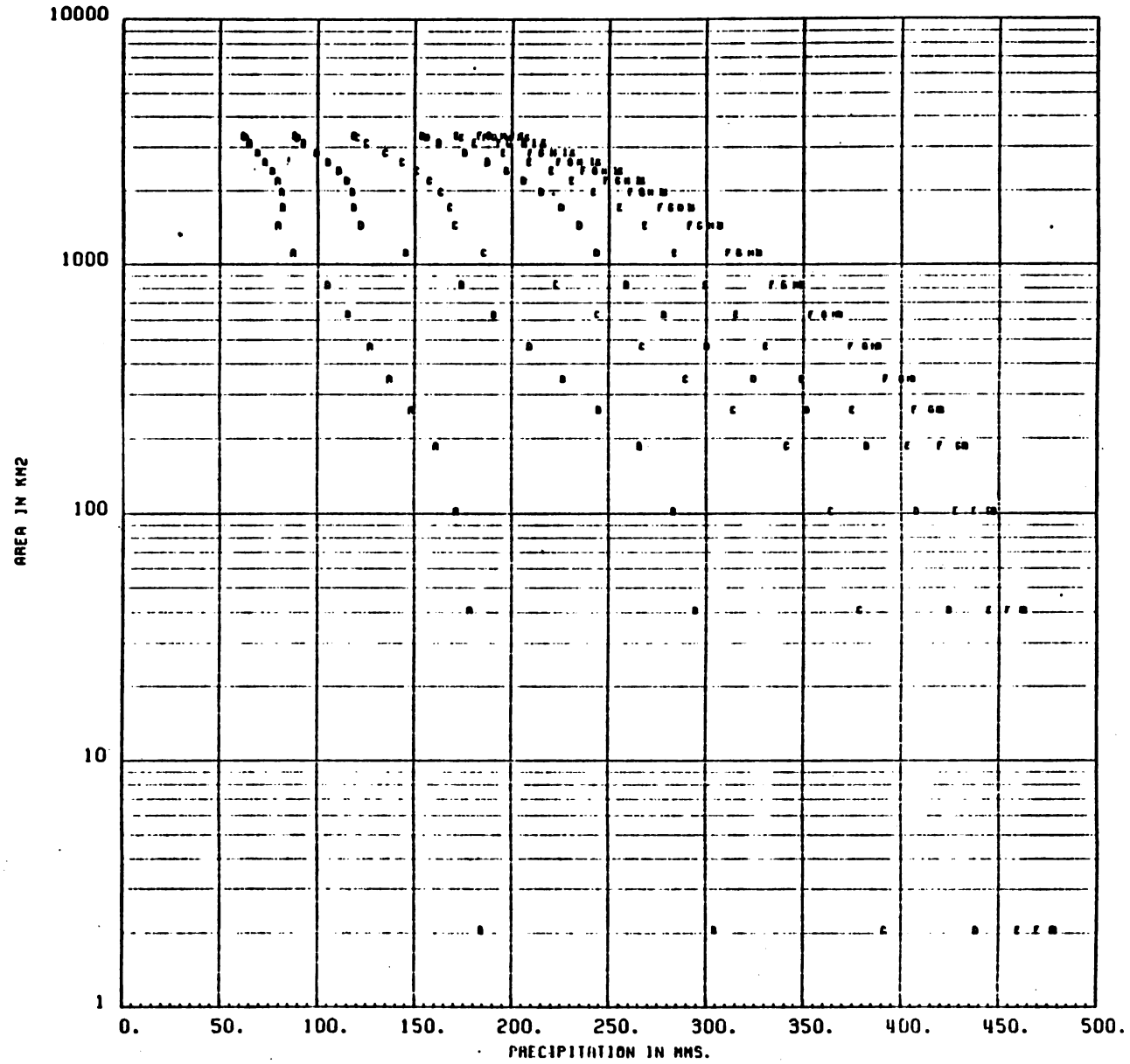

Figure 1.6.B.21

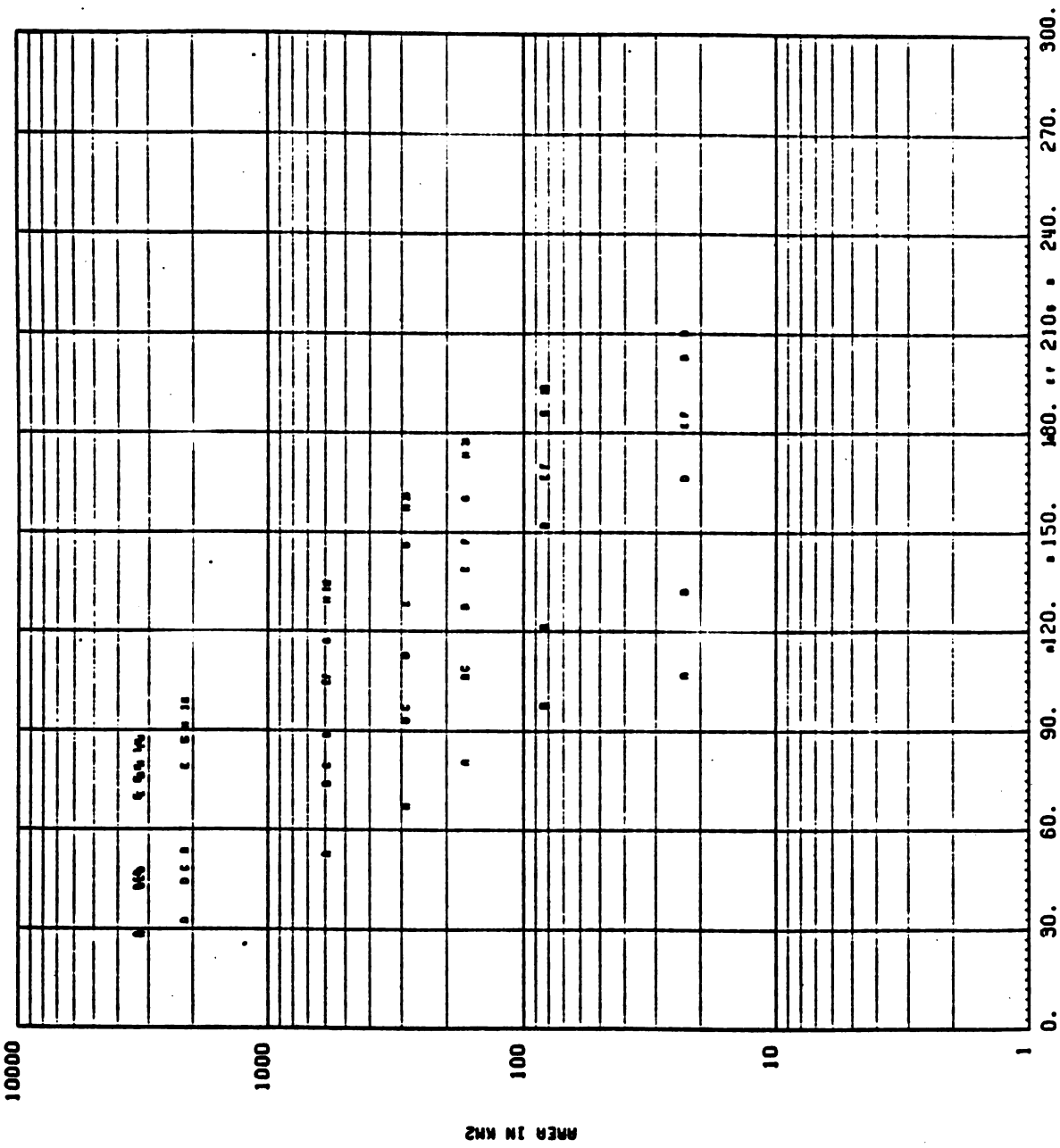

Figure 1.6.B.22

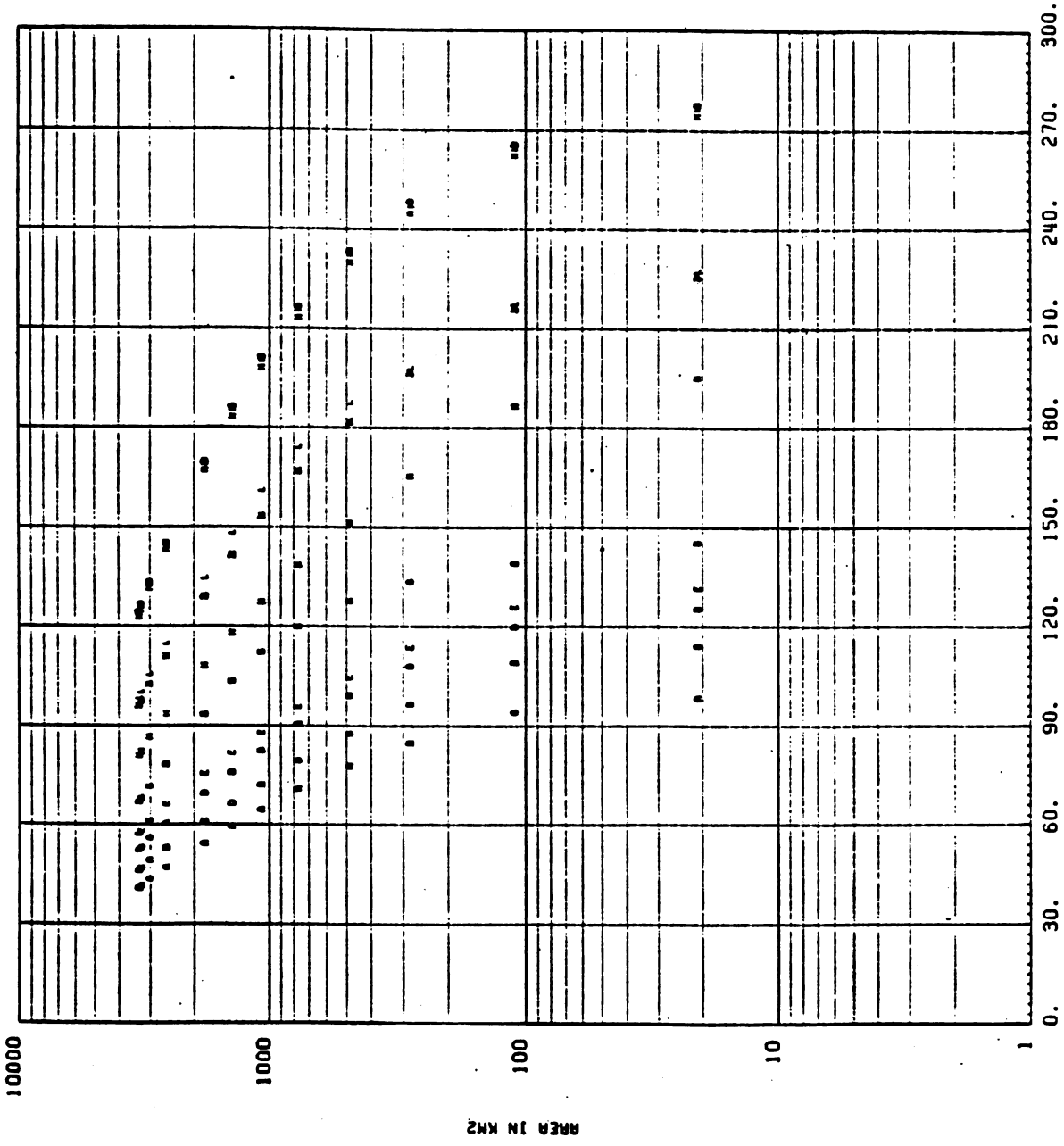

Figure 1.6.B.23

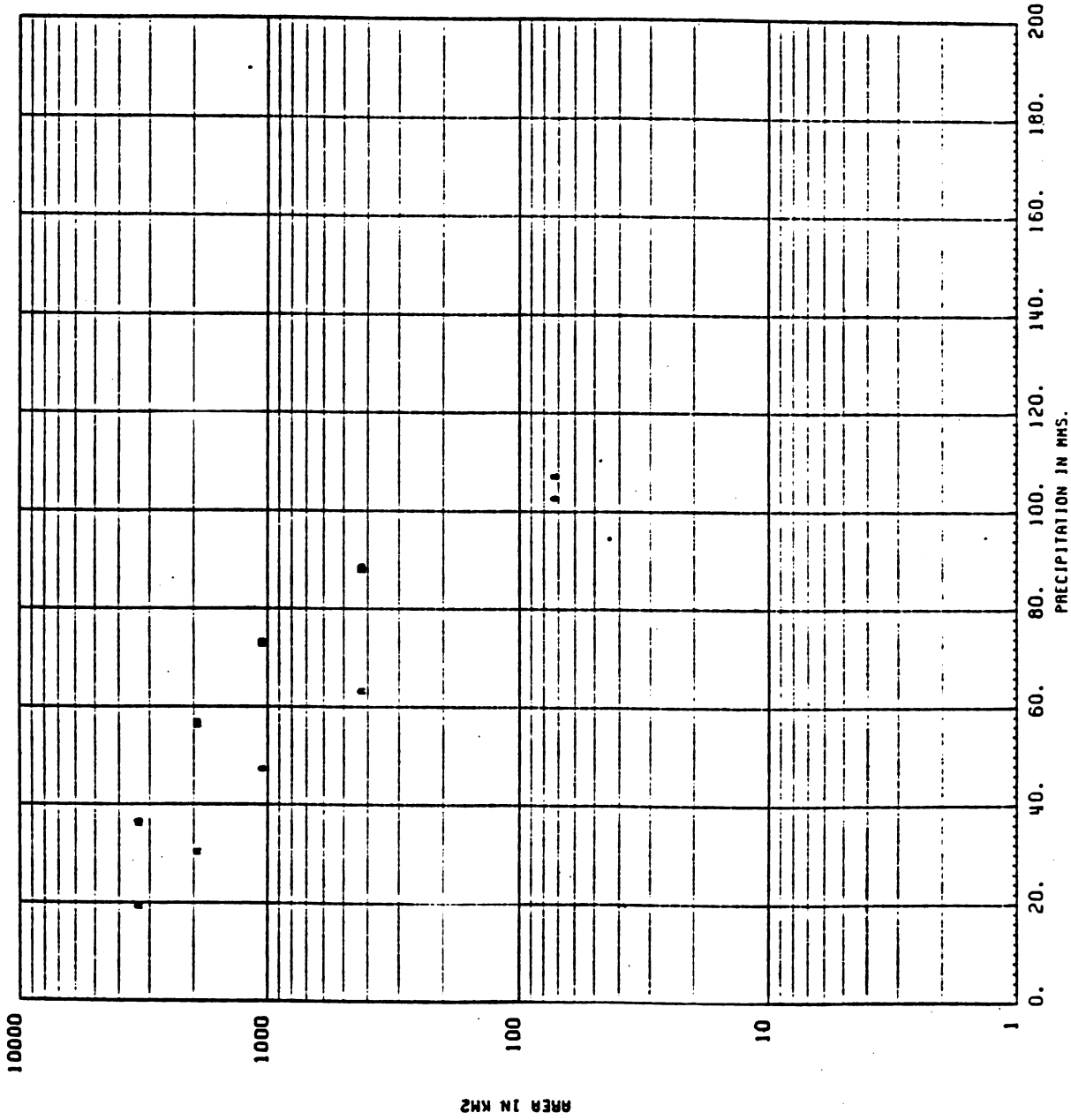

Figure 1.6.8.24

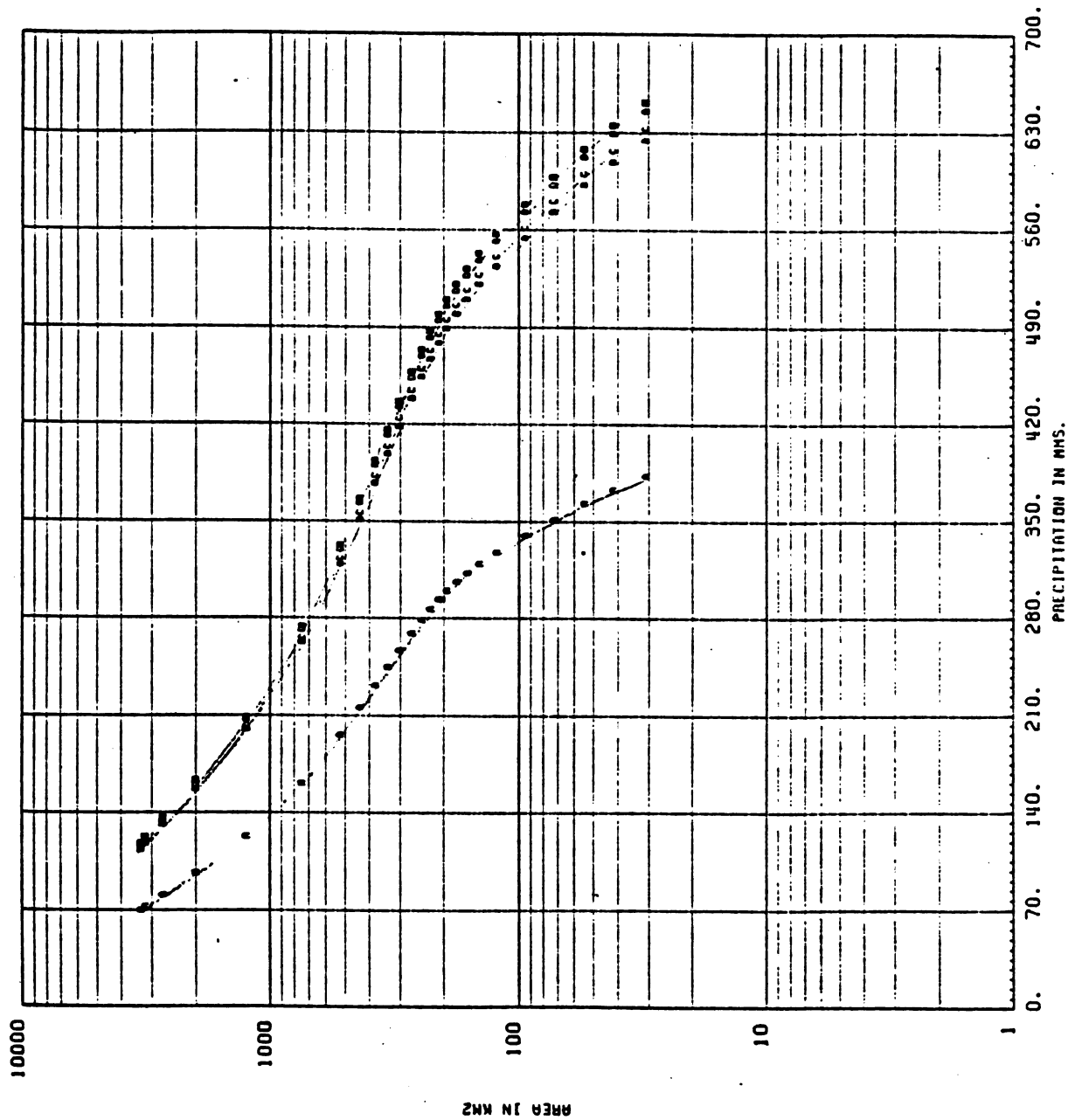

Figure I.6.B.25

1.7 RAINFALL-RUNOFF MODELING

1.7.1 Selection of Model

Several existing simulation models were considered for various applications in this project. In particular, a close scrutiny was exercised for models Flood Hydrograph Package (HEC-1) of U.S. Army Corps of Engineers, National Weather Service River Forecast System (NWSRFS), Hydrologic Simulation Program-Fortran (HSPF), and Simulation of Flood Control and Conservation Systems (HEC5). Most of these models obtained by Colorado State University require a large computer memory and storage and they cannot be implemented readily in the IBM System 34 or in the personal computers available at INDRHI or CDE. Moreover, the available data for Nizao basin do not satisfy the requirements of some of the models.

Since flood hydrographs entering Valdesia reservoir are to be simulated from historic and hypothetical storms, an event type rainfall-runoff model is needed. From all the event models considered, the HEC-1 was chosen based on the data availability and ease of implementation. A version of HEC-1 which fits into an IBM personal computer (PC) has been obtained and installed in the IBM-PC at INDRHI.

1.7.2 HEC-1 Model Calibration

Clark Unit Hydrograph and Muskingum Routing: The HEC-1 rainfall-runoff model has many options for computing rainfall excess, watershed routing, and channel routing. Many of these options can be used with the optimization model which computes the "best" parameters on the basis of "best fit" of the observed and computed flood hydrographs. A common approach is to use the HEC-1 exponential loss rate function with the Clark unit hydrograph to compute subbasin flood hydrographs and then to

use Muskingum method to route flood hydrographs to the basin outlet. Naturally, this was the initial approach to calibrate HEC-1 for Nizao watershed. Unfortunately, the results obtained by this method were unacceptable. The poor quality of rainfall and runoff data used in our optimization runs was partly responsible for this poor initial calibration results. The variation of parameters from one storm event to another was too large to be acceptable (see Table 1.7.1).

The particular topography of Nizao basin (high slopes with no significant flood plains) is thought to be another reason for the failure of storage routing techniques such as Clark Unit hydrograph and Muskingum method. Consequently, the kinematic wave approach of overland flow routing and channel routing was deemed to be more appropriate for rainfall-runoff modeling in Nizao basin.

Kinematic wave model: The first step taken in the Kinematic Wave Model formulation was to subdivide the basin into 10 subbasins, in an effort to simulate each important tributary of the Nizao basin independently. Also, one additional subdivision was included at gaging station La Estrechura, to be able to compare simulated and observed hydrographs at that point. Other two subbasing limits coincide with gaging stations Palo de Caja and Paso del Ermitano. The general configuration is shown in Figure 1.7.1.

The physical characteristics of the basin, such as channel lengths, slopes, widths, areas, etc., as well as the land use were estimated from available maps of the area. Mannings's N was obtained by calibration.

The loss rate method that was chosen was the SCS (Soil Conservation Service) loss rate function. Since very little data on soil type was available it was judged convenient to reduce the number of unknown

TABLE 1.7.1 INITIAL HEC-1 CALIBRATION FOR EXPONENTIAL LOSS RATE AND CLARK UNIT HYDROGRAPH PARAMETERS

	1st RUN	STRKR	DLTKR	RTIOL	TC	R	ERAIN
*	Storm E	12.76	24.82	7.99	11.03	11.25	.44
	Storm F	14.69	95.04	2.76	1.09	12.35	.13
	Storm H	4.05	11.46	1.90	9.12	12.64	.81
	Storm M	19.53	96.78	4.33	16.83	18.09	.28
	Storm N	1.90	7.37	1.26	17.01	18.34	.10
**	2nd RUN						
	Storm E	13.70	26.89	1.98	11.04	10.80	.44
	Storm F	24.00	94.37	2.91	7.03	5.71	.22
	Storm H	4.53	12.59	1.98	6.00	18.01	.50
	Storm M	6.96	88.38	2.15	11.26	10.47	.13
	Storm N	3.20	11.04	1.50	16.83	18.08	.10
***	Storm E	10.75	5.89	1.39	1.36	32.06	.08
	Storm F	3.68	93.94	11.52	4.66	14.73	.06
	Storm H	4.26	10.59	1.73	10.12	12.74	.38
	Storm M	9.66	86.96	2.14	11.24	10.28	.13
	Storm N	6.03	16.77	1.67	11.55	13.91	.31

* Using all precipitation stations (recording and non-recording) all hydrograph ordinates

** Range of optimization limited to period around peak outflow

*** Inconsistent precipitation data removed from record.

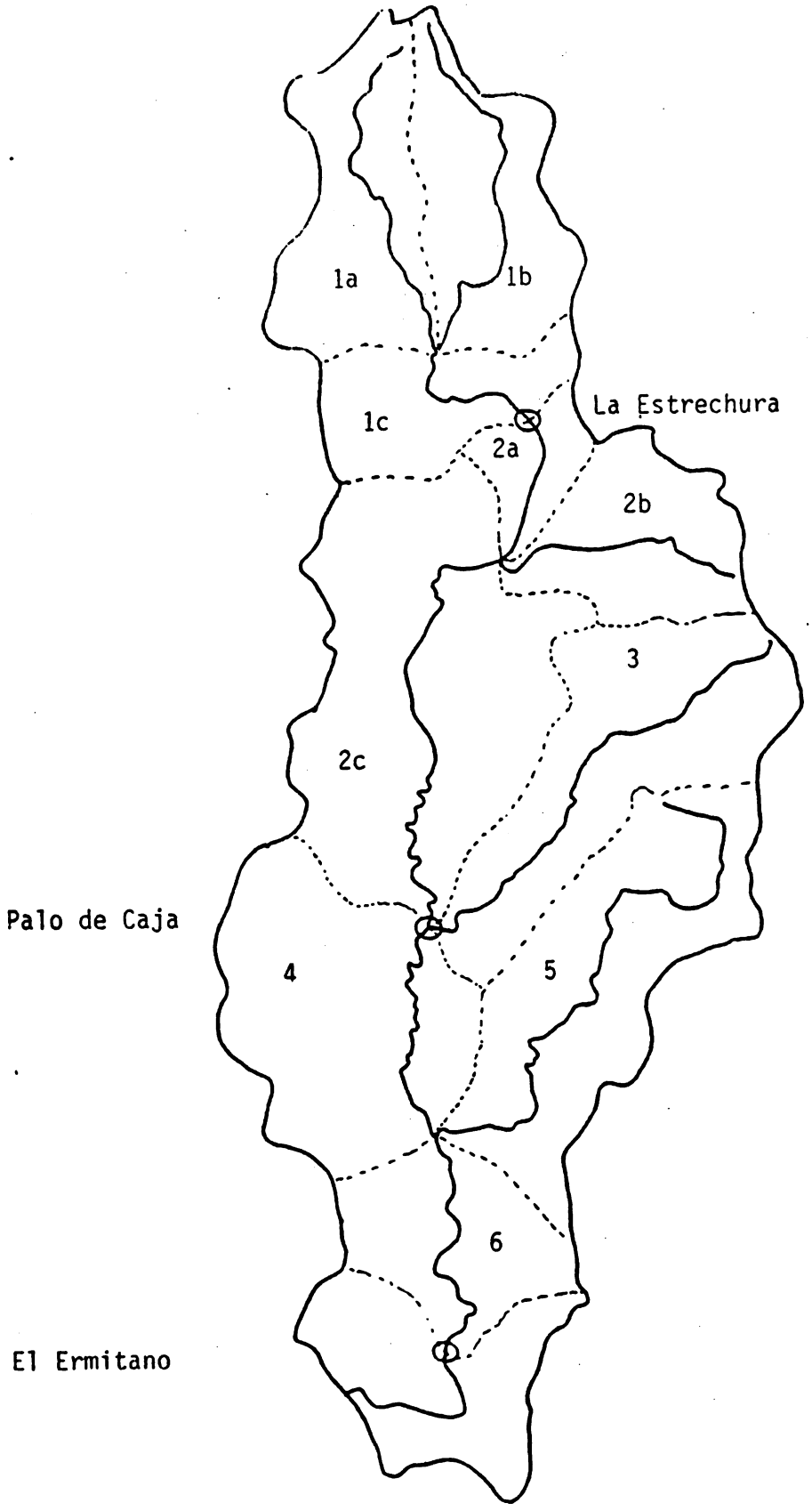

Figure 1.7.1. Nizao river basin configuration used in kinematic wave routing model.

parameters in the model to a minimum, and the SCS method only uses the Curve Number as input (once it is assumed that the initial abstraction is 20% of the storage capacity). The SCS method has proven to give good results in similar situations.

The selection of the storms used for the calibration was a little difficult. After the revision of the stage-discharge relations and the computation of the new hydrographs, very carefully the plots of precipitation and runoff of all the available storms were inspected. Most of them showed dramatic inconsistencies in terms of timing and volume of water. In many cases the hydrographs show a peak before the stations show any record of precipitation. This is why only four storms were selected for calibration. The corresponding hydrographs are shown in Figures 1.7.2 through 1.7.5.

The creation of each storm file starts by assigning weights to each of the precipitation stations with available data for each storm. The HEC-1 model computes an average total storm depth based on given weights and storm values for each precipitation station. Then an average time distribution is computed based on given weights and precipitation patterns of the recording stations. The weights were assigned by using program PCMAPS (CSU-HMS, Users Manual, 1986) to map the Thiessen polygons which were superimposed on the basin subdivision. In this way, each subbasin has an individual average storm depth and an individual time distribution pattern.

The calibration procedure starts by trying to adjust the volume under the computed hydrograph to the volume under the observed hydrograph. In most of the cases the curve number fall in the range 60 to 80 which is reasonable for the vegetation cover and expected soil

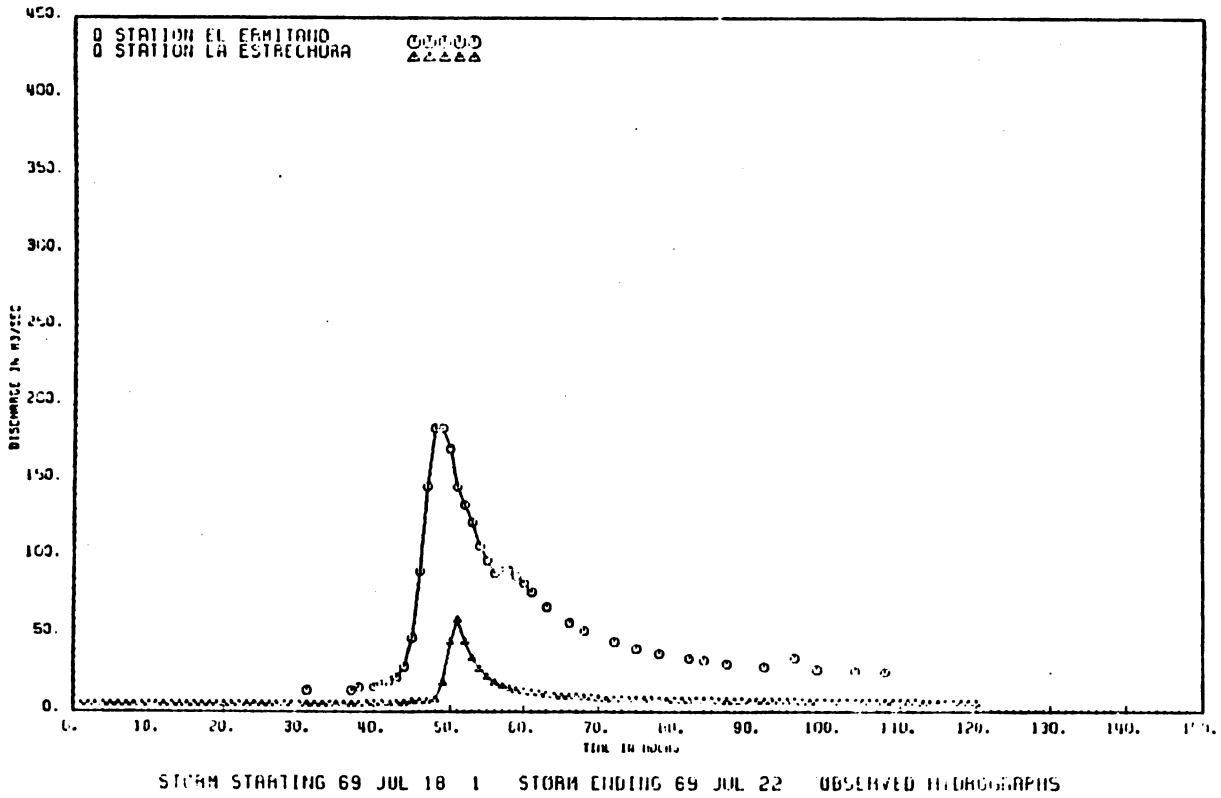

Figure 1.7.2. Streamflow hydrographs for period July 18-22, 1969 (storm A).

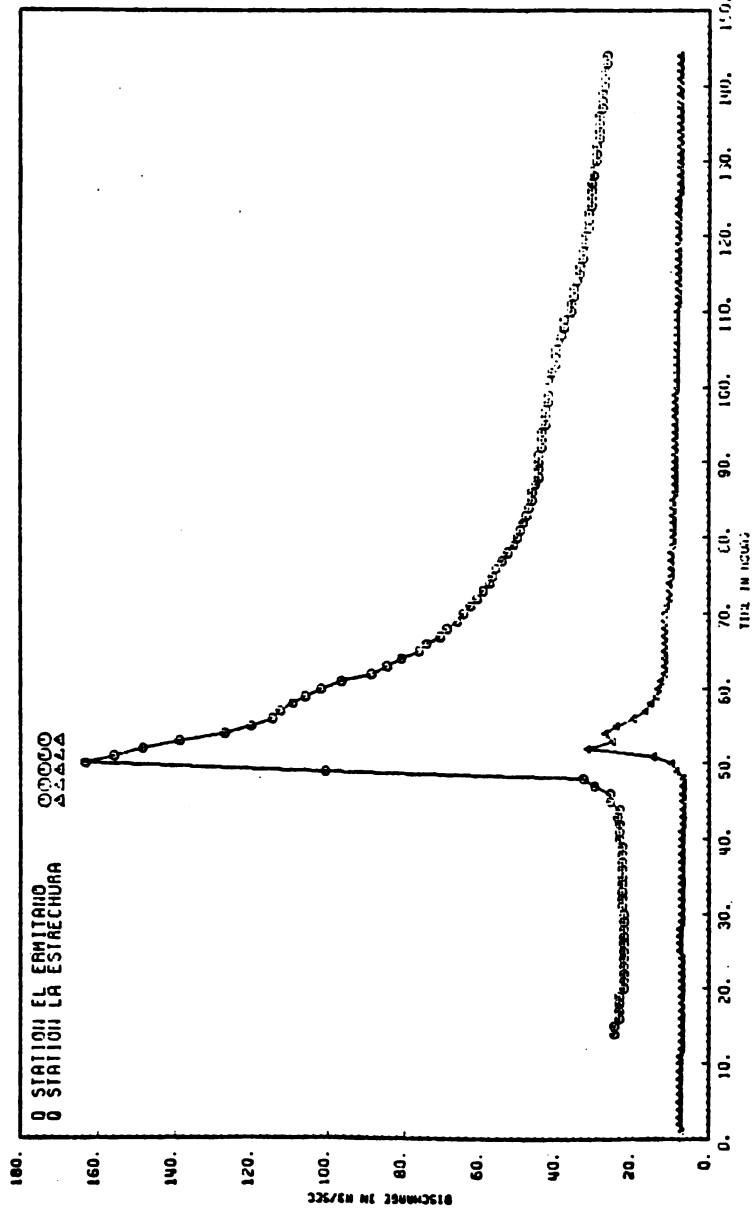

Figure 1.7.3. Streamflow hydrographs for period July 1-12, 1970 (storm B).

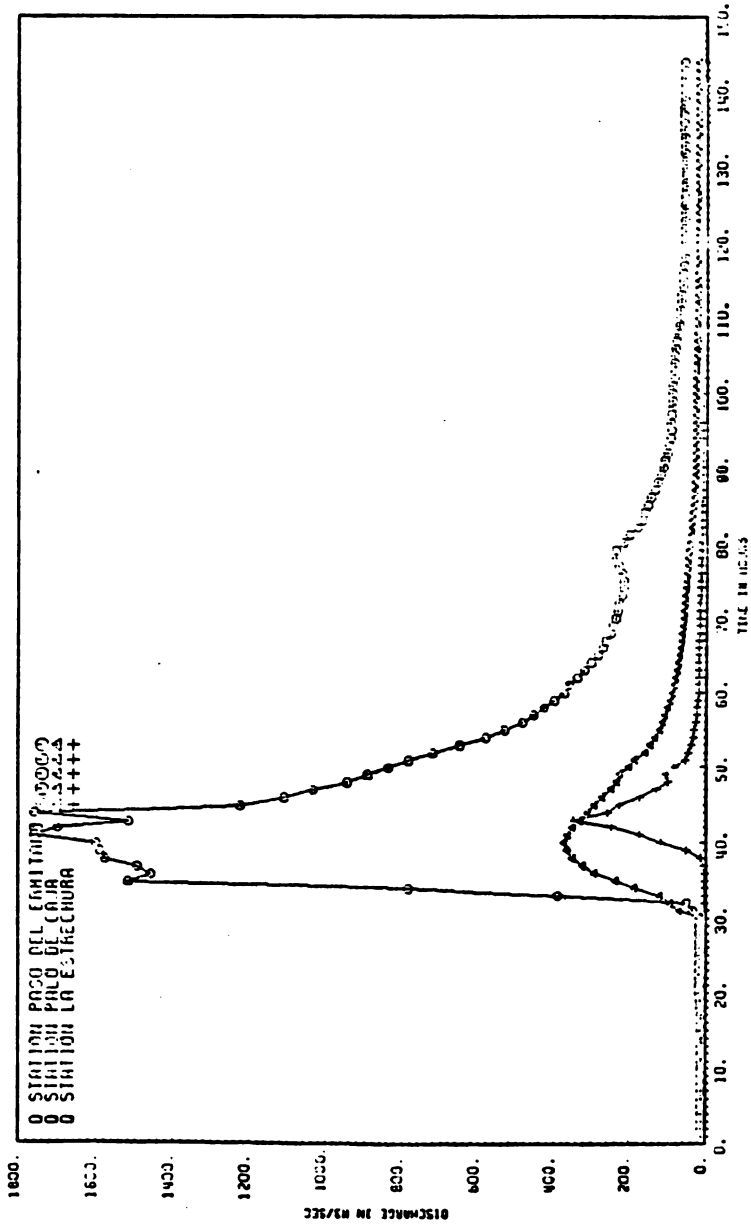

Figure 1.7.4. Streamflow hydrographs for period May 20-25, 1972 (storm F).

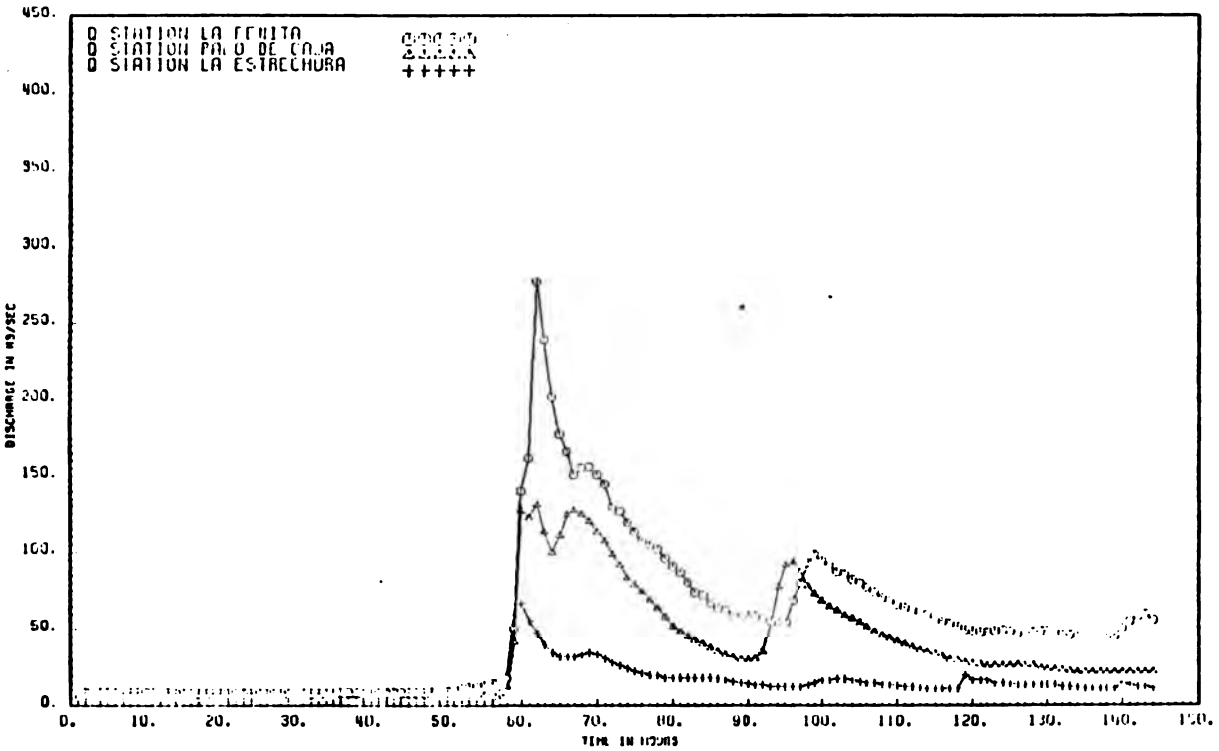

Figure 1.7.5. Streamflow hydrographs for period May 20-25, 1977 (storm 3).

type in the area. Some extremes as low as 45 and high as 100 are observed in case of storms F and M. The low of 45 could be reasonable for a very dry antecedent condition but in the case of CN = 100, i.e. with practically no infiltration, (which was used for lower subbasins) there is a deficit of 45% of the observed volume. It is concluded that some errors are present in the data.

Once the runoff volumes are matched, next step is to change the Manning's N, within reasonable values, to try to adjust the timing of the hydrographs. The best set of parameters so obtained is shown in Tables 1.7.2 and 1.7.3. Unfortunately, the computer outputs showed that the match is not too good in most of the cases. Since, in some cases, the observed peak comes before the computed, and in other cases is the opposite, it was not possible to arrive at a unique set of parameters that will fit all the storms. Suspecting errors in data, additional data consisting of reservoir levels and operation records of the Valdesia reservoir,during certain major storm events were requested. The data for two reasonably large storms in September and October 1985 were received which proved to be very useful. The calibration results for the September storm are illustrated in Figure 1.7.6. The timing of the reconstructed inflow hydrographs to the reservoir matches reasonably well those computed with the calibrated model.

TABLE 1.7.2 KINEMATIC WAVE MODEL SUBBASIN CHARACTERISTICS

SUBBASIN	OVERLAND FLOW PLANE LENGTH	OVERLAND FLOW PLANE SLOPE	MANNING N	DRAINAGE AREA (sq km)	LAND USE
1a	2500	0.60	0.400	70	Forest
1b	2500	0.60	0.400	70	Forest
1c	4500	0.50	0.300	45	Pasture
2a	2000	0.40	0.300	24	Pasture/Forest
2b	3500	0.20	0.300	56	Agriculture/Forest
2c	4500	0.40	0.300	164	Pasture/Forest
3	2000	0.40	0.300	106	Pasture/Forest
4	5000	0.50	0.300	103	Pasture/Forest
5	3000	0.40	0.300	109	Forest
6	5000	0.60	0.300	53	Forest

TABLE 1.7.3 KINEMATIC WAVE MODEL CHANNEL CHARACTERISTICS

SUBBASIN	LENGTH (m)	SLOPE (m/m)	MANNING N	WIDTH	SIDE SLOPE (m/m)	UPSTREAM INFLOW
1a	16000	0.1050	0.060	45	1	no
1b	20000	0.0837	0.060	45	1	no
1c	8500	0.0133	0.040	85	1	yes
2a	7500	0.0108	0.040	85	1	yes
2b	13500	0.0452	0.050	45	1	no
2c	33500	0.0086	0.040	70	1	yes
3	33000	0.0293	0.050	45	1	no
4	18000	0.0148	0.040	80	1	yes
5	34000	0.0323	0.050	45	1	no
6	18000	0.0119	0.040	80	1	yes

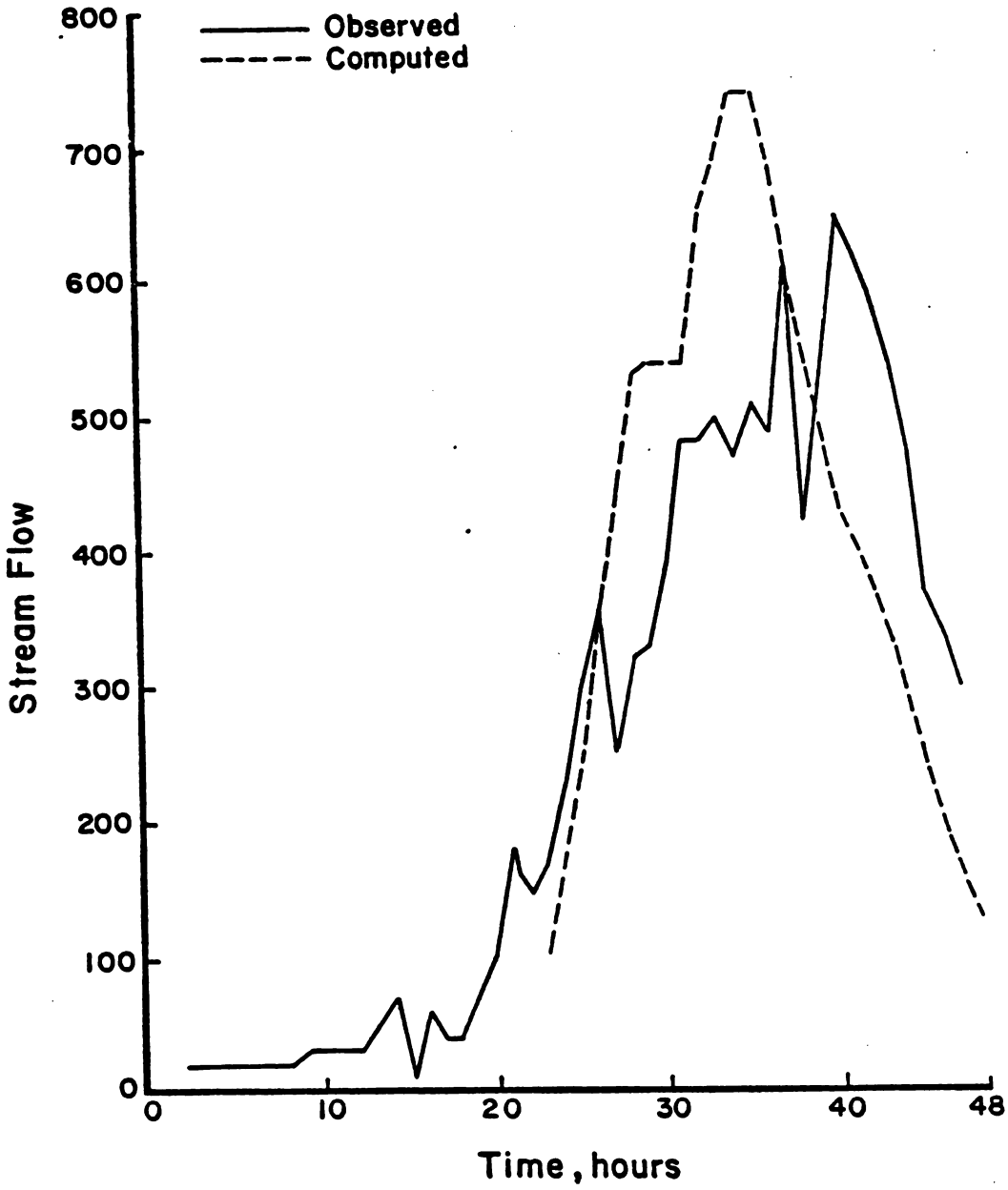

Figure 1.7.6. Comparison of computed (from reservoir levels) and calibrated (HEC-1) inflow hydrographs to Valdesia Reservoir due to storm on September 13-14, 1985.

1.7.3 Design Flood Hydrographs

The primary use of the calibrated HEC-1 model is in computing design flood hydrographs from hypothetical design storm events. The hypothetical storms under consideration are (a) Standard Project storm for non-hurricane conditions; (b) Standard Project storm for hurricane conditions; and (c) probable maximum precipitation. The calibrated HEC-1 model was used to compute hydrographs corresponding to all three design storms.

An important consideration in computing design flood hydrographs is the antecedent moisture condition of the basin under consideration. Since the SCS curve number method of HEC-1 model is being used for computing losses, the antecedent basin condition is reflected in the curve numbers corresponding to each subbasin. The actual curve number magnitude depend on three types of basin conditions: (a) Antecedent Moisture Condition type-I (AMC-I). This corresponds to the dry soil conditions; (b) Antecedent Moisture Condition type-II (AMC II). This corresponds to average soil moisture conditions; (c) Antecedent Moisture Condition type-III (AMC-III). This corresponds to the nearly saturated soil condition. The soil conservation service provides the Curve Numbers for AMC II conditions for a variety of land uses and four types of soil cover complexes. Based on a past study on soil types and land uses in Nizao basin (personal communication, Perez, 1985), the curve numbers were identified for various subbasins in the watershed subdivision made for kinematic wave model. These curve numbers correspond to AMC II. The curve numbers for AMC I and AMC III were identified from another table provided by soil conservation service. These results are summarized in Table 1.7.4.

TABLE 1.7.4 CURVE NUMBERS USED IN HEC-1 MODEL

SUB-BASIN	AMC-I	AMC-II	AMC-III
1a	40	60	78
1b	40	60	78
1c	51	70	85
2a	51	70	85
2b	51	70	85
2c	45	65	82
3	45	65	82
4	45	65	82
5	45	65	82
6	40	60	78

Finally, by using the curve numbers corresponding to AMC I, AMC II and AMC III in the calibrated HEC-1 model three design flood hydrographs were computed for each of the three hypothetical design storms mentioned above. The resulting hydrographs are presented in Figures 1.7.7 through 1.7.9.

1.7.4 Reconstruction of Hydrographs for Hurricane DAVID

Hurricane DAVID constitutes the largest storm event recorded in Nizao. Unfortunately, the hydrograph corresponding to this event is not available due to failure of equipment during the hurricane. The HEC-1 model was used to reconstruct the hydrograph corresponding to recorded precipitation pattern of hurricane DAVID. Since the antecedent basin condition prior to the hurricane is unknown, the hydrograph corresponding to all three antecedent moisture conditions AMC I, AMC II, and AMC III were computed. These results are presented in Figure 1.7.10. It is noted that the peak flow corresponding to even AMC I is considerably larger than the peak discharge of about 3800 m^3/s reported in some documents obtained from INDRHI. For the present study however,

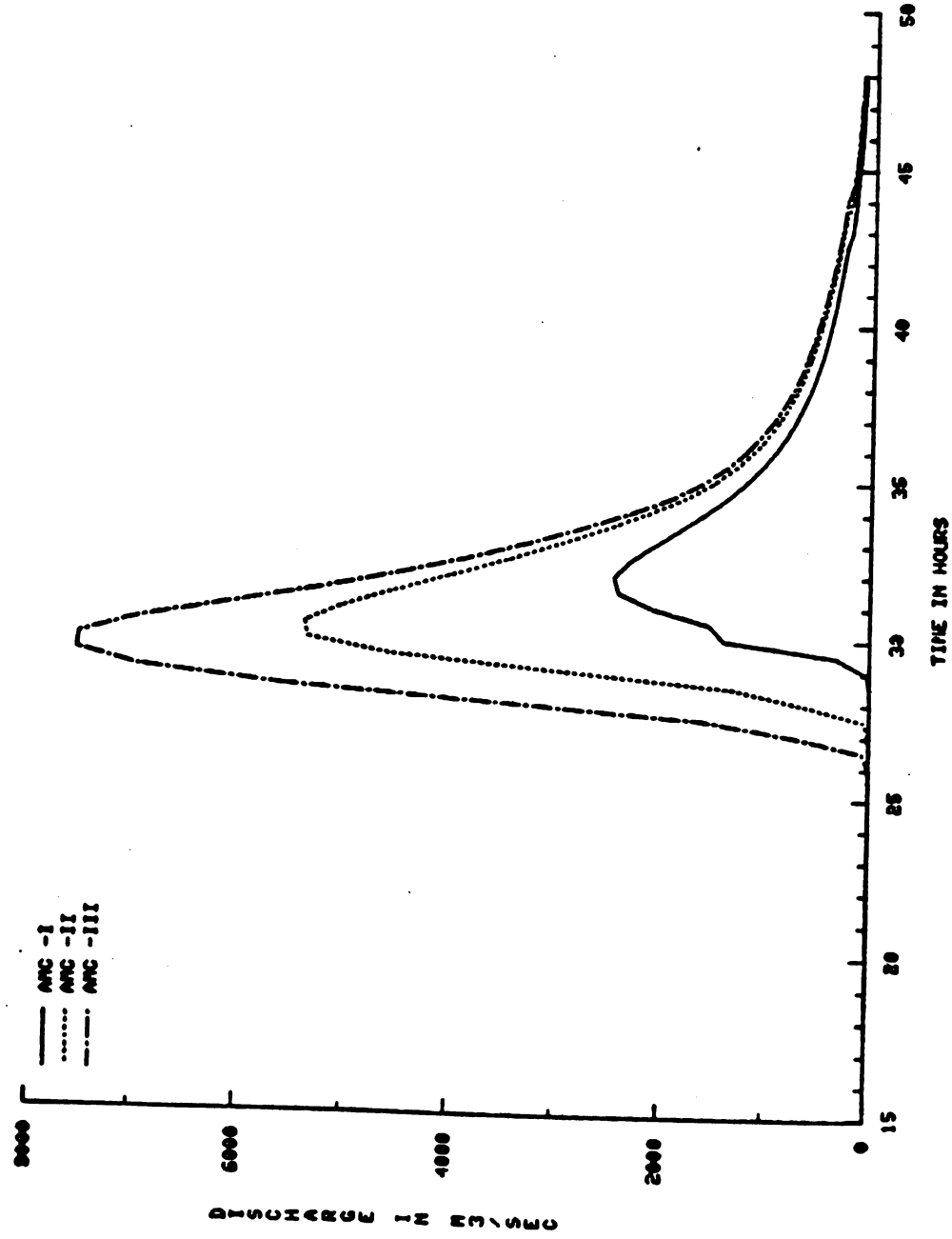

Figure 1.7.7. Non-hurricane standard project flood.

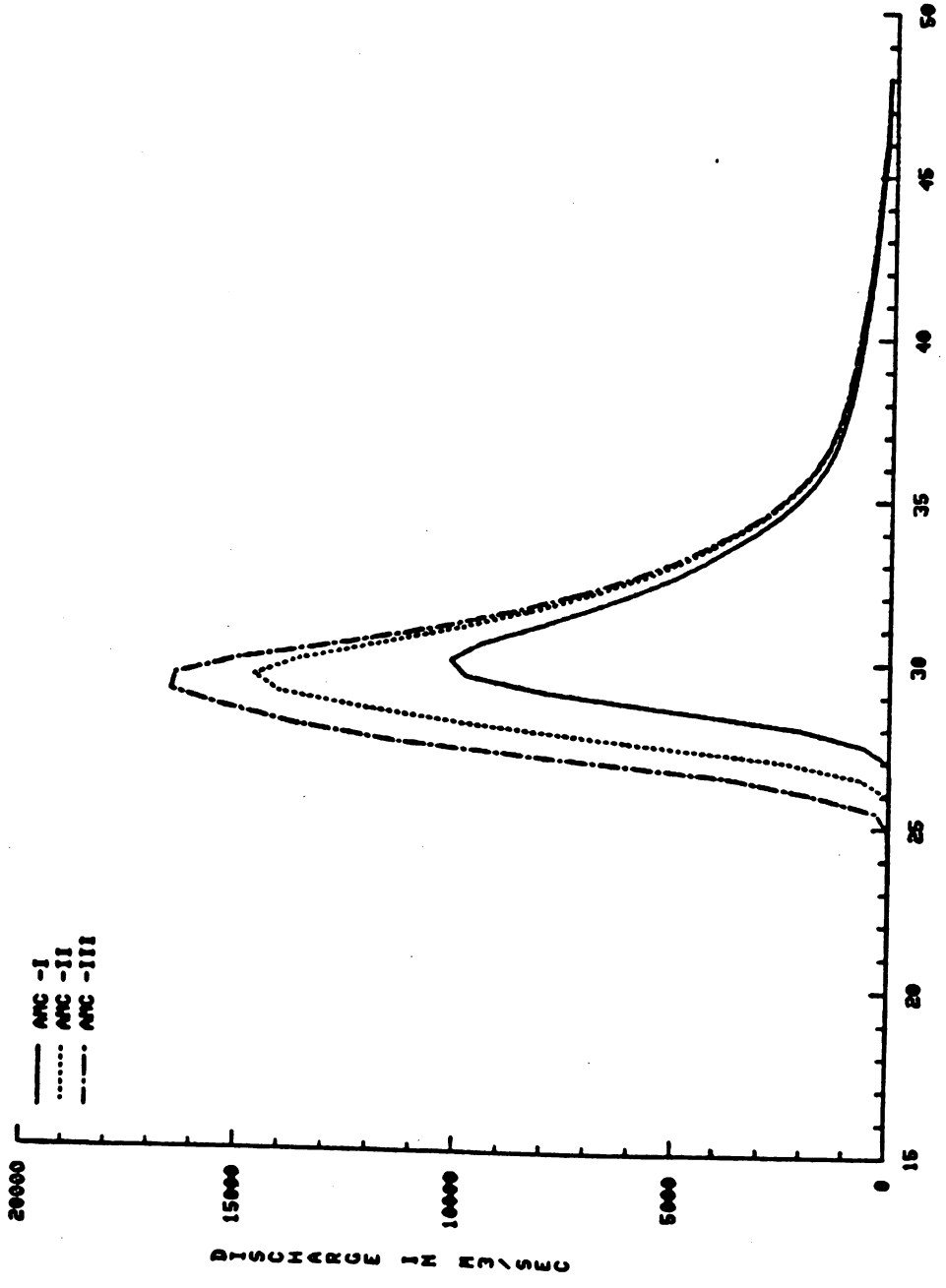

Figure 1.7.8. Hurricane standard project flood.

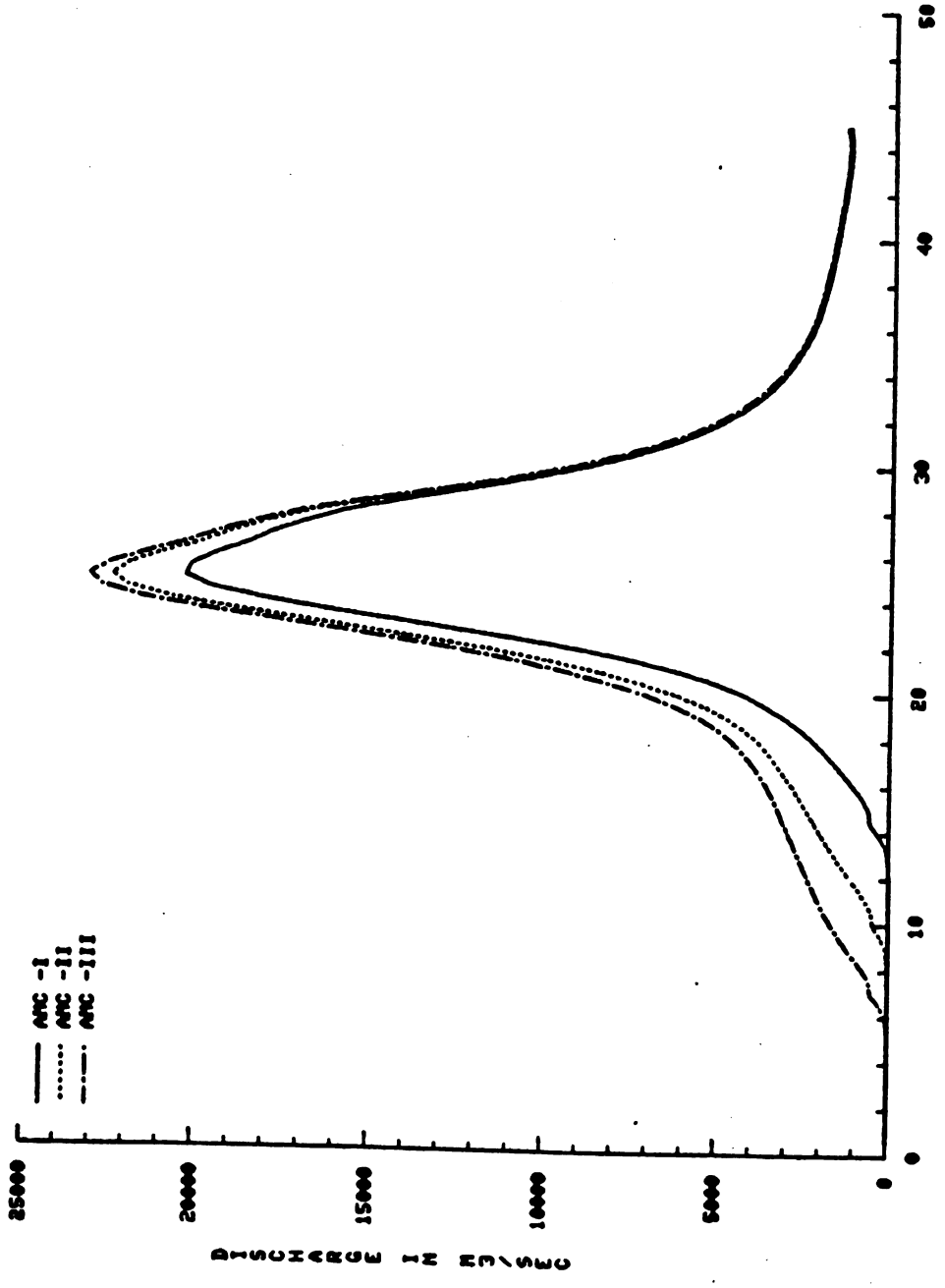

Figure 1.7.9. Simulated probable maximum flood.

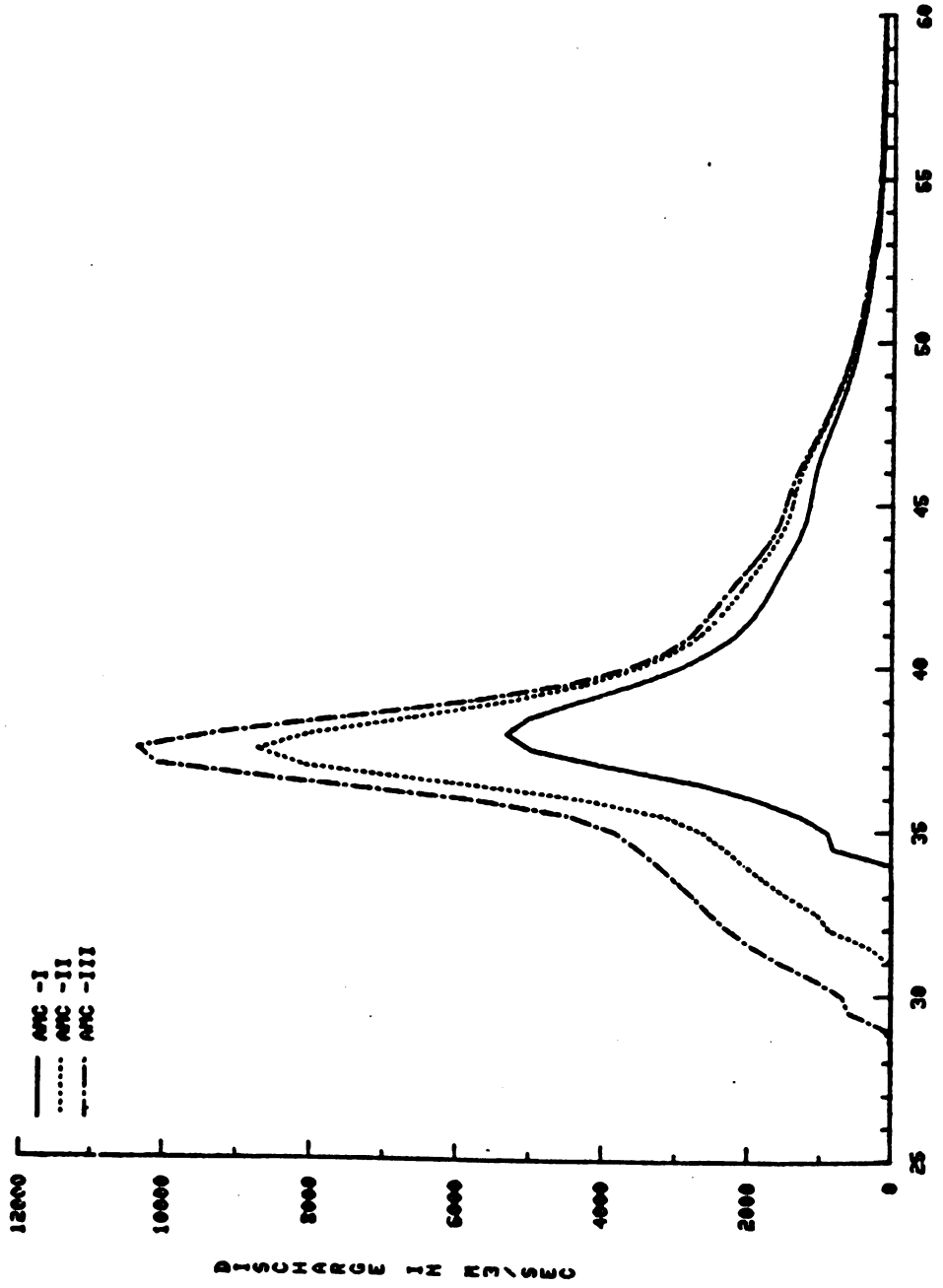

Figure 1.7.10. Simulated hydrograph for hurricane David (August, 1979).

exact reproduction of the actual peak discharge of flood due to hurricane DAVID is not critical.

1.7.5 Effects of Natural Storages in the Watershed

It is noted here that the kinematic wave approach of HEC-1 does not have a facility to attenuate a flood hydrograph due to natural storages such as those present in flood plains. However, it is important to account for such storages wherever they exist since the hydrograph can be greatly modified by attenuation due to storage effects. A study was undertaken to investigate the presence of natural storage which may have the potential to substantially attenuate the flood hydrograph computed by the kinematic wave model.

Two possible storage areas were identified in the main channel of the Nizao River. The first one is located upstream of Rio Abajo and the second one upstream the junction of Banilejo River and the main channel.

Based on the new information made available by INDRHI (cross sections and map scale 1:20000) for the area upstream of Rio Abajo, it was concluded that the storage in the channal is not significant even for very high flows. Because a detailed map for the area upstream the junction of Banilejo and Nizao is not available a definite conclusion about the effect of storage in this location during high flows could not be made. However an approximate sensitivity analysis was conducted to see the effect of different storages on the peak discharge.

An estimate of elevation-discharge relation was obtained by using Manning's equation in the narrowest section downstream the junction. The values used for this estimation are:

Slope = = 0.0055

Manning's N = 0.04

Base width = 85 m

z (side slope) = $\frac{11}{40}$ = 0.275

Using the parameters the following table was obtained.

Depth	A	R	Q	V
0.5	42.6	0.49	49.4	1.16
1.0	85.3	0.98	156	1.83
1.5	128.1	1.45	305	2.38
2.0	171.1	1.92	490	2.86
2.5	214.0	2.38	707	3.30
3.0	257.0	2.82	953	3.70
3.5	301.0	3.26	1227	4.08
4.0	344.0	3.69	1525	4.43
4.5	388.0	4.11	1847	4.76
5.0	432.0	4.53	2192	5.07
5.5	476.0	4.94	2557	5.37
6.0	520.0	5.34	2943	5.66

Note: A = Area; R = Hydraulic radius; Q = Discharge; and V = Volume of storage.

From the maps scale 1:50000 one can estimate the volume of storage for different depths. Two runs with different storage values were made to see their effect on the hydrograph at Paso del Ermitano.

(a) FIRST RUN: (Upper Limit)

For a maximum stage level of 6.0 m assume a maximum average flooded area of 3 km^2. The storage for this stage is $\frac{1}{3} \times 3 \times 10^6 \times 6 = 6 \times 10^6$ m^3. Assuming storage S is related to stage ,d, in the form, $S = ad^3$ the stage-storage data are obtained as given below:

Depth (m)	STORAGE x 10^3 m^3
0.5	3.5
1.0	27.8
1.5	93.8
2.0	222.2
2.5	434.0
3.0	750.0
3.5	1191.0
4.0	1777.8
4.5	2531.3
5.0	3472.2
5.5	4621.5
6.0	6000.0

(b) SECOND RUN

Assume that the maximum storage for a stage of 6 m is 2000 x $10^3 m^3$. Then the storage ordinate in the storage-elevation curve will be one third of the one used in the first run.

These two assumed reservoirs were incorporated into the Hurricane David HEC-file. It was seen that the effect of the storage on the peak discharge is insignificant in both cases and therefore it was not considered in subsequent analysis.

1.7.6 Sensitivity Analysis

The previous section illustrated that the effect of the two potential natural storages in the Nizao basin is insignificant in the peak of a large flood such as that of Hurricane David. The sensitivity of other key components of the flood hydrograph computation, namely the routing and loss rates are investigated for the case of PMF. particularly in view of its large magnitude.

A comment regarding kinematic wave routing is in order. This method, at least in theory, does not provide for attenuation of the flood although the particular numerical scheme used may artificially introduce some attenuation. In view of this, the peak flow may be overestimated and the magnitude of overestimation depends on the validity of the kinematic wave method for the case at hand. Some past studies have shown that this method is suitable for cases of high slopes and slow rising floods. In view of very high slopes found in Nizao basin and the fact that no significant flood plain storage are present, the kinematic wave method appears to be a valid approach to use in case of Nizao.

The storage routing technique which employs the Clark unit hydrograph is also employed to investigate the effect of using a different routing technique on the magnitude of PMF. This particular approach has two parameters: (a) time of concentration, T_c; and (b) storage constant, R. A complete description of the method can be found in HEC-1 users manual (U.S. Army, 1985). It is noted that the application of this method was attempted earlier on each subbasin but with little success as reported in the previous sections. However, in the present study, the Clark unit hydrograph is fitted to the entire basin. The time-area diagram required in the method was developed on the basis of channel slopes, channel lengths and other geomorphic characteristics. The optimization capability of HEC-1 was employed to calibrate the entire basin for largest flood in the record which occurred on May 20, 1972. The optimization yielded values of T_c = 2.28 hrs and R = 1.8 hrs. A graphical analysis of the hydrograph recession gives R = 2.6 hrs.

In view of high slopes in the basin and the large magnitude of PMF, the use of such a loss value for T_c may be justified. A low R value indicates that the effect of watershed storage on the flood hydrograph is not significant. The use of these computed T_c and R (from HEC-1 optimization) to route PMP with CN = 60 yielded the PMF shown in Figure 1.7.11. It is noted that this hydrograph shape is quite similar to the one obtained by kinematic wave method (see Fig. 1.7.9) whereas the peak flow of 19495 m^3/s is quite comparable to the values obtained earlier. The use of a higher curve number (say 80) will increase this peak flow. A further sensitivity studies reported in Table 1.7.5 shows that quite high values of both T_c and R need to be used to reduce the peak flow

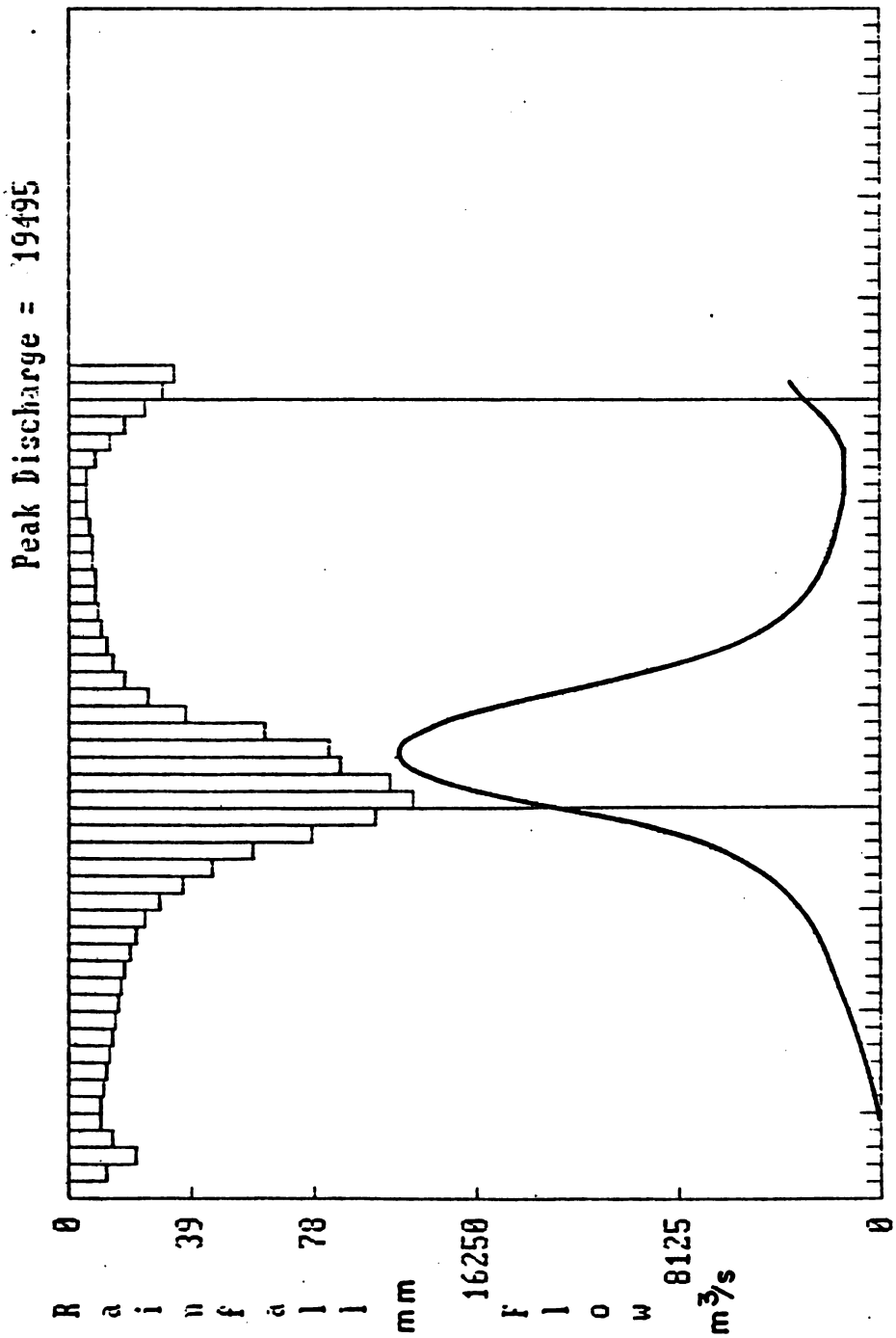

Figure 1.7.11. The PMF derived by using T_c and R of Clark's method which are computed by calibrating May, 1972 flood in the historic record.

below 15,000 m^3/s and that the influence of curve number on the peak flow is relatively insignificant.

Table 1.7.5. Sensitivity of time of concentration T_c and storage constant R of Clark unit hydrograph method on the PMF peak flow.

Parameters		Peak Flow (m^3/s)	
T_c hrs	R hrs	CN = 60	CN = 80
6	2	14568	18233
6	4	15151	15907
6	6	13226	13989
10	4	13174	13851
10	10	9763	10436
3	3	17520	18304

A further analysis was made by changing the loss rate function. In particular, the HEC-1 exponential loss rate function is used for computing PMF from PMP. The values of the parameters used are:

STRKR = 19 Initial value of loss coefficent

DLTKR = 36 Initial loss

RTIOL = 2.0 Loss coefficient recession constant

ERAIN = 0.5 Exponent of precipitation.

These values are based on results of previous calibration attempts for recorded hydrographs. For the case of T_c = 6 hrs and R = 4 hrs, the use of these parameters resulted in a peak of 15835 m^3/s. This is within the range of peak flows for same case of T_c and R reported in Table 1.7.5 and it is apparent that the use of a different loss function has a little influence on the peak flow. This was confirmed with many other runs made for other events including the reconstructed flood of Hurricane David.

1.8 STREAMFLOW FORECASTING MODEL

1.8.1 Selection of Models

Several existing simulation models were considered and reviewed to constitute the flood forecasting model for this project. The selection of the model considered, the computer facility capabilities at INDHRI, and that the model provides suitable and acceptable results at reasonable cost within the forecast lead time frame. In view of these, two models were particularly examined namely the National Weather Service River Forecast System (National Weather Service, 1984) and the Flood Hydrograph Package (HEC-1) of the U.S. Army Corps of Engineers (1985). The NWSRFS is an operational model for continuous time streamflow simulation and real-time river forecasting. It is composed of several models developed independently including Sacramento soil moisture accounting model (SAC), snow accumulation and ablation model, routing models such as layered coefficient routing technique, Muskingum routing and unit hydrograph, precipitation and temperature models and extended streamflow prediction model. Also, this model contains procedures for data processing and analyses for calibration, testing and forecasting and auxiliary programs for data preprocessing and data file manipulation prior to and after model runs. On the other hand, the HEC-1 model simulates single event rainfall/snowmelt runoff processes. In this model, the surface runoff response of the river basin to precipitation is represented as a network system of hydrologic and hydraulic components such as overland flow plane, stream channel, pump station, diversion channel or a reservoir. For a given precipitation hydrograph the rainfall excess in derived using loss rate equations and routed via a unit hydrograph or kinematic wave method to obtain the

surface runoff hydrograph. A baseflow component can also be added to the surface runoff at a basin or subbasin outlet using empirical methods. Sophisticated hydrologic analysis of basin wide flow-frequencies and analysis of expected annual flood damages may also be accomplished.

So far, the NWSRFS and HEC-1 models had found applications in several countries especially in the United States. Both models, however, have advantages and disadvantages which are unique but complementary to each other. On one hand, an attractive component of the NWSRFS model is the Sacramento soil moisture accounting model which has conceptually sound rainfall to channel inflow components transformation as compared to using precipitation loss equations in the HEC-1 model. On the other hand, the use of kinematic wave routing model of HEC-1 is more favored to the other routing techniques but is not available in the NWSRFS model. Thus combining the Sacramento soil moisture accounting model of the NWSRFS and the kinematic wave routing procedure of HEC-1 is believed to have more promising applications.

1.8.2 Development of SACKW Model

The latest version of the NWSRFS model obtained for this project is too large and requires a tremendous amount of core memory. Besides a PC-version of the NWSRFS model is not yet available. In view of this, steps were taken to develop a small version of NWSRFS model which specifically involved adapting the Sacramento soil-moisture accounting model (SAC) of the huge NWSRFS model. Similarly, the kinematic wave (KW) routing model of the HEC-1 model has been incorporated in the SAC model. In essence therefore, the streamflow forecasting model finally

developed is the combination of Sacramento soil moisture accounting and kinematic wave routing referred to as SACKW model here.

For purposes of model calibration, the constrained Rosenbrock optimization routine presented by Kuester and Mize (1973) has also been adapted as an option to automatically calibrate the parameters of the SAC component of the model. This method is a sequential search technique which has been proven affective in finding the maximum or minimum of a multivariable, nonlinear objective function subject to nonlinear inequality constraints. This optimization technique is readily adaptable to SAC model since no derivatives are required.

1.8.3 Description of Model Components

Primarily, the SACKW model can be partitioned into two major components, namely: The Sacramento soil moisture accounting, and the kinematic wave routing. Given below are descriptions of each component. A subsection is also included to describe the watershed partitioning and timing considerations of the model.

1.8.3.1 Sacramento Soil Moisture Accounting Model

Referring to Figure 1.8.1, the Sacramento model computes various runoff components which are added together as total channel inflow and subsurface discharge through a soil moisture accounting procedure from a linkage of five basic soil moisture storages. Another function of the Sacramento model deals with the evapotranspiration process which has significant role in moisture movement in the hydrologic cycle.

The use of five basic storages and their linking mechanism is intended to provide a simple but effective representation of the vertical and horizontal movement of water through and over the soil. As shown in Figure 1.8.1, the five storages are: 1) the upper zone tension

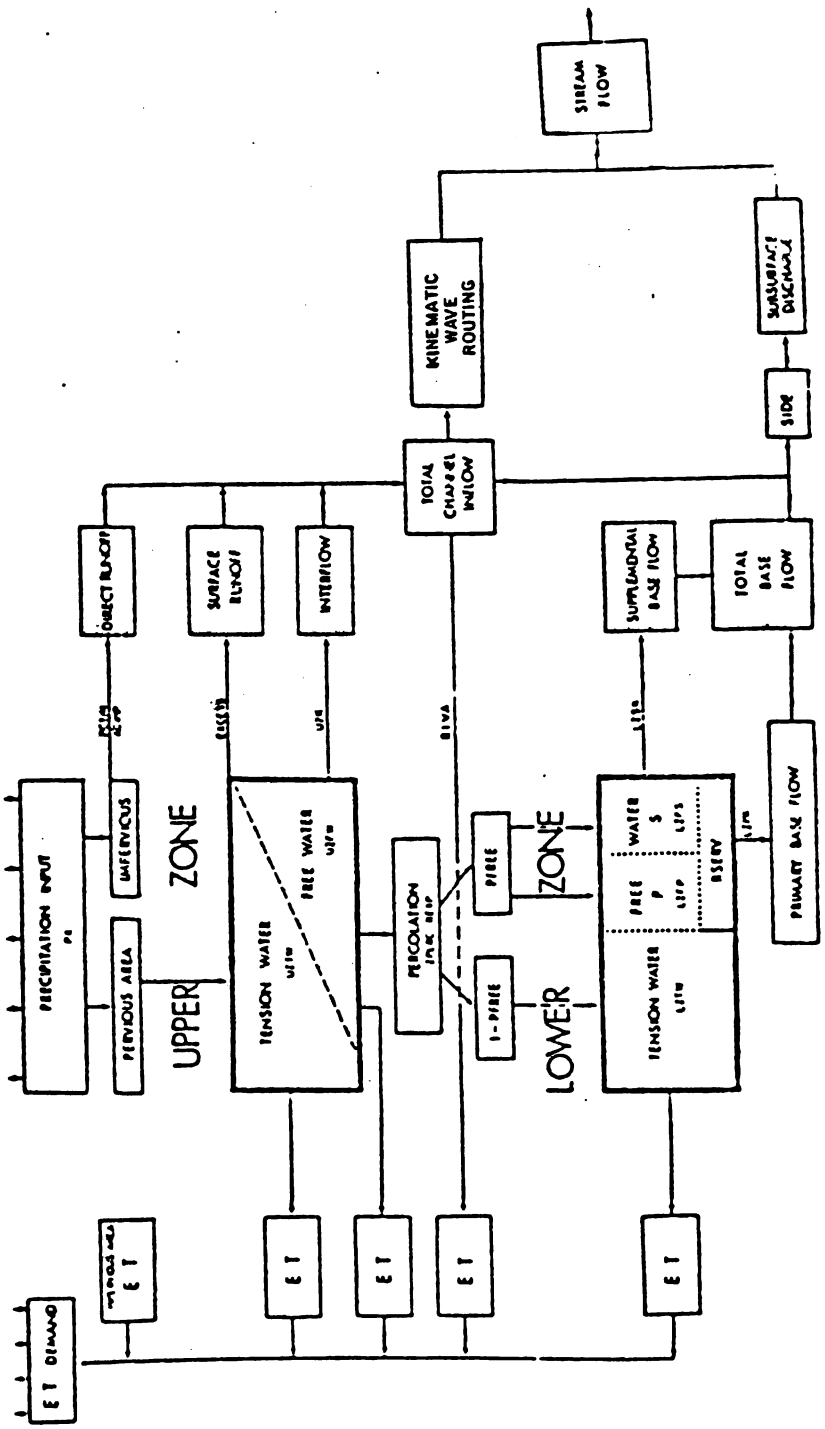

Figure 1.8.1. Flow chart of Sacramento soil-moisture accounting model. After National Weather Service (1984).

water which is the volume of water tightly bound to soil molecules but can be removed by evapotranspiration but occurs within such a shallow layer of soil that it is rapidly replaced by rainfall before sufficient moisture can accumulate to initiate the runoff process, 2) the upper zone free water is that water needed to produce fully effective wetting front which is a key factor to the percolation process and provides the source for rapid drainage in the form of interflow, 3) the lower zone tension water is that volume of water utilized by plants for evapotranspiration but not readily transferred from roots to leaf systems as in the shallower upper zone tension water, 4) the lower zone supplemental free water represents the source of rapidly draining component of subsurface runoff known as supplemental baseflow, and, 5) the lower zone primary water provides the source of slowly draining runoff component referred to as primary baseflow.

Three subprocesses in the Sacramento model worthwhile mentioning are the percolation process, evapotranspiration process and runoff process. The percolation process essentially centers on computing the water that percolates to deeper soil through vertical drainage prior to interflow calculation. The percolation rate is controlled by the amount of water available for percolation in the upper zone free water and the deficiency of lower zone moisture volume translated into the lower zone percolation demand as shown in Figure 1.8.2. The evapotranspiration process consists of evaporation from the area covered by surface water or phreatophyte vegetation and evapotranspiration from upper zone and lower zone water storages. Evaporation is computed at a potential rate while evapotranspiration from the soil moisture storages varies with the volume and distribution of tension water storage and evapotranspiration

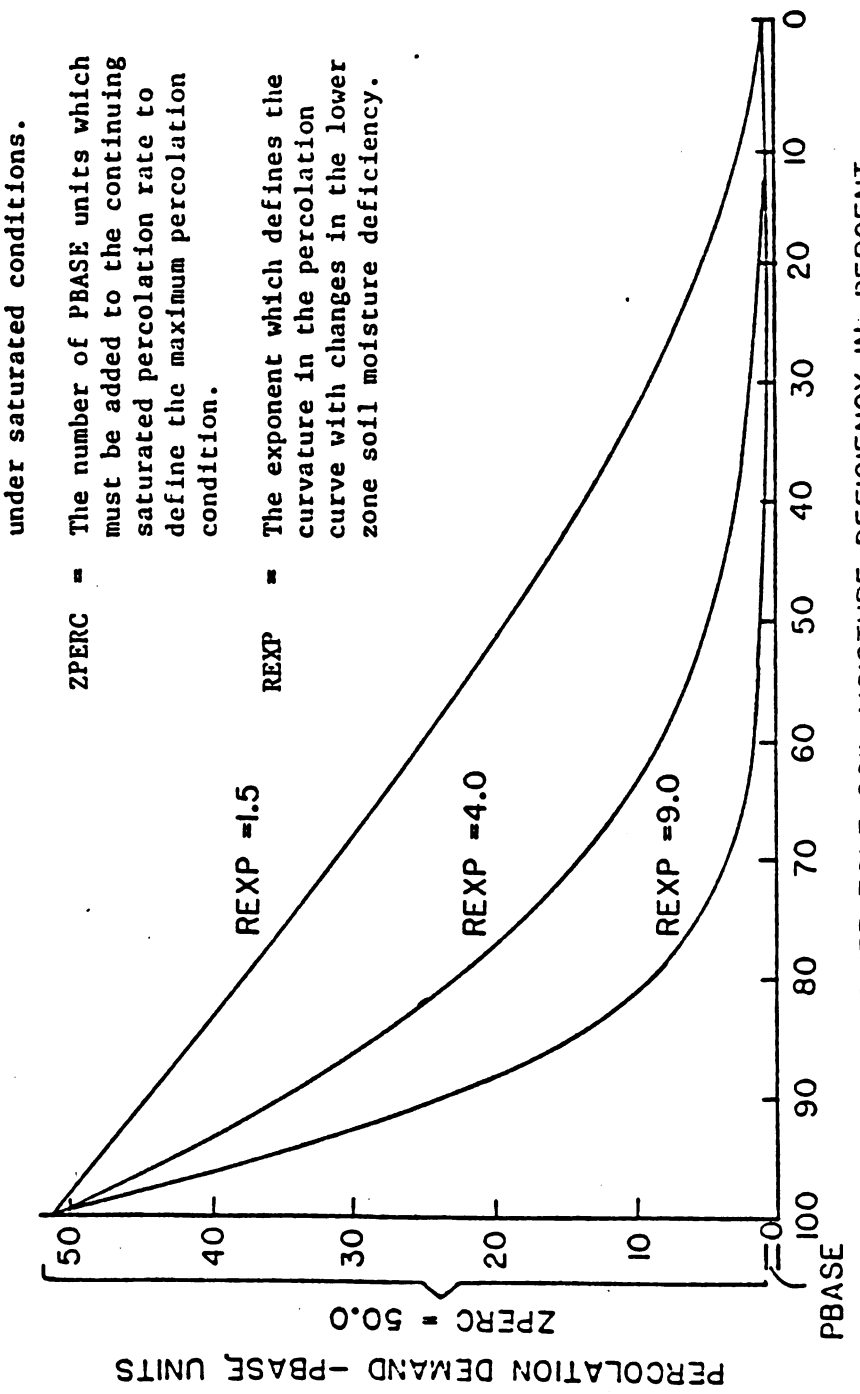

Figure 1.8.2. Relationship of percolation demand and lower zone moisture deficiency. After National Weather Service (1984).

demand. Starting with a saturated soil, and exposing it to a constant evapotranspiration demand would produce an effective evapotranspiration use curve of the type illustrated in Figure 1.8.3.

The runoff resulting from soil-moisture accounting are given in five basic forms. These are: 1) the impervious runoff from impervious areas, and direct runoff from temporary impervious area, 2) surface runoff which occurs when the upper zone free water storage is full and the precipitation intensity exceeds the rate of percolation and interflow, 3) interflow resulting from lateral drainage of the upper zone free water storage, 4) supplemental baseflow, and 5) primary baseflow. The first three runoff components represents the total channel inflow while the latter two is the total baseflow. In the SACKW model, the so called total channel inflow constitute the surface runoff contribution to the stream flow hydrograph routed via the kinematic wave routing methodology and the total baseflow is the subsurface runoff contribution to streamflow. This baseflow component is added to the routed streamflow at the basin or subbasin outlet using a linear, decay weighting function of current and some specified previous time total baseflows.

1.8.3.2 Kinematic Wave Routing Model

The kinematic wave model provides the mechanism of water movement over the land surface and in stream channels towards the basin or subbasin outlet. The input to this model is the total channel inflow or hydrograph which is assumed to be uniform over the subbasin. In determining the subbasin runoff by the kinematic wave method, three conceptual elements are used: flow planes, collector channels and a main channel as shown in Figure 1.8.4. The kinematic wave method

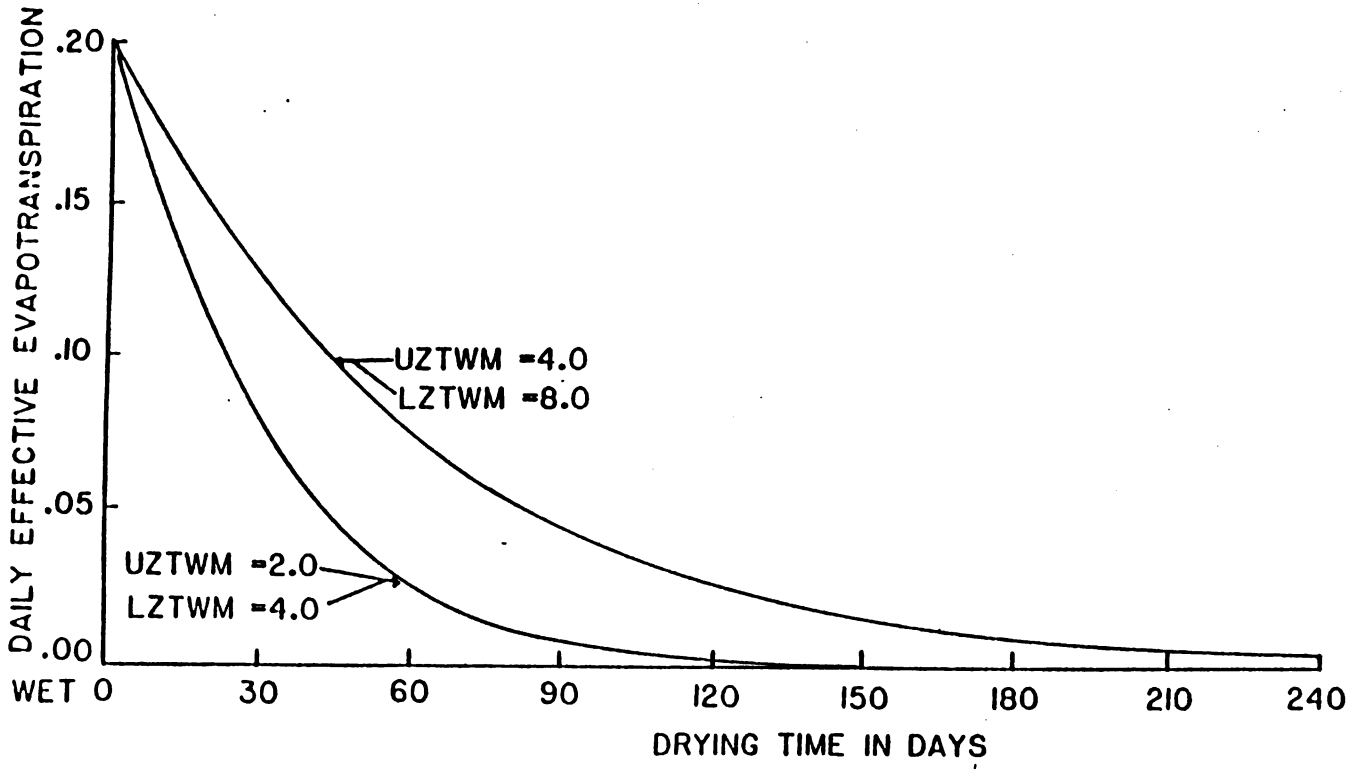

Figure 1.8.3. Daily effective evapotranspiration from initially wet soils exposed to a constant evapotranspiration demand. After National Weather Service (1984).

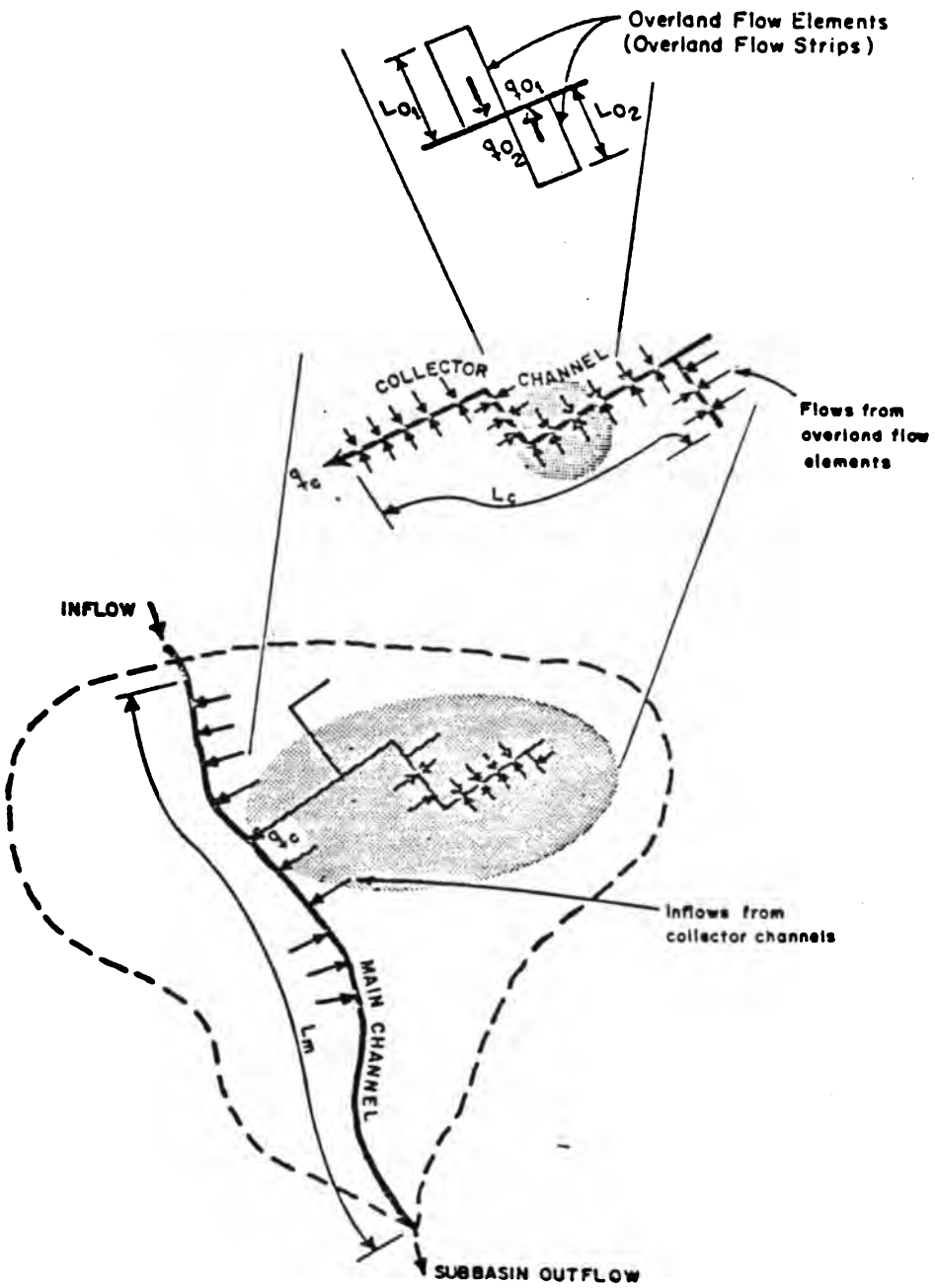

Figure 1.8.4. Relationship between flow elements in kinematic wave routing. After U.S. Army Corps of Engineers (1985).

assumes that the bed slope and water surface slope are equal and acceleration effects are negligible. In this manner, the overland or channel flow can be represented as a power function of cross-sectional area with power coeficients related to flow geometry and surface roughness. The movement of flood wave is described solely by the continuity equation in partial differential form. Through combining the flow and continuity equations, a finite difference approximation can be developed and likewise solved by finite difference methods. For further details of the kinematic wave method and its solution, the HEC-1 User's Manual (U.S. Corps of Engineers, 1985) may be consulted.

1.8.3.3 Watershed Partitioning and Timing Considerations

Partitioning of the watershed provides the distributed parameter capability of the model. This is done to account for the spatial and temporal variabilities of the physical and hydrological characteristics of the basin, the climatic variables, and basin-wide response characteristics. In the SACKW model, the watershed can be partitioned into two levels. The first level, partitions the watershed into subwatersheds where each subwatershed is a homogeneous unit of the SAC model in terms of the SAC model parameters. Rainfall and evapotranspiration are assumed homogeneous or uniform over one subwatershed. The second level of partitioning divides further a subwatershed into smaller homogeneous units representing individual flow planes. Each flow plane is assumed to have homogeneous kinematic wave parameters.

The timing considerations for the model refers to the time basis of model operation. The model is set up to simulate basin hydrology on an hourly basis and on longer time intervals which is a multiple integer of

1 hour. In the SAC model, the computational time interval is always done in an hourly basis so that rainfall, evapotranspiration and streamflow if given in longer time intervals are uniformly transformed into hourly data. Model outputs however are given on time intervals equal to those specified in the input data. In the kinematic wave routing computations, the time interval may vary depending on the stability criteria requirements of the finite-difference numerical sequence.

1.8.4 Model Calibration

This section reports the SACKW model calibration for the Nizao basin. Shown in Figure 1.8.5 is the Nizao basin and its watershed partitioning. It is decided that the basin be partitioned into three subwatersheds: La Estrechura, Palo de Caja and Paso del Ermitano, for purposes of the SAC model (first level partitioning). For each subwatershed, further partitioning is made to constitute the homogeneous flowplanes in the kinematic wave routing (second level partitioning).

A total of four years (1972-1975) of data is used for model calibration. The rainfall data used which are available hourly are areal averages from nine stations using optimal interpolation. Three sets of areal averaged time series were obtained corresponding to the three first level subwatersheds. Since not all of the nine rainfall stations are recording at one time or another, the areal averaging was done on a case to case basis. As an example, in case of nine stations recording at the same time, Figure 1.8.6. to 1.8.8 show the optimal interpolation areal averages and the weights of each station using a hypothetical data. Nevertheless, Figures 1.8.9 through 1.8.11 show the areal averaged rainfall series plotted on a daily basis for each

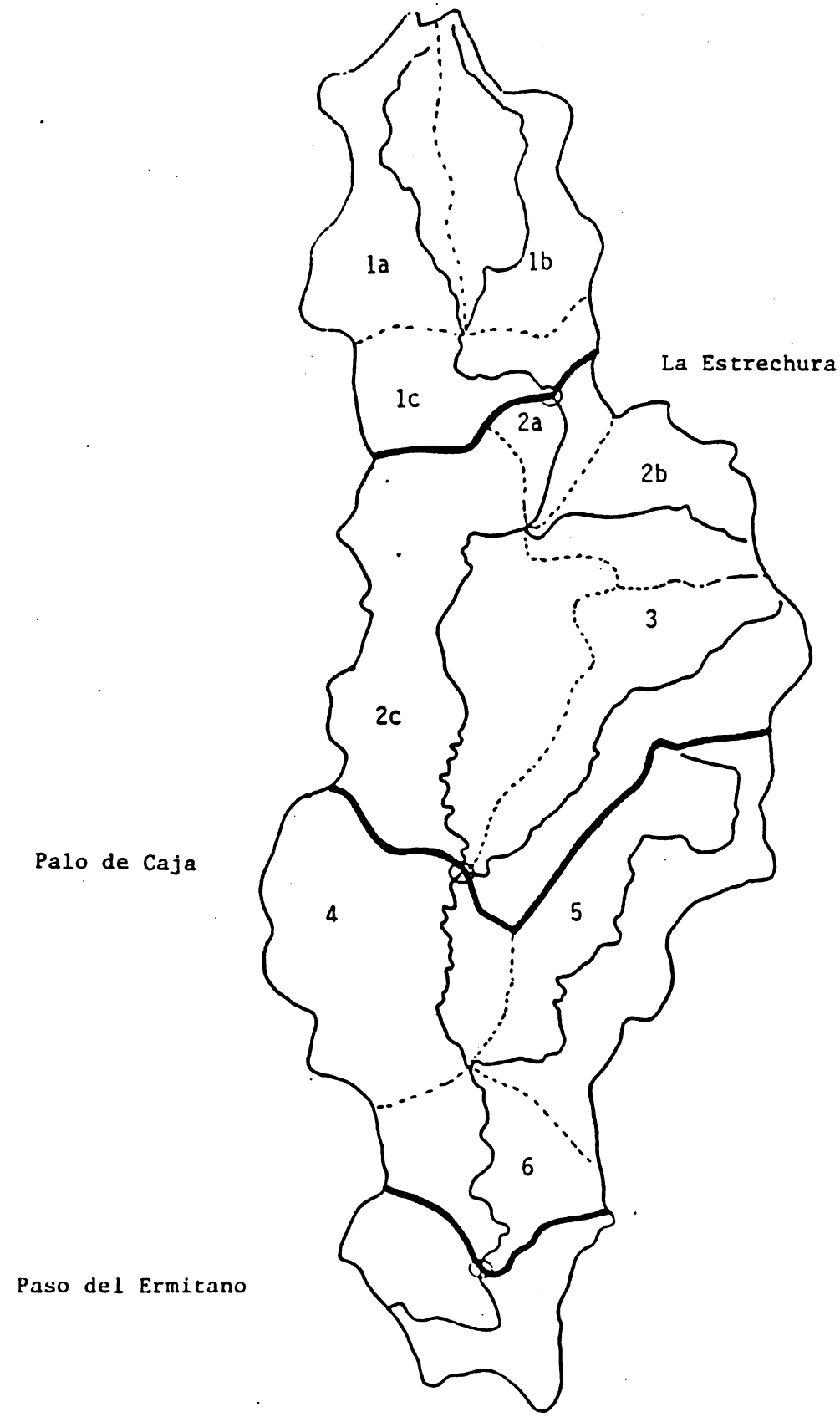

Figure 1.8.5. First and second level watershed partitions of Nizao basin for SACKW model.

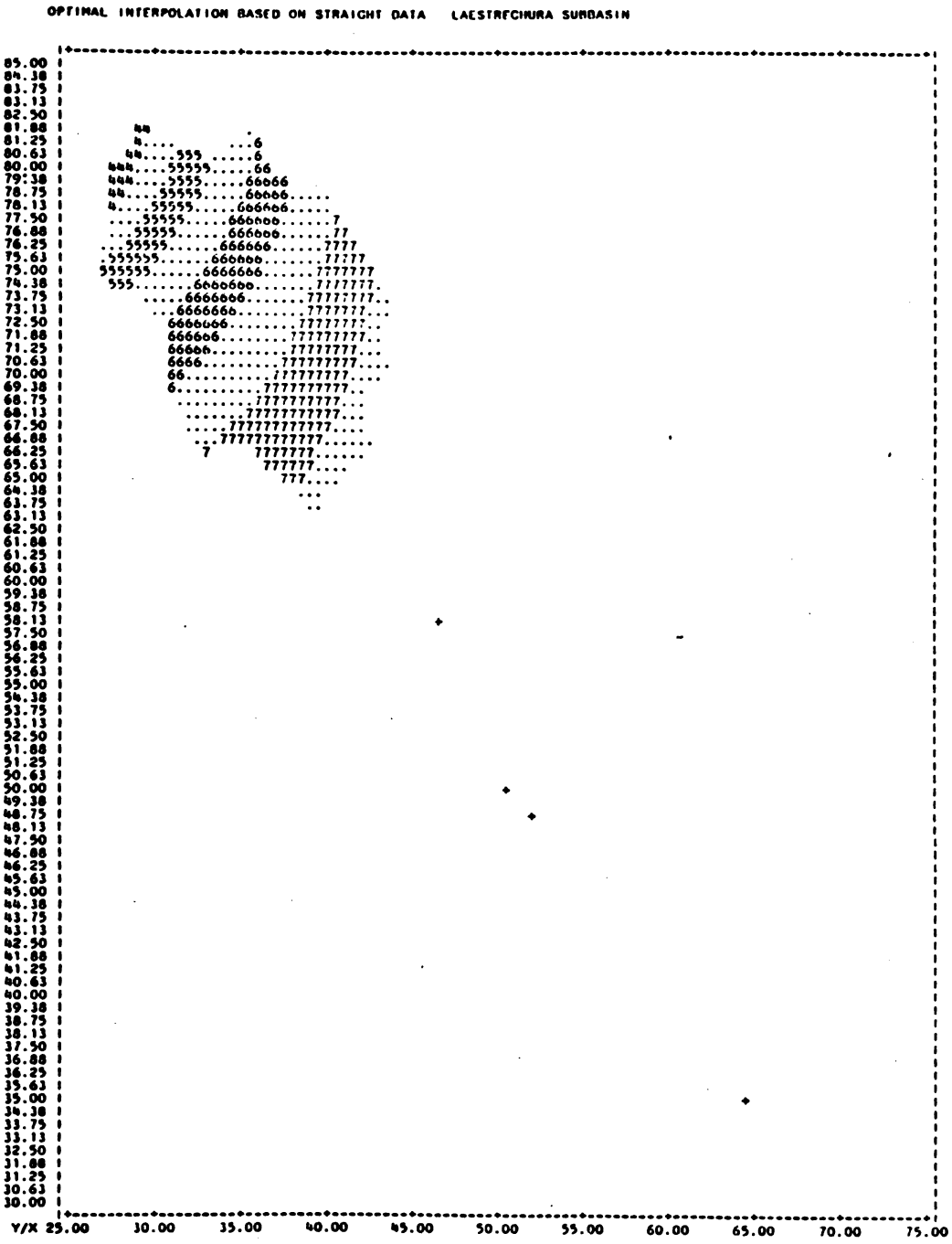

OPTIMAL AREAL AVERAGING

STA.NO.	STA. NAME	INPUT DATA	OPTIMAL WEIGHT
1	EL RIO	28.700	.0784
2	ENCOMRE	94.200	.0374
3	JUMA RON	54.000	.0664
4	LALALUNA	50.800	.0334
5	QUEMADOS	46.400	.1696
6	RIZAO	46.200	.2406
7	PALOUECA	52.200	.0240
8	VALDESIA	64.800	.0364
9	VALLENUE	22.640	.3141

SUM OF OPTIMAL WEIGHT = 1.00000
OPTIMAL AREAL MEAN = 40.917
STD. ERROR OF AREAL MEAN = 12.7183

Figure 1.8.6. Sample output of rainfall areal averaging for La Estrechura subbasin.

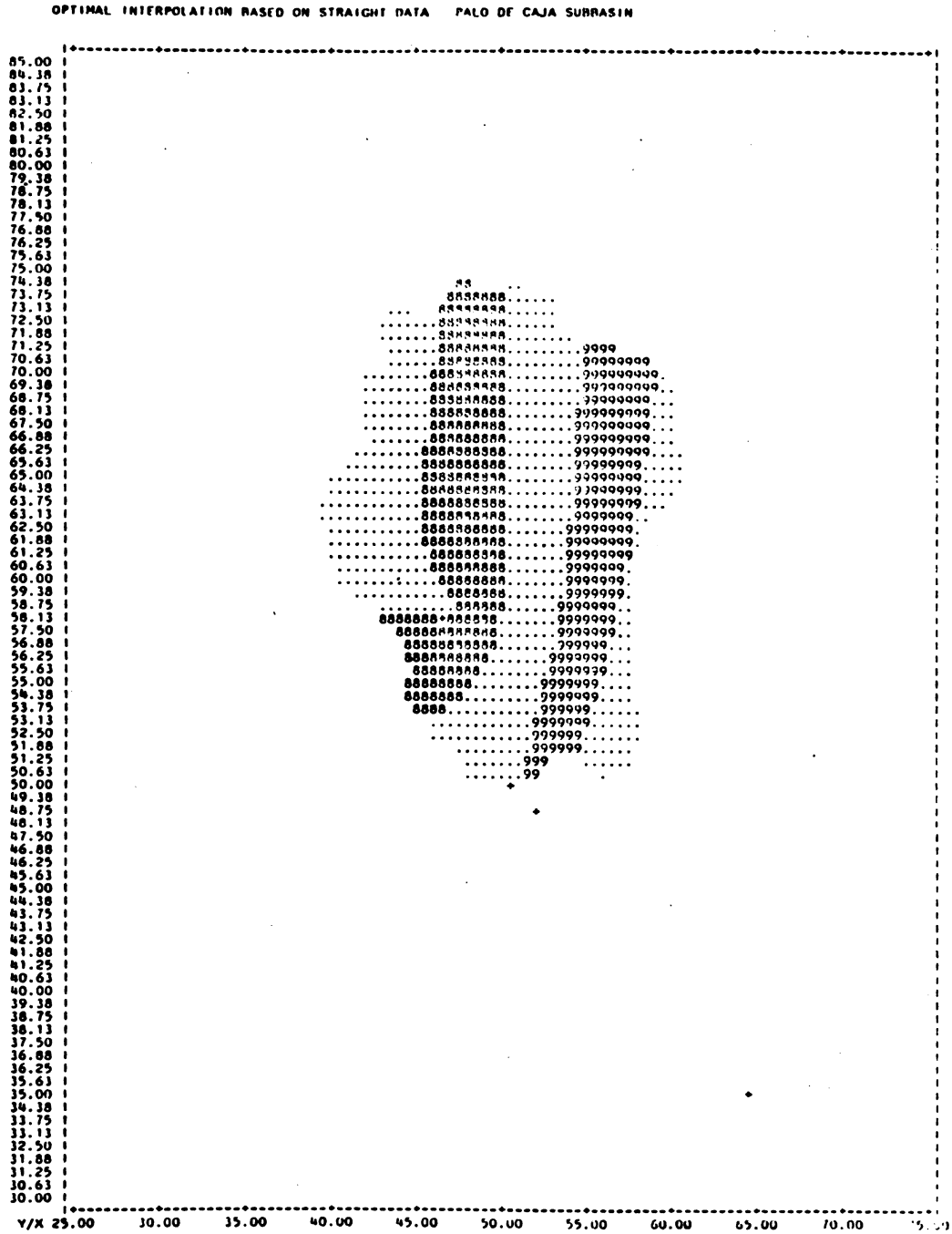

OPTIMAL AREAL AVERAGING

STA.NO.	STA. NAME	INPUT DATA	OPTIMAL WEIGHT
1	EL PIO	28.700	.0269
2	ENGOMBE	98.200	.0456
3	JUMA RUN	54.000	.0839
4	LALAGUNA	90.800	.1298
5	QUEMADOS	66.400	.0765
6	RIZAO	56.900	.4423
7	PALOBECA	52.200	.0872
8	VALDESIA	64.800	.0482
9	VALLENUE	22.640	.0596

SUM OF OPTIMAL WEIGHT = 1.00000
OPTIMAL AREAL MEAN = 49.510
STD. ERROR OF AREAL MEAN = 9.9004

Figure 1.8.7. Sample output of rainfall areal averaging for Palo de Caja subbasin.

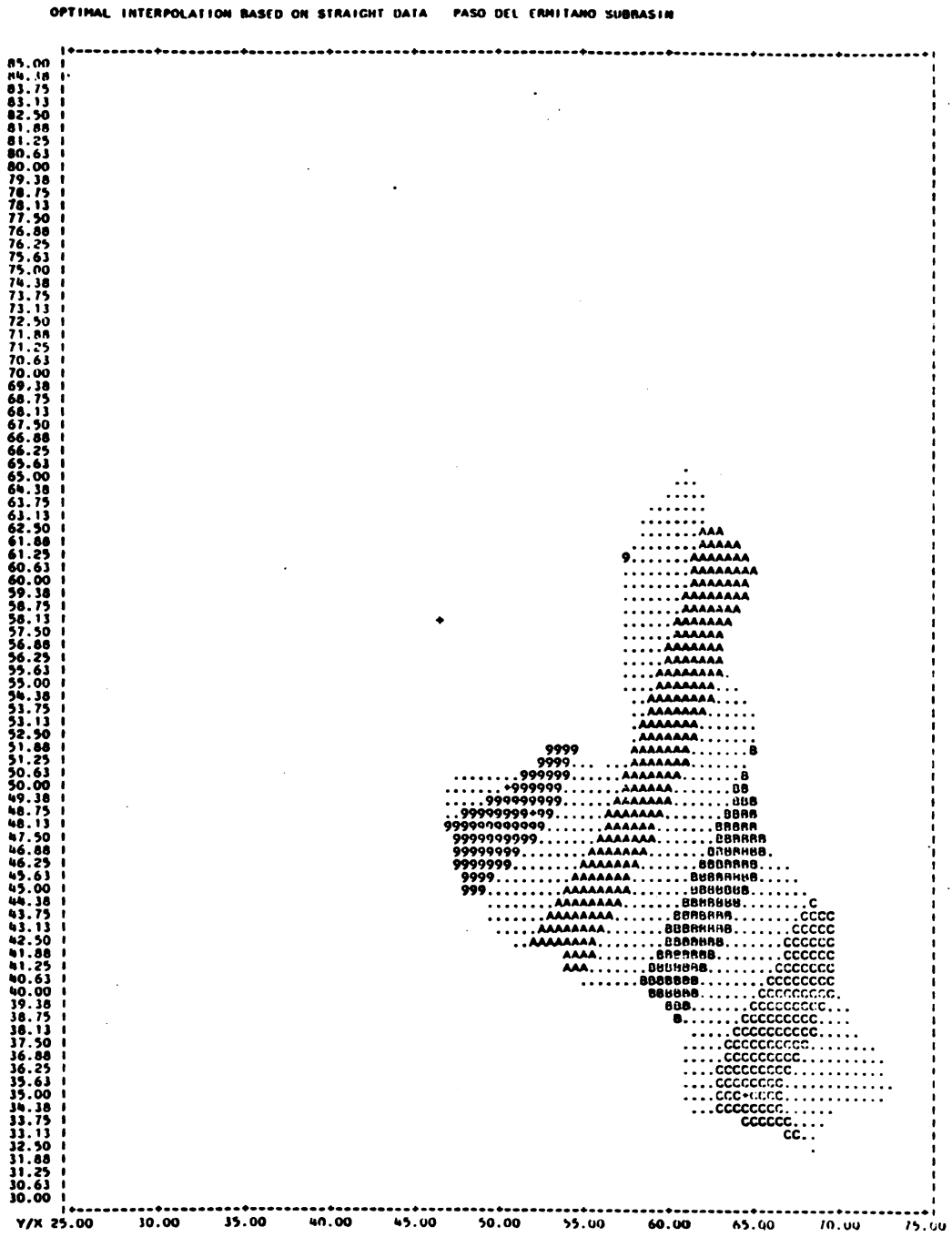

OPTIMAL AREAL AVERAGING

STA.NO.	STA. NAME	INPUT DATA	OPTIMAL WEIGHT
1	EL RIO	28.700	.0191
2	ENGOMME	94.200	.0907
3	JUNA RON	56.000	.0404
4	LALAGUNA	50.800	.0930
5	QUEMADOS	46.600	.0204
6	RIZAO	46.900	.0216
7	PALODECA	52.200	.2492
8	VALDESTA	64.800	.3430
9	VALLENUE	22.640	.0226

SUM OF OPTIMAL WEIGHT = 1.00000
OPTIMAL AREAL MEAN = 58.112
STD. ERROR OF AREAL MEAN = 10.9190

Figure 1.8.8. Sample output of rainfall areal averaging for Paso del Ermitano subbasin.

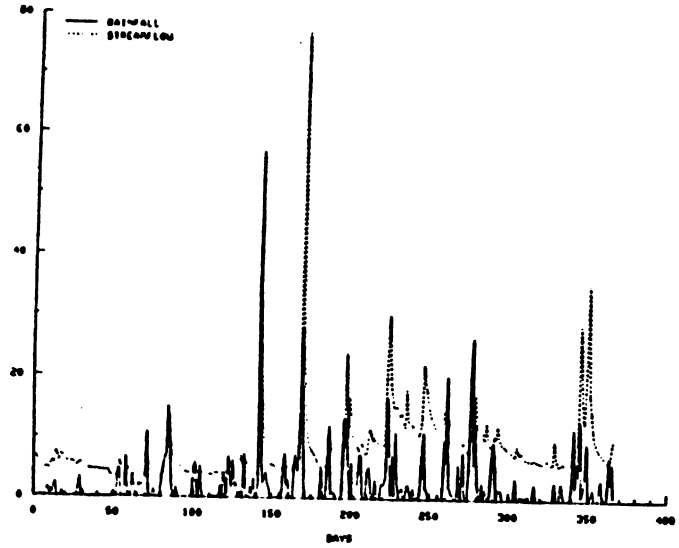

LA ESTRECHURA - 1972

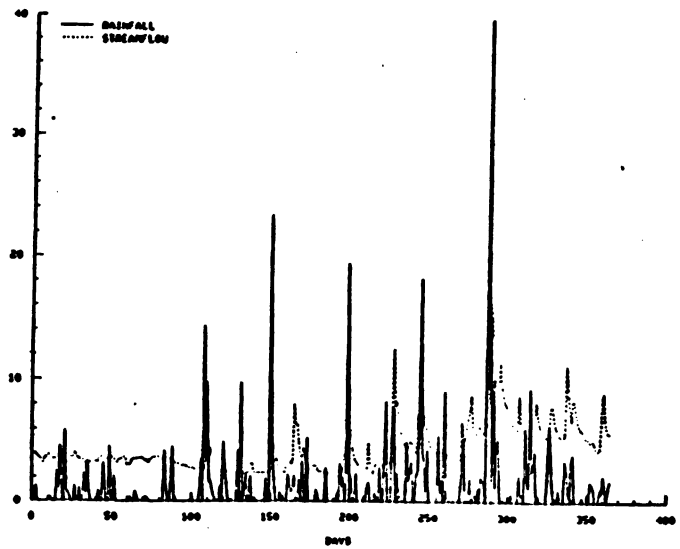

LA ESTRECHURA - 1973

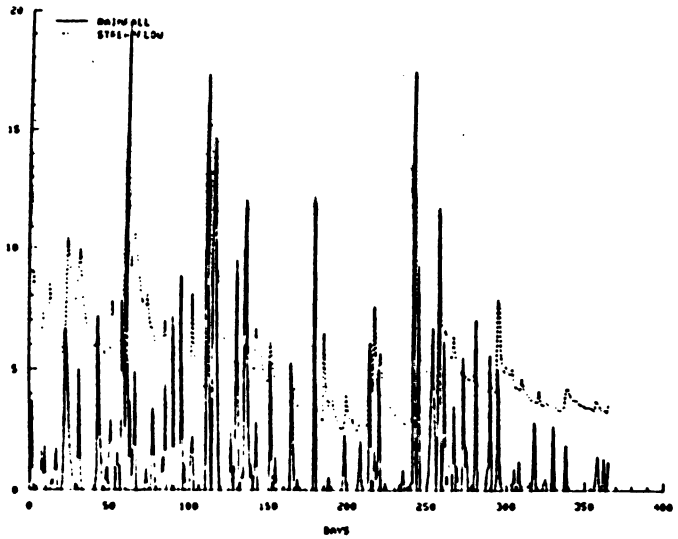

LA ESTRECHURA - 1974

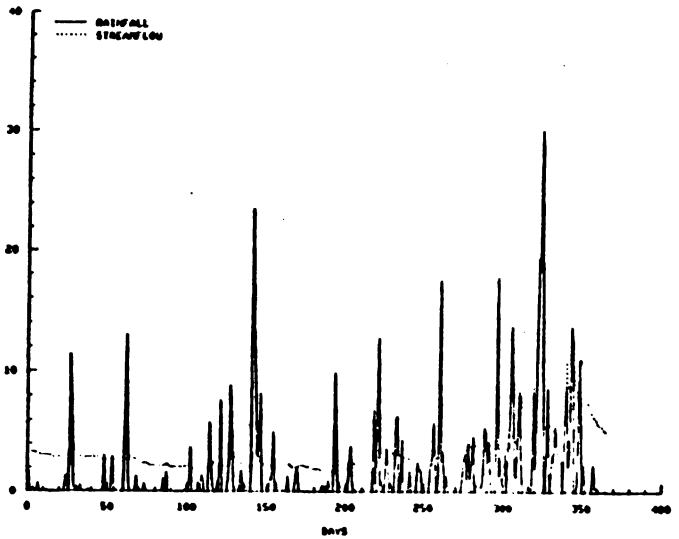

LA ESTRECHURA - 1975

Figure I.8.9. Time plots of weighted rainfall and observed streamflows at La Estrechura used in model calibration.

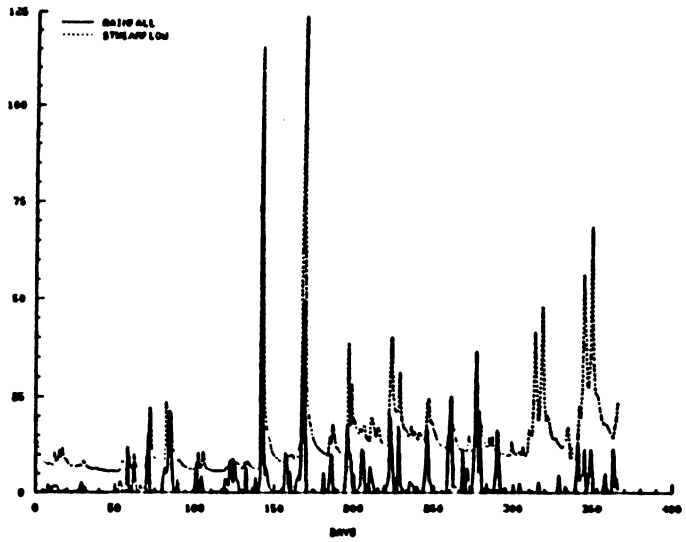

PALO DE CAJA - 1972

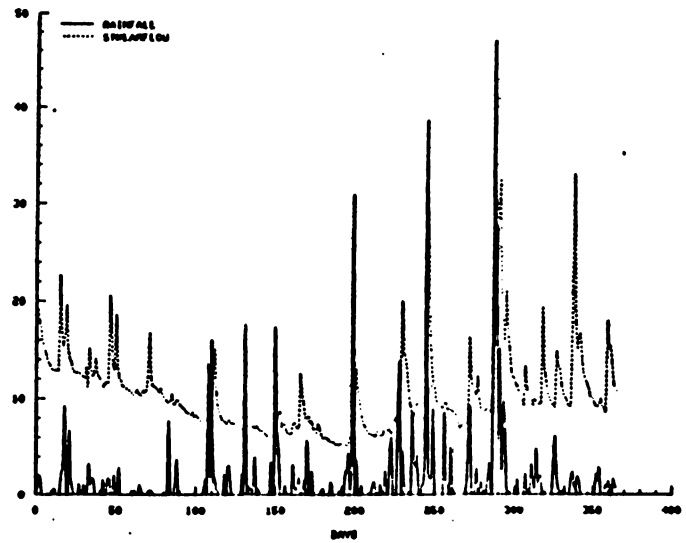

PALO DE CAJA - 1973

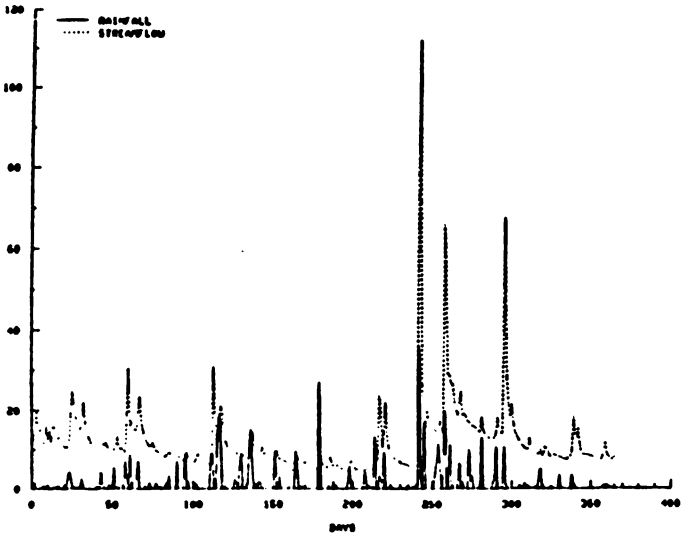

PALO DE CAJA - 1974

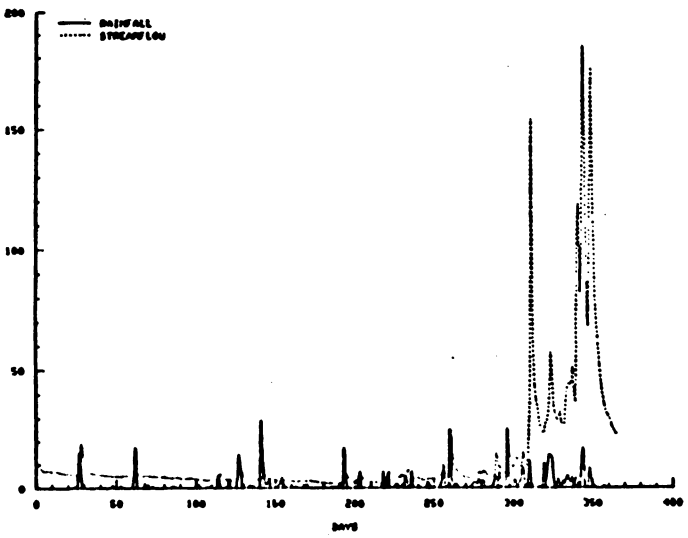

PALO DE CAJA - 1975

Figure 1.8.10. Time plots of weighted rainfall and observed streamflows at Palo de Caja used in model calibration.

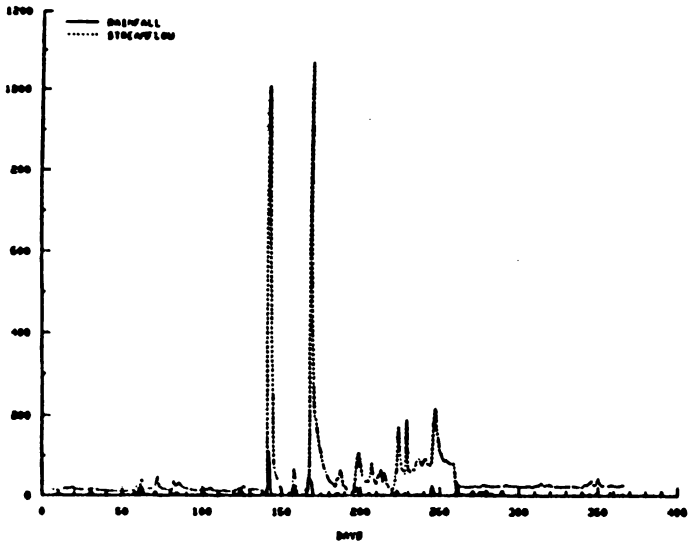

PASO DEL ERMITANO - 1972

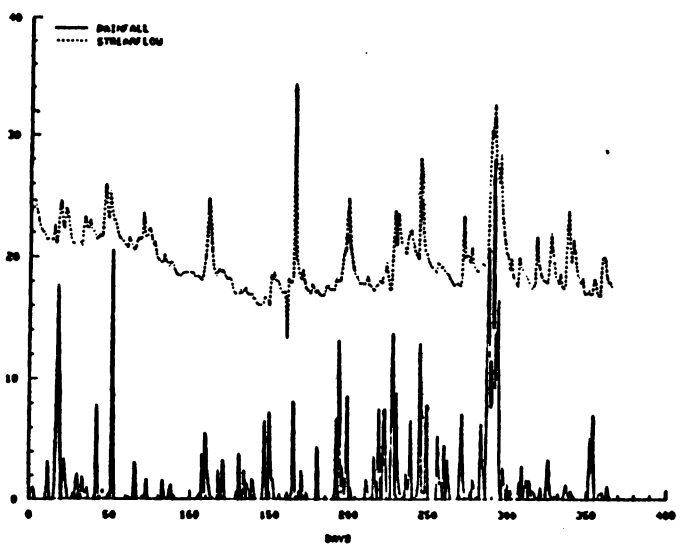

PASO DEL ERMITANO - 1973

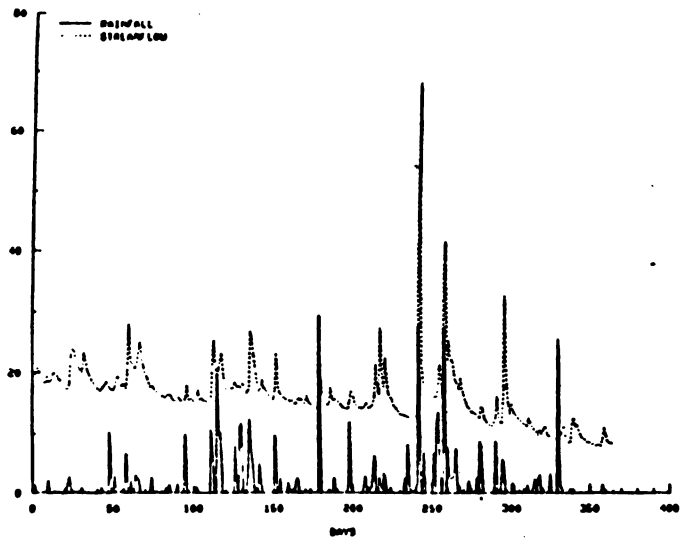

PASO DEL ERMITANO - 1974

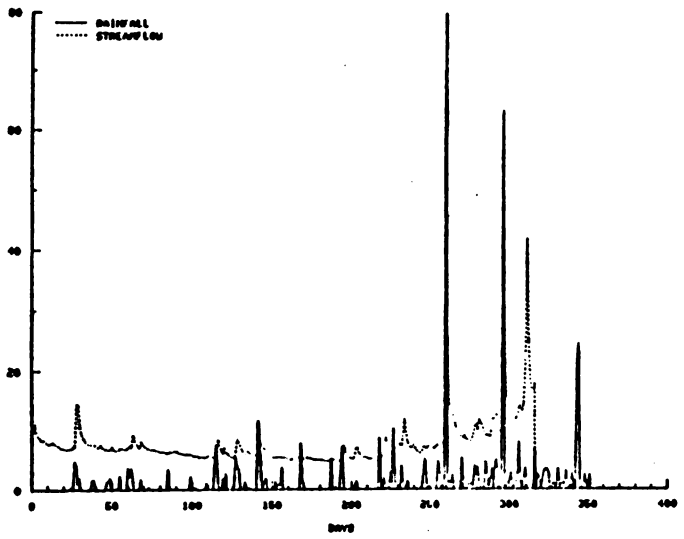

PASO DEL ERMITANO - 1975

Figure I.8.11. Time plots of weighted rainfall and observed streamflows at Paso del Ermitano used in model calibration.

subwatershed and for each year. Daily streamflow at the outlet of each subwatershed were used for purposes of calibration. Figures 1.8.9 to 1.8.11 also show the daily streamflow for each subwatershed and for each year. The daily evapotranspiration demand data required in the model is obtained from the monthly pan evaporation of Valdesia station after converting them to daily values and multiplying by an adjustment coefficient of 0.7. This demand data is assumed to be uniform all over the basin.

Based on some guidelines suggested for model calibration and references herein, the model input parameters were set up for the first year of data to be calibrated. The input file for this first year is given in Figure 1.8.12. The kinematic wave routing model parameters used were those obtained from the HEC-1 model calibration which is presented in Section 1.7.2 of the report. Beginning with year 1972, the best parameter estimates of the SAC model are obtained where some refinements were made using the optimization routine. The least squares objective function was used in the optimization runs between observed and computed daily stream flows at each subwatershed. Based on these 1972 model parameters, the calibration proceeds to 1973, then to 1974, and finally 1975. It is assumed that for four years, the kinematic wave parameters are the same such that only the SAC model parameters change. Given in Figure 1.8.13 is the summary SAC model parameters for each year and for each subwatershed. Figures 1.8.14 through 1.8.16 show the observed and computed streamflow for each year and for each subwatershed.

It is seen from these figures that some years in some subwatersheds are not fairly satisfactory. Generally, the fit between observed and

```
BASIN A - LA ESTRECHURA (1972)
   17     0  730 8784     1
0.0001          1    25     1     1
ZPERC       87.00       15.0        150.        5.0
REXP        0.709       0.5         5.0         0.1
SIDE        0.176       0.0001      10.0        0.001
UZK         0.010       0.01        0.90         0.01
ADIMP       0.115       0.001       0.5         0.001
RSERV       0.35        0.01        .50         0.01
RIVA        0.57        0.25        0.90         0.01
PCTIM       0.089       0.05        .80         0.01
LZPK        0.010       0.005       .80         0.01
LZSK        0.006       0.005       .50         0.01
PFREE       0.793       0.01        .999        0.0001
UZTWC       96.0        50.0        150.0       2.0
UZFWC       34.0        30.0        80.0        2.0
LZTWC       197.0       40.0        200.0       5.0
LZFSC       34.00       30.0        150.0       2.0
LZFPC       405.0       400.0       800.0       5.0
ADIMC       115.0       100.0       400.0       10.0
UZTWM       150.0
UZFWM       100.0
LZTWM       300.0
LZFSM       200.0
LZFPM       800.0
PXADJ       1.0
PEADJ       0.7
END
ROUTE
70.0
2500.0      0.6         0.4         100.0
16000.      0.105       0.06        0.0
5.0         15.0        1.0         7.30        0.0
BASEF     2
0.3          0.5        0.2
ROUTE
70.0
2500.       0.6         0.4         100.
20000.      0.0837      0.06        70.0
5.0         15.0        1.0         7.30        0.0
BASEF     2
0.3          0.5        0.2
ADD       2
ROUTE
45.0
4500.0      0.5         0.3         100.0
8500.0      0.0133      0.040       45.0
5.0         85.0        1.0         7.30        1.0
BASEF     2
0.3          0.5        0.2
END
RAIN
    1 8784     7     1     1
(10X,F10.0)
ETDATA
```

Figure 1.8.12 SACKW model input file for year 1972.

```
   24    9    1    1
(10F8.0)
FLOW
   24  366    8    1    1
(10X,F10.0)
END
BASIN B - PALO DE CAJA (1972)
   17.   0  730 8784    1
1.0        25.0       0.0001     1.0        1.0
ZPERC      178.0      15.0       180.       5.0
REXP       0.400      0.4        5.0        0.1
SIDE       1.050       0.001     10.0       0.001
UZK        0.030      0.03       0.90        0.01
ADIMP      0.145      0.001      0.6        0.001
RSERV      0.225      0.01       .50        0.01
RIVA       0.339      0.25       0.90        0.01
PCTIM      0.015      0.005      .80        0.01
LZPK       0.003      0.001      .80        0.01
LZSK       0.002      0.001      .50        0.0001
PFREE      0.987      0.01       .999       0.0001
UZTWC      43.0       40.0       150.0      2.0
UZFWC      32.5       30.0       80.0       2.0
LZTWC      42.50      40.0       200.0      5.0
LZFSC      44.00      40.0       150.0      2.0
LZFPC      324.5      300.0      800.0      5.0
ADIMC      217.5      100.0      400.0      10.0
UZTWM      150.0
UZFWM      100.0
LZTWM      300.0
LZFSM      200.0
LZFPM      800.0
PXADJ      1.0
PEADJ      0.7
END
ROUTE
24.0
2000.0     0.4        0.3        100.0
7500.0     0.108      0.040      0.0
5.0        85.0       1.0        14.0       1.0
BASEF    2
0.3        0.5        0.2
ROUTE
56.0
3500.      0.2        0.3        100.
13500.     0.0452     0.05       0.0
5.0        10.0       1.0        14.0       0.0
BASEF    2
0.3        0.5        0.2
ADD      2
ROUTE
164.0
4500.0     0.4        0.3        100.0
33500.0    0.0086     0.040      00.0
5.0        70.0       1.0        14.0       1.0
BASEF    2
```

Figure 1.8.12 (continuation)

```
0.3         0.5         0.2
ROUTE
103.0
2000.       0.4         0.3         100.
33000.      0.0293      0.05        00.0
5.0         10.0        1.0         14.0        0.0
BASEF     2
0.3         0.5         0.2
ADD       2
END
RAIN
     1 8784     7     1     1
(20X,F10.0)
ETDATA
    24     9     1     1
(10F8.0)
FLOW
    24  366     8     1     1
(20X,F10.0)
END
BASIN C - PASO DEL ERMITANO (1972)
    17     0  730 8784     1
1.0         25.0        0.0001      1.0         1.0
ZPERC       33.70       15.0        150.        5.0
REXP        4.83        0.5         5.0         0.1
SIDE        0.006       0.001       10.0        0.001
UZK         0.900       0.15        0.95         0.01
ADIMP       0.092       0.001       0.5         0.001
RSERV       0.440       0.01        .50         0.01
RIVA        0.829       0.25        0.90         0.01
PCTIM       0.908       0.10        .90         0.01
LZPK        0.012       0.01        .80         0.01
LZSK        0.476       0.01        .50         0.01
PFREE       0.994       0.001       .999        0.0001
UZTWC       98.0        50.0        150.0       2.0
UZFWC       57.0        40.0        80.0        2.0
LZTWC       195.0       40.0        200.0       5.0
LZFSC       74.65       60.0        150.0       2.0
LZFPC       501.0       400.0       800.0       5.0
ADIMC       350.0       100.0       400.0       10.0
UZTWM       150.0
UZFWM       100.0
LZTWM       300.0
LZFSM       200.0
LZFPM       800.0
PXADJ       1.0
PEADJ       0.7
END
ROUTE
103.0
5000.0      0.5         0.3         100.0
18000.      0.0148      0.04        0.0
5.0         80.0        1.0         23.6        1.0
BASEF     2
0.3         0.5         0.2
```

Figure 1.8.12 (continuation)

```
ROUTE
109.0
3000.      0.4        0.3        100.
34000.     0.0323     0.05       00.0
5.0        10.0       1.0        23.6        0.0
BASEF      2
0.3        0.5        0.2
ADD        2
ROUTE
53.0
5000.0     0.4        0.3        100.0
18000.     0.0119     0.040      00.0
5.0        80.0       1.0        23.6        1.0
BASEF      2
0.3        0.5        0.2
END
RAIN
    1 8784     7     1     1
(30X,F10.0)
ETDATA
   24     9     1     1
(10F8.0)
FLOW
   24  366     8     1     1
(30X,F10.0)
```

Figure 1.8.12 (continuation)

LA ESTRECHURA

	1972	1973	1974	1975	AVE
ZPERC	87.000	97.000	17.000	147.000	87.000
REXP	.709	.659	1.909	1.819	1.274
SIDE	.176	.207	.175	.219	.194
UZK	.010	.006	.005	.005	.007
ADIMP	.115	.115	.085	.073	.097
RSERV	.350	.500	.593	.621	.516
RIVA	.570	.880	.880	.990	.830
PCTIM	.089	.014	.003	.001	.027
LZPK	.010	.009	.013	.025	.014
LZSK	.006	.005	.015	.029	.014
PFREE	.793	.793	.800	.801	.797
UZTWC	96.000	100.000	148.300	84.600	
UZFWC	34.000	2.320	.103	.010	
LZTWC	197.000	300.000	295.100	274.000	
LZFSC	34.000	99.000	84.680	19.790	
LZFPC	405.000	320.000	267.200	92.020	
ADIMC	115.000	390.000	439.800	349.000	
UZTWM	150.000	150.000	150.000	150.000	150.000
UZFWM	100.000	100.000	100.000	100.000	100.000
LZTWM	300.000	301.000	301.000	301.000	300.750
LZFSM	200.000	200.000	200.000	200.000	200.000
LZFPM	800.000	800.000	800.000	800.000	800.000
PXADJ	1.000	1.000	1.000	1.000	1.000
PEADJ	.700	.700	.700	.700	.700

PALO DE CAJA

	1972	1973	1974	1975	AVE
ZPERC	178.000	198.000	140.000	145.000	165.250
REXP	.400	.275	.440	.285	.350
SIDE	1.050	1.057	1.049	1.000	1.039
UZK	.030	.020	.050	.002	.026
ADIMP	.145	.141	.171	.121	.145
RSERV	.225	.365	.585	.585	.440
RIVA	.339	.439	.739	.939	.614
PCTIM	.015	.001	.031	.001	.012
LZPK	.003	.008	.011	.041	.016
LZSK	.002	.002	.004	.015	.006
PFREE	.987	.987	.989	.999	.991
UZTWC	43.000	100.000	148.300	85.400	
UZFWC	32.500	4.160	.008	.006	
LZTWC	42.500	278.000	214.800	160.800	
LZFSC	44.000	183.000	118.200	65.360	
LZFPC	324.500	721.700	322.900	137.200	
ADIMC	217.500	385.500	437.500	348.900	
UZTWM	150.000	150.000	150.000	150.000	150.000
UZFWM	100.000	100.000	100.000	100.000	100.000
LZTWM	300.000	300.000	300.000	300.000	300.000
LZFSM	200.000	200.000	200.000	200.000	200.000
LZFPM	800.000	800.000	800.000	800.000	800.000
PXADJ	1.000	1.000	1.000	1.000	1.000
PEADJ	.700	.700	.700	.700	.700

PASO DEL ERMITANO

	1972	1973	1974	1975	AVE
ZPERC	33.700	199.300	218.700	199.600	162.825

Figure 1.8.13 Summary of SAC model parameters calibrated for years 1972 to 1975.

REXP	4.830	.502	.130	.100	1.391
SIDE	.006	.372	.360	.236	.244
UZK	.900	.125	.135	.152	.328
ADIMP	.092	.004	.003	.002	.025
RSERV	.440	.470	.750	.190	.463
RIVA	.829	.879	.880	.320	.727
PCTIM	.908	.155	.040	.051	.289
LZPK	.012	.010	.010	.004	.009
LZSK	.476	.075	.016	.003	.143
PFREE	.994	.975	.948	.742	.915
UZTWC	98.000	100.000	148.300	84.800	
UZFWC	57.000	.000	.000	.010	
LZTWC	195.000	160.000	137.400	126.500	
LZFSC	74.650	4.600	3.824	20.230	
LZFPC	501.000	165.000	187.400	127.900	
ADIMC	350.000	386.000	438.800	348.400	
UZTWM	150.000	150.000	150.000	150.000	150.000
UZFWM	100.000	100.000	100.000	100.000	100.000
LZTWM	300.000	300.000	300.000	300.000	300.000
LZFSM	200.000	200.000	200.000	200.000	200.000
LZFPM	800.000	800.000	800.000	800.000	800.000
PXADJ	1.000	1.000	1.000	1.000	1.000
PEADJ	.700	.700	.700	.700	.700

Figure 1.8.13 (continuation)

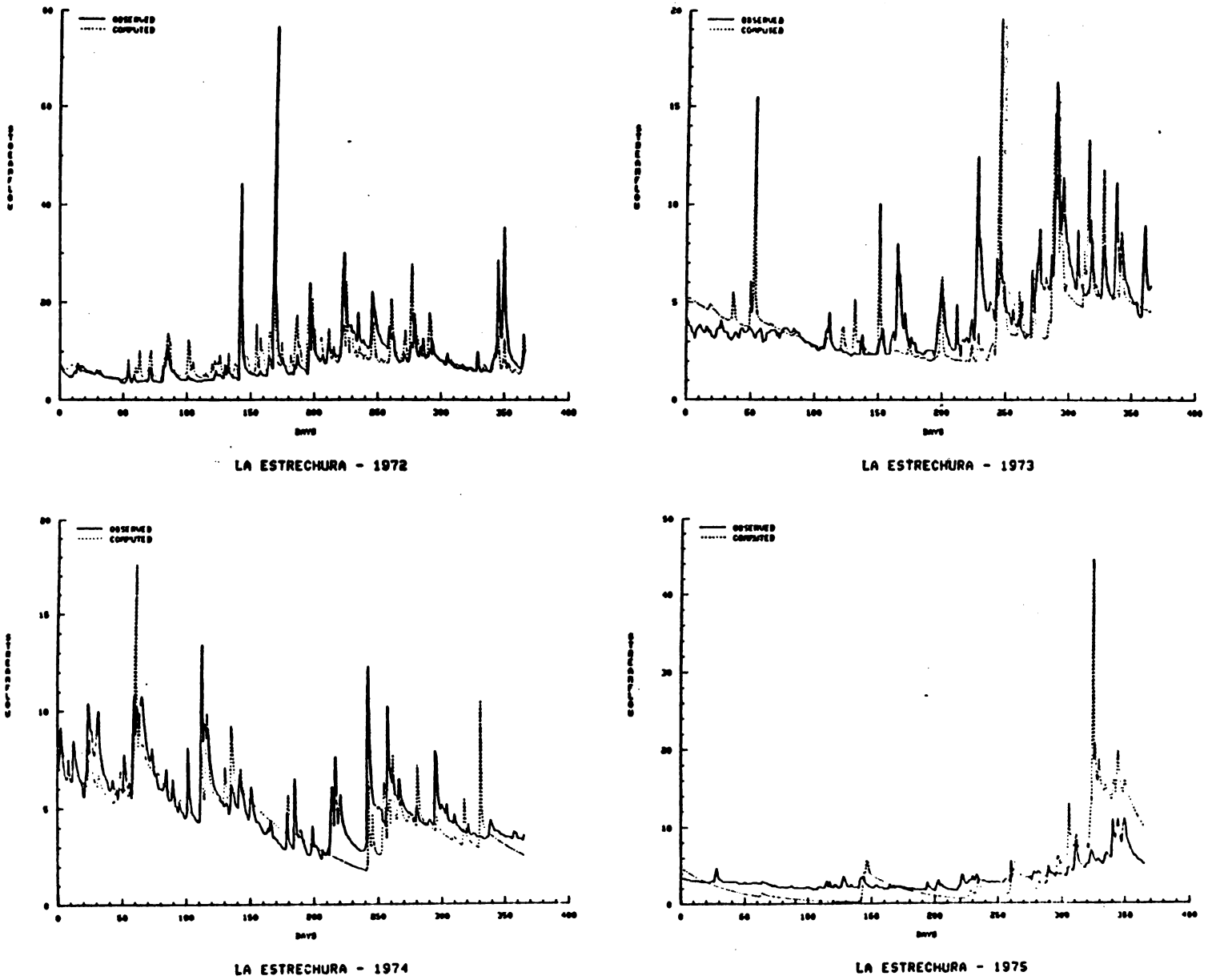

Figure 1.8.14. Observed and computed streamflows at La Estrechura resulting from model calibration.

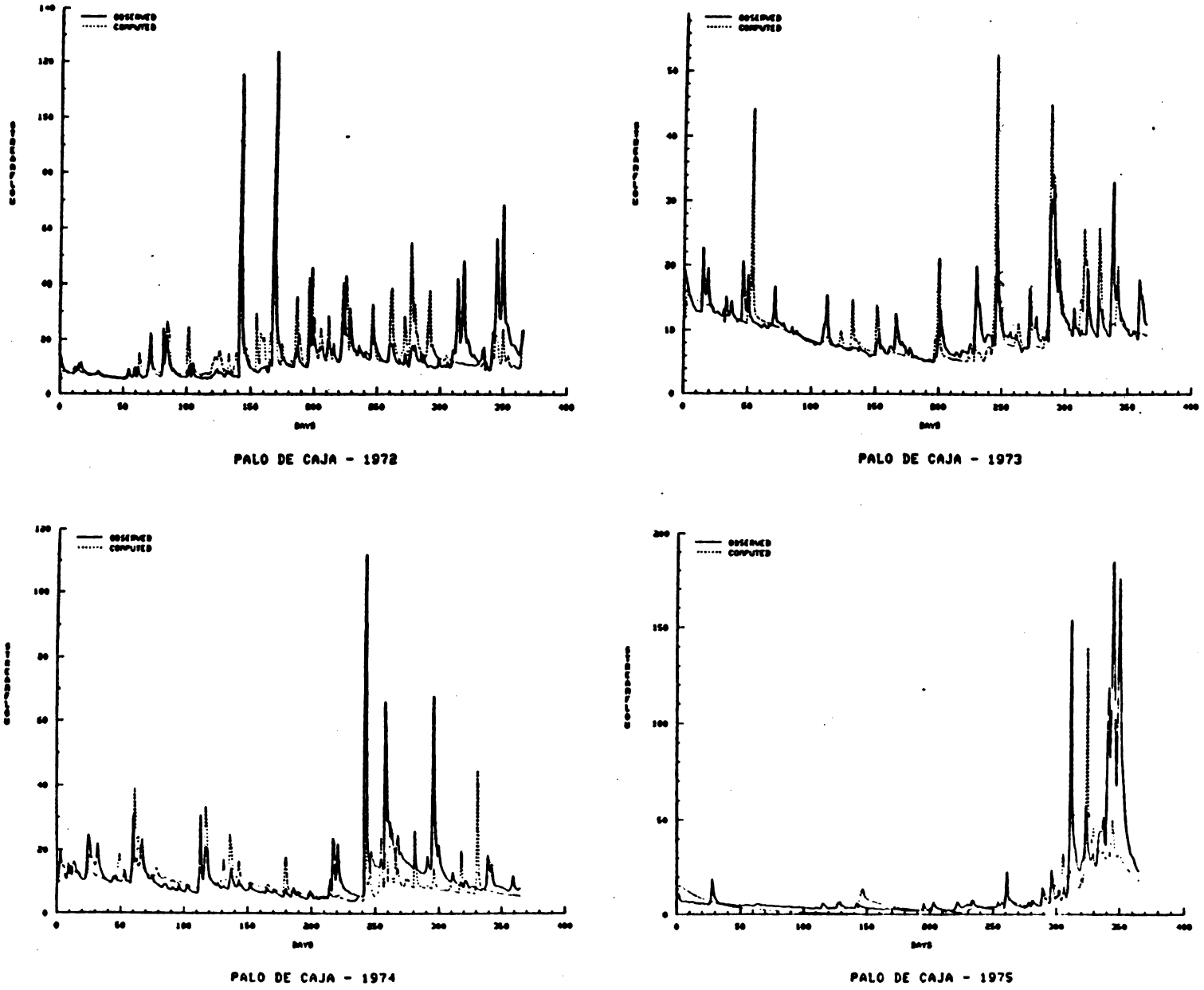

Figure 1.8.15. Observed and computed streamflows at Palo de Caja resulting from model calibration.

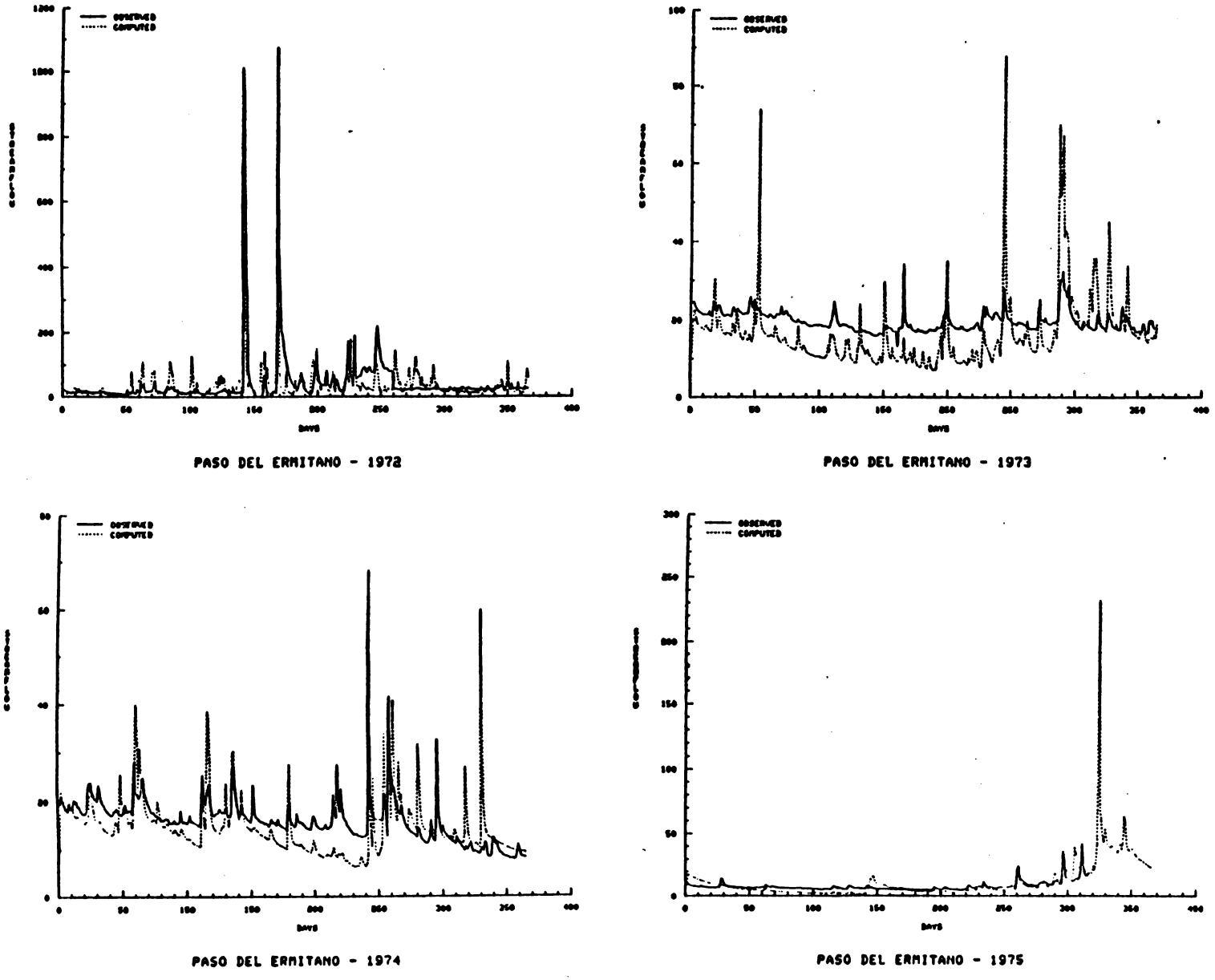

Figure 1.8.16. Observed and computed streamflows at Paso del Ermitano resulting from model calibration.

computed streamflows worsens in going from La Estrechura to Paso del Ermitano (i.e. upstream to downstream). This can be expected since any calibration inadequacy at the upstream flow points are carried to the downstream flow points. It appears that the best fit is in year 1972.

One major problem encountered in the model calibration is the rainfall data where inconsistencies with respect to streamflow are found. For example, the worst fit between observed and computed streamflow experienced in La Estrechura in 1974 can well be attributed to the rainfall data as seen in the plots of rainfall with streamflow in Figure 1.8.9. Admittedly, this is difficult to resolve since the inconsistency can be caused by inadequacies in areal averaging, representativeness of rainfall stations recording at this time, or sampling errors. It may be noted that the rainfall data could be the most critical input to the SACKW model. This is attested by Burnash (1985) in which from several tests conducted on the sensitivity of the Sacramento model, a particular runoff hydrograph is ten times as sensitive to a shift in the rainfall input as it is to a similar change in the most sensitive parameters.

1:8.5 Model Applications

This section presents two applications of the SACKW model in simulation mode. Both applications are designed to estimate the streamflows at Paso del Ermitano associated with: Hurricanes David and Frederic data; and, the probable maximum precipitation (PMP) data taking from the TP-42 model which was provided by the project counterparts.

Hurricane David and Frederic Data

Hurricanes David and Frederic hit the Dominican Republic around late August, 1979 and early September, 1979, respectively. No

streamflow data was recorded during this period. However, hourly rainfall data is available. For purposes of this exercise, the model parameters calibrated for year 1972 are used since it is found to have the best fit as well as this year experienced a high flood flow regime which occurred around late May.

The input data file for the model is shown in Figure 1.8.17. To obtain the streamflows during the hurricane period of interest, the model has to be ran from year 1976 up to 1979. Results from this run are shown in Figures 1.8.18 and 1.8.19 assuming that there is an evapotranspiration (ET) demand and without ET demand, respectively. For hurricane David, the highest streamflows estimated are 6983 cms for the case where there is ET demand and 7074 cms for the case with no ET demand. Both highest flows occurred on the 21st hour of August 31, 1979.

Probable Maximum Precipitation Data

The probable maximum precipitation (PMP) data was provided by the project counterpart which was obtained using the TP-42 model. A total of 48 hours of hourly rainfall data are available. As in the previous model application, the SAC parameters calibrated for year 1972 were used here. For purposes here, two sets of initial soil-moisture regimes are used which are for dry condition and wet condition. Results of the SACKW model run are given in Figures 1.8.20 and 1.8.21, for the dry condition and wet condition, respectively. Only the results for Paso del Ermitano subbasin are shown in these figures. For the case of initially dry soil condition, the peak flow estimated is 19,237.94 cms while that for wet condition is 22,618.10 cms. These results are quite

```
BASIN A - LA ESTRECHURA (1976-1979)  1972 PARAMETERS
    0     0 8766 8766     1
ZPERC      87.00
REXP       0.709
SIDE       0.176
UZK        0.010
ADIMP      0.115
RSERV      0.35
RIVA       0.57
PCTIM      0.089
LZPK       0.010
LZSK       0.006
PFREE      0.793
UZTWM      150.0
UZFWM      100.0
LZTWM      300.0
LZFSM      200.0
LZFPM      800.0
UZTWC      120.4
UZFWC      0.005
LZTWC      297.27
LZFSC      41.06
LZFPC      185.43
ADIMC      416.5
PXADJ      1.0
PEADJ      0.7
END
ROUTE
70.0
2500.0     0.6        0.4        100.0
16000.     0.105      0.06       0.0
5.0        15.0       1.0        5.10       0.0
BASEF      2
0.3        0.5        0.2
ROUTE
70.0
2500.      0.6        0.4        100.
20000.     0.0837     0.06       70.0
5.0        15.0       1.0        5.10       0.0
BASEF      2
0.3        0.5        0.2
ADD        2
ROUTE
45.0
4500.0     0.5        0.3        100.0
8500.0     0.0133     0.040      45.0
5.0        85.0       1.0        5.10       1.0
BASEF      2
0.3        0.5        0.2
END
RAIN
    135064     7     1     1
(10X,F10.0)
ETDATA
   24     9     1     1
```

Figure 1.8.17. Model input file for model testing by forecasting hurricanes David and Frederic flood flow regime.

```
(10F8.0)
FLOW
    1     0
END
BASIN B - PALO DE CAJA (1976-1979)  1972 PARAMETERS
    0     0 8766 8766     1
ZPERC      178.0
REXP       0.400
SIDE       1.050
UZK        0.030
ADIMP      0.145
RSERV      0.225
RIVA       0.339
PCTIM      0.015
LZPK       0.003
LZSK       0.002
PFREE      0.987
UZTWM      150.0
UZFWM      100.0
LZTWM      300.0
LZFSM      200.0
LZFPM      800.0
UZTWC      120.4       40.0        150.0       2.0
UZFWC      .000        00.0        80.0        2.0
LZTWC      75.0        40.0        300.0       5.0
LZFSC      56.05       40.0        200.0       2.0
LZFPC      92.07       100.0       500.0       5.0
ADIMC      414.4       100.0       450.0       10.0
PXADJ      1.0
PEADJ      0.7
END
ROUTE
24.0
2000.0     0.4         0.3         100.0
7500.0     0.108       0.040       0.0
5.0        85.0        1.0         23.1        1.0
BASEF      2
0.3        0.5         0.2
ROUTE
56.0
3500.      0.2         0.3         100.
13500.     0.0452      0.05        0.0
5.0        10.0        1.0         23.1        0.0
BASEF      2
0.3        0.5         0.2
ADD        2
ROUTE
164.0
4500.0     0.4         0.3         100.0
33500.0    0.0086      0.040       00.0
5.0        70.0        1.0         23.1        1.0
BASEF      2
0.3        0.5         0.2
ROUTE
103.0
```

Figure 1.8.17 (continuation)

```
2000.       0.4         0.3         100.
33000.      0.0293      0.05        00.0
5.0         10.0        1.0         23.1        0.0
BASEF       2
0.3         0.5         0.2
ADD         2
END
RAIN
    135064      7     1     1
(20X,F10.0)
ETDATA
   24     9     1     1
(10F8.0)
FLOW
    1     0
END
BASIN C - PASO DEL ERMITANO (1976-1979)  1972 PARAMETERS
    0     0 8766 8766     1
ZPERC       33.70
REXP        4.83
SIDE        0.006
UZK         0.900
ADIMP       0.092
RSERV       0.440
RIVA.       0.829
PCTIM       0.908
LZPK        0.012
LZSK        0.476
PFREE       0.994
UZTWM       150.0
UZFWM       100.0
LZTWM       300.0
LZFSM       200.0
LZFPM       800.0
UZTWC       84.8        50.0        150.0       2.0
UZFWC       0.01        00.0        80.0        2.0
LZTWC       126.5       40.0        200.0       5.0
LZFSC       20.23       60.0        150.0       2.0
LZFPC       127.9       0.0         800.0       5.0
ADIMC       348.4       100.0       400.0       10.0
PXADJ       1.0
PEADJ       0.7
END
ROUTE
103.0
5000.0      0.5         0.3         100.0
18000.      0.0148      0.04        0.0
5.0         80.0        1.0         29.18       1.0
BASEF       2
0.3         0.5         0.2
ROUTE
109.0
3000.       0.4         0.3         100.
34000.      0.0323      0.05        00.0
5.0         10.0        1.0         29.18       0.0
```

Figure 1.8.17 (continuation)

```
BASEF     2
0.3        0.5        0.2
ADD       2
ROUTE
53.0
5000.0     0.4        0.3        100.0
18000.     0.0119     0.040      00.0
5.0        80.0       1.0        29.18      1.0
BASEF     2
0.3        0.5        0.2
END
RAIN
    135064     7     1     1
(30X,F10.0)
ETDATA
   24     9     1     1
(10F8.0)
FLOW
    1     0
```

Figure 1.8.17 (continuation)

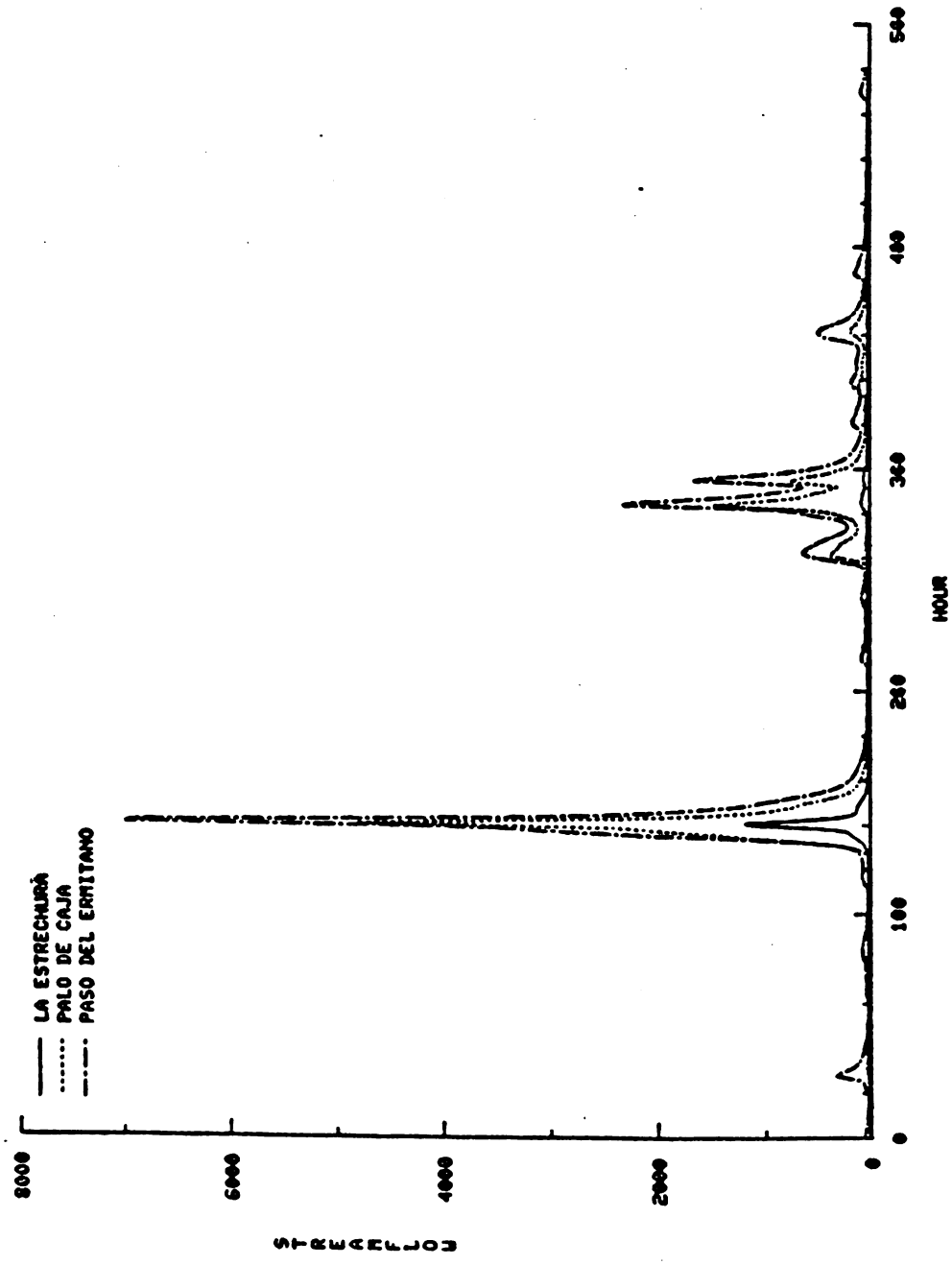

Figure 1.8.18. Results of model run with evapotranspiration demand for hurricanes David and Frederic (Aug 26-Sep 14, 1979).

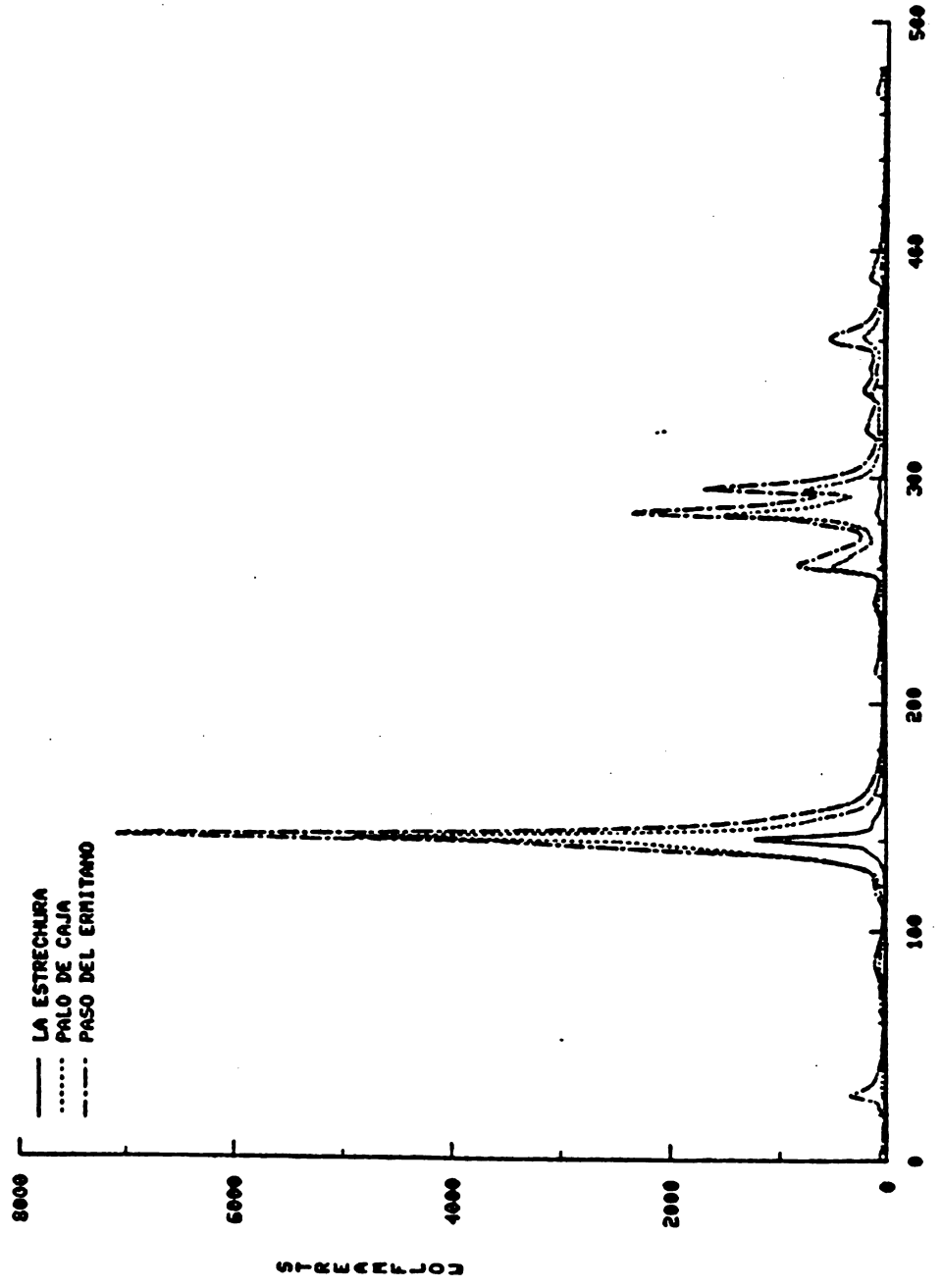

Figure 1.8.19. Results of model run without evapotranspiration demand for hurricanes David and Frederic (Aug 26-Sep 14, 1979).

```
BASIN 3 RUN: BASIN C - PASO DEL ERMITANO (PMF - DRY CONDITION)

LIST OF PARAMETERS MANUALLY CALIBRATED

  NAME          VALUE

 ZPERC          33.70000
 REXP            4.83000
 SIDE            0.00600
 UZK             0.90000
 ADIMP           0.09200
 RSERV           0.44000
 RIVA            0.82900
 PCTIM           0.90800
 LZPK            0.01200
 LZSK            0.47600
 PFREE           0.77400
 UZTWM         150.00000
 UZFWM         100.00000
 LZTWM         300.00000
 LZFSM         200.00000
 LZFPM         800.00000
 UZTWC           0.00000
 UZFWC           0.00000
 LZTWC           0.00000
 LZFSC           0.00000
 LZFPC           0.00000
 ADIMC           0.00000
 PXADJ           1.00000
 PEADJ           0.70000

OPTIMIZATION PARAMETERS :
  OBJECTIVE FUNCTION TYPE          0
  MAXIMUM NUMBER OF ITERATIONS     0
  CONVERGENCE CRITERION   0.00000E+00
  STEP SIZE UPDATE OPTION          0
  PRINTING FREQUENCY               0

NUMBER OF PARAMETERS TO BE OPTIMIZED =   0
NUMBER OF PARAMETERS MANUALLY CALIBRATED = 24

PARAMETERS MANUALLY CALIBRATED AFTER CHECKING

  ITEM NAME     VALUE

   1  ZPERC     33.70000
   2  REXP       4.83000
   3  SIDE       0.00600
   4  UZK        0.90000
   5  ADIMP      0.09200
   6  RSERV      0.44000
   7  RIVA       0.82900
   8  PCTIM      0.90800
   9  LZPK       0.01200
  10  LZSK       0.47600
```

Figure 1.8.20. Results of model run using PMP data under initially dry soil-moisture conditions.

11	PFREE	0.99400
12	UZTWM	150.00000
13	UZFWM	100.00000
14	LZTWM	300.00000
15	LZFSM	200.00000
16	LZFPM	800.00000
17	UZTWC	0.00000
18	UZFWC	0.00000
19	LZTWC	0.00000
20	LZFSC	0.00000
21	LZFPC	0.00000
22	ADIMC	0.00000
23	PXADJ	1.00000
24	PEADJ	0.70000

1

SACRAMENTO SOIL-MOISTURE ACCOUNTING OPERATION

PARAMETER VALUES - CAPACITIES ARE IN MM.

PX-ADJ	PE-ADJ	UZTWM	UZFWM	UZK	PCTIM	ADIMP	RIVA
1.000	0.700	150.000	100.000	0.900	0.908	0.092	0.829

DAILY ET DIST. ASSUMED UNIFORM

PBASE	ZPERC	REXP	LZTWM	LZFSM	LZFPM	LZSK	LZPK	PFREE	RSERV	SIDE
104.800	33.700	4.830	300.000	200.000	800.000	0.476	0.012	0.994	0.440	0.006

SOIL-MOISTURE CONTENTS (MM)

UZTWC	UZFWC	LZTWC	LZFSC	LZFPC	ADIMC
0.000	0.000	0.000	0.000	0.000	0.000

DETAILED SOIL-MOISTURE ACCOUNTING OUTPUT UNITS ARE IN MM.

DAY	HR	UZTWC	UZFWC	LZTWC	LZFSC	LZFPC	ADIMC	PERC	IMP	DIR	SUR	INT	SUP	PRI	TOT-RO	ET-DMD	ACT-ET	RAIN
1	1	12.0	0.000	0.00	0.000	0.00	11.99	0.000	10.807	0.000	0.000	0.000	0.000	0.000	10.887	0.000	0.000	11.99
1	2	33.6	0.000	0.00	0.000	0.00	33.57	0.000	19.595	0.000	0.000	0.000	0.000	0.000	19.595	0.000	0.000	21.58
1	3	47.8	0.000	0.00	0.000	0.00	47.81	0.000	12.930	0.000	0.000	0.000	0.000	0.000	12.930	0.000	0.000	14.24
1	4	58.0	0.000	0.00	0.000	0.00	57.96	0.000	9.216	0.000	0.000	0.000	0.000	0.000	9.216	0.000	0.000	10.15
1	5	68.0	0.000	0.00	0.000	0.00	68.01	0.000	9.125	0.000	0.000	0.000	0.000	0.000	9.125	0.000	0.000	10.05
1	6	78.9	0.000	0.00	0.000	0.00	78.06	0.000	9.852	0.000	0.000	0.000	0.000	0.000	9.852	0.000	0.000	10.85
1	7	90.6	0.000	0.00	0.000	0.00	90.58	0.000	10.642	0.000	0.000	0.000	0.000	0.000	10.642	0.000	0.000	11.72
1	8	103.2	0.000	0.00	0.000	0.00	103.19	0.000	11.450	0.000	0.000	0.000	0.000	0.000	11.450	0.000	0.000	12.61
1	9	116.7	0.000	0.00	0.000	0.00	116.72	0.000	12.285	0.000	0.000	0.000	0.000	0.000	12.285	0.000	0.000	13.53
1	10	131.2	0.000	0.00	0.000	0.00	131.21	0.000	13.157	0.000	0.000	0.000	0.000	0.000	13.157	0.000	0.000	14.49
1	11	146.7	0.000	0.00	0.000	0.00	146.71	0.000	14.074	0.000	0.000	0.000	0.000	0.000	14.074	0.000	0.000	15.50
1	12	150.0	6.367	0.04	1.351	5.43	163.30	6.824	15.064	0.000	0.000	0.000	0.000	0.000	15.064	0.000	0.000	16.59
1	13	150.0	8.891	0.13	4.239	17.23	181.04	14.851	16.190	0.008	0.000	0.000	0.000	0.000	16.198	0.000	0.000	17.83
1	14	150.0	10.297	0.23	7.544	31.01	200.10	17.353	17.615	0.031	0.000	0.000	0.000	0.000	17.646	0.000	0.000	19.40
1	15	150.0	12.026	0.35	11.072	46.01	220.71	18.902	19.468	0.077	0.000	0.000	0.000	0.000	19.545	0.000	0.000	21.44
1	16	150.0	14.409	0.47	14.898	62.52	243.18	20.830	22.001	0.162	0.000	0.000	0.000	0.000	22.163	0.000	0.000	24.23
1	17	150.0	18.179	0.61	19.207	81.28	268.44	23.696	26.132	0.323	0.000	0.000	0.000	0.000	26.455	0.000	0.000	28.78
1	18	150.0	24.358	0.78	24.308	103.51	297.54	28.125	32.788	0.645	0.000	0.000	0.000	0.000	33.433	0.000	0.000	36.11
1	19	150.0	33.675	0.99	30.496	130.39	329.88	34.057	41.732	1.254	0.000	0.000	0.000	0.000	42.985	0.000	0.000	45.96

Figure 1.8.20 (continuation)

1	20	150.0	47.313	1.23	37.961	162.62	363.13	40.931	52.909	2.302	0.000	0.000	0.000	0.000	55.211	0.000	0.000	58.27
1	21	150.0	69.577	1.53	46.993	201.29	394.98	49.214	69.852	4.147	0.000	0.000	0.000	0.000	74.000	0.000	0.000	76.93
1	22	150.0	100.000	1.87	57.595	246.29	419.82	57.465	88.430	6.649	0.026	0.000	0.000	0.000	95.105	0.000	0.000	97.39
1	23	150.0	100.000	2.19	67.109	287.54	429.77	52.895	99.644	8.494	0.636	0.000	0.000	0.000	103.824	0.000	0.000	109.74
1	24	150.0	100.000	2.45	74.472	320.90	435.63	43.043	92.552	8.337	0.502	0.000	0.000	0.000	101.392	0.000	0.000	101.93
2	25	150.0	100.000	2.67	80.364	348.83	439.35	36.288	78.133	7.274	0.300	0.000	0.000	0.000	85.707	0.000	0.000	86.05
2	26	150.0	100.000	2.86	85.196	372.79	441.87	31.393	75.210	7.153	0.236	0.000	0.000	0.000	82.599	0.000	0.000	82.83
2	27	150.0	100.000	7.44	85.322	393.35	443.64	27.701	56.505	5.453	0.109	0.000	0.000	0.000	62.067	0.000	0.000	62.23
2	28	150.0	100.000	16.23	81.406	410.96	444.93	24.814	33.996	3.315	0.0H	0.000	0.000	0.000	37.321	0.000	0.000	37.44
2	29	150.0	94.276	24.06	78.273	425.84	445.72	21.832	22.981	2.256	0.000	0.000	0.000	0.000	25.238	0.000	0.000	25.31
2	30	150.0	85.009	30.87	75.612	438.06	446.19	18.565	16.153	1.593	0.000	0.000	0.000	0.000	17.746	0.000	0.000	17.79
2	31	150.0	75.511	36.56	73.397	447.98	446.52	15.547	12.394	1.225	0.000	0.000	0.000	0.000	13.620	0.000	0.000	13.65
2	32	150.0	67.362	41.22	71.594	456.11	446.78	13.105	10.642	1.054	0.000	0.000	0.000	0.000	11.696	0.000	0.000	11.72
2	33	150.0	60.618	45.04	70.115	462.91	447.00	11.228	9.570	0.950	0.000	0.000	0.000	0.000	10.520	0.000	0.000	10.54
2	34	150.0	54.978	48.22	68.860	468.70	447.19	9.771	8.717	0.866	0.000	0.000	0.000	0.000	9.583	0.000	0.000	9.60
2	35	150.0	50.173	50.90	67.760	473.69	447.35	8.617	7.972	0.793	0.000	0.000	0.000	0.000	8.765	0.000	0.000	8.78
2	36	150.0	46.069	53.19	66.769	478.06	447.49	7.680	7.373	0.734	0.000	0.000	0.000	0.000	8.107	0.000	0.000	8.12
2	37	150.0	42.512	55.16	65.857	481.91	447.61	6.909	6.837	0.681	0.000	0.000	0.000	0.000	7.519	0.000	0.000	7.53
2	38	150.0	39.372	56.87	65.003	485.34	447.72	6.263	6.338	0.632	0.000	0.000	0.000	0.000	6.970	0.000	0.000	6.98
2	39	150.0	36.540	58.36	64.190	488.40	447.81	5.706	5.857	0.585	0.000	0.000	0.000	0.000	6.441	0.000	0.000	6.45
2	40	150.0	33.943	59.67	63.408	491.16	447.90	5.220	5.394	0.539	0.000	0.000	0.000	0.000	5.932	0.000	0.000	5.94
2	41	150.0	31.530	60.81	62.647	493.64	447.97	4.789	4.949	0.495	0.000	0.000	0.000	0.000	5.443	0.000	0.000	5.45
2	42	150.0	29.603	61.80	61.910	495.89	448.04	4.418	4.867	0.487	0.000	0.000	0.000	0.000	5.353	0.000	0.000	5.36
2	43	150.0	30.464	62.68	61.271	498.04	448.15	4.280	7.219	0.722	0.000	0.000	0.000	0.000	7.941	0.000	0.000	7.95
2	44	150.0	35.358	63.51	60.853	500.36	448.29	4.621	11.432	1.145	0.000	0.000	0.000	0.000	12.576	0.000	0.000	12.59
2	45	150.0	43.930	64.47	60.726	503.15	448.49	5.491	16.144	1.618	0.000	0.000	0.000	0.000	17.762	0.000	0.000	17.78
2	46	150.0	56.080	65.74	60.912	506.64	448.71	6.815	21.501	2.158	0.000	0.000	0.000	0.000	23.660	0.000	0.000	23.68
2	47	150.0	71.619	67.48	61.433	511.02	448.94	8.512	27.331	2.748	0.000	0.000	0.000	0.000	30.078	0.000	0.000	30.10
2	48	150.0	86.991	69.80	62.203	516.30	449.15	10.263	30.118	3.032	0.000	0.000	0.000	0.000	33.151	0.000	0.000	33.17

1

KINEMATIC WAVE ROUTING FOR SUBBASIN 1

TOTAL AREA = 103.00

OVERLAND FLOW ELEMENT 1

CHLNG = 5000.00
SLOPE = 0.50000
RCMAN = 0.30000
PAREA = 100.000

MAIN CHANNEL

CHLNG = 10000.00
SLOPE = 0.01480
RCMAN = 0.04000
SAREA = 103.000

ISHAPE= 5
CHWDT = 80.000
ZLNG = 1.000

FLOIC = 70.227

ROUTE UPSTREAM FLOW

=

Figure 1.8.20 (continuation)

```
COMPUTED KINEMATIC PARAMETERS

 ELEMENT     ALPHA        M       DT (MIN)   DX (MT)
    1        3.5120     1.667       60.00     2500.64
    2        0.1177     1.653       60.00     9002.30

ADD BASEFLOW TO SUBBASIN  1 USING A LINEAR DECAY FUNCTION OF THE FORM:

 ADDED BF AT TIME T = SUM OF W(L) * BF(T-L) FOR L = 0 TO  2 ; WHERE

 W(L):  0.3000     0.5000     0.2000


KINEMATIC WAVE ROUTING FOR SUBBASIN  2

 TOTAL AREA =    109.00

OVERLAND FLOW ELEMENT 1

 CHLNG =   3000.00
 SLOPE =   0.40000
 RCMAN =   0.30000
 PAREA =   100.000


MAIN CHANNEL

 CHLNG =  34000.00
 SLOPE =   0.03230
 RCMAN =   0.05000
 SAREA =   109.000

 ISHAPE=         5
 CHWDT =    10.000
 ZLNG  =     1.000

 FLOIC =    70.227

COMPUTED KINEMATIC PARAMETERS

 ELEMENT     ALPHA        M       DT (MIN)   DX (MT)
    1        3.1412     1.667       60.00     1500.38
    2        0.6485     1.580       60.00    17004.35

ADD BASEFLOW TO SUBBASIN  2 USIHG A LINEAR DECAY FUNCTION OF THE FORM:

 ADDED BF AT TIME T = SUM OF W(L) * BF(T-L) FOR L = 0 TO  2 ; WHERE

 W(L):  0.3000     0.5000     0.2000

ADD FLOWS OF SUBBASINS   1,  2,


KINEMATIC WAVE ROUTING FOR SUBBASIN  3

 TOTAL AREA =     53.00
```

Figure 1.8.20 (continuation)

```
OVERLAND FLOW ELEMENT 1

 CHLNG =   5000.00
 SLOPE =   0.40000
 RCMAN =   0.30000
 PAREA =   100.000


MAIN CHANNEL

 CHLNG =  18000.00
 SLOPE =   0.01190
 RCMAN =   0.04000
 SAREA =    53.000

 ISHAPE=         5
 CHWDT =    80.000
 ZLNG  =     1.000

 FLOIC =    70.227

ROUTE UPSTREAM FLOW


COMPUTED KINEMATIC PARAMETERS

 ELEMENT     ALPHA       M       DT (MIN)   DX (MT)
    1        3.1412    1.667       60.00    2500.64
    2        0.1055    1.653       60.00    9002.30

ADD BASEFLOW TO SUBBASIN  3 USING A LINEAR DECAY FUNCTION OF THE FORM:

 ADDED BF AT TIME T = SUM OF W(L) * BF(T-L) FOR L = 0 TO  2 ; WHERE

 W(L):  0.3000     0.5000     0.2000
```

Figure 1.8.20 (continuation)

DAY	HOUR	OBSERVED	COMPUTED
1	1	*	4.298
1	2	*	23.853
1	3	*	568.851
1	4	*	1480.494
1	5	*	2268.498
1	6	*	2531.872
1	7	*	2516.416
1	8	*	2455.489
1	9	*	2461.468
1	10	*	2553.496
1	11	*	2709.648
1	12	*	2904.342
1	13	*	3120.296
1	14	*	3369.174
1	15	*	3651.147
1	16	*	3982.814
1	17	*	4406.605
1	18	*	5015.511
1	19	*	5947.134
1	20	*	7475.765
1	21	*	9720.617
1	22	*	12884.356
1	23	*	17051.033
1	24	*	21053.096
2	25	*	22618.102
2	26	*	21384.750
2	27	*	19672.680
2	28	*	17216.273
2	29	*	13555.004
2	30	*	9940.715
2	31	*	7114.887
2	32	*	5260.435
2	33	*	4065.766
2	34	*	3308.151
2	35	*	2816.745
2	36	*	2477.936
2	37	*	2229.349
2	38	*	2035.698
2	39	*	1875.896
2	40	*	1738.053
2	41	*	1615.301
2	42	*	1503.064
2	43	*	1404.104
2	44	*	1363.355
2	45	*	1472.751
2	46	*	1873.348
2	47	*	2697.434
2	48	*	4002.458

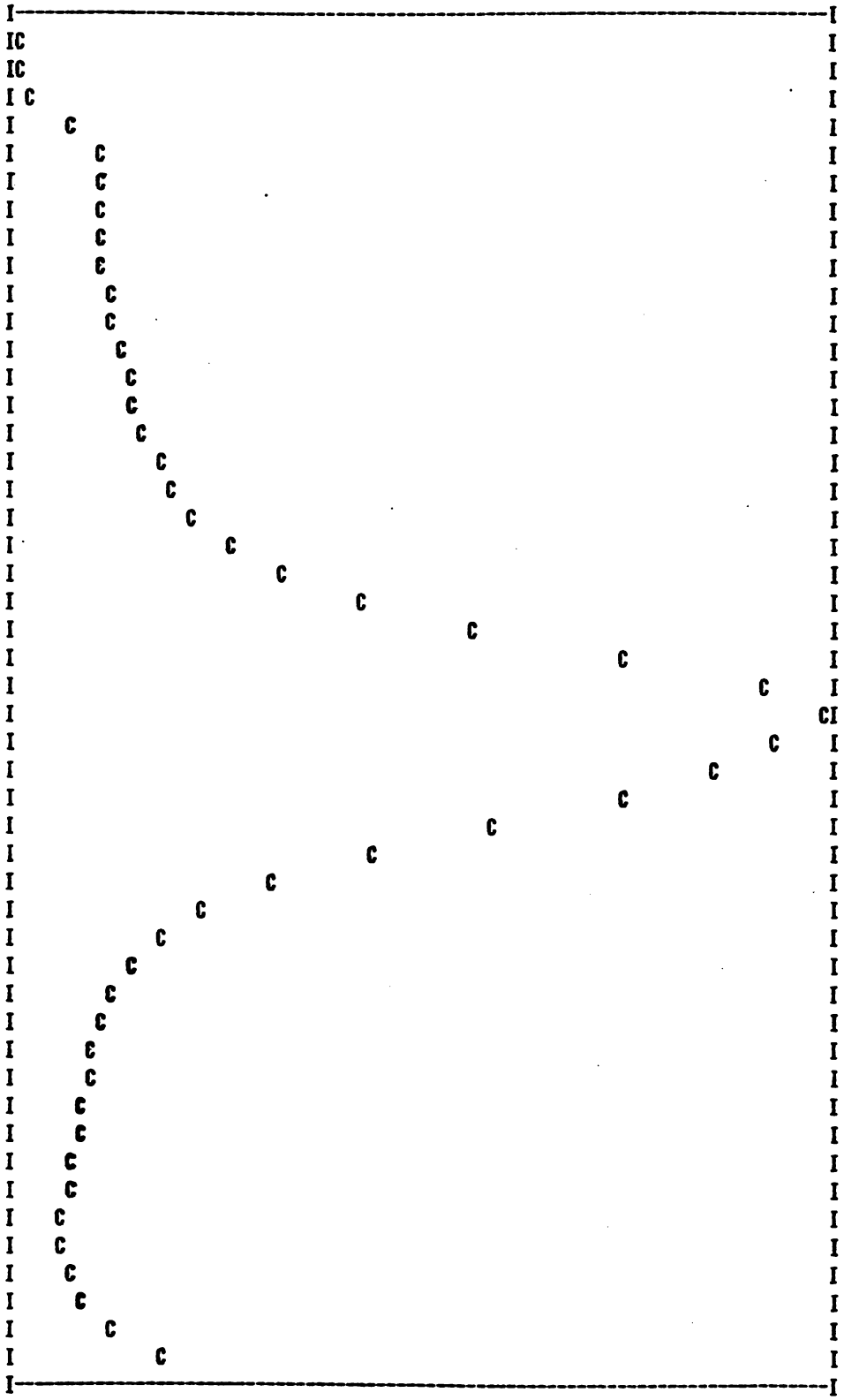

MINIMUM ORDINATE = 4.30
MAXIMUM ORDINATE = 22618.10

SYMBOLS USED:
COMPUTED - C
OBSERVED - O
IF EQUAL - E

Figure 1.8.21 (continuation)

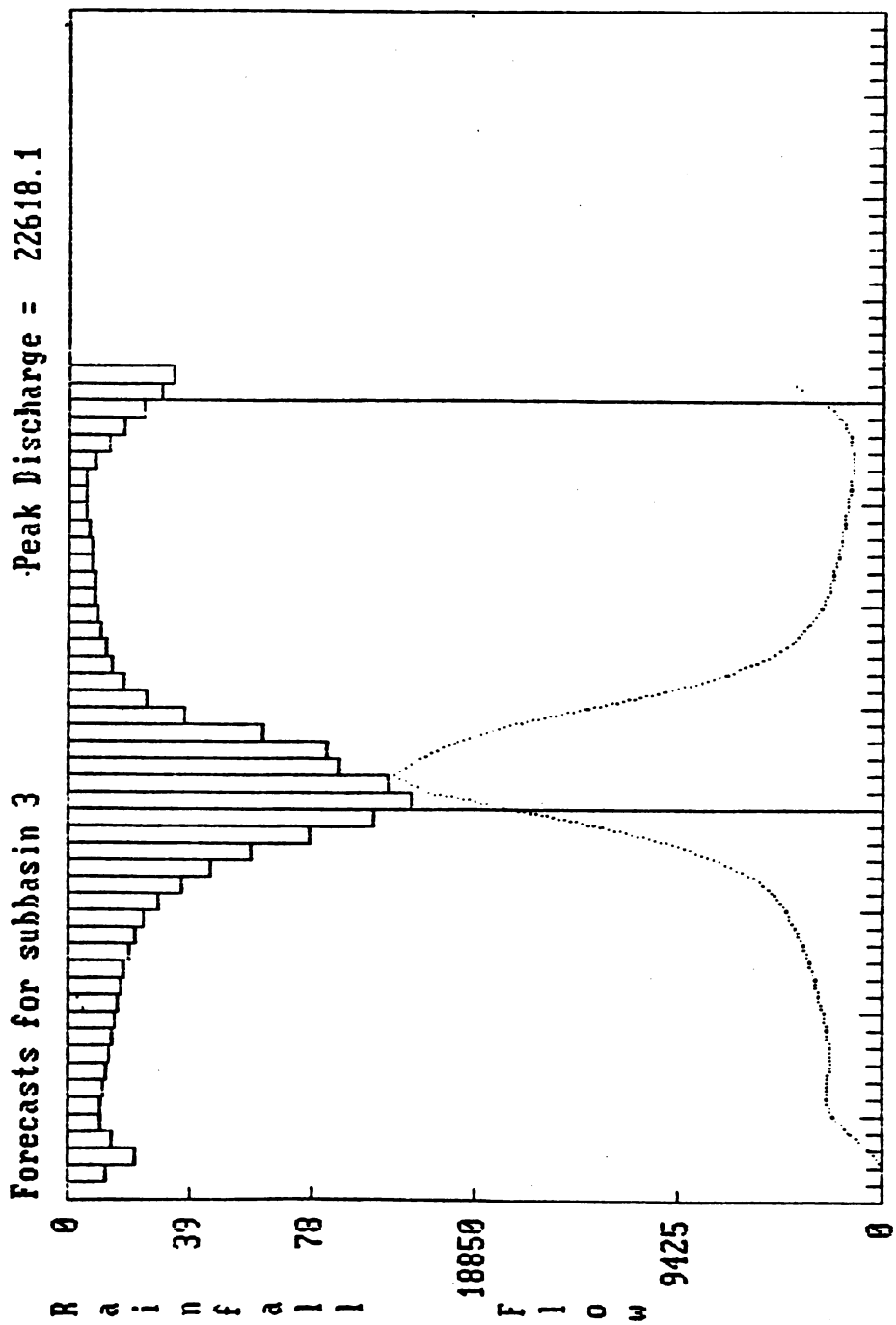

Figure 1.8.21 (continuation)

consistent with those peak flows estimated using the HEC-1 model in section 1.7.3.

1.9 STOCHASTIC GENERATION OF STREAMFLOWS AND TURBINE OPERATING HOURS

1.9.1 Introduction

This report presents the stochastic modeling and data generation of monthly and weekly streamflows in the Nizao Basin, Dominican Republic and monthly turbine operating hours for Valdesia reservoir. For streamflow modeling three gaging stations were selected for analysis, namely: Palo de Caja, Paso del Ermitaño and Rancho Arriba. Prior to data analysis, the gaps in the historical data were filled-in and short records were extended to improve the reliability of statistical parameters to be used in modeling. The stochastic models used for both monthly and weekly streamflows were developed following standard (currently used) modeling procedures. The modeling and generation of monthly turbine operating hours were based on the monthly flows of Paso del Ermitaño.

The report presented herein is divided into four major sections, namely: 1) description of hydrologic data used, 2) filling-in and extension of historical data, 3) stochastic modeling of streamflows, 4) streamflow data generation, and, 5) modeling and generation of turbine operating hours. Some general remarks are given at the end of this report as well as literature cited and appendices.

1.9.2 Description of Hydrologic Data Used

Daily data from four streamflow stations and two rainfall stations provided by Dominican Republic were used in this study. The six gaging stations are listed in Table 1.9.1 and their corresponding years of records. The locations of these stations are shown in Fig. 1.9.1 indicated by station names. For purposes of this study, the monthly data were derived from averaging the daily data of each month. The

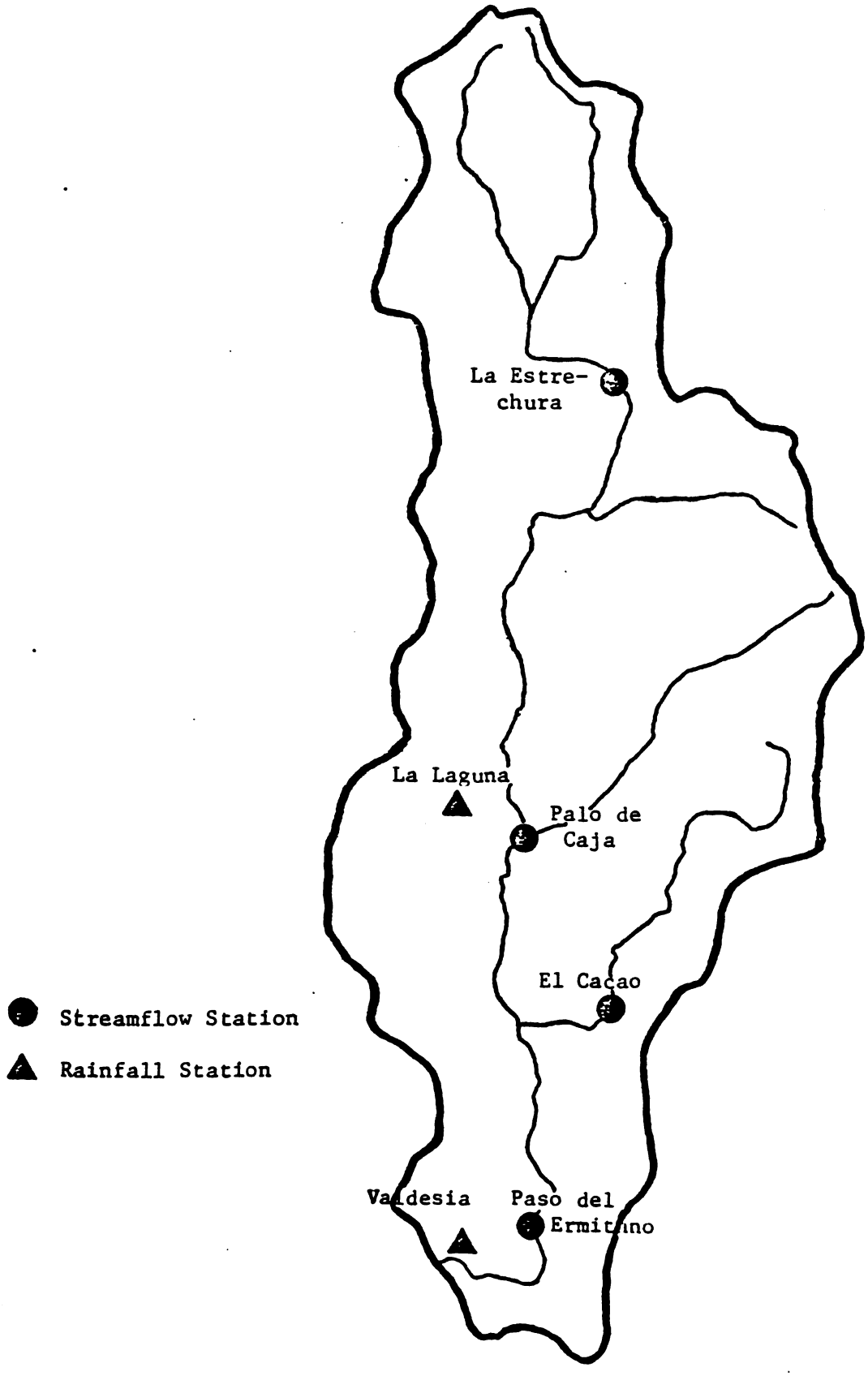

Figure 1.9.1. Map showing Nizao basin and gaging stations used in this study.

weekly data were derived from averaging daily data every seven days starting in January 1 (e.g., January 1-7 is first week, January 8-14 is second week, etc.) except for the last or 52nd week of the year (i.e., December 26 to 31) which is an eight-day average. In the case of leap years, the 9th week data is average from eight days comprising February 26, 27, 28 and 29, and March 1, 2, 3 and 4. Time series plots on a monthly basis for each station are given in Figs. 1.9.2 through 1.9.7. The weekly time series plots are not given due to space limitations. It has been seen however, that the basic seasonal and other time series patterns observed in the monthly time series are likewise exhibited in the weekly series.

Table 1.9.1. List of gaging stations used in this study.

Station Name	Location		Period of Record	Type of Data
	Latitude	Longitude		
Palo de Caja	18°33'17"	70°22'52"	Sept. 1956 - July, 1979	Streamflow
Paso del Ermitaño	18°26'02"	70°15'43"	Dec. 1967 - Oct. 1975	Streamflow
Rancho Arriba	18°42'58"	70°27'59"	Mar. 1959 - Oct. 1966	Streamflow
El Cacao*	18°31'44"	70°17'59"	Jan. 1962 - Dec. 1981	Streamflow
La Laguna	18°32'30"	70°24'45"	Jan. 1963 - Dec. 1979	Rainfall
Valdesia	18°24'30"	70°16'50"	Feb. 1963 - Aug. 1984	Rainfall

*Records fragmentary between 1966 to 1979.

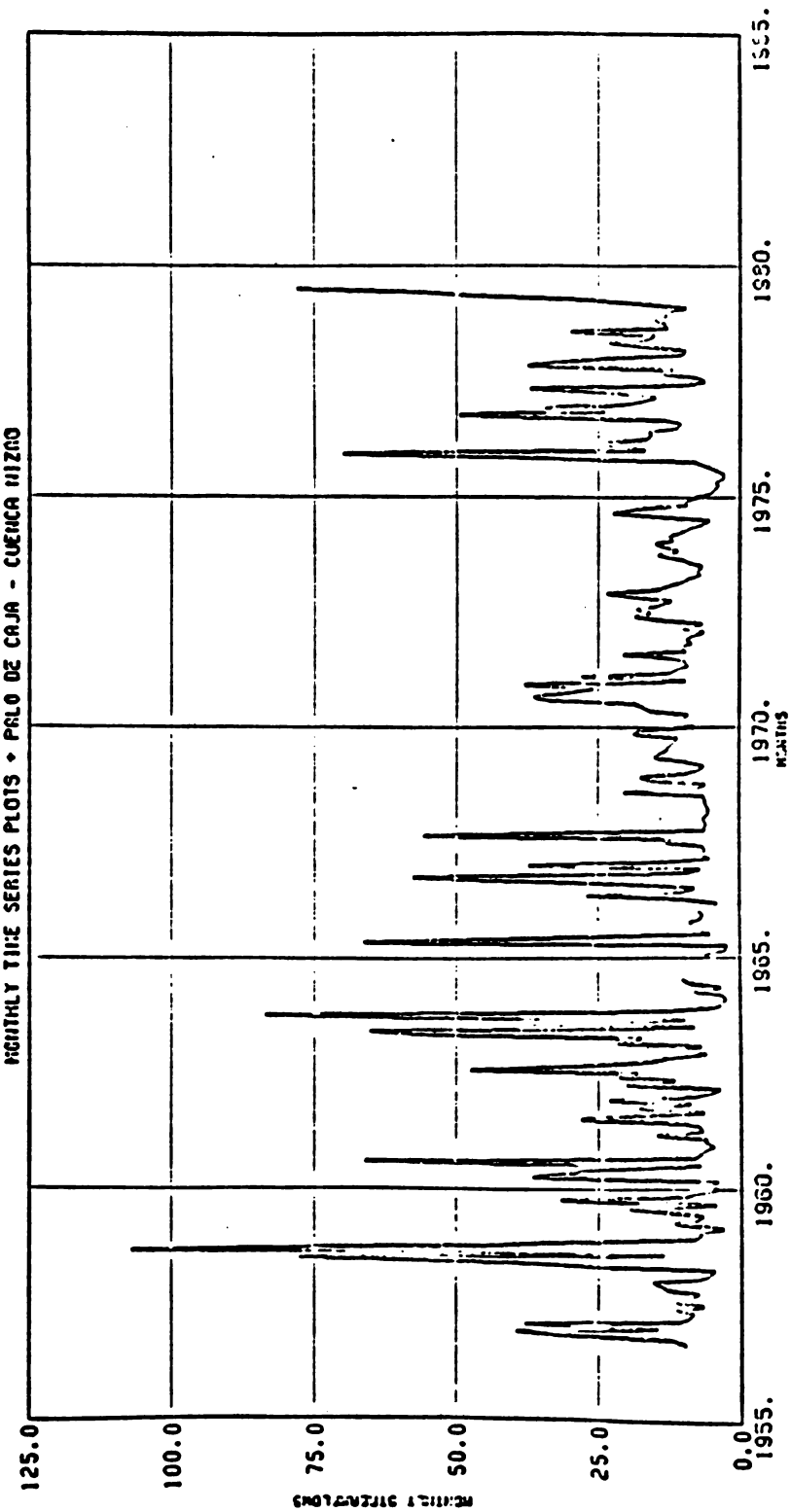

Figure 1.9.2. Time series plots of monthly streamflows of Palo de Caja.

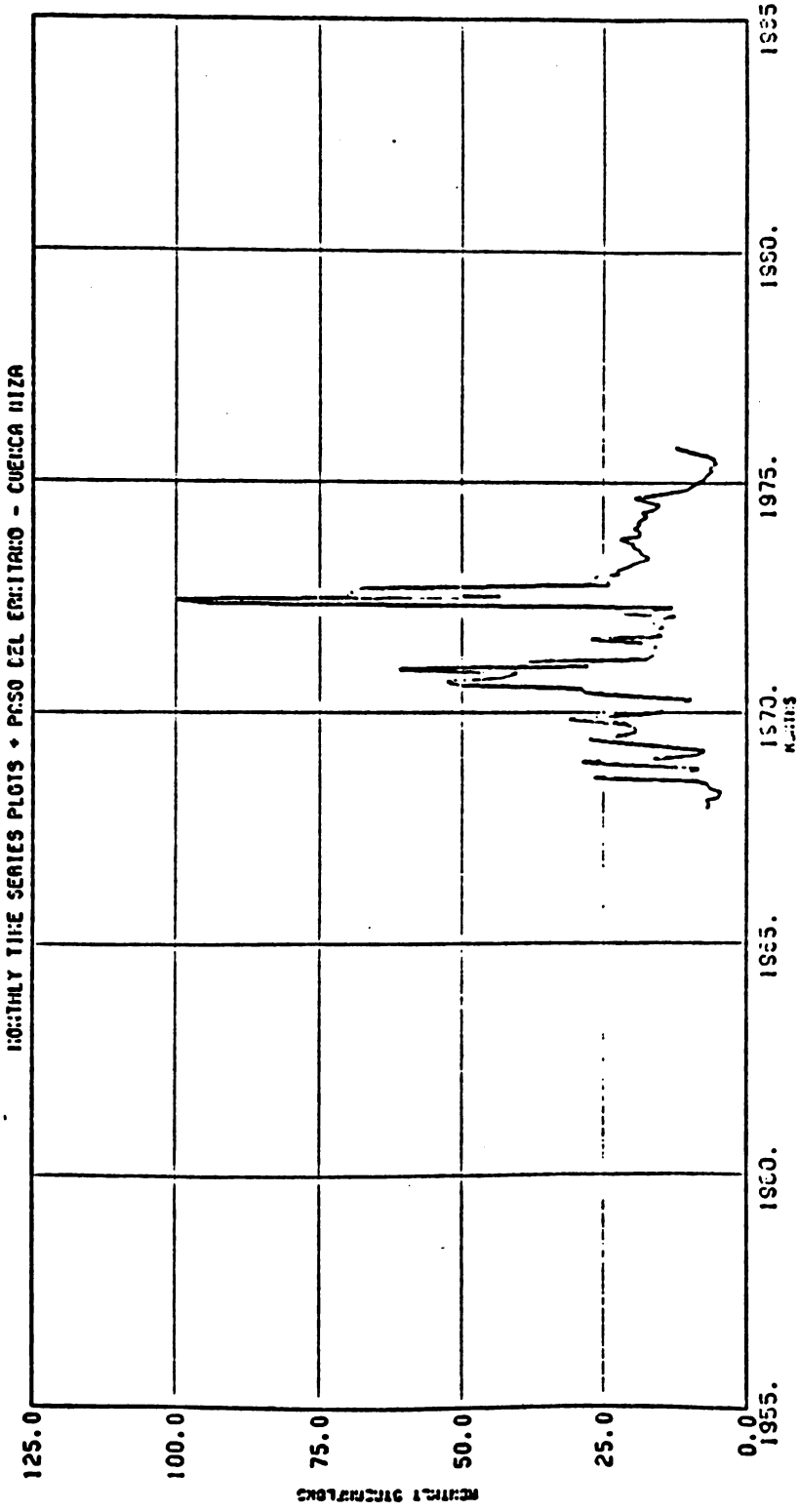

Figure 1.9.3. Time series plots of monthly streamflows of Paso del Ermitaño.

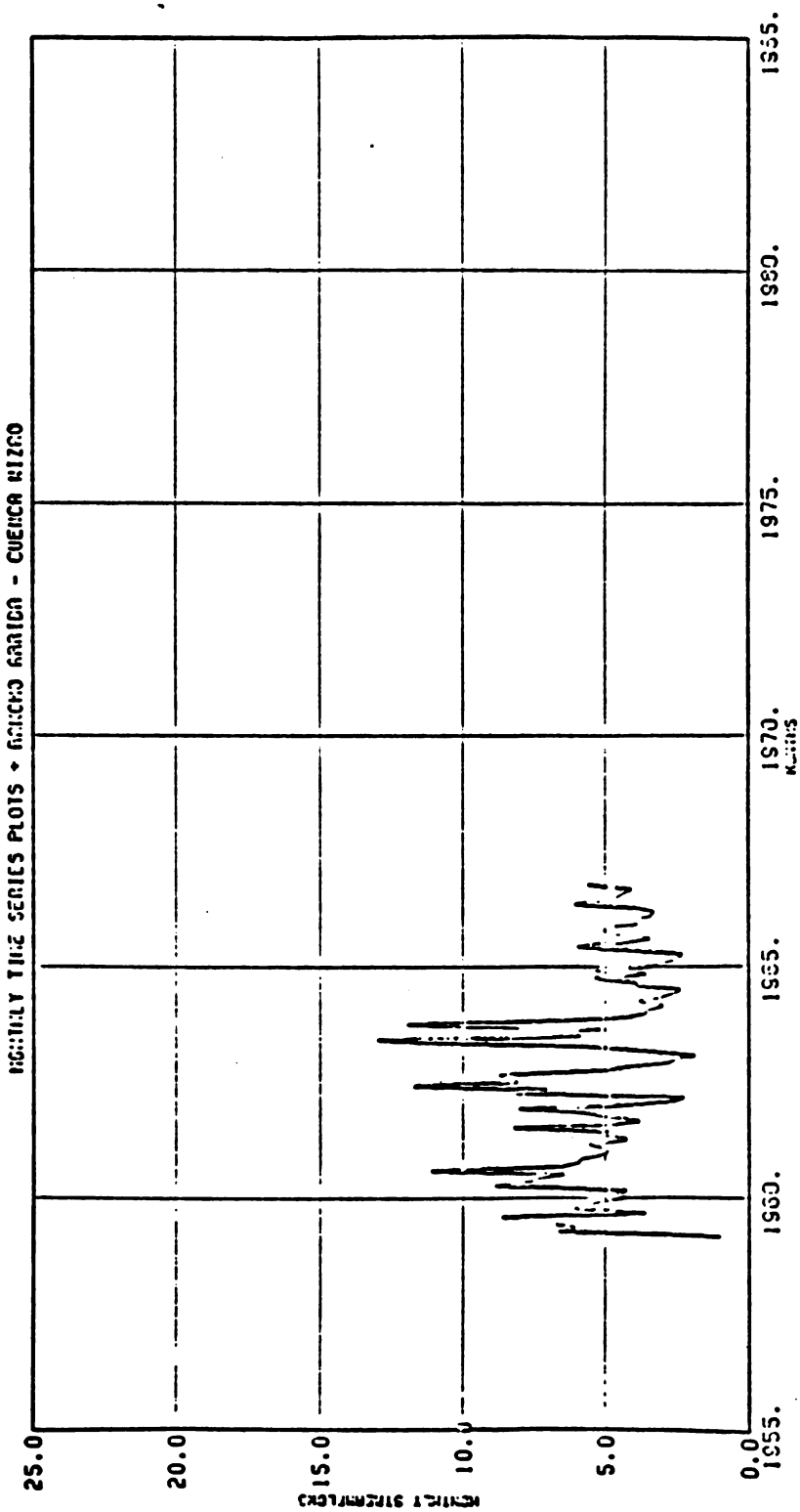

Figure 1.9.4. Time series plots of monthly streamflows of Rancho Arriba.

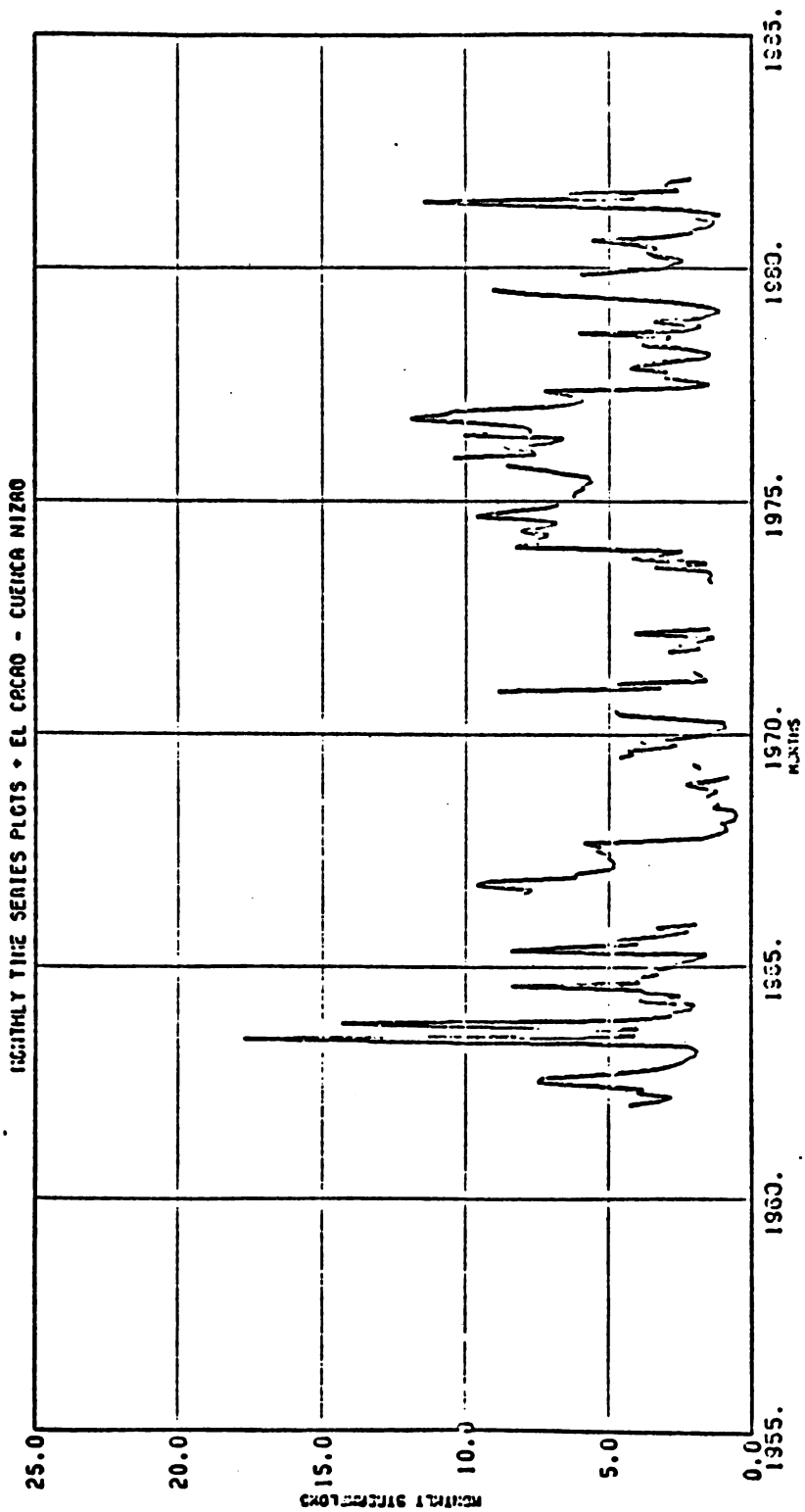

Figure 1.9.5. Time series plots of monthly streamflows of El Cacao.

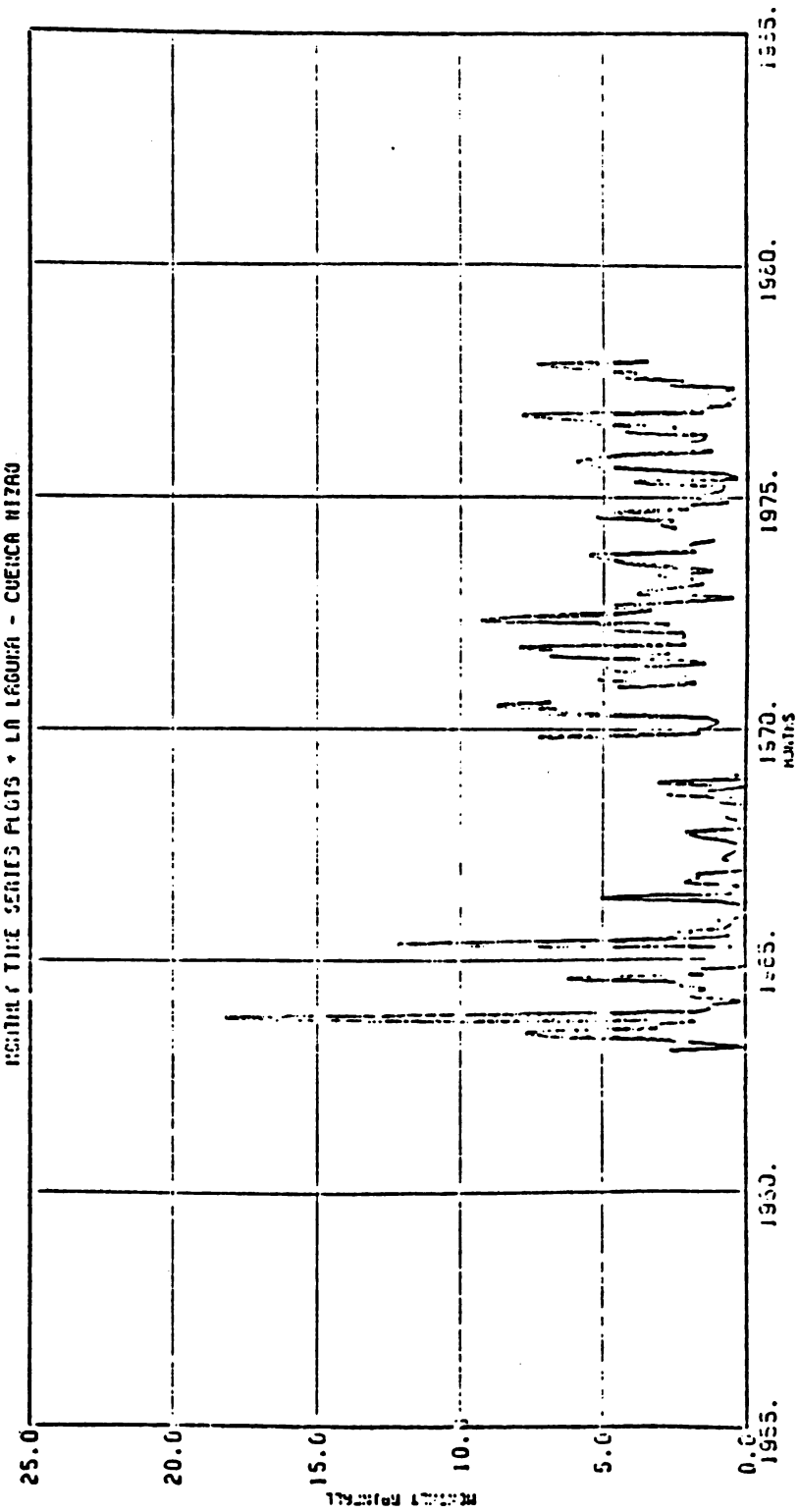

Figure 1.9.6. Time series plots of monthly rainfall of La Laguna.

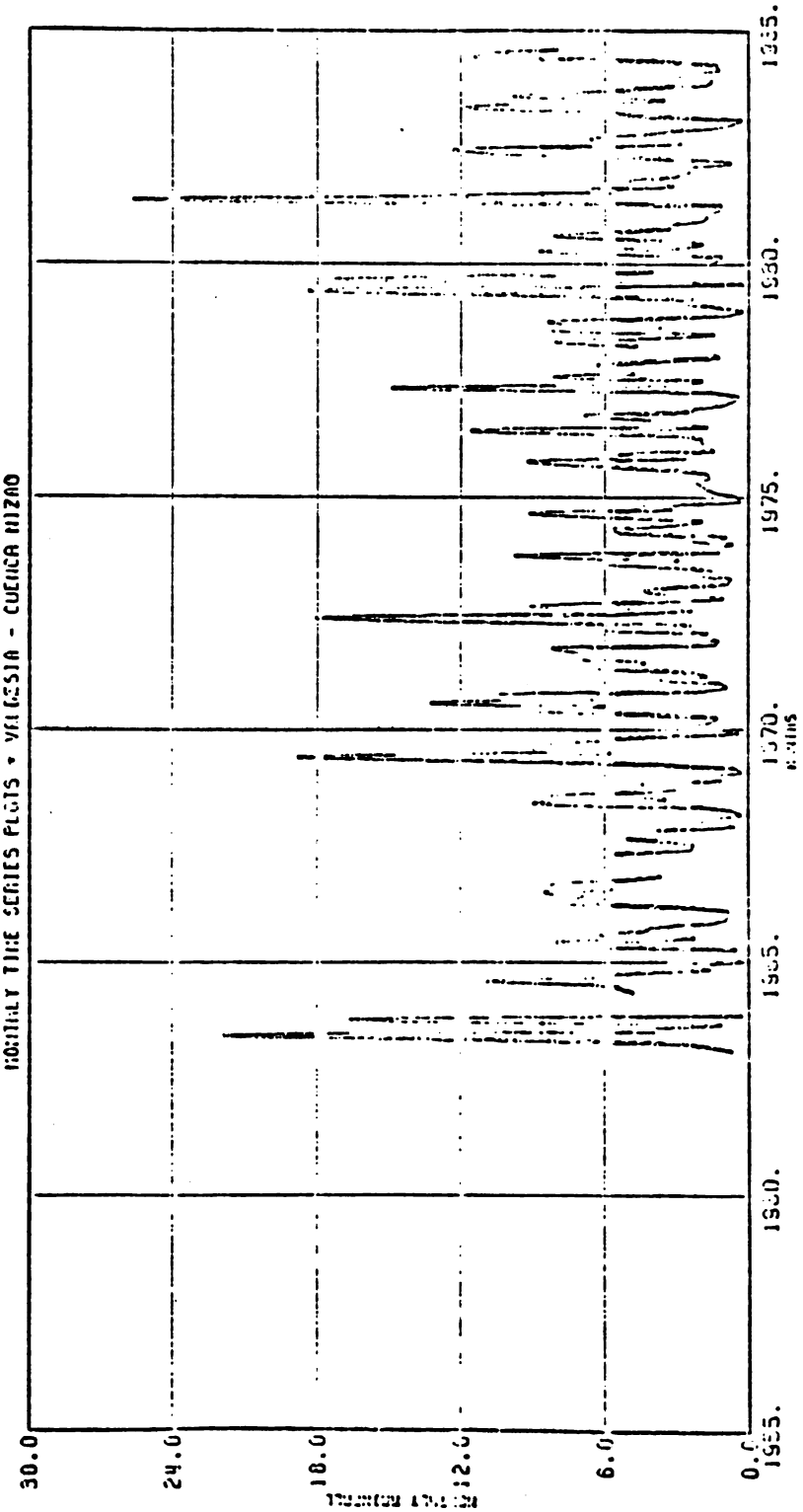

Figure 1.9.7. Time series plots of monthly rainfall of Valdesia.

1.9.3 Filling-in and Extension of Historical Data

To improve the reliability of statistical parameters such as the means, variances, skewness, autocorrelations and cross correlations which will be used for stochastic modeling, the historical data of each station are filled-in and/or extended first based on other stations. The monthly and weekly streamflows of Palo de Caja contain only some data gaps in years 1964 and 1966 thus requiring only minor filling-in of missing data. However, both Paso del Ermitaño and Rancho Arriba require major data extension since their records are short. The succeeding subsections present filling-in of missing data of Palo de Caja and extension of records of Paso del Ermitaño and Rancho Arriba respectively.

1.9.3.1 Filling-in of Missing Data of Palo de Caja

On a monthly basis, the data of months August, October and December of year 1964 and February 1966 are missing. On a weekly basis, weeks 33, 34, 35, 42, 43, 44, 51 and 52 of year 1964 and weeks 6 and 7 of 1966 are missing. It is decided that a simple or multiple linear regression model be used in filling-in the missing data of Palo de Caja based on neighboring stations within the Nizao basin. As a requirement to linear regression models, the regression variables must be nominally normally distributed. Thus, prior to fitting these models, the streamflows of Palo de Caja and the time series variables of other stations are suitably transformed to become normal. Five normalizing transformations were tried, namely: 1) square-root, 2) cube root, 3) logarithmic, 4) Wilson-Hilferty, and 5) combined logarithmic and Wilson-Hilferty transformations. Details of the normalization schemes and results for each station are given in Appendix 1.9.A. Using the transformed data of

each station, the overall monthly and weekly cross correlations between stations were computed to form the basis of choosing the regressor variables. The computed cross correlations for monthly and weekly data are given in Tables 1.9.2 and 1.9.3, respectively. The choice of the regressor variables is also dependent on the availability of data from these stations with respect to those periods of missing data of Palo de Caja and the coefficient of correlation of the fitted regression model.

On the above basis, the monthly missing values of Palo de Caja are filled-in using the bivariate regression model given by

$$Z^{(1)}_{\nu,\tau} = -0.038 + 0.358\ Z^{(5)}_{\nu,\tau} + 0.257\ Z^{(6)}_{\nu,\tau} + 0.814\ \epsilon_{\nu,\tau} \qquad (1.9.1)$$

where $Z^{(1)}_{\nu,\tau}$ is the log-Wilson-Hilferty domain streamflow of Palo de Caja of year ν and month τ; $Z^{(5)}_{\nu,\tau}$ and $Z^{(6)}_{\nu,\tau}$ are the Wilson-Hilferty domain rainfalls of La Laguna and Valdesia, respectively; and $\epsilon_{\nu,\tau}$ is an added noise term which is identically and independently distributed standard normal random deviates. The addition of the noise term $\epsilon_{\nu,\tau}$ is necessary because otherwise the variance of the filled-in data may be reduced (Salas, et al., 1980). Equation (1.9.1) has a multiple correlation coefficient (R) equal to 0.540. Note that in Table 1.9.2, the overall monthly cross-correlation between Palo de Caja and Paso del Ermitaño is the highest. But during those months where Palo de Caja has missing values, the values of Paso del Ermitaño are also missing. The filled-in monthly values of Palo de Caja in the original domain of streamflows are obtained using the inverse log-Wilson-Hilferty transformation (see Appendix 1.9.A or section 1.9.6.1).

Table 1.9.2. Overall monthly cross-correlations of transformed data between stations.

	Palo de Caja	Paso del Ermitaño	Rancho Arriba	El Cacao	La Laguna	Valdesia
Palo de Caja (LWH)	1.000 (271)*					
Paso del Ermitaño (LWH)	0.789 (95)	1.000 (95)				
Rancho Arriba (LWH)	0.473 (87)	-- (0)	1.000 (91)			
El Cacao (LWH)	0.443 (177)	0.260 (72)	0.542 (51)	1.000 (206)		
La Laguna (WH)	0.463 (162)	0.661 (81)	0.272 (46)	0.307 (140)	1.000 (166)	
Valdesia (WH)	0.447 (182)	0.460 (95)	0.226 (40)	0.274 (180)	0.543 (154)	1.000 (246)

*Numbers enclosed in parentheses are total number of concurrent observations.

-- denotes no concurrent record between these two stations.

Note: LWH or WH indicates whether data for that station was transformed either by combined log-Wilson-Hilferty transformation or Wilson-Hilferty transformation, respectively.

For filling-in the weekly values of Palo de Caja, the following simple linear regression model is used:

$$Z^{(1)}_{\nu,\tau} = a_\tau + b_\tau Z^{(3)}_{\nu,\tau} + c_\tau \epsilon_{\nu,\tau} \qquad (1.9.2)$$

where $Z^{(1)}_{\nu,\tau}$ and $Z^{(3)}_{\nu,\tau}$ are the weekly log-Wilson-Hilferty domain streamflows of Palo de Caja and Rancho Arriba, respectively and the regression models parameters as a function week τ are computed either on a week-to-week basis or overall-weekly basis depending on which of the two give the highest coefficient of correlation (R). Note again that Palo de Caja and Paso del Ermitaño has the highest correlation as shown in Table 1.9.3, but values of Paso del Ermitaño are missing during these weeks when Palo de Caja had missing values. The model coefficients of Eq. (1.9.2) and corresponding coefficient of correlations (R) for each missing week are given in Table 1.9.4. As in monthly filling-in of missing data, the original domain of weekly streamflows of Palo de Caja are obtained using the inverse log-Wilson-Hilferty transformation. Effectively now, the monthly and weekly data available for Palo de Caja is from 1957 to 1978 (1956 and 1979 are excluded since they are incomplete) which is a total of 22 years.

1.9.3.2 Extension of Records of Paso del Ermitaño and Rancho Arriba

For extending the records of Paso del Ermitaño and Rancho Arriba, three model forms are tentatively prescribed in the linear and normal domain of time series variables. These models are: i) nonseasonal multiple regression model, ii) seasonal multiple regression model, and

Table 1.9.4. Regression model parameters of Equation (1.9.2) for filling-in weekly missing values of Palo de Caja.

Year, ν	Week, τ	a_τ	b_τ	c_τ	R_τ
1964	33	-0.456	1.143	1.696	0.554
	34	0.363	1.079	0.310	0.971
	35	0.259	0.815	0.576	0.856
	42	0.360	0.809	1.072	0.579
	43	-0.197	0.936	0.776	0.813
	44	-0.324	0.613	0.964	0.507
	51	-0.324	0.613	0.964	0.507
	52	-0.324	0.613	0.964	0.507
1966	6	-0.324	0.613	0.964	0.507
	7	-0.843	0.608	0.882	0.644

iii) nonseasonal bivariate first-order autoregressive model. For the case of nonseasonal models, it is assumed that any inherent seasonality in the data is adequately removed by seasonal standardization which is included in the normalizing transformation used (see Appendix 1.9.A). In the multiple regression models, the choice of regressors were made on the basis of best regression correlation coefficients using one or two stations.

With these three model forms, sample extensions of monthly data were then performed. On this basis, it is found that the nonseasonal bivariate first-order autoregressive model best preserves the means, variances, autocorrelations and cross-correlations of the data. Thus, the short records of Paso del Ermitaño and Rancho Arriba for both monthly and weekly levels were extended using a bivariate first-order

autoregressive model with Palo de Caja. In equation form, this model is written as:

$$\begin{bmatrix} z^{(1)}_{\nu,\tau} \\ z^{(2)}_{\nu,\tau} \end{bmatrix} = \begin{bmatrix} a_{11} & a_{12} \\ a_{21} & a_{22} \end{bmatrix} \begin{bmatrix} z^{(1)}_{\nu,\tau-1} \\ z^{(2)}_{\nu,\tau-1} \end{bmatrix} + \begin{bmatrix} b_{11} & 0 \\ b_{21} & b_{22} \end{bmatrix} \begin{bmatrix} \epsilon^{(1)}_{\nu,\tau} \\ \epsilon^{(2)}_{\nu,\tau} \end{bmatrix} \qquad (1.9.3a)$$

For purposes of data extension, the equation above is written as:

$$z^{(2)}_{\nu,\tau} = \frac{b_{21}}{b_{11}} z^{(1)}_{\nu,\tau} + \left(a_{21} - \frac{a_{11}b_{21}}{b_{11}}\right) z^{(1)}_{\nu,\tau-1}$$

$$+ \left(a_{22} - \frac{b_{21}a_{12}}{b_{11}}\right) z^{(2)}_{\nu,\tau-1} + b_{22}\, \epsilon^{(2)}_{\nu,\tau} \qquad (1.9.3b)$$

where $z^{(2)}_{\nu,\tau}$ is the data of either Paso del Ermitaño or Rancho Arriba, $z^{(1)}_{\nu,\tau}$ is the data of Palo de Caja, $\epsilon^{(2)}_{\nu,\tau}$ is a standard normal random number, and the a's and b's are model parameters.

Since the data of Paso del Ermitaño and Rancho Arriba are to be extended forward in time and backward in time to coincide with those of Palo de Caja (see Table 1.9.1 for periods of available records), the model in Eqs. (1.9.3) are applied likewise forward and backward in time as the case requires. This scheme is possible for linear-normal time series models owing to the notions of time-reversibility and distributional symmetry in the linear and normal domain of time series variables.

The model parameters of Eqs. (1.9.3) are estimated using the method of moments (Salas, et al., 1980). Tables 1.9.5 and 1.9.6 show the model parameters for monthly and weekly levels, respectively. Referring to

Table 1.9.5. Model parameters for monthly data extensions.

Forward in Time	A		B	
Paso del Ermitaño and	-0.0459	0.6325	0.8023	0.0
Palo de Caja	0.0214	0.8250	0.3574	0.4040
Rancho Arriba and	0.5817	-0.2896	0.8531	0.0
Palo de Caja	-0.0757	0.5493	0.5819	0.6253
Backward in Time	**A**		**B**	
Paso del Ermitaño and	-0.2035	0.8324	0.7300	0.0
Palo de Caja	-0.1783	0.9825	0.2863	0.4440
Ranch Arriba and	0.4710	-0.0408	0.8909	0.0
Palo de Caja	-0.3245	0.6601	0.5396	0.5988

Table 1.9.6. Model parameters for weekly data extensions.

Forward in Time	A		B	
Paso del Ermitaño and	0.5755	0.1963	0.6765	0.0
Palo de Caja	0.0537	0.7764	0.3423	0.4620
Rancho Arriba and	0.7617	-0.0725	0.6853	0.0
Palo de Caja	-0.0382	0.7756	0.4206	0.4997
Backward in Time	**A**		**B**	
Paso del Ermitaño and	0.5553	0.2226	0.6731	0.0
Palo de Caja	0.0273	0.7965	0.3404	0.4644
Ranch Arriba and	0.7343	-0.0176	0.6881	0.0
Palo de Caja	-0.0932	0.8030	0.4164	0.4977

Eq. (1.9.3b), the extension of records is done by generating the normal standard random noise $\epsilon^{(2)}_{\nu,\tau}$ to obtain $z^{(2)}_{\nu,\tau}$, then followed by back transformation to the original domain of flows. Due to the addition of the random term, a single series is only one possible (equally likely) sequence that may have occurred. In view of this, fifty data extensions are made. The intent here is simply to utilize the fifty extended

series for improving the estimates of the parameters to be used in modeling and data generation.

For each extended series, the seasonal statistics are then computed constituting a total of 50 samples of statistics for each season. From these, the averages and standard errors of each statistic are determined. The averages in this case are considered as the improved estimates representing the seasonal statistic while their corresponding standard errors indicate the degree of variation of each statistic from the averages. The computed averages and standard errors for monthly and weekly statistics are given in Appendix 1.9.B.

A reliability test for the improvement of the means and variances was performed after extending the records of Paso del Ermitaño and Rancho Arriba. The test is based on comparing the variances of "historical" means (or variances) with the corresponding variances of "extended" means (or variances). The statistics are improved if the "extended" variances are smaller than the "historical" variances. The variances of historical means and variances for seasonally autocorrelated processes are given respectively as:

$$\mathrm{var}(\bar{x}_\tau) = \frac{S_\tau^2}{N}\left[1 + \frac{2}{N}\sum_{\nu=1}^{N-1}(N-\nu)\rho_\tau(w\nu)\right] \qquad (1.9.4a)$$

and

$$\mathrm{var}(S_\tau^2) = 2\,S_\tau^4\left[\frac{N}{1 + \sum_{\nu=1}^{N-1}\rho_\tau^2(w\nu)} - 1\right]^{-1} \qquad (1.9.4b)$$

where S_τ^2 is the historical variance at season τ, N is the number of years of record, w is the number of seasons and $\rho_\tau(w\nu)$ is the

seasonal autocorrelation at lag $w\nu$. Assuming that the historical series follows a seasonal first-order autoregressive process, the

$$\rho_\tau(w\nu) = \rho_\tau(1)\ \rho_{\tau-1}(1)\ \ldots\ \rho_{\tau-w\nu+1}(1)$$

in which $\rho_\tau(1)$ is the lag-1 autocorrelation at season τ. The variances of the extended series statistics are the square of the standard errors computed from each statistic based on fifty series extensions.

Results from these tests show that for all monthly means and variances, all extended statistics are improved. For the weekly statistics, a maximum of 2 weeks out of 52 weeks failed the test. For all practical purposes, the extention of records has definitely improved the reliability of statistical parameters.

1.9.4 Stochastic Modeling of Streamflows

The stochastic models for both monthly and weekly streamflows adopted herein for data generation studies belong to the family of multivariate linear models. Similar to the models used in extension, the models are developed by first normalizing and standardiz-ing each series. Thereafter the correlation structure of the residual series is derived to form the basis of the stochastic model. In normalization, the combination of logarithmic and Wilson-Hilferty transformations is used for both monthly and weekly streamflows. For Wilson-Hilferty transformation, the seasonal skewness coefficients (in the logarithmic domain of flows) are Fourier fitted functions using the first two harmonics for monthly skews and first four harmonics for weekly skews. The skewness coefficients were also corrected for bias under the

assumption that the process in the log domain are approximately gamma distributed. Details of the Fourier series fitting of the seasonal skewness coefficients are given in Appendix 1.9.C.

Three alternative stochastic model formulations were tried in this study. The first model, referred to here as "MODEL A," is a contemporaneous seasonal mixed autoregressive-moving average model (ARMA) which involves fitting first appropriate seasonal univariate ARMA models to each series. The model residuals of each series are then obtained and fitted to a zero-order multivariate model. In equation form, the univariate seasonal ARMA model can be generally written as:

$$z_{\nu,\tau}^{(s)} = \sum_{i=1}^{p} \phi_{i,\tau}^{(s)} z_{\nu,\tau-i}^{(s)} + \sum_{j=1}^{q} \theta_{j,\tau}^{(s)} e_{\nu,\tau-j}^{(s)} + e_{\nu,\tau}^{(s)} \qquad (1.9.5)$$

where $z_{\nu,\tau}^{(s)}$ is the normalized and standardized series of station s, year ν and season τ; $e_{\nu,\tau}^{(s)}$ is the residual series independent in time but the residuals of each station are contemporaneously correlated with each; and $\phi_{i,\tau}^{(s)}$ and $\theta_{j,\tau}^{(s)}$ are model parameters of orders p and q, respectively. For both monthly and weekly streamflows, the model parameters are estimated based on Fourier fitted functions of the seasonal sample autocorrelations. Details of the Fourier series fitting of autocorrelations for monthly and weekly levels of the three stations are given in Appendix 1.9.C. The autocorrelations fitted with the first two harmonics were used for monthly models and the fitted first four harmonics were used for weekly models. The zero-order multivariate model written for three stations takes the form below:

$$\begin{bmatrix} e^{(1)}_{\nu,\tau} \\ e^{(2)}_{\nu,\tau} \\ e^{(3)}_{\nu,\tau} \end{bmatrix} = \begin{bmatrix} b_{11} & 0 & 0 \\ b_{21} & b_{22} & 0 \\ b_{31} & b_{32} & b_{33} \end{bmatrix} \begin{bmatrix} \epsilon^{(1)}_{\nu,\tau} \\ \epsilon^{(2)}_{\nu,\tau} \\ \epsilon^{(3)}_{\nu,\tau} \end{bmatrix} \tag{1.9.6}$$

where $\epsilon^{(s)}_{\nu,\tau}$'s are identically and independently distributed normal deviates and the b's are nonseasonal model parameters. The second model tried in this study uses both Eqs. (1.9.5) and (1.9.6) except that in Eq. (1.9.6), the model parameter b's are allowed to vary seasonally. This latter model is referred to here as "MODEL B." The third model, referred to as "MODEL C," is a nonseasonal vector first-order autoregressive model written for three stations as:

$$\begin{bmatrix} z^{(1)}_{\nu,\tau} \\ z^{(2)}_{\nu,\tau} \\ z^{(3)}_{\nu,\tau} \end{bmatrix} = \begin{bmatrix} a_{11} & a_{12} & a_{13} \\ a_{21} & a_{22} & a_{23} \\ a_{31} & a_{32} & a_{33} \end{bmatrix} \begin{bmatrix} z^{(1)}_{\nu,\tau-1} \\ z^{(2)}_{\nu,\tau-1} \\ z^{(3)}_{\nu,\tau-1} \end{bmatrix} + \begin{bmatrix} b_{11} & 0 & 0 \\ b_{21} & b_{22} & 0 \\ b_{31} & b_{32} & b_{33} \end{bmatrix} \begin{bmatrix} \epsilon^{(1)}_{\nu,\tau} \\ \epsilon^{(2)}_{\nu,\tau} \\ \epsilon^{(3)}_{\nu,\tau} \end{bmatrix} \tag{1.9.7}$$

where the a's are nonseasonal model parameters and the other notations are defined as in Eqs. (1.9.5) and (1.9.6).

For the three tentative models above, the model parameters were estimated using the method of moments presented in Salas, et al., 1980. In choosing the appropriate model order of univariate seasonal ARMA in Eq. 1.9.5, the computer program UMOSE1 developed by Salas and Smith (1981) was used. A seasonal ARMA(1,0) or AR(1) model is found adequate and parsimonious to describe both monthly and weekly flows.

1.9.5 Streamflow Data Generation

1.9.5.1 Data Generation Scheme

For the three alternative stochastic models given previously, the data generation commences by generating the sequence $\epsilon_{\nu,\tau}^{(s)}$ using the Box-Muller formula written as (Salas, et al., 1980):

$$\epsilon_1 = [2 \ln (1/u_1)]^{1/2} \cos (2\pi u_2) \tag{1.9.8a}$$

and

$$\epsilon_1 = [2 \ln (1/u_1)]^{1/2} \sin (2\pi u_2) \tag{1.9.8b}$$

where u_1 and u_2 are two independent uniformly distributed (0,1) random numbers. Note that two random numbers can be generated at one time. Then these generated values are applied to either Eq. (1.9.6) or (1.9.7). For models A and B, Eq. (1.9.6) is used with nonseasonal or seasonal b's respectively to obtain $e_{\nu,\tau}^{(s)}$, followed by Eq. (1.9.5) to arrive at $z_{\nu,\tau}^{(2)}$. For model C, Eq. (1.9.7) is used to arrive at $z_{\nu,\tau}^{(s)}$.

Having obtained the sequence $z_{\nu,\tau}^{(s)}$ for any model, the backward Wilson-Hilferty transformation is applied using the inverse of Eq. (1.9.A:6) such that

$$x'^{(s)}_{\nu,\tau} = \frac{2}{G_\tau^{(s)}(x)} \left\{ \frac{G_\tau^{(s)}(x)}{6} \left[z_{\nu,\tau}^{(s)} - \frac{G_\tau^{(s)}(x)}{6} \right] + 1 \right\}^3 - \frac{2}{G_\tau^{(s)}(x)} \tag{1.9.9}$$

in which $G_\tau^{(s)}(x) \neq 0$, where $G_\tau^{(s)}(x)$ is the seasonal Fourier fitted skewness coefficient in the log domain. The variable $x_{\nu,\tau}^{(s)}$ is further transformed by

$$x_{\nu,\tau}^{(s)} = \begin{cases} \max \left[x'^{(s)}_{\nu,\tau},\ -2/G_{\tau}^{(s)}(x) \right] & \text{if } G_{\tau}^{(s)}(x) > 0 \\ \min \left[x'^{(s)}_{\nu,\tau},\ -2/G_{\tau}^{(s)}(x) \right] & \text{if } G_{\tau}^{(s)}(x) < 0 \end{cases}$$

and

$$x_{\nu,\tau}^{(s)} = z_{\nu,\tau}^{(s)} \qquad \text{if } G_{\tau}^{(s)}(x) = 0 \qquad (1.9.10)$$

where $x_{\nu,\tau}^{(s)}$ is the generated data in the log domain. Finally, the data $y_{\nu,\tau}^{(s)}$ in the actual or original domain is obtained from

$$w_{\nu,\tau}^{(s)} = \bar{w}_{\tau}^{(s)} + S_{\tau}^{(s)}(w)\ x_{\nu,\tau}^{(s)} \qquad (1.9.11)$$

and

$$y_{\nu,\tau}^{(s)} = \exp\left[w_{\nu,\tau}^{(s)} \right] \qquad (1.9.12)$$

where $\bar{w}_{\tau}^{(s)}$ and $S_{\tau}^{(s)}(w)$ are the seasonal mean and standard deviation in the log-domain of flows.

The program GENSEA developed by Salas and Smith (1981) was utilized for data generation which was slightly modified for purposes here.

1.9.5.2 Analysis of Generated Data

A total of 50 samples of size 22 years each of monthly and weekly streamflows were generated using the three alternative model formulations above. The best monthly and weekly models were then selected based on the comparison of historical and generated seasonal means, standard deviations, skewness coefficients, autocorrelations, and cross-correlations. For each generated sample, the above mentioned statistical properties are computed, then the arithmetic averages and standard errors for all samples are determined. Given in Appendix 1.9.D are plots of the monthly and weekly historical and generated statistics of the three models in the original domain of flows. Only the computed

averages are shown for clarity in presentation. Based on these plots, the best model selected for both monthly and weekly streamflows is MODEL B (i.e., univariate seasonal first-order autoregressive process with seasonal multivariate zero-order station-to-station dependence).

Given in Appendix 1.9.E are the monthly and weekly, historical and generated statistics of MODEL B in the three domains of streamflows, namely: original domain, log domain, and log-Wilson-Hilferty domain. Plotted along the generated average statistics are the positive and negative one-standard errors relative to these averages. In general, the results show that the historical statistics are satisfactorily reproduced in the different domain of flows. Notice that in almost all cases, the confidence bands of the generated statistics encloses the historical statistics. It may be noted also that in the different domain of flows, the mean, standard deviations are best reproduced in the log-domain while the auto- and cross-correlations are best reproduced in the log-Wilson-Hilferty domain. This is only logical since such statitical properties are parameterized in the model at these corresponding domain of flows.

1:9.6 Modeling and Generation of Turbine Operating Hours

A preliminary analysis done in this study showed that the monthly inflows to Valdesia reservoir is significantly correlated to the monthly turbine operating hours of the said reservoir based on 9 years of data covering the period of 1976 to 1984. On this basis, it is decided to model and generate the turbine operating hours monthly time series based on reservoir inflows. Due to the proximity of Paso del Ermitaño and Valdesia reservoir, it is assumed that the said reservoir inflows are the same streafmlows as those of Paso del Ermitaño. Subsequently, the

turbine operating hours can be generated by solely using the generated streamflows of Paso del Ermitaño. However, since the available turbine operating hours (i.e., 1976-1984 period) has no corresponding recorded streamflow at Paso del Ermitaño, the monthly inflow data at Valdesia reservoir are used to derive the stochastic model for data generation.

The model selected for purposes here is a bivariate, contemporaneous, first-order autoregressive model with monthly parameters. Specifically, the model takes the following form:

$$\begin{bmatrix} z^{(1)}_{\nu,\tau} \\ z^{(2)}_{\nu,\tau} \end{bmatrix} = \begin{bmatrix} a_{11,\tau} & 0 \\ 0 & a_{22,\tau} \end{bmatrix} \begin{bmatrix} z^{(1)}_{\nu,\tau-1} \\ z^{(2)}_{\nu,\tau-1} \end{bmatrix} + \begin{bmatrix} b_{11,\tau} & 0 \\ b_{21,\tau} & b_{22,\tau} \end{bmatrix} \begin{bmatrix} \epsilon^{(1)}_{\nu,\tau} \\ \epsilon^{(2)}_{\nu,\tau} \end{bmatrix} \quad (1.9.13)$$

where $z^{(1)}_{\nu,\tau}$ is the Paso del Ermitaño streamflows, $z^{(2)}_{\nu,\tau}$ is the turbine operating hours, and, a's and b's are model parameters. The model above is similar to the model used for data extension (see Eq. 1.9.3a, Section 1.9.3.2) except for the seasonality of its model parameters and the parametric matrix of a's which renders the model as contemporaneous (Salas et al., 1985). For generating the turbine operating hours $z^{(2)}_{\nu,\tau}$, Eq. (1.9.13) can be rewritten as

$$z^{(2)}_{\nu,\tau} = \frac{b_{21,\tau}}{b_{11,\tau}} z^{(1)}_{\nu,\tau} - \frac{a_{11,\tau} b_{21,\tau}}{b_{11,\tau}} z^{(1)}_{\nu,\tau-1} + a_{22,\tau} z^{(2)}_{\nu,\tau-1} + b_{22,\tau} \epsilon^{(2)}_{\nu,\tau} \quad (1.9.14)$$

The time series variables $z^{(1)}_{\nu,\tau}$ and $z^{(2)}_{\nu,\tau}$ are monthly normalized and standardized using the Wilson-Hilferty transformation (see Appendix 1.9.A). The use of Wilson-Hilferty (WH) transformation alone for Paso del Ermitaño instead of in combination with logarithmic transformation

as done previously is simply for convenience and consistency with respect to the type of transformation used for turbine hours. Besides, either the log-WH or plain WH transformations are valid for Paso del Ermitaño monthly streamflows as shown in Table 1.9.A.1.

The monthly model parameters estimated for Eq. (1.9.14) are given in Table 1.9.7. Data generation of turbine operating hours follows in the same manner as the extension of records in section 1.9.3.2. Once, $z^{(2)}_{\nu,\tau}$ in the Wilson-Hilferty domain of turbine hours are obtained, the backtransformation to its original domain is performed as in section 1.9.5.1 using Eqs. (1.9.9), (1.9.10) and (1.9.11), i.e., without the anti-log operation.

Table 1.9.7. Monthly parameters of turbine operating hours model in Eq. (1.9.14).

Month, τ	$a_{11,\tau}$	$a_{22,\tau}$	$b_{11,\tau}$	$b_{21,\tau}$	$b_{22,\tau}$
1	0.6694	0.9753	0.7429	0.1002	0.1969
2	0.3083	0.1667	0.9513	0.2410	0.9561
3	0.5255	0.2728	0.8508	0.4014	0.8744
4	0.5900	0.6270	0.8074	-0.2026	0.7522
5	0.4592	0.0780	0.8883	0.5654	0.8211
6	0.4547	0.5428	0.8906	0.6946	0.4721
7	0.5435	0.5640	0.8394	0.3352	0.7547
8	0.3396	-0.1422	0.9406	0.4205	0.8961
9	0.1236	0.4279	0.9923	0.6525	0.6254
10	0.3649	0.5630	0.9310	0.3378	0.7543
11	0.1527	0.4804	0.9883	0.2200	0.8490
12	0.4888	0.2435	0.8724	0.7023	0.6690

As in streamflow data generation, 50 samples of 22 years of monthly turbine operation hours were generated. A comparison of important statistical parameters between historical and generated turbine hours was also performed. Results of the comparison are shown in Appendix 1.9.F which show satisfactory reproduction of monthly means, standard

deviations skewness coefficients, autocorrelations and cross-correlations.

1.9.7 Final Remarks

Considerable data analysis and manipulations have been done prior to data modeling and generation. First of all, the missing data of Palo de Caja has to be filled-in using an appropriate regression model. Then data extension has to be performed for Palo del Ermitaño and Rancho Arriba. In data extension, 50 series extensions are made where in principle, any one of the extended series can be used for deriving the statistical parameters for modeling and data generation. However, since our objective is to improve the reliability of these statitical estimates, the 50 series extensions were used to represent the statistical parameters in terms of averages.

As a requirement for linear normal models in this study, the combination of logarithmic and Wilson-Hilferty transformation is proven to be effective in normalizing the streamflow. It may be noted that the Wilson-Hilferty transformation is developed on the basis of the Pearson Type III (gamma) distribution. Thus, it can be said that streamflow data follows a log-Pearson Type III distribution.

In time series modeling of the extended data, three alternative stochastic models were found. The main reason for tentatively prescribing three model forms is for us to select the best model in terms of model parsimony (i.e., economy of parameters) and overall modeling efficiency without compromising the adequacy and ability of the final model adopted to represent the time series process studied at hand. The paper by Salas, et al., 1985 may be consulted for further

elaborations on alternative multivariate models similar to the ones used here, and applications of multivariate models in general.

APPENDIX 1.9.A

STANDARDIZATION AND NORMALIZATION

The purpose of standardization is to remove the seasonalities in the means and variances of the data. Removal of such seasonalities may be made by using the raw estimates of the means and variances or their corresponding smoothed estimates by say, Fourier series fitting. For this study, the raw estimates of the semi-monthly means and variances are used. As mentioned in section 1.9.3, a transformation is made to render the data normal. Currently, there are various transformations of frequent use in hydrology such as square-root, cube-root, logarithmic, Wilson-Hilferty or log-Wilson-Hilferty transformations. Depending on the type of normalization (transformation) used, standardization is applied before or after transformation. The five normalizing transformations mentioned above were used in this study.

1) Square-root transformation:

Denoting the original time series data by $Y_{\nu,\tau}$ of year ν and season τ, the square-root transformation is done by

$$X_{\nu,\tau} = \sqrt{Y_{\nu,\tau}} \qquad (1.9.A.1)$$

for all $\nu = 1,\ldots,n$ years and $\tau = 1,\ldots,w$ seasons. Then standardization follows given by:

$$Z_{\nu,\tau} = \frac{X_{\nu,\tau} - \bar{X}_{\tau}}{S_{\tau}(x)} \qquad (1.9.A.2)$$

where $\bar{X}_\tau$ and $S_\tau(x)$ are the semi-monthly mean and standard deviation of the square-root transformed data.

2) Cube-root transformation:

In this case, the original series $Y_{\nu,\tau}$ is transformed using the equation

$$X_{\nu,\tau} = Y_{\nu,\tau}^{1/3} \qquad (1.9.A.3)$$

then, standardization is performed using Eq. (1.8.A.2) where $\bar{X}_\tau$ and $S_\tau(x)$ are evaluated using the cube-root transformed data.

3) Logarithmic transformation:

The raw series $Y_{\nu,\tau}$ is transformed by

$$X_{\nu,\tau} = \log(Y_{\nu,\tau}) \qquad (1.9.A.4)$$

where log stands for the base-e logarithms. This is followed by standardization as in Eq. (1.9.A.2).

4) Wilson-Hilferty transformation:

The original series $Y_{\nu,\tau}$ is first standardized as in Eq. (1.9.A.2) by

$$X_{\nu,\tau} = \frac{Y_{\nu,\tau} - \bar{Y}_\tau}{S_\tau(Y)} \qquad (1.9.A.5)$$

where $\bar{Y}_\tau$ and $S_\tau(Y)$ are the semi-monthly mean and standard deviation of the series $(Y_{\nu,\tau})$. The Wilson-Hilferty transformation is given by (Matals, 1967)

$$Z_{\nu,\tau} = \frac{6}{G_\tau(x)} \left\{ \left[\frac{G_\tau(x)\, X'_{\nu,\tau}}{2} + 1 \right]^{1/3} - 1 \right\} + \frac{G_\tau(x)}{6} \qquad (1.9.A.6)$$

which is valid for $G_\tau(x) \neq 0$, where $G_\tau(x)$ is the semi-monthly skewness coefficient of $X_{\nu,\tau}$ and $X'_{\nu,\tau}$ is given by McGinnis and Sammons (1970) as

$$X'_{\nu,\tau} = \begin{cases} \max[X_{\nu,\tau},\ -2/G_\tau(x)] & \text{if } G_\tau(x) \geq 0 \\ \min[X_{\nu,\tau},\ -2/G_\tau(x)] & \text{if } G_\tau(x) < 0 \end{cases} \qquad (1.9.A.7)$$

If $G_\tau(x) = 0$ no transformation is necessary then $Z_{\nu,\tau} = X_{\nu,\tau}$.

5) Log-Wilson-Hilferty transformation:

This transformation is a combination of logarithmic transformation (item 3) and Wilson-Hilferty transformation (item 4). For the sake of clarity, let us rewrite some of the equations above. First the original data $Y_{\nu,\tau}$ is transformed as in Eq. (1.9.A.4) as

$$W_{\nu,\tau} = \log (Y_{\nu,\tau}) \qquad (1.9.A.8)$$

Then, standardization is performed using

$$X_{\nu,\tau} = \frac{W_{\nu,\tau} - \bar{W}_\tau}{S_\tau(w)} \qquad (1.9.A.9)$$

where $\bar{W}_\tau$ and $S_\tau(w)$ are the seasonal means and standard deviations of the logarithmic transformed sequence $\{W_{\nu,\tau}\}$. Then, the Wilson-Hilferty transformation is performed using Eqs. (1.9.A.6) and (1.9.A.7) to arrive at $Z_{\nu,\tau}$.

The criteria for selecting the type of normalizing transformation to be used in this study is the skewness test for normality. This test assumes that if the observations are independent and sampled from the normal distribution, then, the sample skewness coefficient must fall within the $(1-\alpha)$ confidence limits

$$[-u_{1-\alpha/2}\sqrt{6/n}\ ,\quad u_{1-\alpha/2}\sqrt{6/n}] \tag{1.9.A.10}$$

where $u_{1-\alpha/2}$ is the $1-\alpha/2$ quantile of the standard normal distribution and n is the sample size. Since we have a total of 12 monthly and 52 weekly skewness coefficients computed after each transformation, the relative number of skews within the confidence limits are counted. The greatest number of passes forms the basis of choice of the suitable transformation used here.

The results of these analysis are given in Tables 1.9.A.1 and 1.9.A.2 for monthly and weekly levels, respectively. From these results it can be concluded that the streamflow data of Palo de Caja, Paso del Ermitaño, Rancho Arriba and El Cacao be normalized using the log-Wilson-Hilferty transformation, while the rainfall data of La Laguna and Valdesia be normalized using Wilson-Hilferty transformation.

Table 1.9.A.1. Relative scores of passing and failing the skewness test on a monthly basis using the five normalizing transformations including no transformation.

	No Transformation	Square-Root	Cube-Root	Logarithmic	Wilson-Hilferty	Log-Wilson-Hilferty
Palo de Caja						
Pass	0	3	6	10	8	12*
Fail	12	9	6	2	4	0
Paso del Ermitaño						
Pass	5	9	10	12	11	12*
Fail	7	3	2	0	1	0
Rancho Arriba						
Pass	10	10	10	10	11	11*
Fail	2	2	2	2	1	1
El Cacao						
Pass	6	12	11	9	12	12*
Fail	6	0	1	3	0	0
La Laguna						
Pass	7	11	8	2	12*	5
Fail	5	1	4	10	0	7
Valdesia						
Pass	5	10	11	9	12*	10
Fail	7	2	1	3	0	2

*Indicate transformation used.

Table 1.9.A.2. Relative scores of passing and failing the skewness test on a weekly basis using the five normalizing transformations including no transformation.

	No Transformation	Square-Root	Cube-Root	Logarithmic	Wilson-Hilferty	Log-Wilson-Hilferty
Palo de Caja						
Pass	1	30	28	30	28	48*
Fail	51	22	24	22	24	4
Paso del Ermitaño						
Pass	33	47	47	48	47	52*
Fail	19	5	5	4	5	0
Rancho Arriba						
Pass	36	43	48	43	49	50*
Fail	16	9	4	9	3	2
El Cacao						
Pass	29	46	45	48	46	52*
Fail	23	6	7	4	6	0
La Laguna						
Pass	10	41	50	41	51*	34
Fail	42	11	2	11	1	18
Valdesia						
Pass	7	36	44	37	46*	32
Fail	45	16	8	15	6	20

*Indicate transformation used.

APPENDIX 1.9.B

HISTORICAL AND EXTENDED SERIES STATISTICS OF MONTHLY AND WEEKLY DATA OF PASO DEL ERMITAÑO AND RANCHO ARRIBA IN THE ORIGINAL DOMAIN OF FLOWS

Note: In the figures given below, the extended series statistics are averages computed from the fifty series extensions and correspondingly the positive and negative one-standard errors relative to these averages.

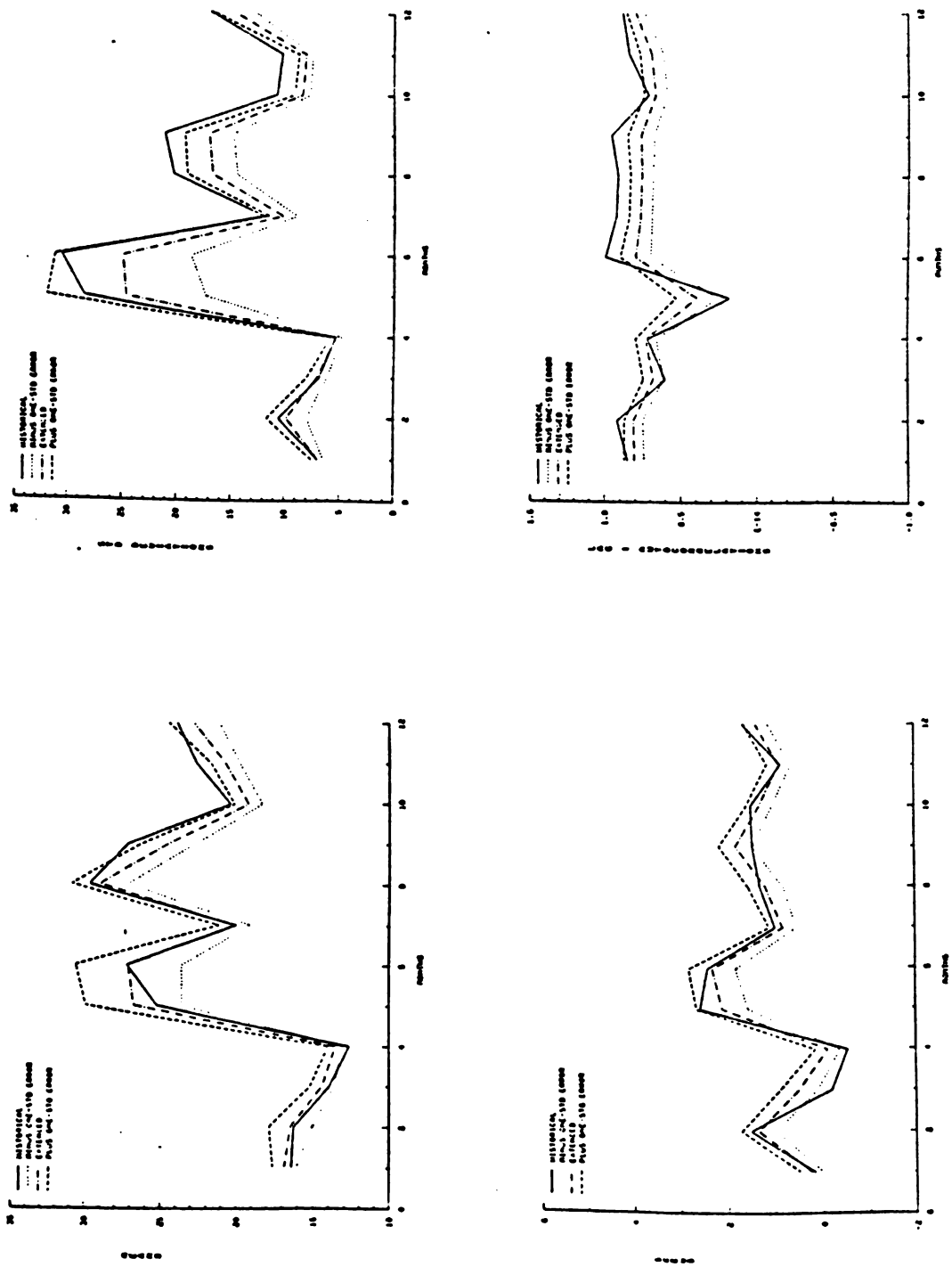

Figure 1.9.B.1 Historical and extended series monthly statistics of Paso del Ermitano in the original domain of flows.

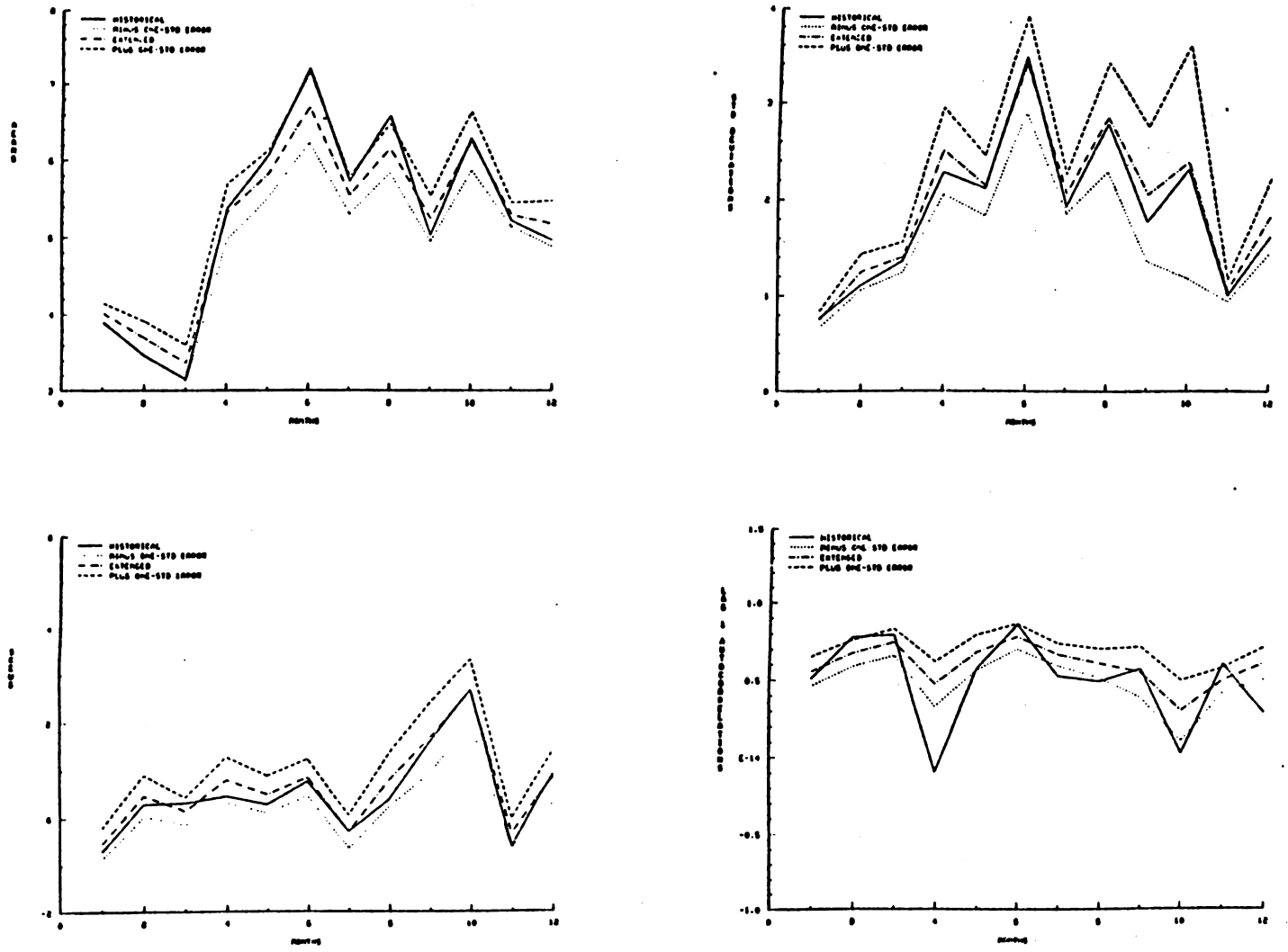

Figure 1.9.B.2. Historical and extended series monthly statistics of Rancho Arriba in the original domain of flows.

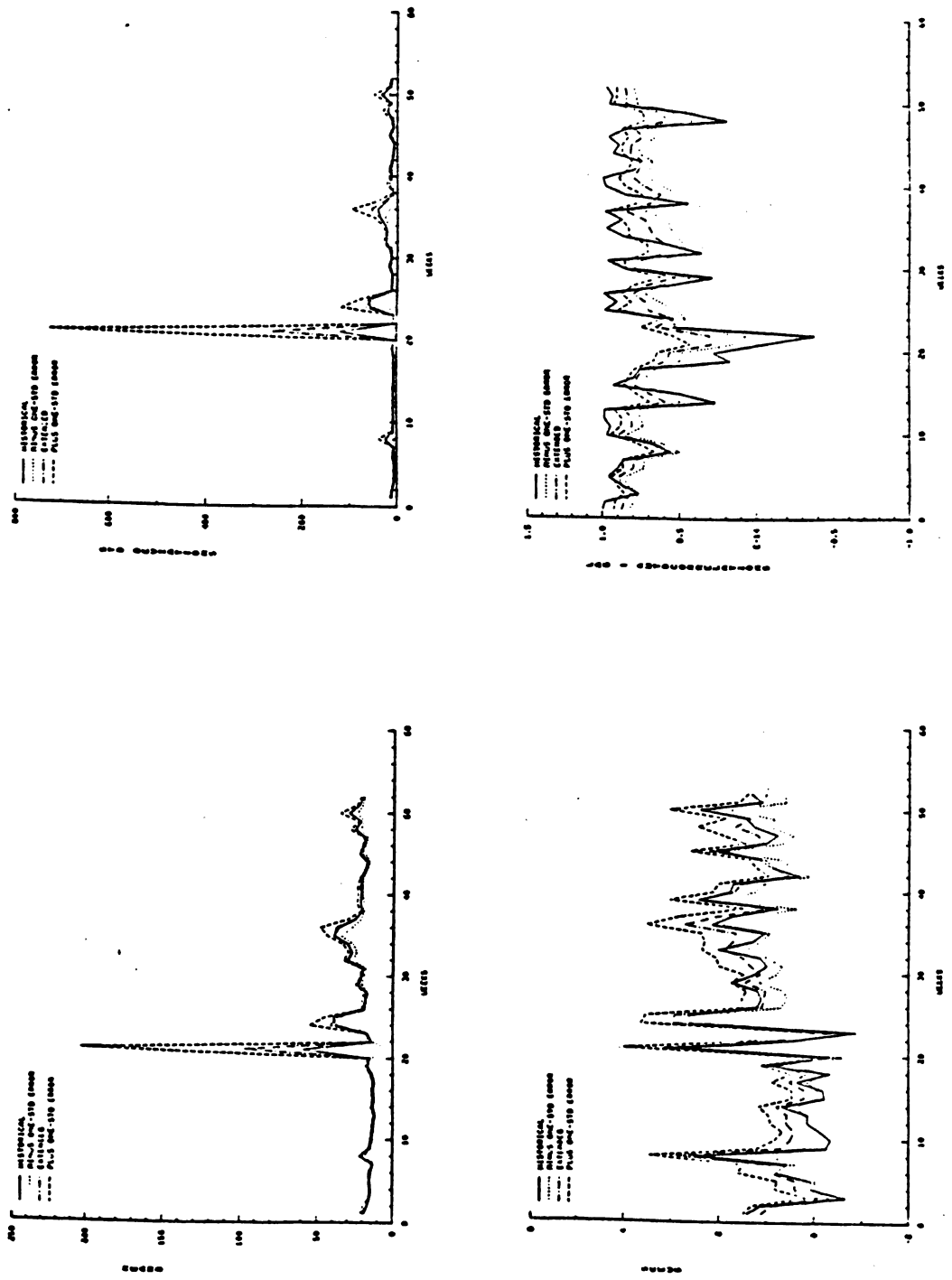

Figure 1.9.B.3. Historical and extended series weekly statistics of Paso del Ermitano in the original domain of flows.

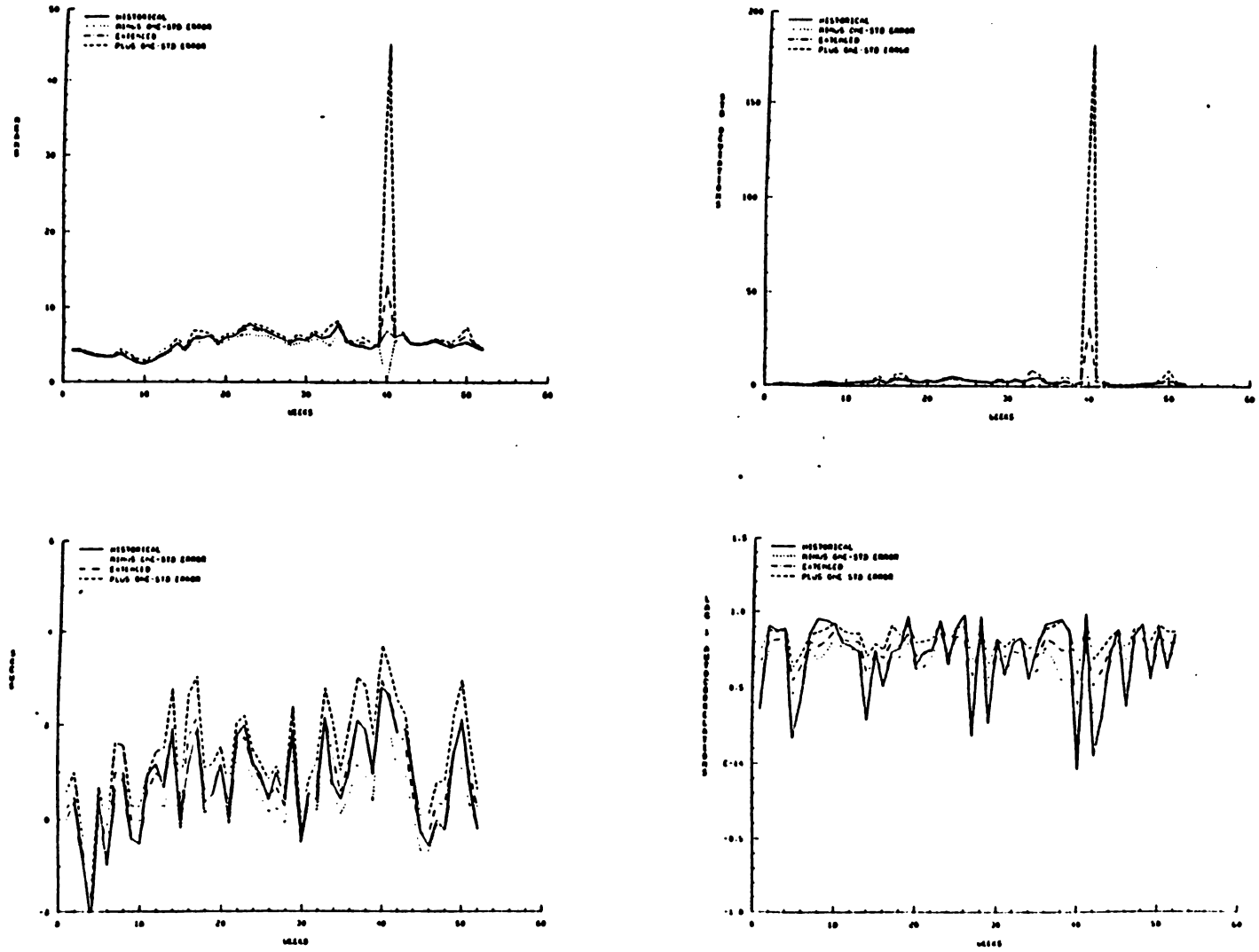

Figure 1.9.B.4. Historical and extended series weekly statistics of Rancho Arriba in the original domain of flows.

APPENDIX 1.9.C

FOURIER SERIES FITTING OF PERIODIC STATISTICAL PARAMETERS

Consider that U_τ represents the periodic statistical parameter such as skewness G_τ or the autocorrelation coefficient $R_\tau(k)$. The Fourier series representation of U_τ denoted by U_τ^* is obtained from (Salas, et al., 1980):

$$U_\tau^* = \bar{U} + \sum_{j=1}^{h} [A_j \cos(2\pi j\tau/\omega) + B_j \sin(2\pi j\tau/\omega)] \qquad (1.9.C.1)$$

for $\tau = 1,\ldots,\omega$ semi-months. The mean $\bar{U}$ and Fourier coefficients A_j and B_j are determined by

$$\bar{U} = \frac{1}{\omega} \sum_{t=1}^{\omega} U_\tau \qquad (1.9.C.2a)$$

$$A_j = \frac{2}{\omega} \sum_{\tau=1}^{\omega} U_\tau \cos\left(\frac{2\pi j\tau}{\omega}\right) ; \quad j = 1,\ldots,h \qquad (1.9.C.2b)$$

and

$$B_j = \frac{2}{\omega} \sum_{\tau=1}^{\omega} U_\tau \sin\left(\frac{2\pi j\tau}{\omega}\right) ; \quad j = 1,\ldots,h \qquad (1.9.C.2c)$$

The total number of harmonics h is theoretically equal to $\omega/2$ for ω an even number or equal to $(\omega-1)/2$ for ω an odd number. However, for purposes of removing sampling variabilities in the sample series U_τ, only a few harmonics are necessary. The selection of

harmonics may be decided based on the significance of explained variance of each harmonic component. The so-called explained variance for each harmonic is computed from

$$EV_j = \frac{(A_j^2 + B_j^2)}{S^2(u)} \times 100 \text{ percent} \qquad (1.9.C.3)$$

where EV_j is the explained variance in percent and $S^2(u)$ is the variance of the series $\{U_\tau\}$. Further details of selection of significant harmonics are given by Salas, et al. (1980).

Results of the Fourier series fitting of the monthly and weekly skewness coefficients in the log-domain for Palo de Caja, Paso del Ermitaño and Rancho Arriba are given in Figures 1.9.C.1 through 1.9.C.2. For monthly skewness coefficients, the first 2, 3, and 4 harmonics were fitted while those for weekly, the first 4, 5, and 6 harmonics were fitted. In the figures, the skewness coefficients of the extended series are referred to as "historical" and has been corrected for bias prior to Fourier series fitting. The bias correction for the skewness is based on gamma distribution which implies that the extended series in the log-domain of flows are assumed to be gamma distributed. This assumption is made post-de-facto since the suitable normalizing transformation is found to be the Wilson-Hilferty transformation (which is a gamma-based transformation) which was performed after logarithmic transformation. In equation form, the skewness $(G_\tau)_c$ corrected for bias is given by (Yevjevich and Obeysekera, 1984):

$$(G_\tau)_c = G_\tau \left[\left(1 + \frac{6.51}{N} + \frac{20.20}{N^2}\right) + \left(\frac{1.48}{N} + \frac{6.77}{N^2}\right) G_\tau^2\right]$$

where G_τ is the extended series, average skewness of season τ and N is the number of years of record. From results herein, it is decided that the Fourier fitted functions using the first two harmonics be used for monthly skews while the first four harmonics be used for weekly skews.

Figures 1.9.C.3 to 1.9.C.6 show the results of Fourier series fitting of lag-1 and lag-2, monthly and weekly autocorrelations for the three stations in the log-Wilson-Hilferty domain of flows. From results herein, it is likewise decided that the first two harmonic fitted functions be used for monthly autocorrelations while the first four harmonic functions be used for weekly autocorrelations.

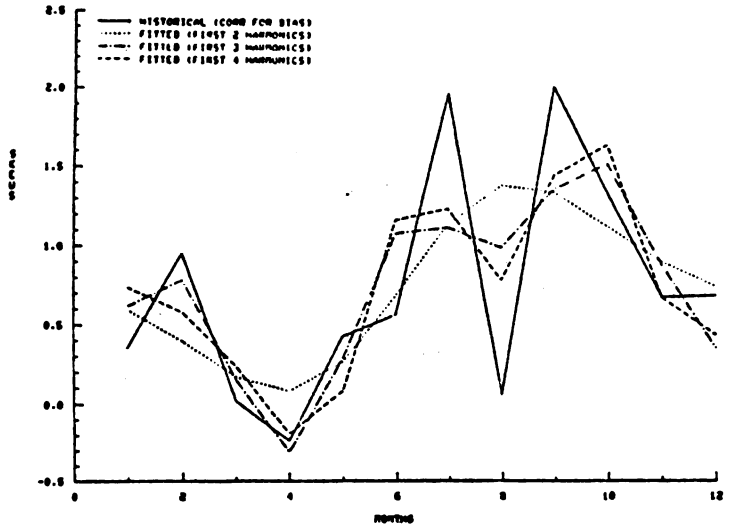

PALO DE CAJA - SKEUS IN LOG DOMAIN

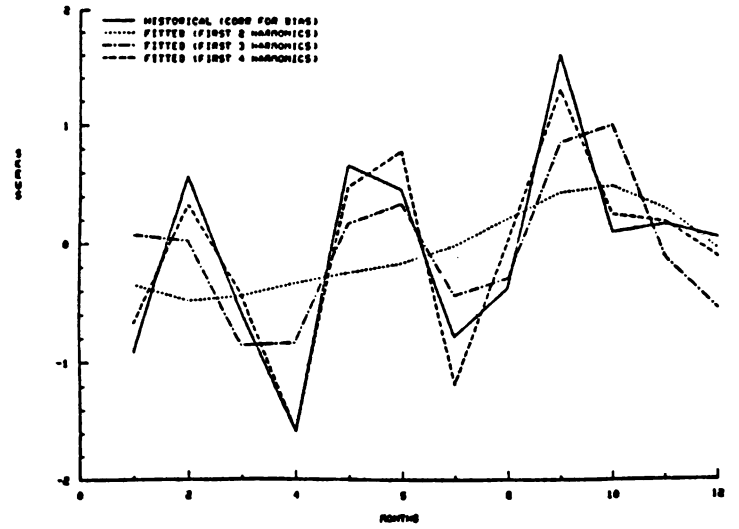

PASO DEL ERMITANO - SKEUS IN LOG DOMAIN

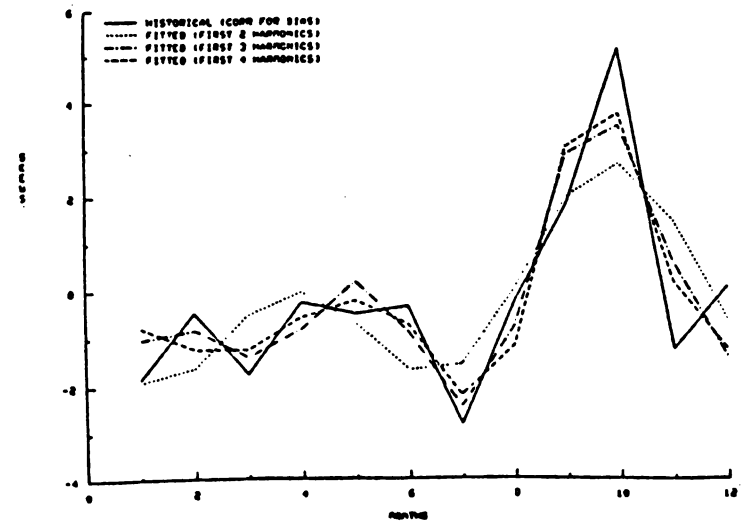

RANCHO ARRIBA - SKEUS IN LOG DOMAIN

Figure 1.9.C.1 Historical and Fourier fitted monthly skews in the log domain.

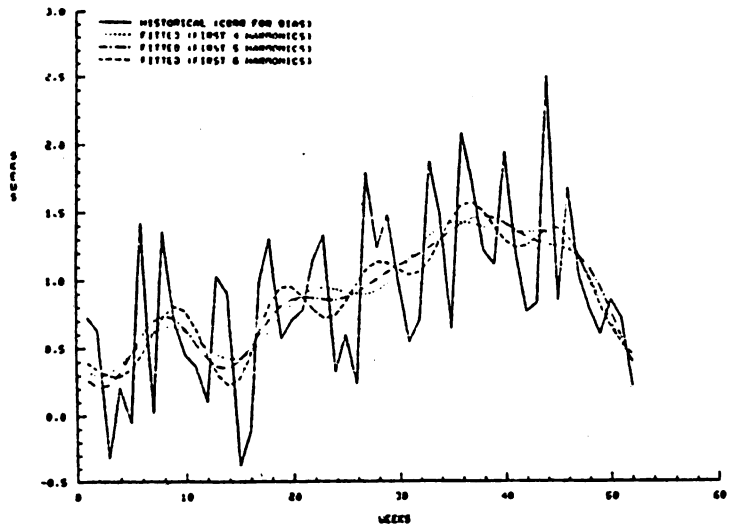

PALO DE CAJA - SKEWS IN LOG DOMAIN

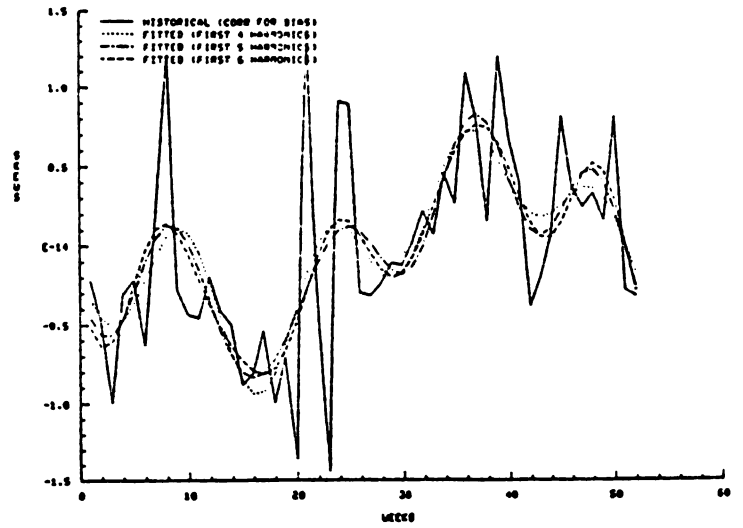

PASO DEL ERMITANO - SKEWS IN LOG DOMAIN

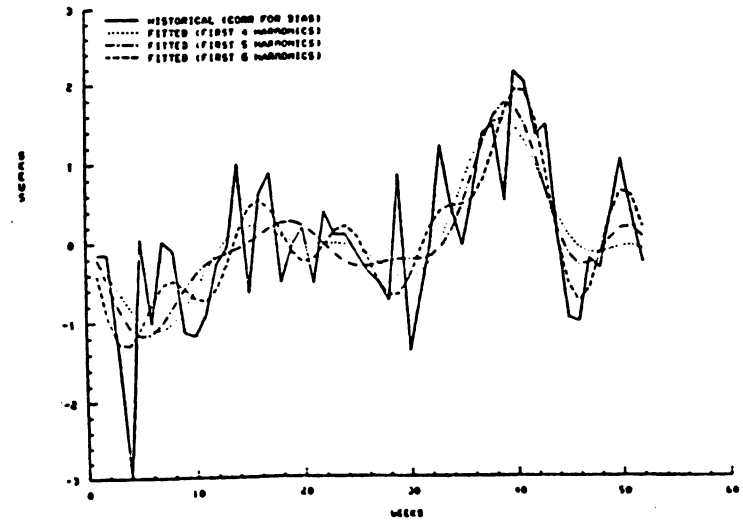

RANCHO ARRIBA - SKEWS IN LOG DOMAIN

Figure 1.9.C.2. Historical and Fourier fitted weekly skews in log domain.

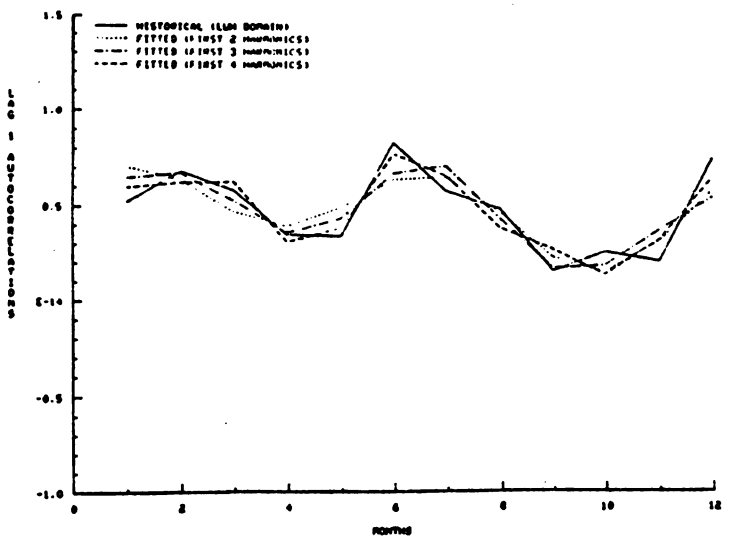

PALO DE CAJA - LAG 1 AUTOCORRELATIONS IN LUH DOMAIN

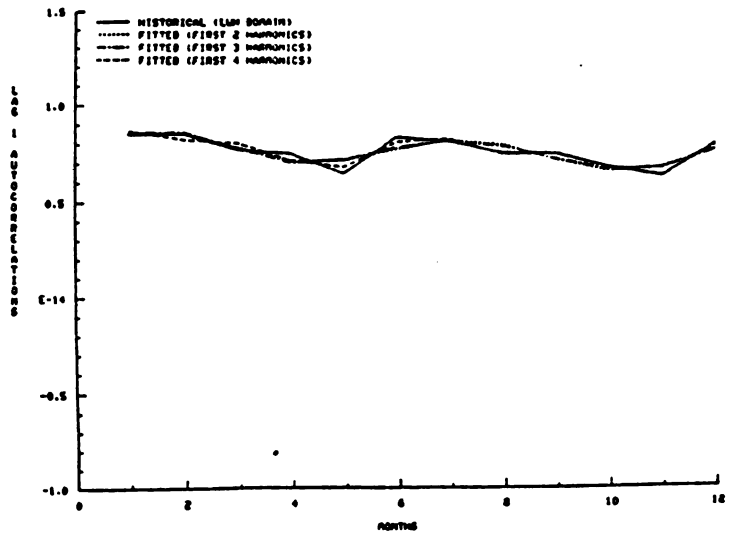

PASO DEL ERMITANO - LAG 1 AUTOCORRELATIONS IN LUH DOMAIN

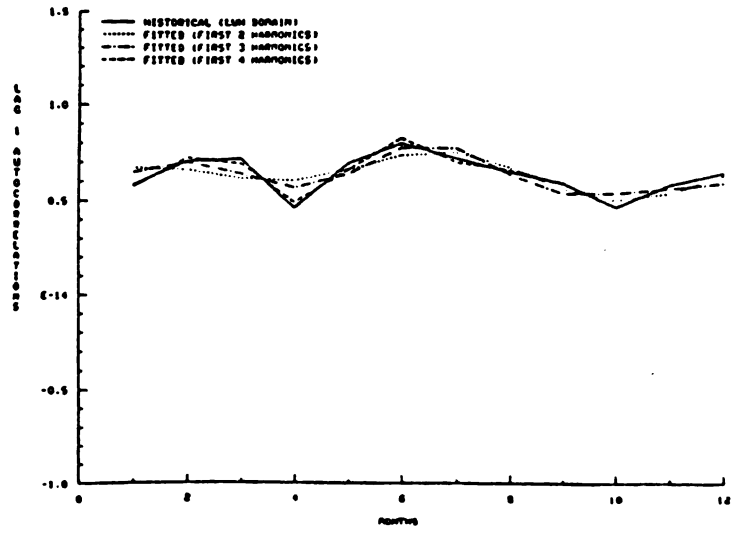

RANCHO ARRIBA - LAG 1 AUTOCORRELATIONS IN LUH DOMAIN

Figure 1.9.C.3 Historical and Fourier fitted monthly lag-1 autocorrelations in log-WH domain.

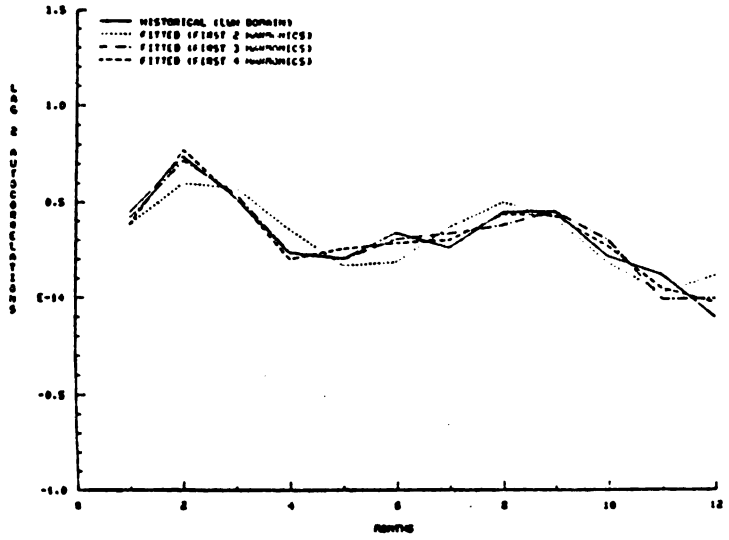

PALO DE CAJA - LAG 2 AUTOCORRELATIONS IN LUH DOMAIN

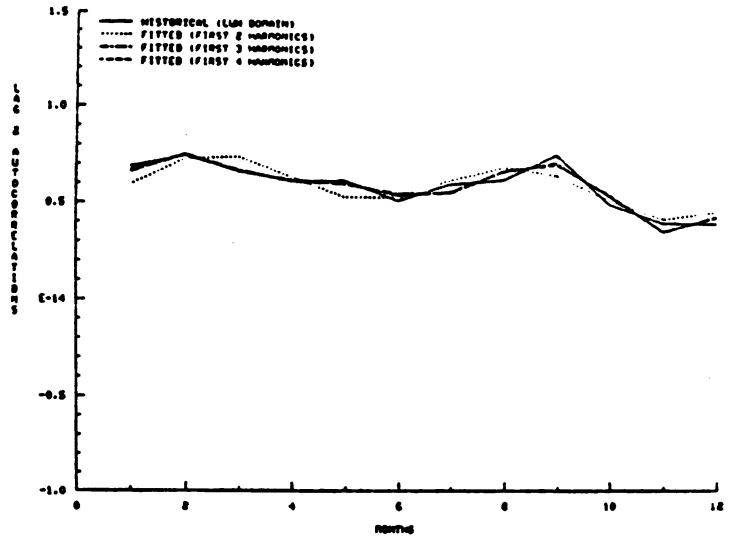

PASO DEL ERMITANO - LAG 2 AUTOCORRELATIONS IN LUH DOMAIN

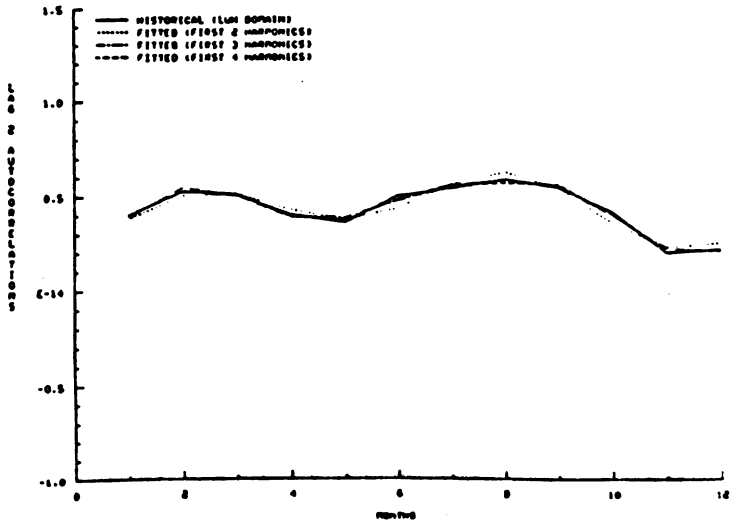

RANCHO ARRIBA - LAG 2 AUTOCORRELATIONS IN LUH DOMAIN

Figure 1.9.C.4. Historical and Fourier fitted monthly lag-2 autocorrelations in log-WH domain.

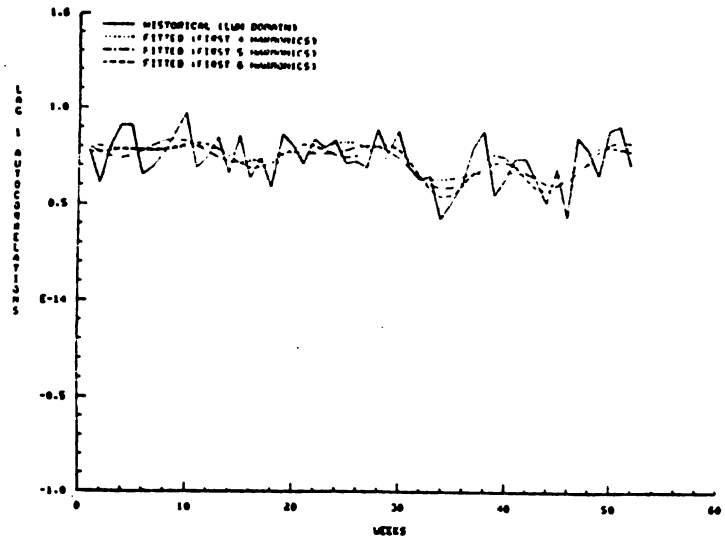

PALO DE CAJA - LAG 1 AUTOCORRELATIONS IN LUH DOMAIN

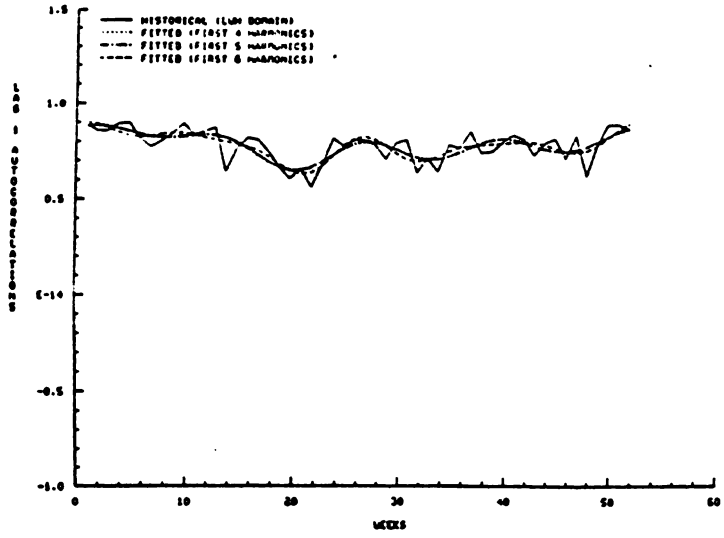

PASO DEL ERMITANO - LAG 1 AUTOCORRELATIONS IN LUH DOMAIN

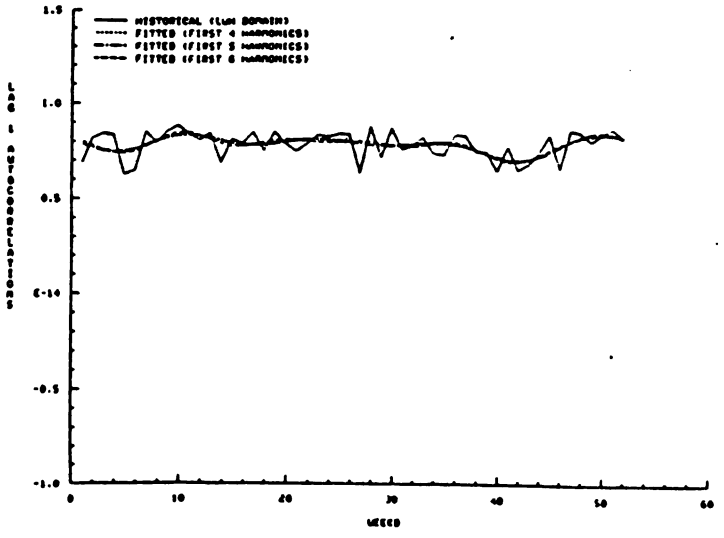

RANCHO ARRIBA - LAG 1 AUTOCORRELATIONS IN LUH DOMAIN

Figure 1.9.C.5. Historical and Fourier fitted weekly lag-1 autocorrelations in log-WH domain.

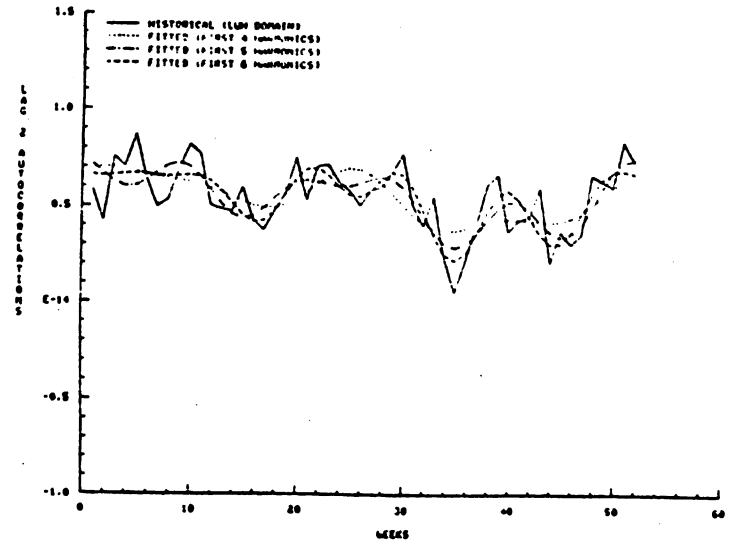

PALO DE CAJA - LAG 2 AUTOCORRELATIONS IN LUH DOMAIN

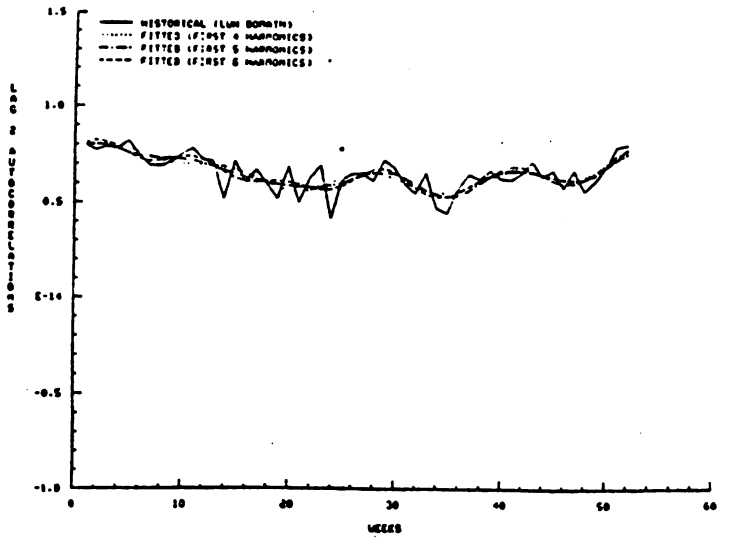

PASO DEL ERMITANO - LAG 2 AUTOCORRELATIONS IN LUH DOMAIN

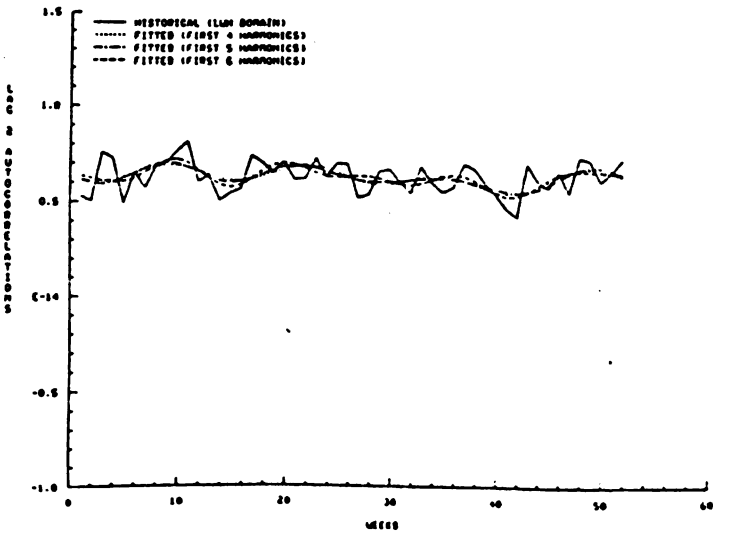

RANCHO ARRIBA - LAG 2 AUTOCORRELATIONS IN LUH DOMAIN

Figure 1.9.C.6. Historical and Fourier fitted weekly lag-2 autocorrelations in log-WH domain.

APPENDIX 1.9.D

HISTORICAL (EXTENDED SERIES) AND GENERATED MONTHLY AND WEEKLY STATISTICS FOR PALO DE CAJA, PASO DEL ERMITAÑO AND RANCHO ARRIBA USING MODELS A, B AND C IN THE ORIGINAL DOMAIN OF FLOWS

Note: See Appendix 1.9.E for details of computing generated statistics.

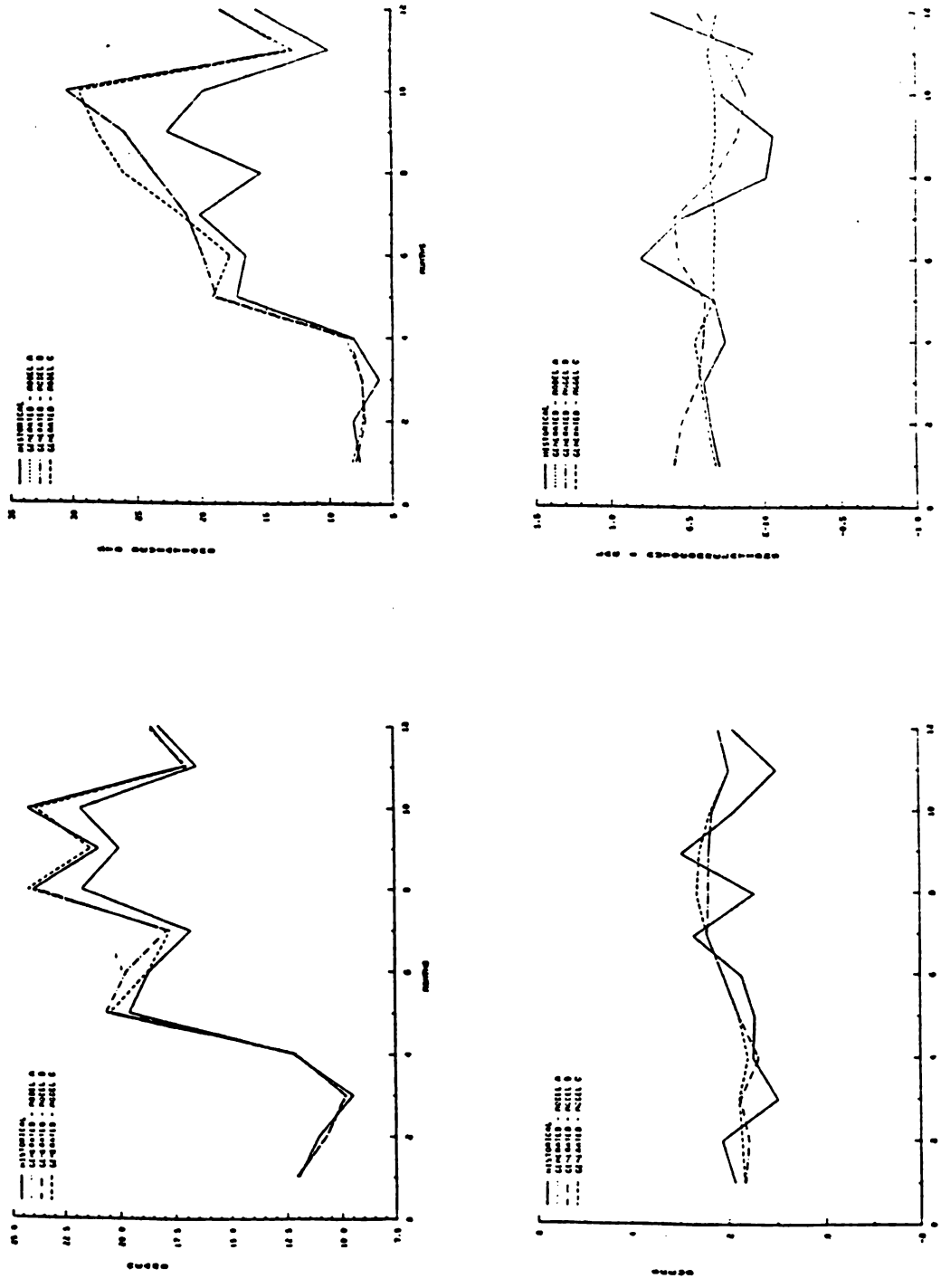

Figure 1.9.D.1. Historical and generated monthly statistics of Palo de Caja in the original domain of flows using models A, B, and C.

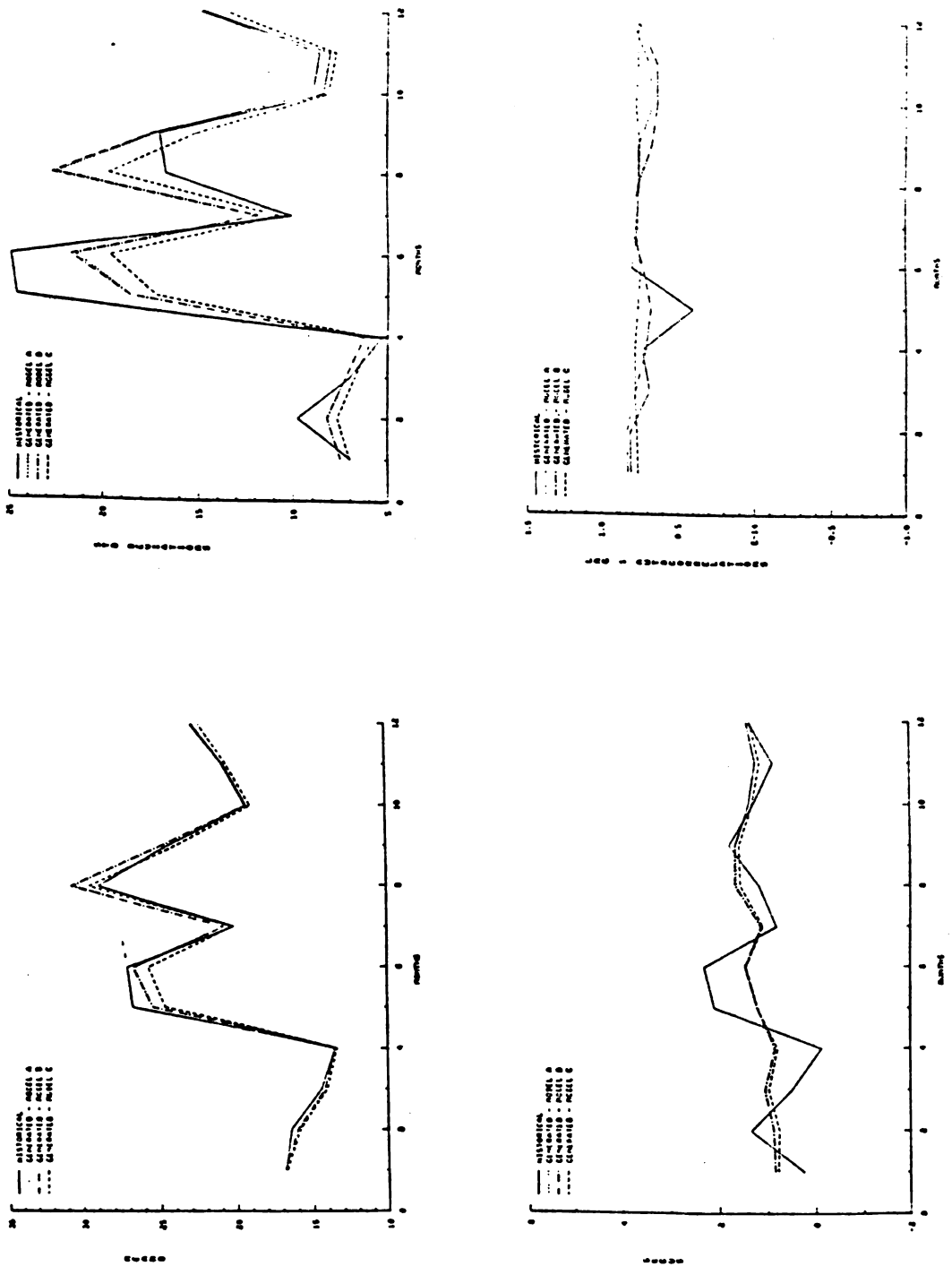

Figure 1.9.D.2. Historical and generated monthly statistics of Paso del Ermitano in the original domain of flows using models A, B, and C.

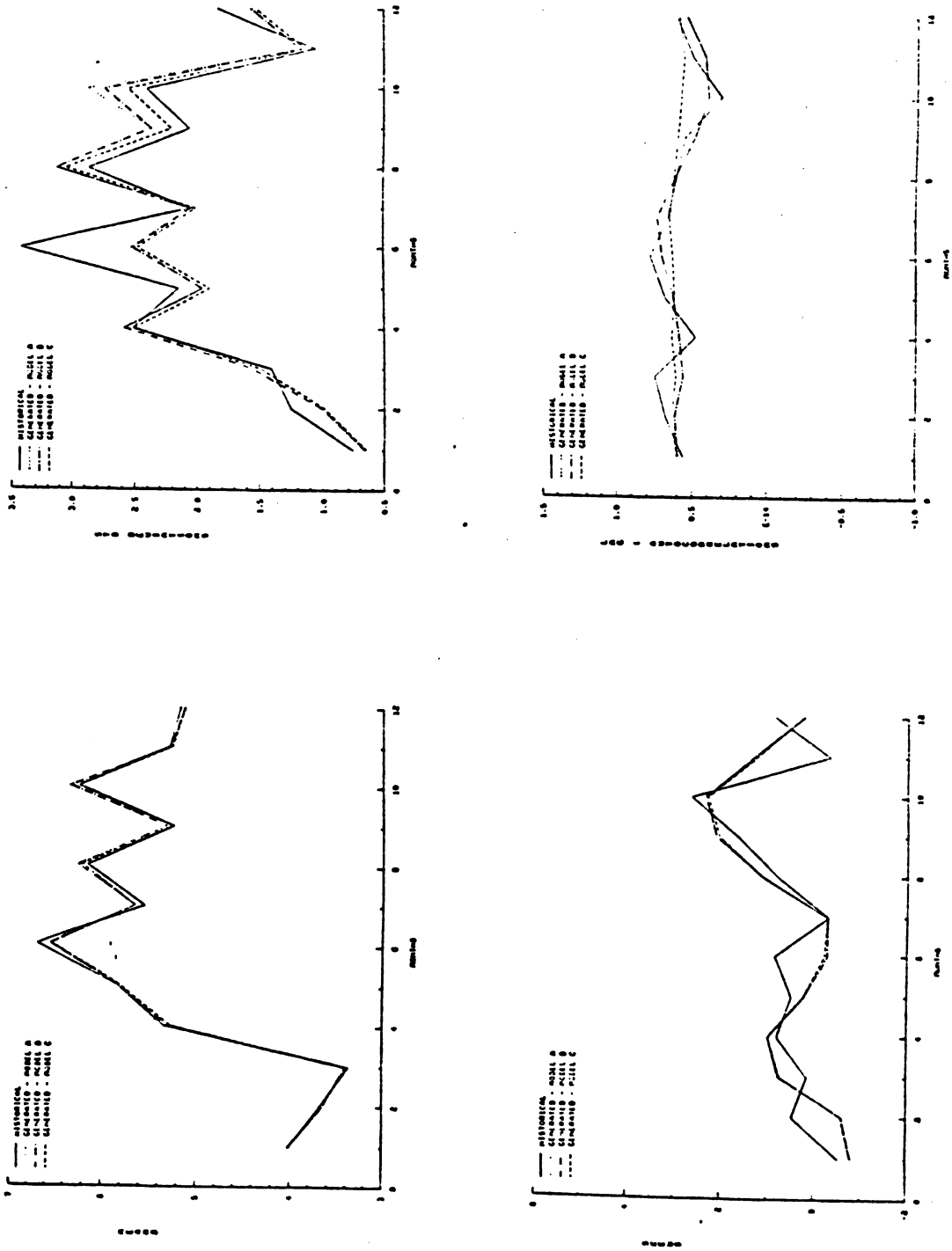

Figure 1.9.D.3. Historical and generated monthly statistics of Rancho Arriba in the original domain of flows using models A,B, and C.

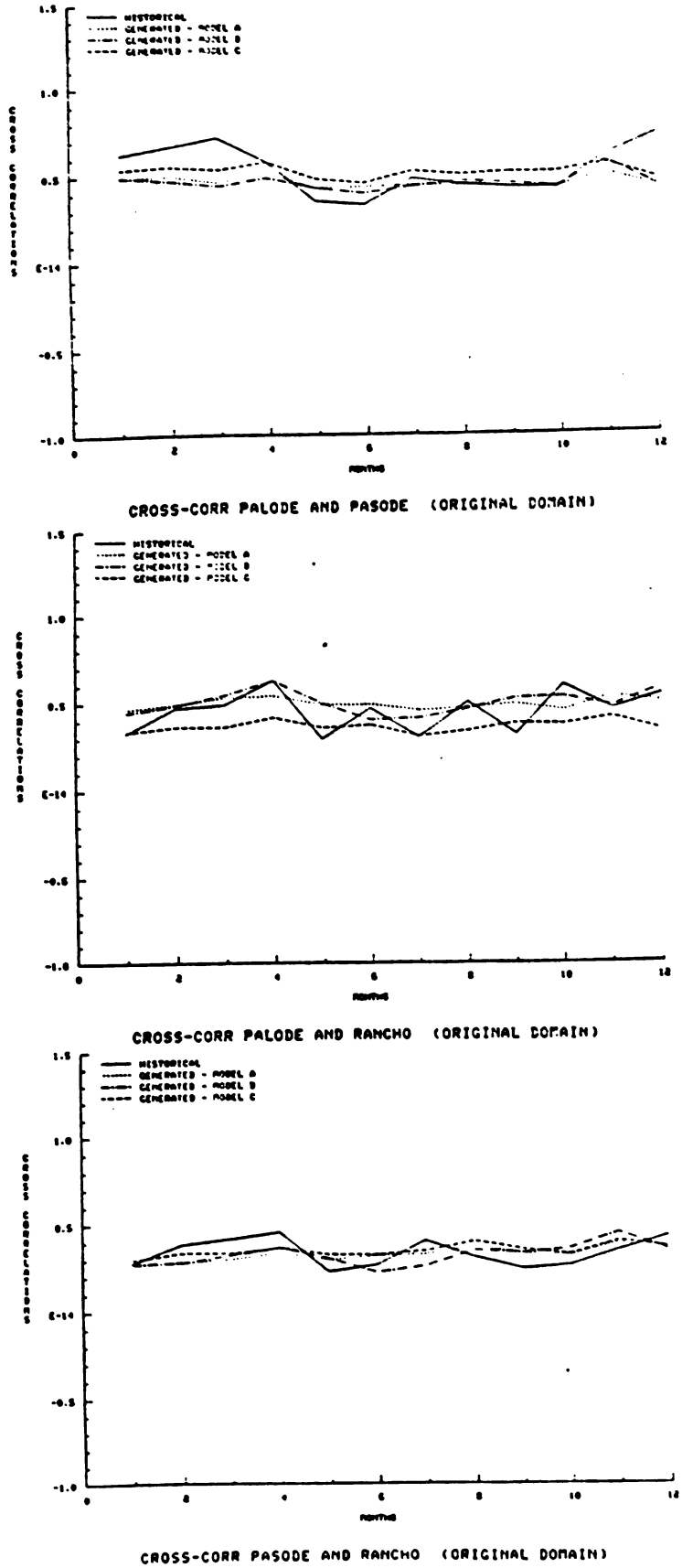

Figure 1.9.D.4. Historical and generated monthly cross-correlations in the original domain using models A, B, and C.

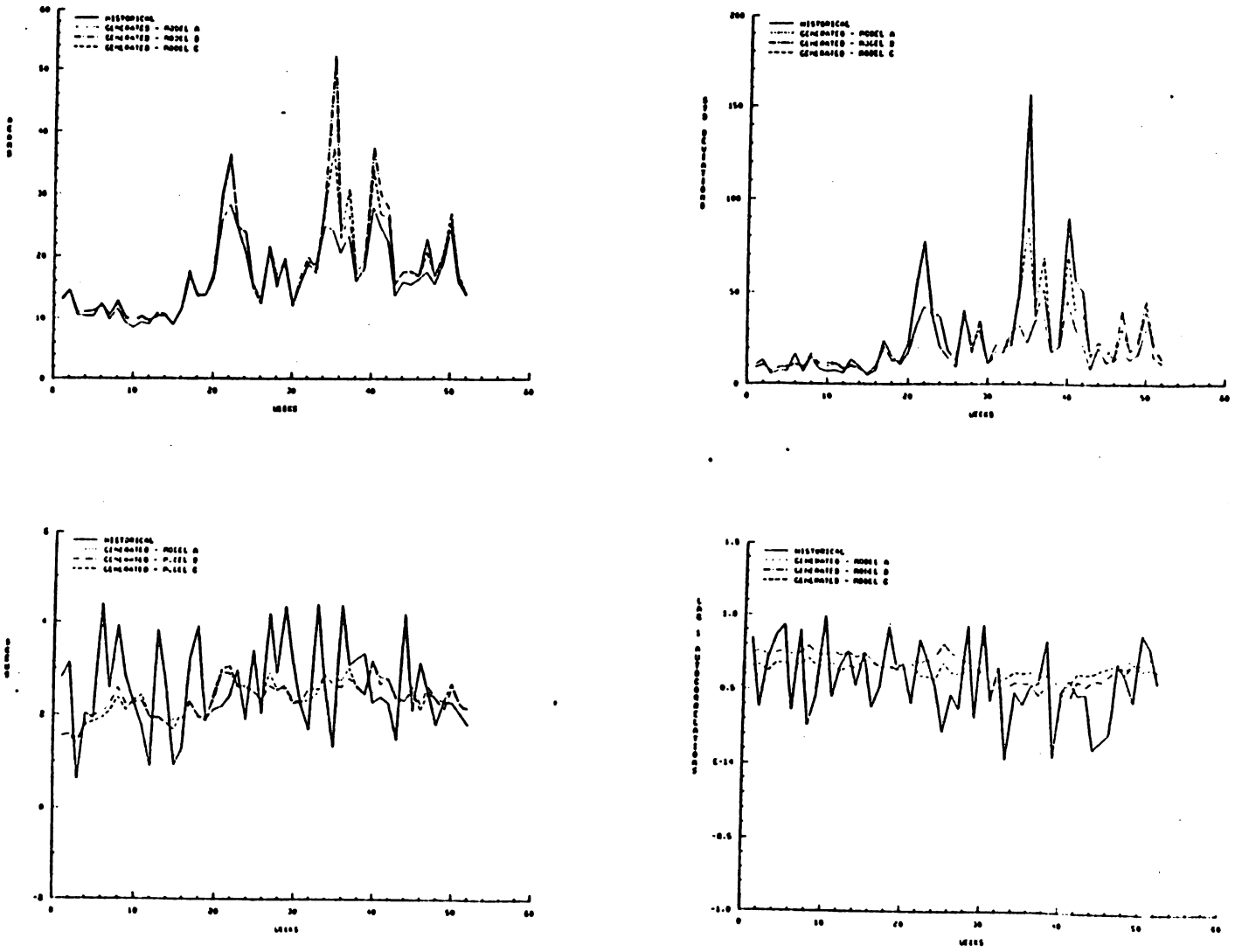

Figure 1.9.D.5. Historical and generated weekly statistics of Palo de Caja in the original domain of flows using models A, B, and C.

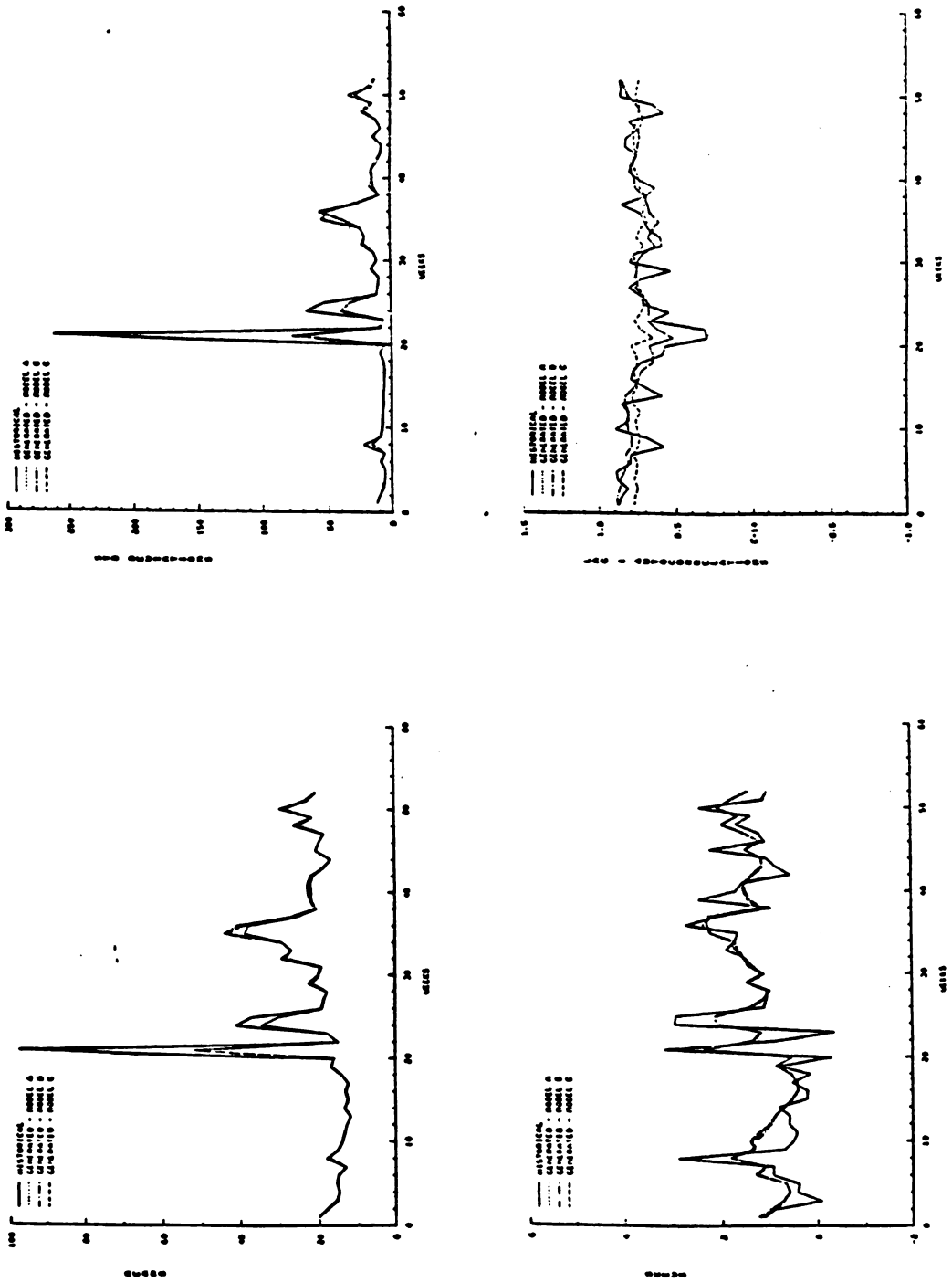

Figure 1.9.D.6. Historical and generated weekly statistics of Paso del Ermitano in the original domain of flows using models A, B, and C.

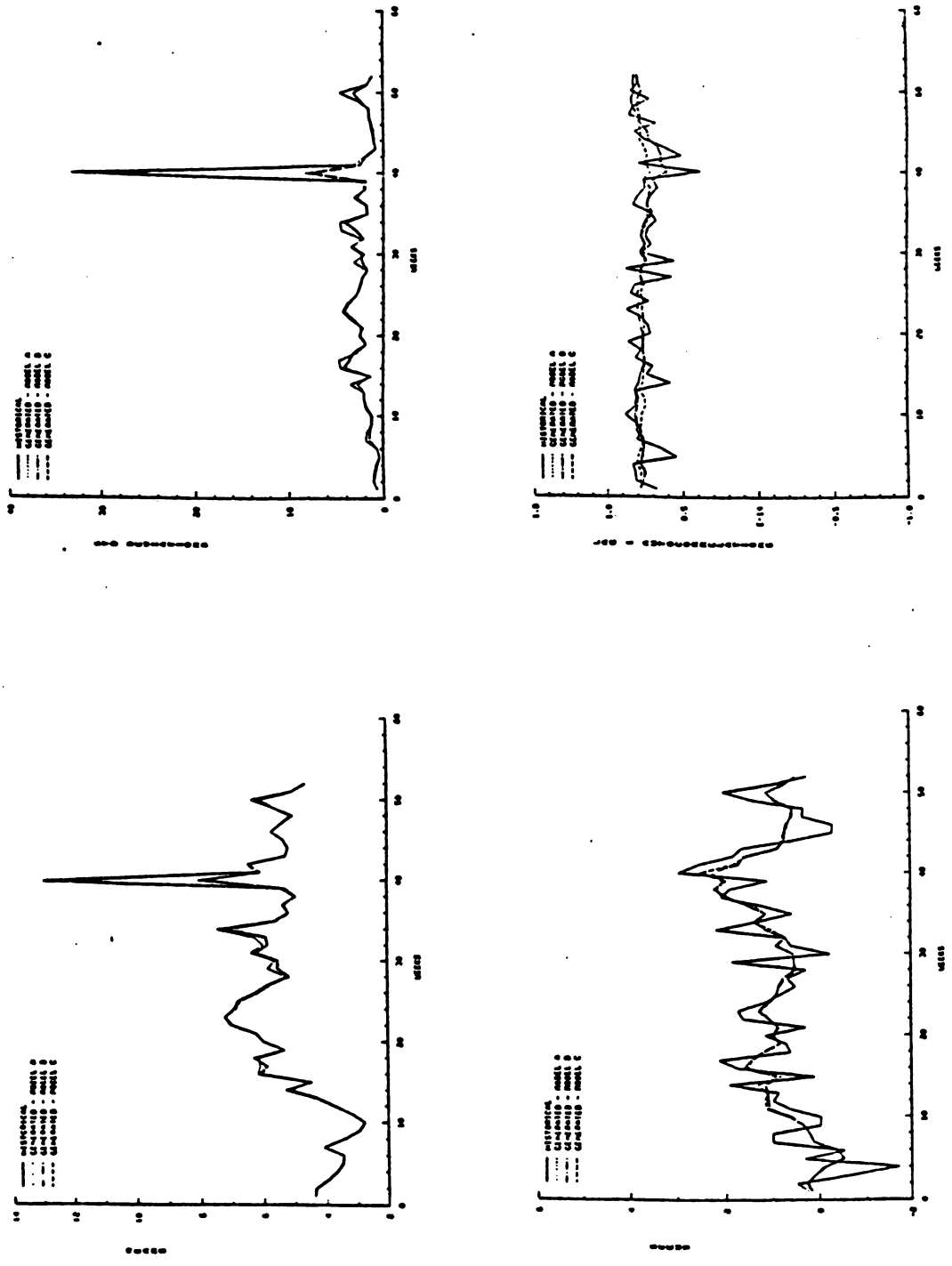

Figure 1.9.D.7. Historical and generated weekly statistics of Rancho Arriba in the original domain of flows using models A, B, and C.

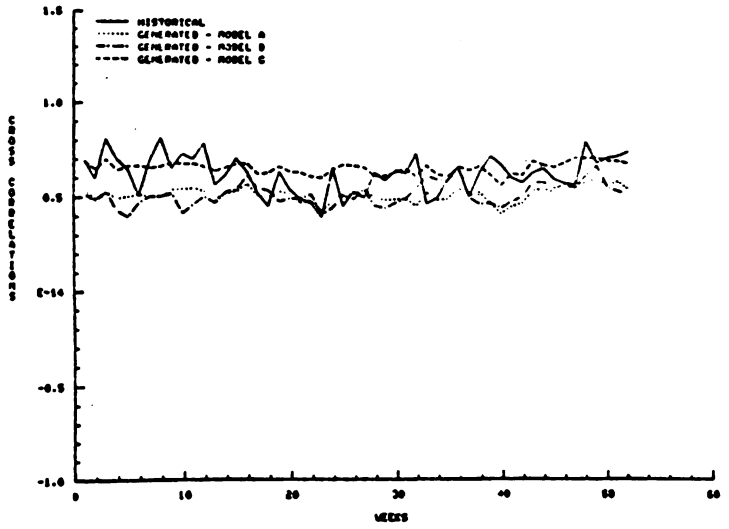

CROSS-CORR PALODE AND PASODE (ORIGINAL DOMAIN)

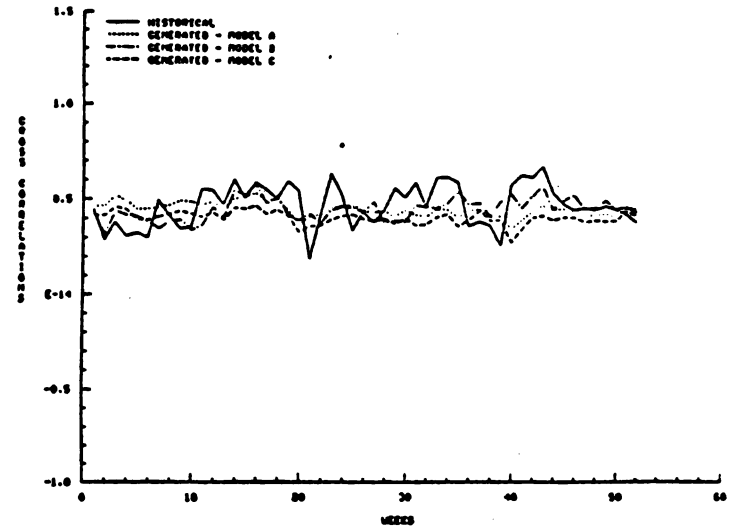

CROSS-CORR PALODE AND RANCHO (ORIGINAL DOMAIN)

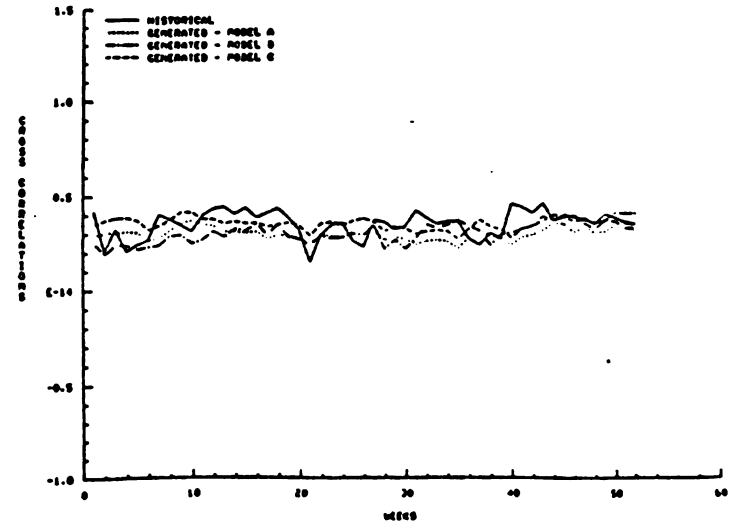

CROSS-CORR PASODE AND RANCHO (ORIGINAL DOMAIN)

Figure 1.9.D.8. Historical and generated weekly cross-correlations in the original domain using models A, B, and C.

APPENDIX 1.9.E

SELECTED HISTORICAL (EXTENDED SERIES) AND GENERATED MONTHLY AND WEEKLY STATISTICS OF PALO DE CAJA, PASO DEL ERMITAÑO AND RANCHO ARRIBA FOR MODEL B

In computing the generated statistics of each sample, Stedinger and Taylor (1982) suggested using the "theoretical" means and standard deviations (i.e., means and standard deviations of the extended data) for computing the generated statistics. This is done in order to reduce any statistical biases introduced from small-sample estimates of the standard deviations, skew coefficients and autocorrelations when computed based on the means and standard deviations of the generated flows. Thus, the unbiased estimates of the generated statistics are:

$$\bar{Y}_\tau = \frac{1}{n} \sum_{\nu=1}^{n} Y_{\nu,\tau} \tag{1.9.E.1}$$

$$S_\tau(Y) = \left\{ \frac{1}{n} \sum_{\nu=1}^{n} [Y_{\nu,\tau} - \hat{\mu}_\tau(Y)]^2 \right\}^{1/2} \tag{1.9.E.2}$$

$$G_\tau(Y) = \frac{1}{n\hat{\sigma}_\tau^3(Y)} \sum_{\nu=1}^{n} [Y_{\nu,\tau} - \hat{\mu}_\tau(Y)]^3 \tag{1.9.E.3}$$

$$R_\tau(k) = \frac{1}{n\hat{\sigma}_\tau(Y)\hat{\sigma}_{\tau-k}(Y)} \sum_{\nu=1}^{n} [Y_{\nu,\tau} - \hat{\mu}_\tau(Y)][Y_{\nu,\tau-k} - \hat{\mu}_{\tau-k}(Y)] \tag{1.9.E.4}$$

where $\hat{\mu}_\tau(Y)$ and $\hat{\sigma}_\tau(Y)$ are the seasonal means and standard deviations, n is the sample size, and τ is the seasonal index where $\tau = 1,\ldots,\omega$ seasons. Equations (1.9.E.1) through (1.9.E.4) are used to compute the generated statistics of each sample not only for the

original domain of flows (represented by Y) but for the other domain of flows by replacing the notation Y by Z for the log-Wilson-Hilferty domain, and by X for the log-domain (see Appendix 1.9.A).

After computing the generated statistics for each sample (a total of 50 for each statistic), the average and standard error are determined. Denoting the mth sample generated statistic by $V_\tau(m)$, the average $\bar{V}_\tau$ and standard error $S_\tau(V)$ are computed from

$$\bar{V}_\tau = \frac{1}{M} \sum_{m=1}^{M} V_\tau(m) \qquad (1.9.E.5)$$

and

$$S_\tau(V) = \left\{ \frac{1}{M} \sum_{m=1}^{M} [V_\tau(m) - \bar{V}_\tau]^2 \right\}^{1/2} \qquad (1.9.E.6)$$

where M is equal to 50 samples.

The computed averages and standard errors of the monthly and weekly generated statistics are given in the figures below for the three stations in the original domain of flows. Plots of skewness coefficients in the log domain, and the lag-1 autocorrelation coefficients in the log-WH domain are also given below. Also plotted in these figures are the historical statistics and the upper and lower confidence bands of the generated statistics. The confidence band B_τ is computed as positive and nega-tive one-standard error relative to the average as

$$B_\tau = \bar{V}_\tau \pm S_\tau(V) \qquad (1.9.E.7)$$

where $\bar{V}_\tau$ and $S_\tau(V)$ are as defined above. Note that for the plots of historical lag-1 autocorrelation coefficients in the log-Wilson-Hilferty domain, and the historical skew coefficients in the log-domain are the fitted Fourier functions (since, these are the parameters used in data generation).

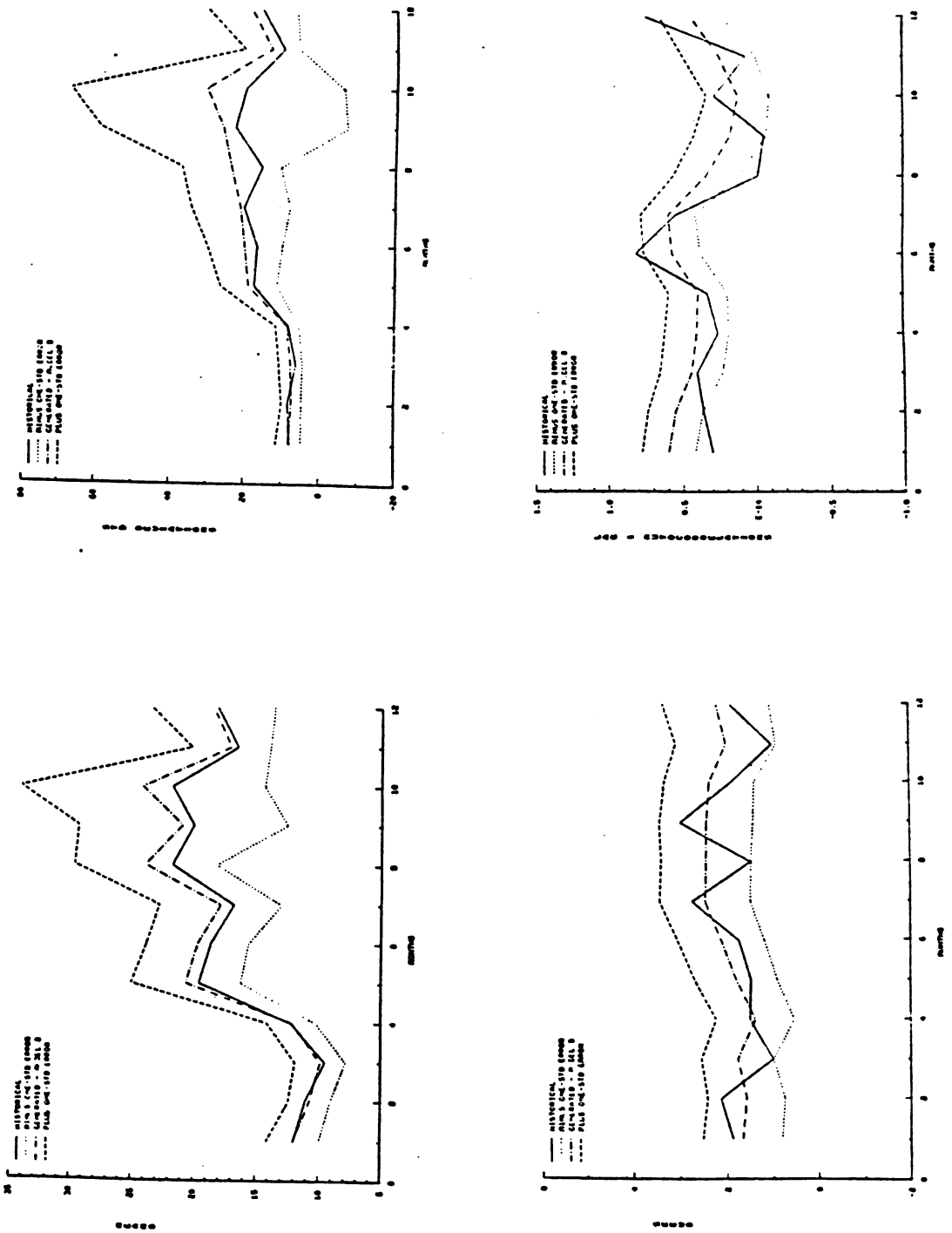

Figure 1.9.E.1. Historical and generated monthly statistics of Palo de Caja in the original domain of flows for model B.

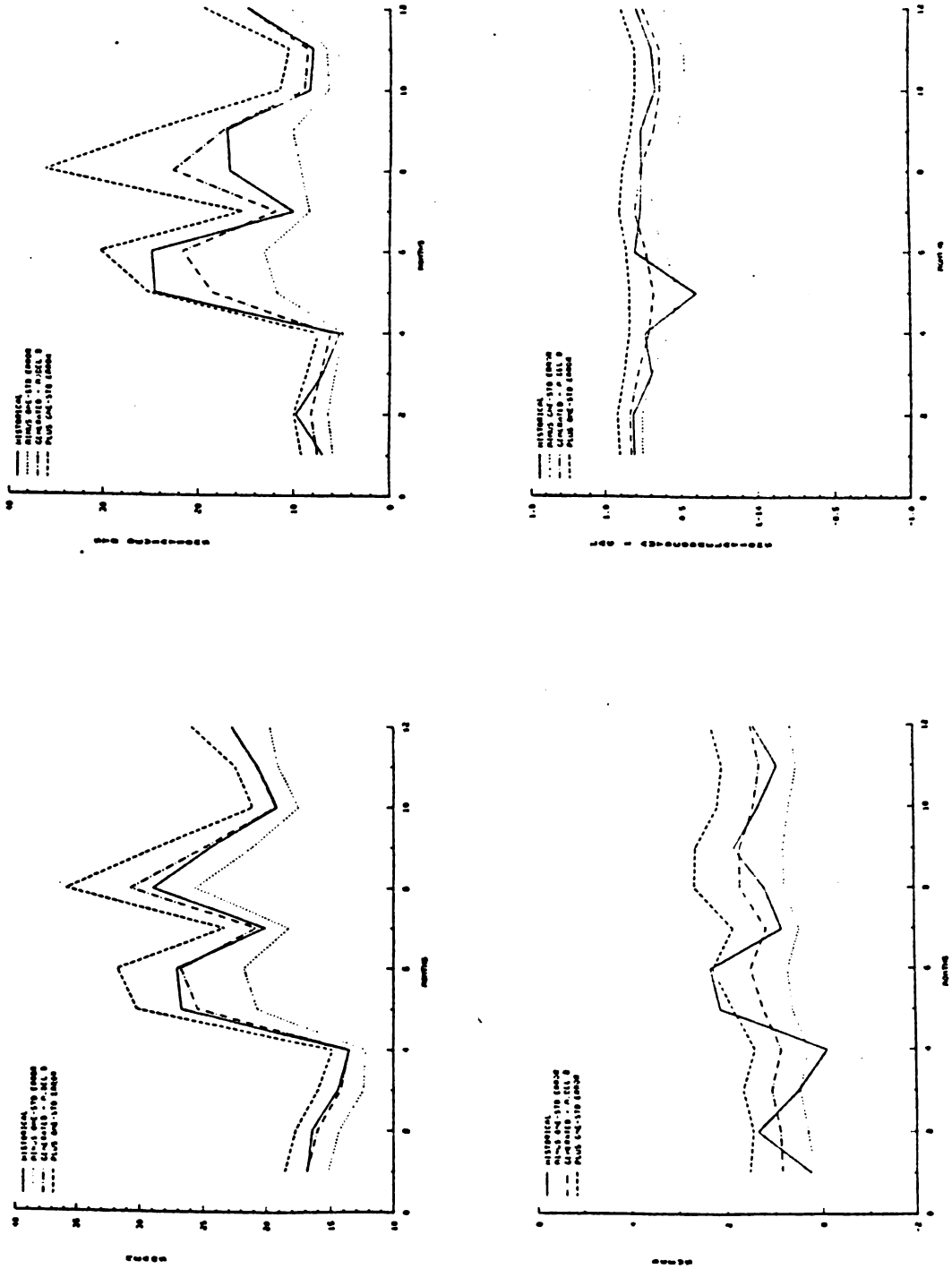

Figure 1.9.E.2. Historical and generated monthly statistics of Paso del Ermitano in the original domain of flows for model B.

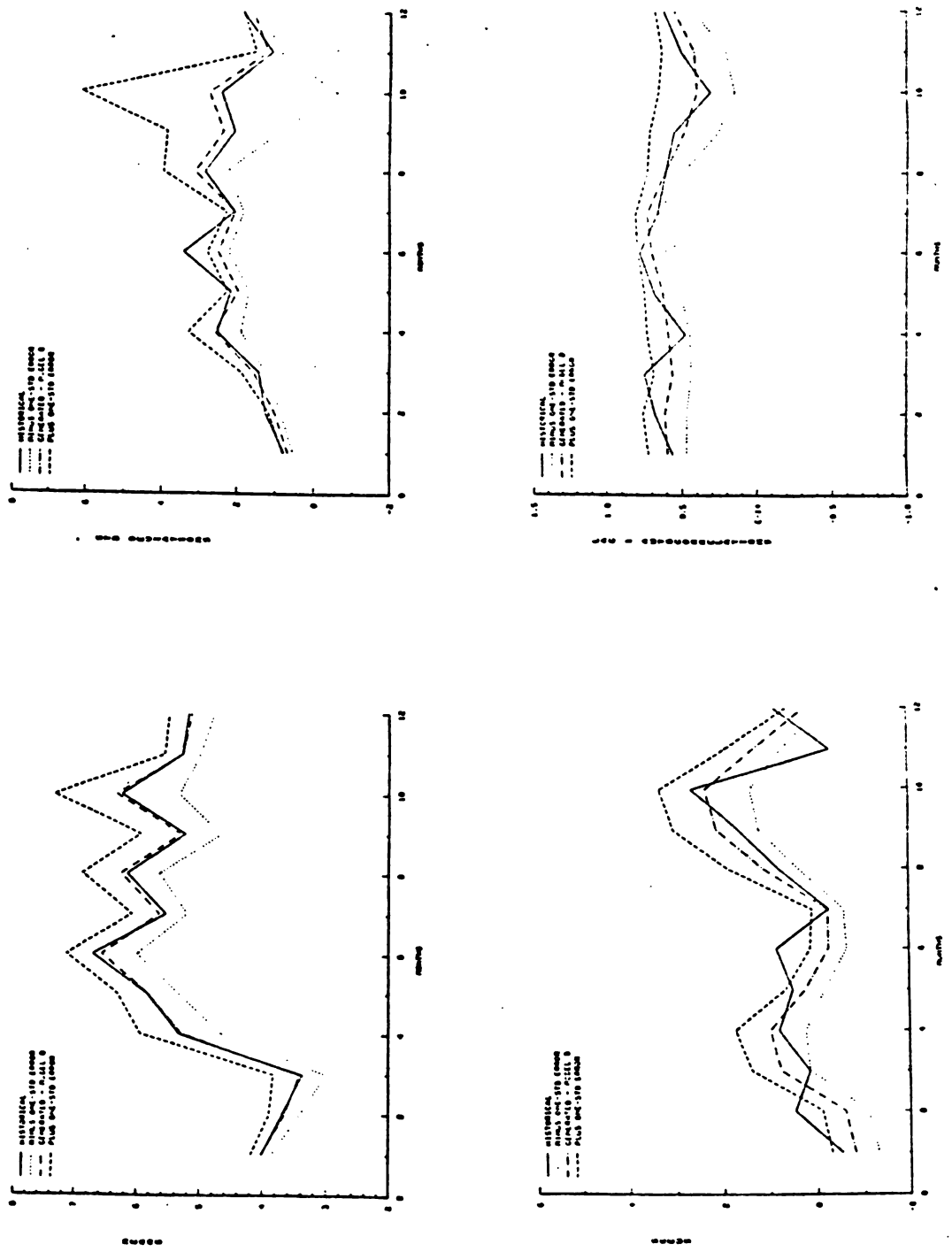

Figure 1.9.E.3. Historical and generated monthly statistics of Rancho Arriba in the original domain of flows for model B.

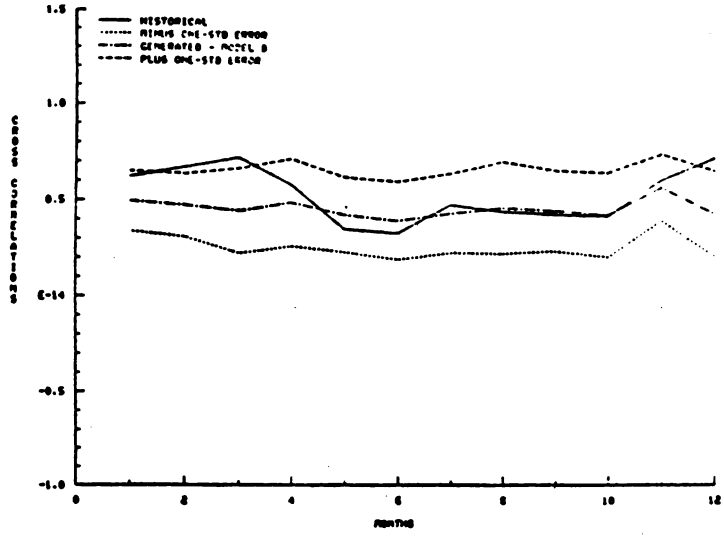

PALODE AND PASODE - CROSS CORRELATIONS (ORIGINAL DOMAIN)

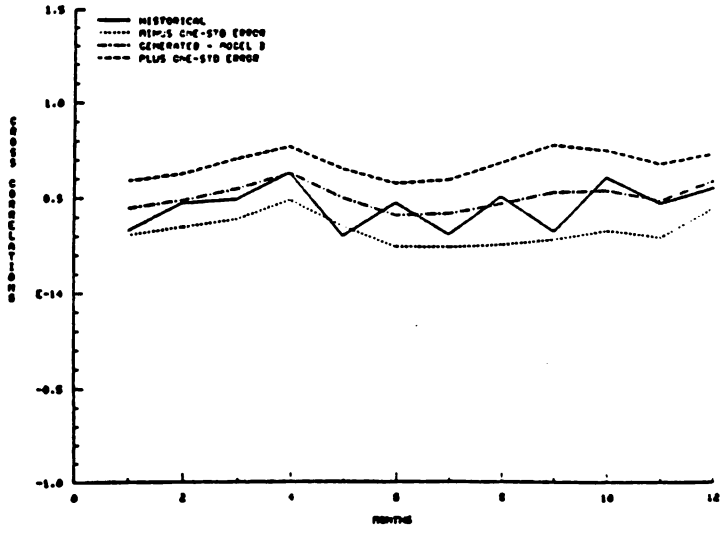

PALODE AND RANCHO - CROSS CORRELATIONS (ORIGINAL DOMAIN)

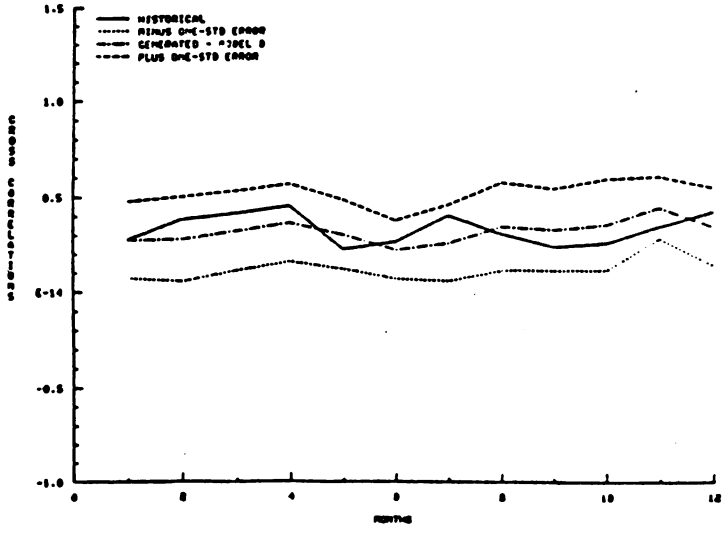

PASODE AND RANCHO - CROSS CORRELATIONS (ORIGINAL DOMAIN)

Figure 1.9.E.4. Historical and generated monthly cross-correlations in original domain for model B.

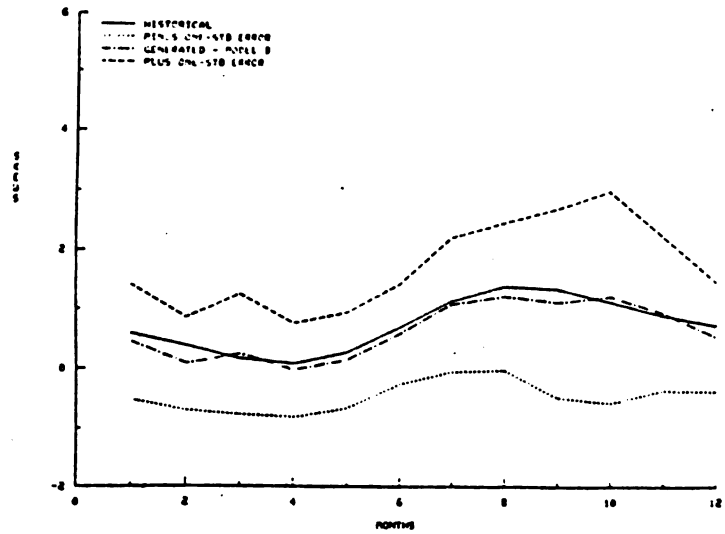

PALODE - SKEWS (LOG DOMAIN)

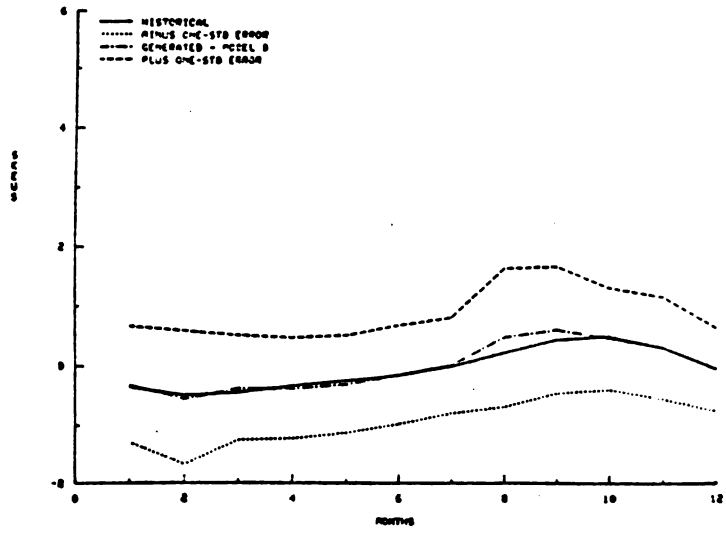

PASODE - SKEWS (LOG DOMAIN)

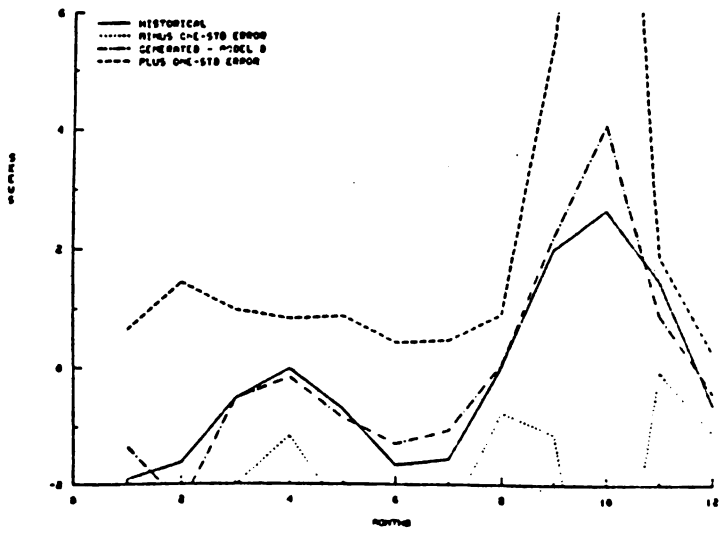

RANCHO - SKEWS (LOG DOMAIN)

Figure 1.9.E.5. Historical and generated monthly skews in log domain for model B.

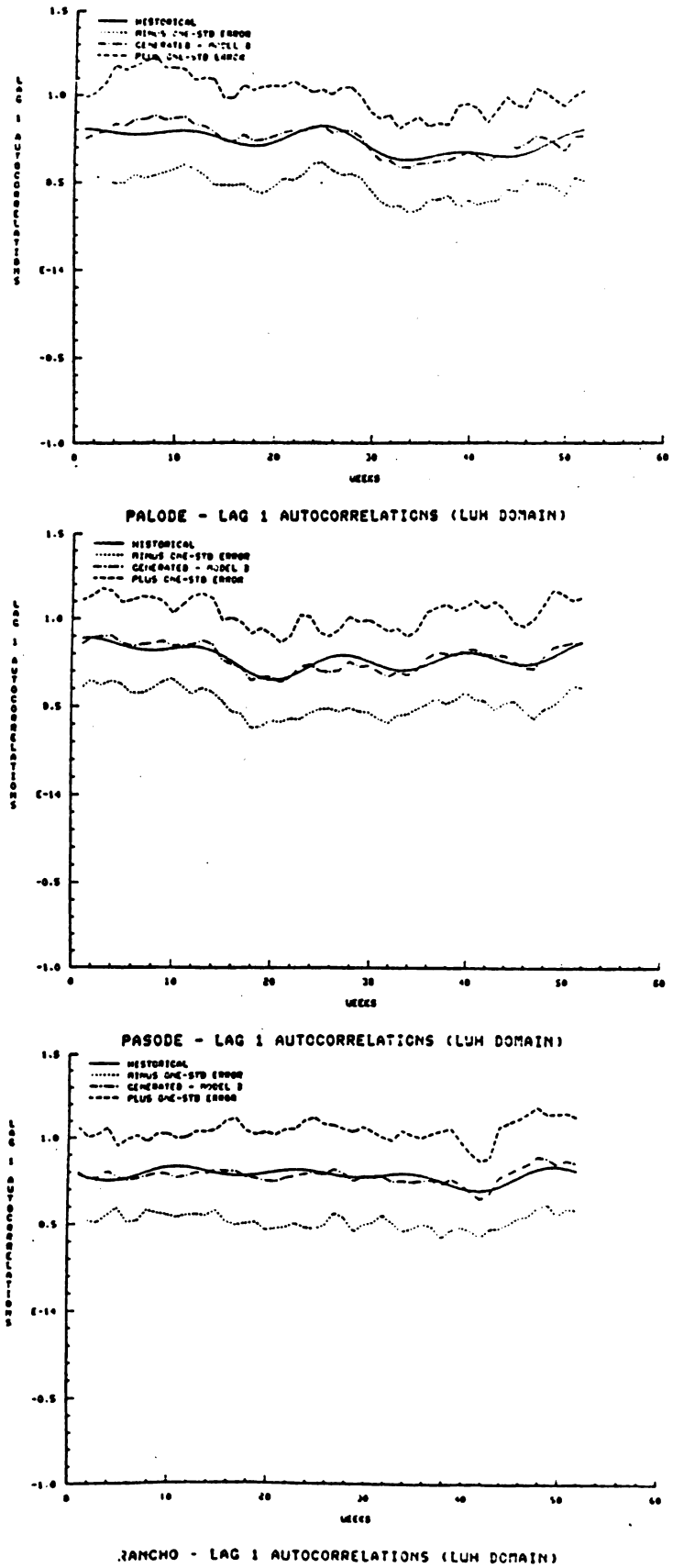

Figure 1.9.E.6. Historical and generated monthly lag-1 autocorrelations in log-wll domain for model B.

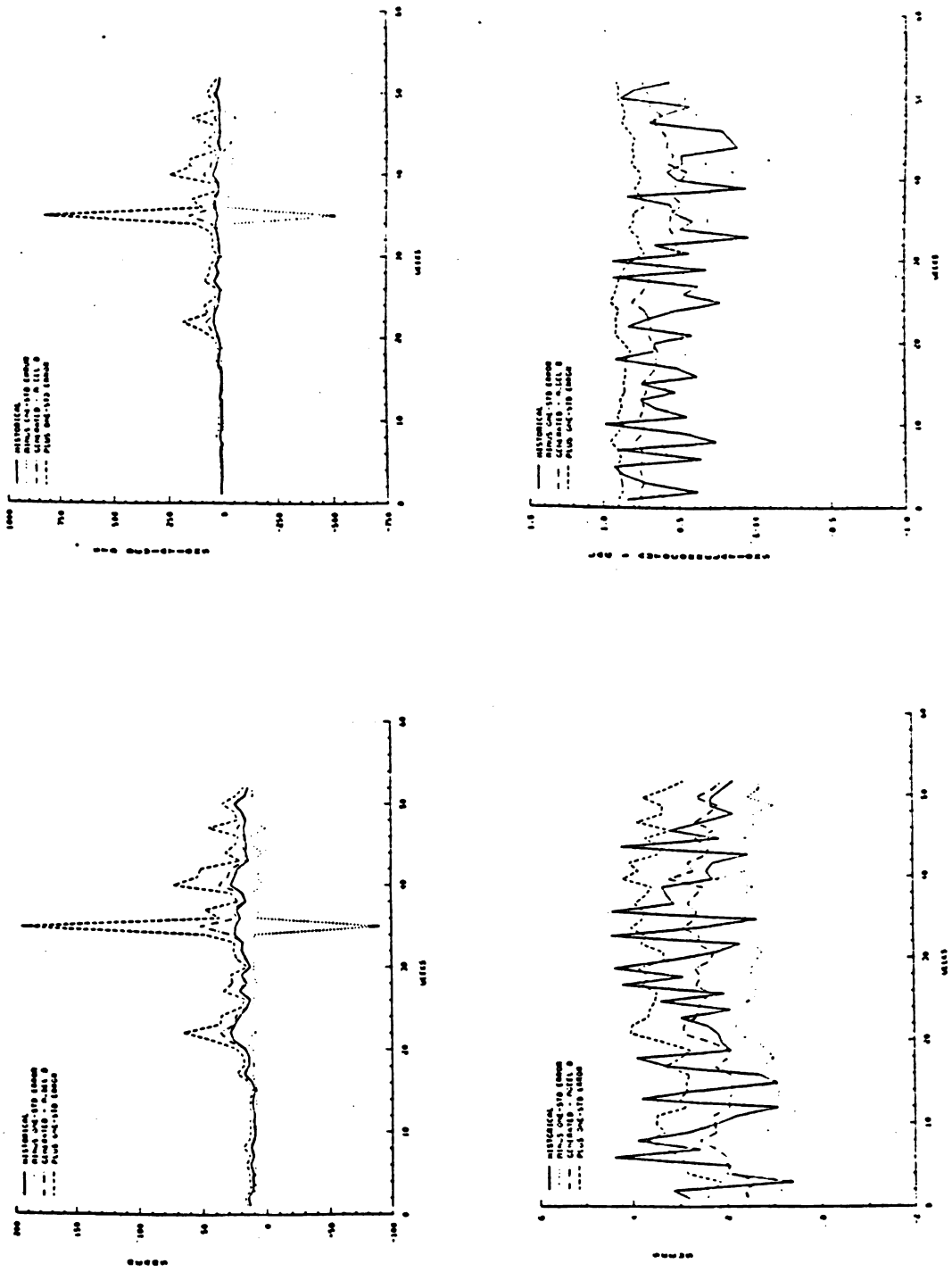

Figure 1.9.E.7. Historical and generated weekly statistics of Palo de Caja in the original domain for model B.

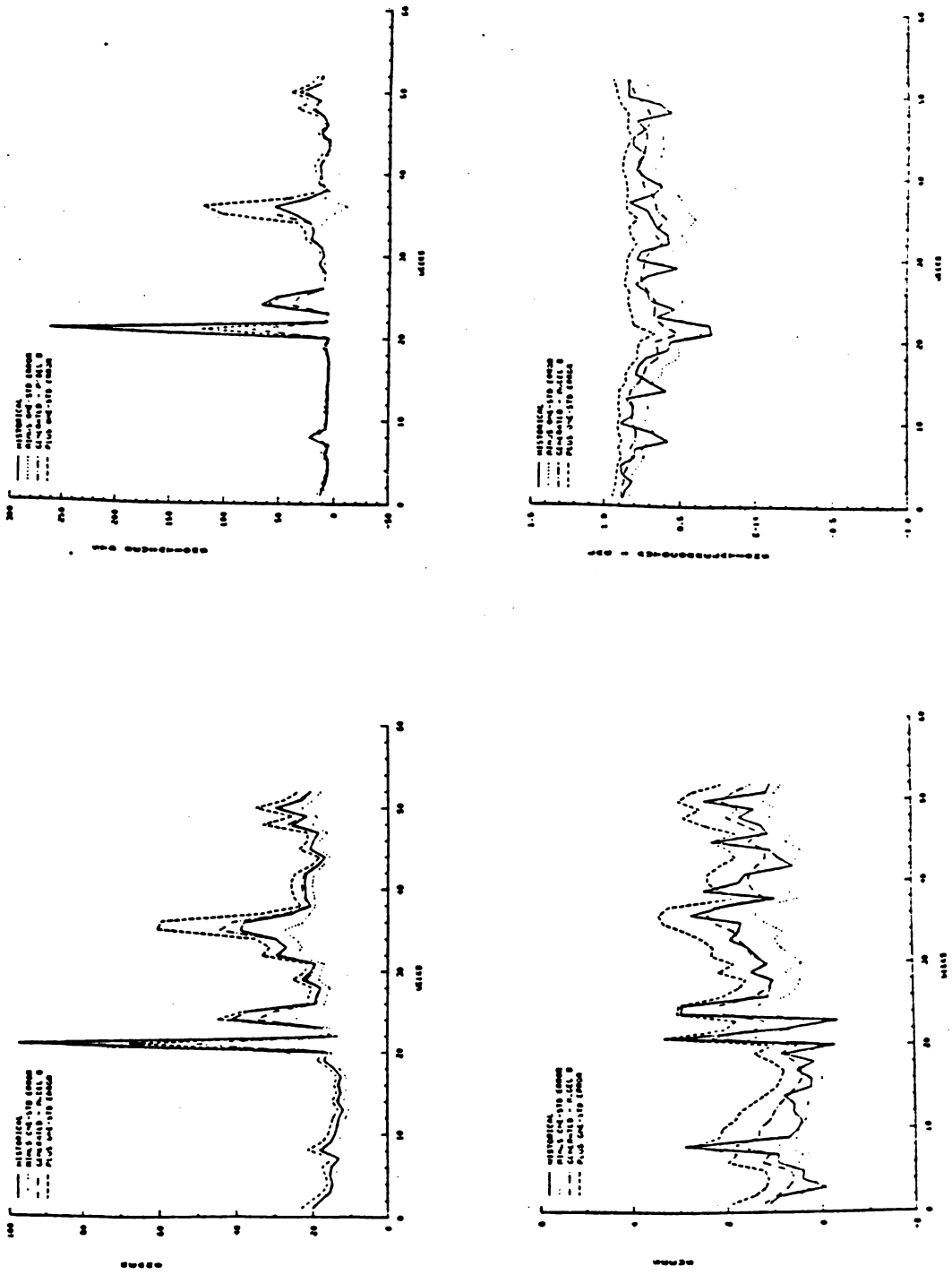

Figure 1.9.E.8. Historical and generated weekly statistics of Paso del Ermitano in the original domain of flows for model B.

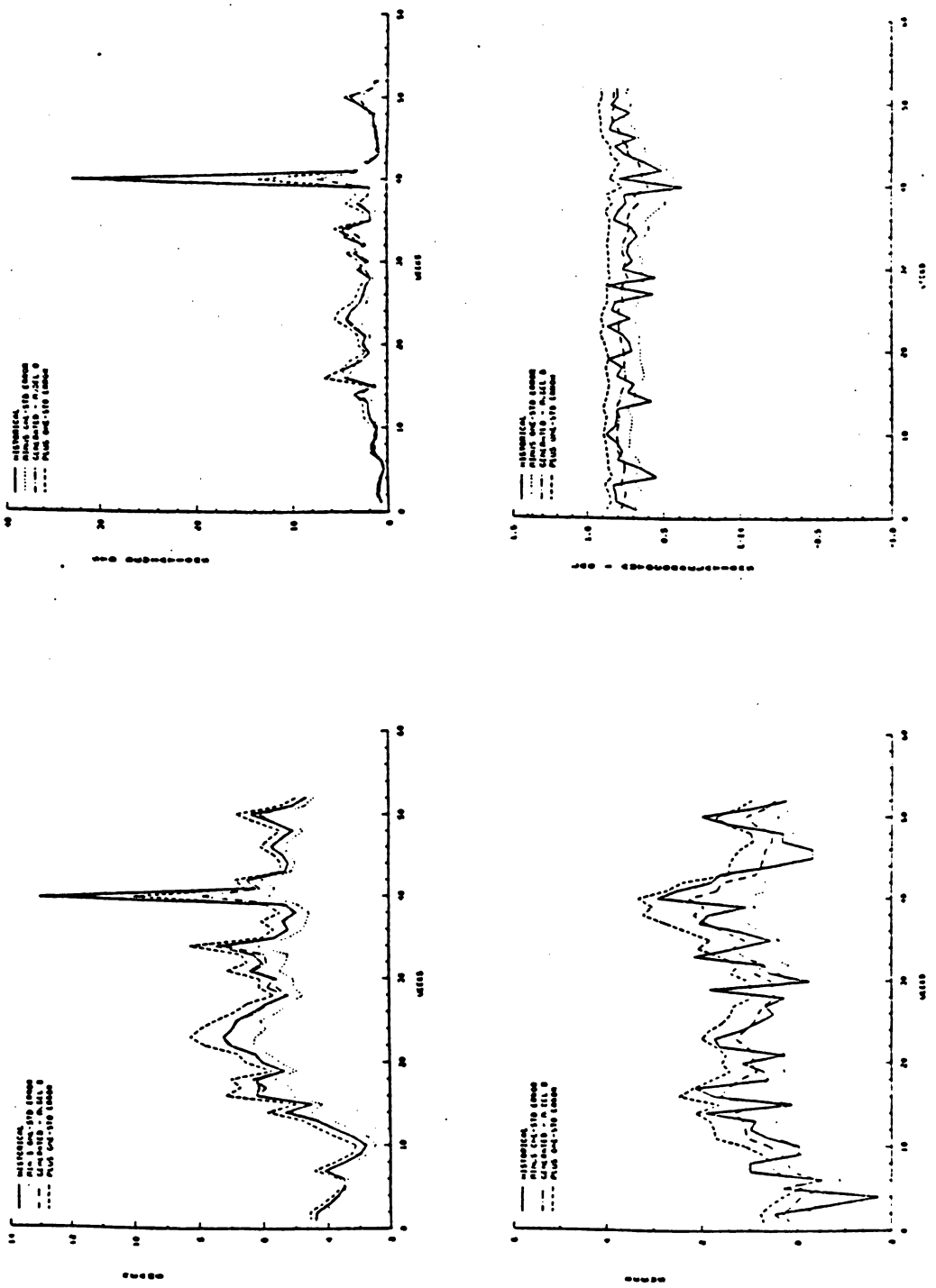

Figure 1.9.E.9. Historical and generated weekly statistics of Rancho Arriba in the original domain of flows for model B.

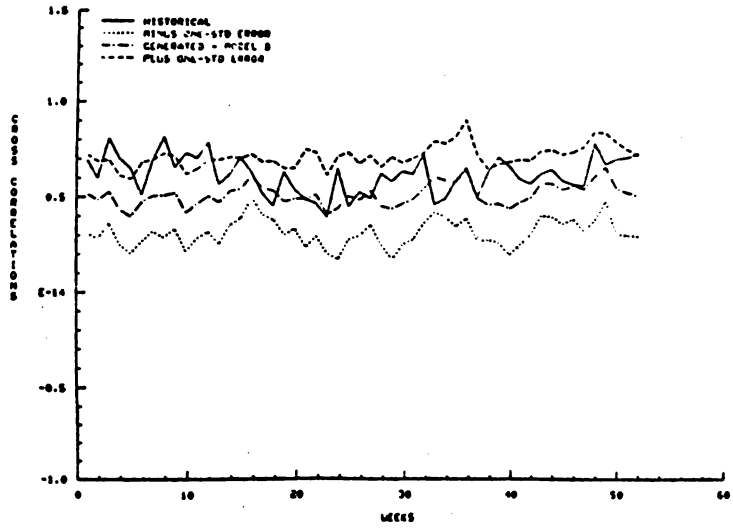

PALODE AND PASODE - CROSS CORRELATIONS (ORIGINAL DOMAIN)

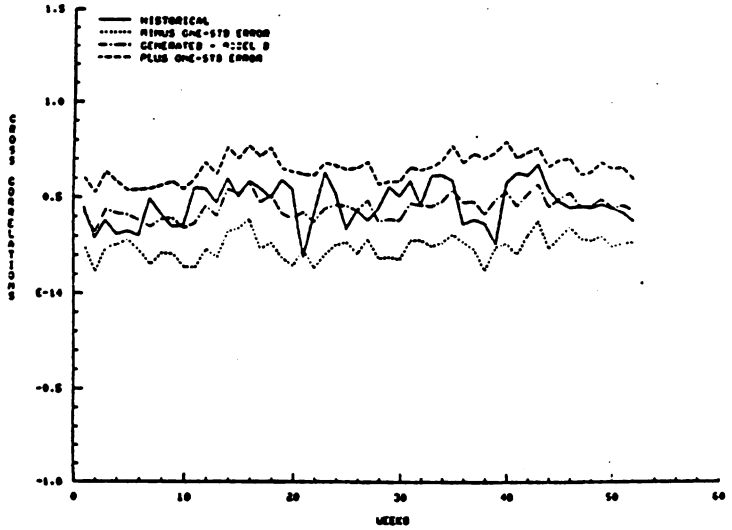

PALODE AND RANCHO - CROSS CORRELATIONS (ORIGINAL DOMAIN)

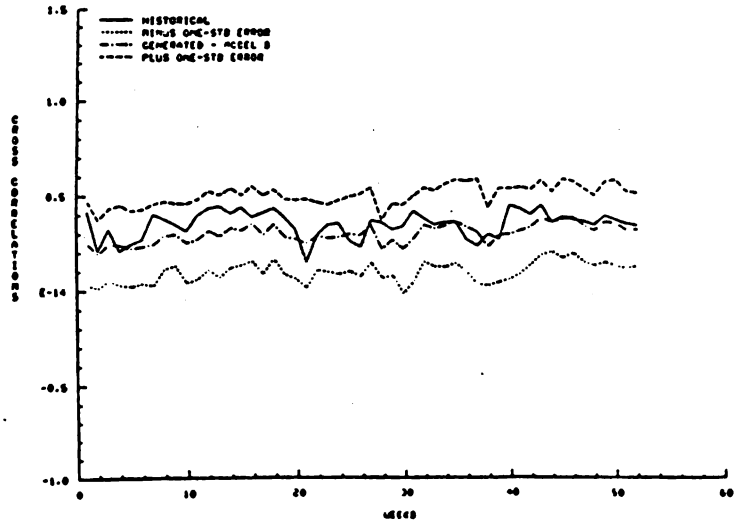

PASODE AND RANCHO - CROSS CORRELATIONS (ORIGINAL DOMAIN)

Figure 1.9.E.10. Historical and generated weekly cross-correlations in original domain for model B.

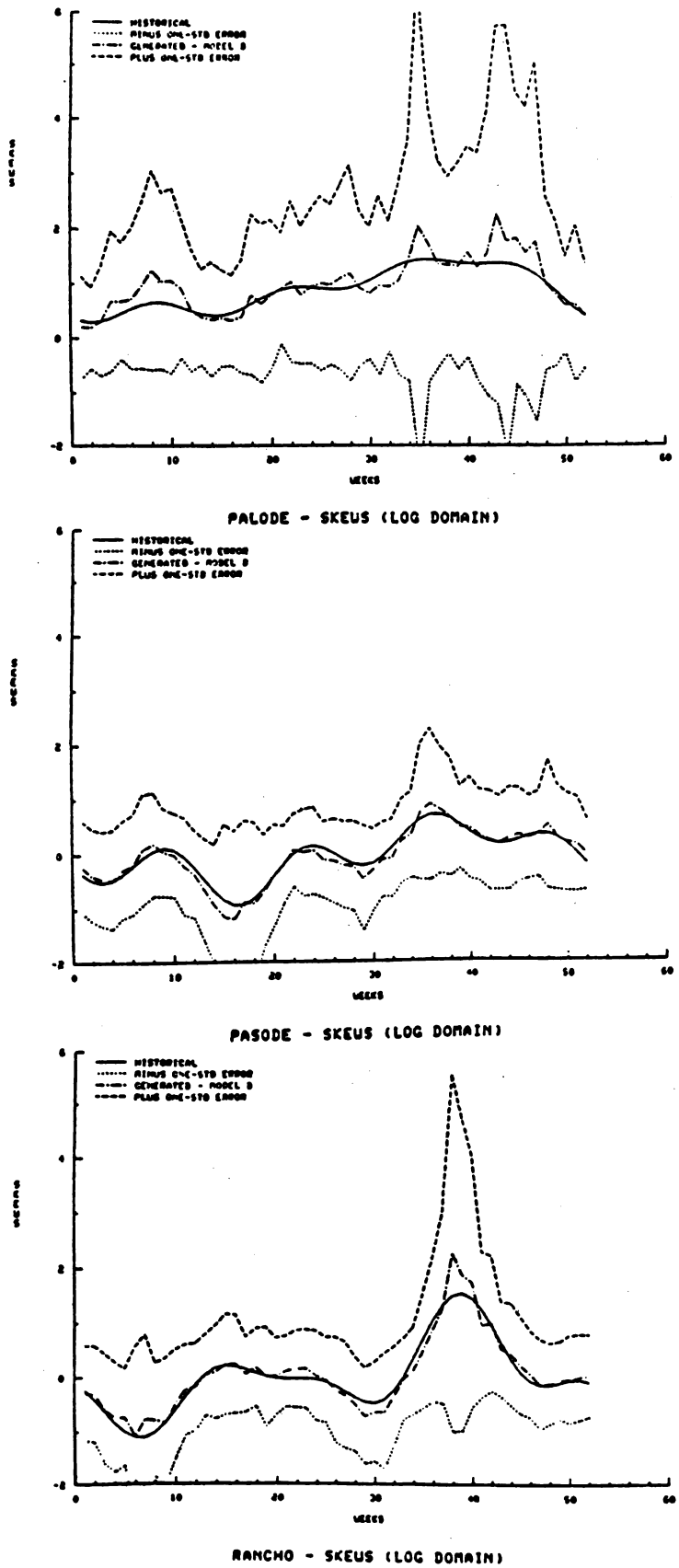

Figure 1.9.E.11. Historical and generated weekly skews in log domain for model B.

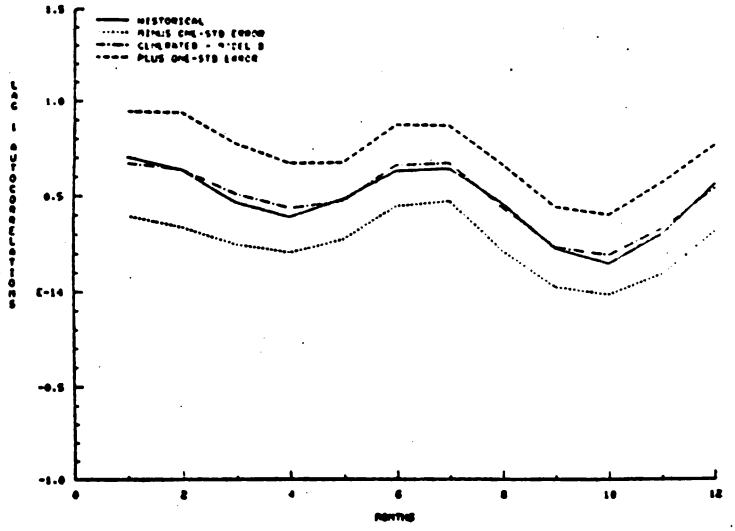

PALODE - LAG 1 AUTOCORRELATIONS (LUH DOMAIN)

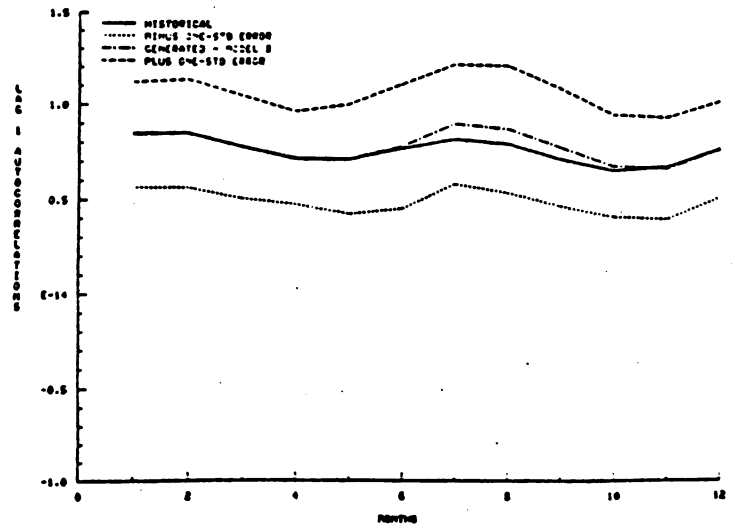

PASODE - LAG 1 AUTOCORRELATIONS (LUH DOMAIN)

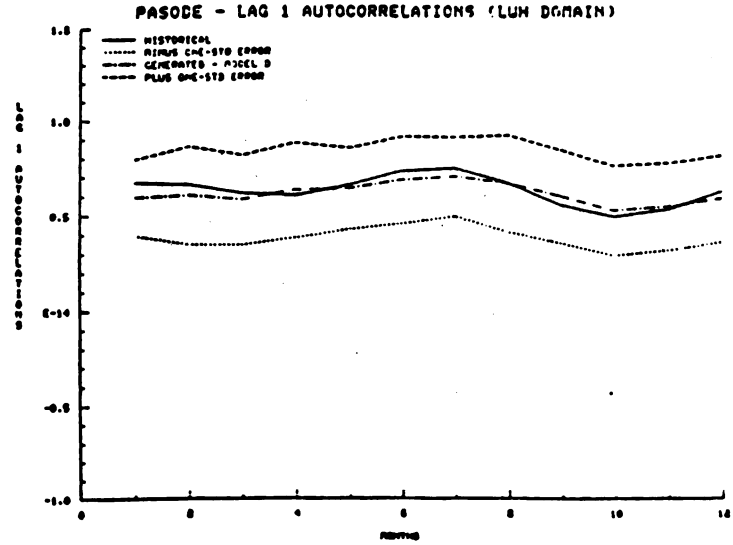

RANCHO - LAG 1 AUTOCORRELATIONS (LUH DOMAIN)

Figure 1.9.E.12. Historical and generated weekly lag-1 autocorrelations in log-WH domain for model B.

APPENDIX 1.9.F

HISTORICAL AND GENERATED STATISTICS OF MONTHLY TURBINE OPERATING HOURS TIME SERIES OF VALDESIA RESERVOIR

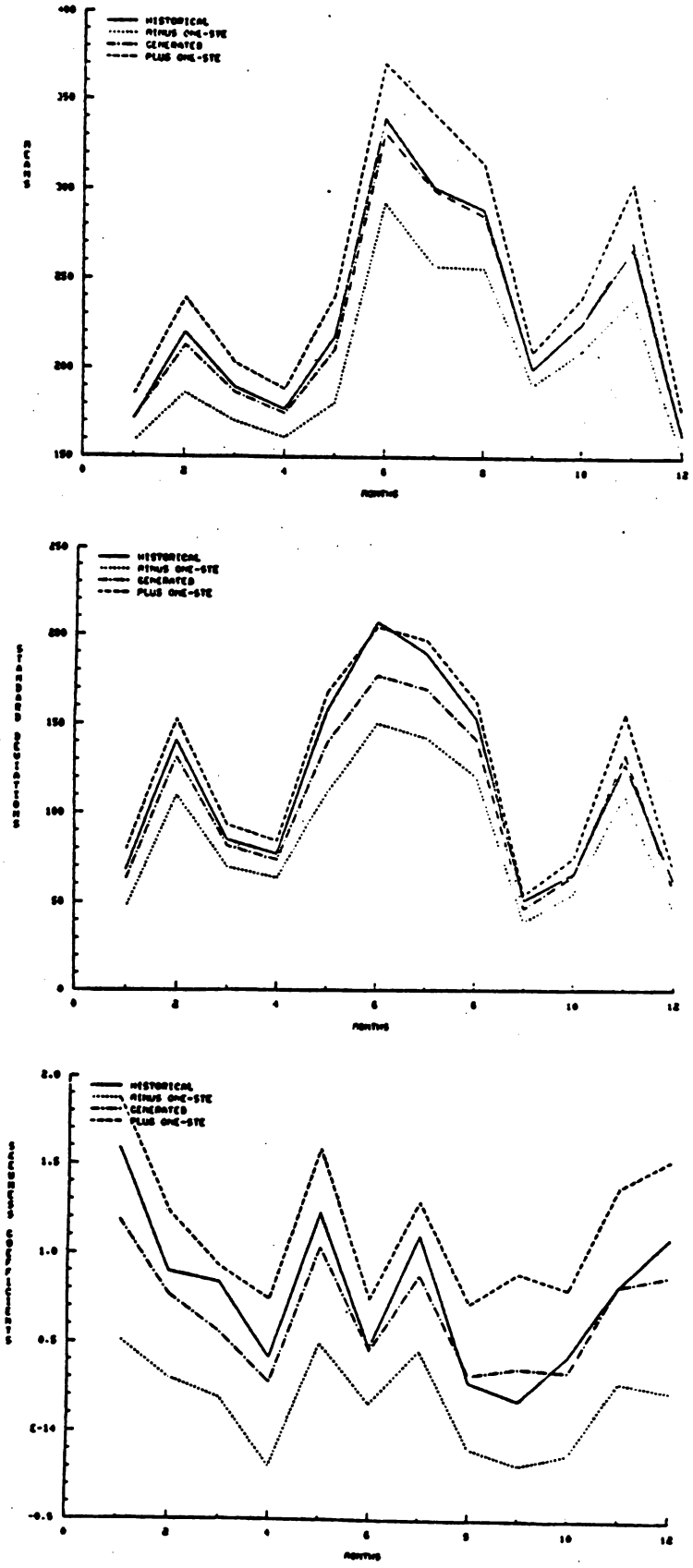

Figure 1.9.F.1. Historical and generated monthly statistics of turbine operating hours at Valdesia reservoir.

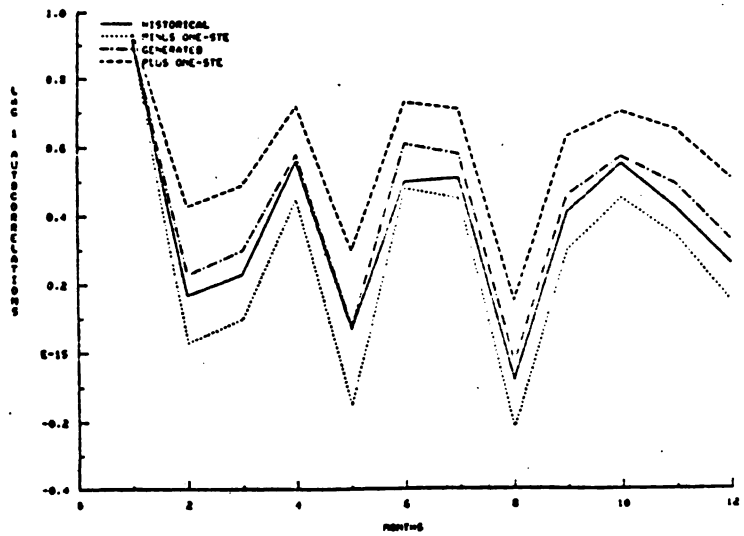

Figure 1.9.F.2. Historical and generated monthly lag-1 autocorrelations of turbine operating hours at Valdesia reservoir.

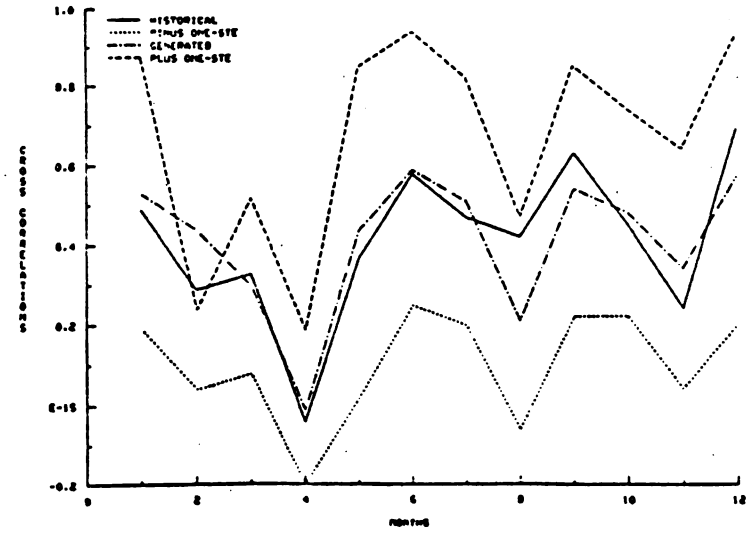

Figure 1.9.F.3. Historical and generated monthly cross-correlations between turbine operating hours and streamflows.

I.10 REFERENCES

Burnash, R.J.C., 1985. Real-time forecasting with the Sacramento watershed model. In Proc. 14th Annual Hydrology Day, Colorado State University, Ft. Collins, CO, pp. 103-113.

Burnash, R.J.C., R.L. Ferral and R.A. McGuire, 1979. A generalized streamflow simulation system conceptual modeling for digital computers. National Weather Service, California Dept. of Water Resources, March, 1979 (second printing).

CSU-HMS, 1986, Colorado State University Hydrologic Modeling System - User's Manual, developed by J.T.B. Obeysekera, G.Q. Tabios III, J.D. Salas, and H.W. Shen, Dept. of Civil Engineering, Fort Collins, Colorado 80523.

Kuester, J.L. and J.H. Mize, 1973. Optimization techniques with FORTRAN. McGraw-Hill Book Co., New York.

Matalas, N.C., 1967. Mathematical assessment of synthetic hydrology. Water Resources Research, Vol. 3, No. 4, 4th Quarter, pp. 931-935.

McGinnis, D.F., Jr., and W.H. Sammons, 1970. Discussion of "Daily streafmlow simulation" by K. Payne, W.D. Neumann and K.D. Kerri. Jour. of the Hydraulics Div., Proc. ASCE, Vol. 96, No. HY5, May, pp. 1201-1206.

National Weather Service, 1984. NWS-river forecast system manual calibration version 3.0. National Weather Service, Silver Spring, Md.

Salas, J.D., J.W. Delleur, V. Yevjevich, and W.L. Lane, 1980. Applied Modeling of Hydrologic Time Series. Water Resources Publ., Littleton, CO.

Salas, J.D. and R.A. Smith, 1981. Computer Programs for Modeling and Generation of Hydrologic Time Series. Dept. of Civil Engineering, Colorado State University, Fort Collins, CO, July.

Salas, J.D., G.Q. Tabios and P. Bartolini, 1985. Approaches to multivariate modeling of water resources time series. Water Resources Bulletin, AWRA, Vol. 21, No. 4, August, pp. 683-708.

Stedinger, J.R. and M.R. Taylor, 1982. Synthetic streamflow generation, 1. Model verification and validation. Water Resources Research, Vol. 18, No. 4, August, pp. 909-918.

U.S. Army Corps of Engineers, 1971. Hydrologic Engineering Methods for Water Resources Development, Volume I, Requirement and General Procedures, Hydrologic Engineering Center, Davis, California.

U.S. Army Corps of Engineers, 1985. HEC-1 flood hydrograph package user's manual, The Hydrologic Engineering Center, Davis, California.

U.S. Weather Bureau, 1961. Generalized Estimates of Probable Maximum Precipitation and Rainfall Frequency for Puerto Rico and Virgin Islands. Technical Paper No. 42, Washington, D.C.

Yevjevich, V. and J.T.B. Obeysekera, 1984. Estimation of skewness of hydrologic variables. Water Resources Research, Vol. 20, No. 7, July. pp. 935-943.

FECHA DE DEVOLUCION

Autor

Título Final report. I. Hydrologic studies

Fecha Devolución	Nombre del solicitante